

Crystallisation and functional studies  
with ethylene receptor ETR1

Inaugural-Dissertation

Elisa Buchen



# **Crystallisation and functional studies with ethylene receptor ETR1**

Inaugural-Dissertation

zur Erlangung des Doktorgrades  
der Mathematisch-Naturwissenschaftlichen Fakultät  
der Heinrich-Heine-Universität Düsseldorf

vorgelegt von

**Elisa Buchen**

aus Remscheid

Düsseldorf, Februar 2011

Aus dem Institut für Biochemie der Pflanzen  
der Heinrich-Heine-Universität Düsseldorf

Gedruckt mit der Genehmigung der  
Mathematisch-Naturwissenschaftlichen Fakultät der  
Heinrich-Heine-Universität Düsseldorf

Referent: Prof. Dr. G. Groth  
Koreferent: Prof. Dr. D. Willbold

Tag der mündlichen Prüfung: 14.04.2011

Titelbild: <i>Arabidopsis thaliana</i> Ökotyp Landsberg <i>erecta</i> . Die Pflanze wurde freundlicherweise zur Verfügung gestellt von Helge Pallakies, Institut für Genetik der Universität Düsseldorf.
--



# Contents

<b>1</b>	<b>Abstract .....</b>	<b>7</b>
<b>2</b>	<b>Zusammenfassung .....</b>	<b>9</b>
<b>3</b>	<b>Introduction .....</b>	<b>11</b>
3.1	Plant hormones: Communication is all!.....	11
3.2	The plant hormone ethylene .....	11
3.2.1	The role of ethylene in plant life cycle .....	12
3.2.2	Ethylene biosynthesis .....	12
3.2.3	The ethylene signalling pathway in <i>Arabidopsis thaliana</i> .....	13
3.2.4	Cross-talk between ethylene and other plant hormones.....	19
3.2.5	Objectives of this thesis.....	20
<b>4</b>	<b>Materials &amp; Methods .....</b>	<b>21</b>
4.1	Materials .....	21
4.1.1	Equipment .....	21
4.1.2	Chromatography supplies .....	22
4.1.3	Crystallographic supplies.....	22
4.1.4	Kits.....	23
4.1.5	Filters and Membranes.....	23
4.1.6	Chemicals and Buffers.....	23
4.1.7	Radiochemicals.....	24
4.1.8	Enzymes .....	24
4.1.9	Antibodies.....	25
4.1.10	Oligonucleotides .....	25
4.1.11	Custom gene synthesis .....	27
4.1.12	Vectors .....	27
4.1.13	Bacterial strains: <i>Escherichia coli</i> .....	29
4.2	Microbiological methods .....	30
4.2.1	Media for cultivation of <i>E. coli</i> cells .....	30
4.2.2	Preparation and transformation of chemically competent <i>E. coli</i> cells.....	30
4.3	Molecular biological methods.....	31
4.3.1	Amplification and isolation of plasmid DNA from <i>E. coli</i> .....	31
4.3.2	Determination of DNA concentration .....	31
4.3.3	Polymerase chain reaction to amplify DNA .....	31
4.3.4	Agarose gel electrophoresis .....	32
4.3.5	Cloning, Mutagenesis and Sequencing.....	33
4.3.6	SLIC: Sequence and ligation independent cloning .....	34
4.4	Protein biochemical methods .....	35
4.4.1	Protein quantification.....	35
4.4.2	SDS polyacrylamide gel electrophoresis.....	36
4.4.3	Silver staining of SDS-PAGE gels.....	36
4.4.4	Western blotting .....	37

4.4.5	Dot blotting .....	37
4.4.6	Immunodetection .....	38
4.4.7	Proteolytic cleavage .....	38
4.5	Expression of recombinant proteins in <i>E. coli</i> .....	39
4.5.1	Expression of full-length receptor protein AtETR1 .....	39
4.5.2	Expression of the extramembrane domain of AtETR1 .....	40
4.5.3	Expression of PpETR1 and LeETR1 .....	40
4.6	Purification of recombinant proteins from <i>E. coli</i> – general methods .....	41
4.6.1	Cell disruption .....	41
4.6.2	Isolation and solubilisation of <i>E. coli</i> membranes .....	41
4.6.3	Isolation and purification of inclusion bodies .....	42
4.6.4	Solubilisation of inclusion bodies .....	42
4.6.5	Refolding of proteins solubilised from inclusion bodies .....	43
4.6.6	Size exclusion chromatography .....	43
4.6.7	Removal of DnaK contamination .....	44
4.7	Purification protocols for individual proteins .....	45
4.7.1	Purification of full-length receptor protein AtETR1 .....	45
4.7.2	Purification of the extramembrane domain of AtETR1 .....	47
4.7.3	Purification of full-length PpETR1 and LeETR1 .....	48
4.7.4	Preparation of truncated PpETR1 and LeETR1 from inclusion bodies .....	48
4.8	Protein characterisation .....	49
4.8.1	<i>In vitro</i> kinase assay .....	49
4.8.2	Circular dichroism spectroscopy .....	50
4.8.3	Fluorescence spectroscopy .....	50
4.8.4	<sup>31</sup> P-NMR spectroscopy .....	51
4.8.5	Protein crystallography .....	52
4.8.6	Bioinformatics methods and software tools .....	57

## 5 Part A: Functional studies on ethylene receptor ETR1 from *A. thaliana*.. 59

5.1	Intrinsic tryptophan fluorescence to resolve ligand binding and conformational changes in ETR1 .....	60
5.1.1	Cloning of single tryptophan substitution mutants .....	61
5.1.2	Expression and purification of recombinant ETR1 .....	64
5.1.3	Characterisation of single tryptophan substitution mutants .....	65
5.2	Ligand binding to ethylene receptor ETR1 .....	71
5.2.1	Binding of copper cofactor and ethylene .....	71
5.2.2	Characterisation of the quenching effect .....	74
5.2.3	Effect of His-tag on copper binding .....	78
5.3	Characterisation of the ETR1 phosphorylation state .....	80
5.3.1	Conformational changes upon phosphorylation of ETR1 probed by engineered Trp reporter groups .....	81
5.3.2	<sup>31</sup> P-NMR spectroscopy to assign the phosphorylation sites in ETR1 .....	86
5.4	Synopsis .....	89

---

<b>6</b>	<b>Part B: Crystallisation of ETR1 from <i>A. thaliana</i></b>	<b>91</b>
6.1	Crystallisation of the extra membrane domain of ETR1	92
6.1.1	Optimising crystallisation conditions	94
6.1.2	Protein modification	100
6.2	Crystallisation of full-length ETR1	107
6.2.1	Effect of histidine affinity tag	108
6.2.2	Influence of the purification method on crystallisation of ETR1	109
6.3	Synopsis	115
<b>7</b>	<b>Part C: Crystallisation of ETR1 orthologs from <i>P. patens</i> and <i>L. esculentum</i></b>	<b>117</b>
7.1	Cloning and expression of receptor constructs	119
7.1.1	Cloning of receptor constructs	120
7.1.2	Expression studies	120
7.2	Purification and characterisation of PpETR1 and LeETR1	126
7.2.1	Receptor constructs lacking the membrane domain	126
7.2.2	Full-length receptor constructs	135
7.3	Crystallisation studies	139
7.3.1	Full-length ethylene receptor ETR1 from <i>L. esculentum</i>	139
7.3.2	Full-length ethylene receptor ETR1 from <i>P. patens</i>	140
7.4	Synopsis	141
7.4.1	Perspective on further crystallisation studies	142
7.4.2	Taxonomic distribution of ethylene receptors in kingdom <i>Viridiplantae</i>	143
7.4.3	Secondary structure analysis of orthologs AtETR1, PpETR1 and LeETR1	145
<b>8</b>	<b>Concluding remarks</b>	<b>149</b>
<b>9</b>	<b>Appendix</b>	<b>151</b>
9.1	Abbreviations	151
9.2	Maps of expression vectors	153
9.3	List of detergents used in this thesis	158
9.4	Refolding buffers	159
<b>10</b>	<b>References</b>	<b>161</b>
<b>11</b>	<b>Acknowledgements</b>	<b>171</b>
<b>12</b>	<b>Erklärung</b>	<b>173</b>



# 1 Abstract

The gas ethylene has a wide influence on various physiological and developmental processes within plants including senescence and abscission of petals, leaves and fruits. The plant hormone is also known as a mediator of biotic and abiotic stress responses upon flooding, drought or pathogen infection. Genetic studies in the model plant *Arabidopsis thaliana* revealed that binding of ethylene occurs at specific receptor proteins located at the endoplasmic reticulum.

To ultimately understand how these membrane proteins perceive and transmit the ethylene signal throughout a complex network and to elucidate potential interactions with other proteins of the signalling cascade, it is essential to analyse and characterise the receptors at the protein level.

Within the first part of this thesis, monitoring of intrinsic tryptophan fluorescence was used in addition to a radioactive assay to characterise ligand binding and phosphorylation events in the ethylene receptor protein ETR1 from *Arabidopsis thaliana*. Fluorescence based studies indicated interaction of the receptor protein with the copper cofactor necessary for binding of ethylene. Phosphorylation experiments revealed that phosphorylation can occur on further residues in the kinase and receiver domain of the receptor other than the putative sites H353 and D659. In this context, preliminary tests were carried out to use  $^{31}\text{P}$ -NMR in future experiments to assign these residues.

The second part of this thesis aimed to a structural characterisation of the receptor protein by X-ray crystallography. For the first time, it was possible to obtain crystals of the full-length ethylene receptor AtETR1. The crystals diffracted to a resolution of about 11 to 12 Å, but data could not be used for structure determination due to the high mosaicity and anisotropic spot distribution. Comprehensive optimisation including protein modification and variations of the experimental setup was tried but did not improve diffraction quality.

For that reason the crystallisation study was expanded to orthologous ETR1s from the moss *Physcomitrella patens subsp. patens* and the tomato *Lycopersicon esculentum*. Expression and purification protocols were established for both proteins, and first crystallisation screens already gave spherulitic crystals. Although these crystalline structures are not suitable for diffraction analysis, they outline starting conditions for future crystallisation approaches.



## 2 Zusammenfassung

Ethylen greift als Pflanzenhormon in eine Vielzahl von physiologischen und entwicklungsrelevanten Prozessen der Pflanze ein. Hierzu gehören unter anderem die Seneszenz und Abszission von Blüten und Blättern, sowie die Förderung der Fruchtreife. Ethylen kann außerdem spezifische Stressantworten auslösen, die durch biotische und abiotische Umweltreize wie z.B. Pathogenbefall oder Trockenheit initiiert werden.

Die Wahrnehmung eines Ethylensignals erfolgt über Rezeptorproteine am endoplasmatischen Retikulum. Der genaue Mechanismus, mit dem die Signalerkennung und -weiterleitung auf molekularer Ebene über ein komplexes Proteinnetzwerk verläuft, ist noch nicht hinreichend bekannt. Sowohl die funktionelle Charakterisierung der beteiligten Proteine als auch strukturelle Ansätze können dazu beitragen, den Signaltransduktionsmechanismus weiter zu entschlüsseln.

Im ersten Teil der vorliegenden Arbeit wurden funktionelle Studien am Rezeptorprotein ETR1 aus *Arabidopsis thaliana* durchgeführt: In einem fluoreszenzbasierten Ansatz ließ sich über Änderungen in der Fluoreszenzintensität intrinsischer Tryptophanreste eine Interaktion zwischen dem Rezeptorprotein und dem für die Bindung von Ethylen notwendigen Kupfer-Kofaktor nachweisen. Phosphorylierungsstudien mit radioaktiv markiertem ATP zeigten außerdem, dass neben den bereits beschriebenen Aminosäuren (H353 und D659) in der Kinase- bzw. Empfängerdomäne von ETR1 weitere Reste phosphoryliert werden können. In diesem Zusammenhang wurden Vorversuche durchgeführt, um zukünftig  $^{31}\text{P}$ -NMR zur Identifizierung der entsprechenden Reste anzuwenden.

Der zweite Teil der Arbeit umfasste die Kristallisation des Ethylenrezeptors AtETR1. Erstmals konnten Kristalle des kompletten Membranproteins gezüchtet werden. Diese streuten bis zu einer Auflösung von 11 bis 12 Å. Allerdings konnten die Daten aufgrund der vorhandenen Mosaizität und anisotropen Verteilung der Reflexe nicht zur Strukturlösung herangezogen werden. Da eine Verbesserung dieser Eigenschaften auch durch vielfältige Variationen der Kristallisationsparameter und durch Modifikationen des Proteins nicht erzielt werden konnte, wurden zwei weitere orthologe Rezeptoren in die Studie aufgenommen: ETR1 aus dem Moos *Physcomitrella patens subsp. patens* und der Tomate *Lycopersicon esculentum*. Nach Etablierung von Expressions- und Reinigungsprotokollen zeigten beide Proteine in ersten Kristallisationsscreens bereits die Bildung von Sphärolithen, so dass diese Bedingungen als Ausgangspunkt für zukünftige Studien dienen können.





### 3 Introduction

#### 3.1 Plant hormones: Communication is all!

Because of their sessile lifestyle, plants need to adapt to a wide range of environmental stimuli like temperature, light or water. Corresponding physiological and developmental processes have to be coordinated throughout the plant—an aspect that equally affects giant organisms like the coast redwood (*Sequoia sempervirens*) or tiny species like the spotless watermeal (*Wolffia arrhiza*), see Figure 1.

Many of the physiological processes are regulated by the *classical* plant hormones auxin, cytokinin, abscisic acid, gibberellin and ethylene<sup>[1]</sup>. Nevertheless, the group of regulatory effective compounds is still expanding, and apart from small chemical substances also peptides have been discovered to have an impact on plant growth<sup>[2]</sup>.

The spectrum of action of the plant hormones is broad and ranges from induction of cell elongation and proliferation to pathogen induced defence mechanisms<sup>[3, 4]</sup>.

Based on genetic analyses, various proteins were identified for each plant hormone to be involved in perception or transduction of the specific signal. These studies also revealed distinct cross-talk between individual pathways and thereby illustrated the complex network necessary for maintaining biological processes<sup>[5]</sup>.

#### 3.2 The plant hormone ethylene

The biological activity of ethylene was first observed in the early 20<sup>th</sup> century as illuminating gas caused senescence and abscission of leafs from plants grown in green houses<sup>[6]</sup>. About 30 years later, it was possible to show that the plant itself can produce the hormone. Today, ethylene is one of the best studied plant effectors<sup>[7]</sup>.

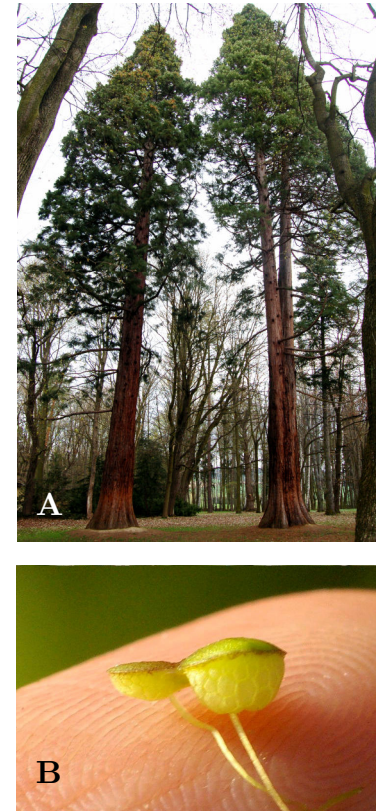


Figure 1: Images of (A) coast redwood, *Sequoia sempervirens* (cc, Martina Pauerová) and (B) spotless watermeal, *Wolffia arrhiza* (cc, Christian Fischer).

Due to its chemical nature—ethylene is the simplest olefin—it is soluble in the aqueous cytosol, but it can also easily pass through lipidic layers such as the cell membrane. As it is gaseous at ambient temperature, ethylene can also diffuse and trigger responses between different organs or even individual plants.

### 3.2.1 The role of ethylene in plant life cycle

Ethylene has a regulatory effect on various processes in the plant life cycle. A known and crucial aspect that is also of agricultural importance is its impact on fruit ripening of climacteric fruits such as apples, bananas or tomatoes. During ripening, the fruit pulp softens and flavouring occurs. Contemporaneously, photosynthetic pigments are degraded—a process that is also observed during senescence of leafs and petals. Finally, cellulases and polygalacturonases are activated at the nodes to induce abscission<sup>[7-10]</sup>.

Ethylene is also important in plant growth where it can regulate cell elongation and is responsible for the formation of the apical hook that protects the sensitive apical meristeme of a seedling when passing through the soil<sup>[11]</sup>. Also the formation of adventitious roots and root hairs has been described to be triggered by the plant hormone as well as sex determination and seed germination<sup>[12, 13]</sup>.

Furthermore, ethylene has been described to play a major role in stress responses. The trigger might either be of abiotic nature like flooding, drought, wounding or hypoxia or biotic such as a pathogen infestation<sup>[14]</sup>. In the latter case, synthesis of phytoalexins can be induced by the plant hormone<sup>[15, 16]</sup>.

### 3.2.2 Ethylene biosynthesis

In plants, the immediate precursor of ethylene is 1-aminocyclopropane-1-carboxylic acid (ACC), which is synthesised from *S*-adenosyl methionine (SAM) by the ACC-synthase. SAM itself is produced by the SAM-synthase from the amino acid methionine and ATP. ACC is degraded by the ACC-oxidase to release ethylene. This step is oxygen dependent and is completely abolished under anaerobic conditions.

ACC-synthase does not only catalyse the formation of SAM but also participates in regeneration of methionine by producing methylthioadenosine (MTA), which is converted back to methionine

during the *Yang* cycle. This mechanism ensures that ethylene synthesis is not reduced due to limitation of methionine<sup>[17]</sup>.

The rate by which ethylene is produced is mainly dependent on the concentration and activity of ACC-synthase. The enzyme is not constitutively expressed, but synthesis is induced through endogenous and exogenous stimuli<sup>[7]</sup>.

### 3.2.3 The ethylene signalling pathway in *Arabidopsis thaliana*

Dark grown seedlings exhibit a typical phenotype when exposed to ethylene. The so-called *triple response* is characterised by a reduced growth of the hypocotyl and the root due to inhibition of internode elongation. An increased apical hook and thickening of the hypocotyl are observed, too<sup>[18]</sup>.

These characteristics were used in genetic studies with *Arabidopsis thaliana* to identify proteins involved in ethylene signalling. Analysis of mutant plants that showed insensitivity towards ethylene or displayed the *triple response* in absence of the hormone, led to discovery of five receptor proteins and further components of the signalling pathway<sup>[19]</sup>.

These proteins were brought into a hierarchic dependence by epistasis analysis and allowed for postulation of two different signalling pathways, the first one involving a MAPKK kinase cascade and the second being similar to two-component signalling as known from bacteria<sup>[20, 21]</sup>.

#### 3.2.3.1 *Ethylene receptor proteins*

The five receptor proteins ETR1, ETR2, ERS1, ERS2 and EIN4 share a sequence similarity of up to 80 % and can be divided into two subfamilies (Figure 2) according to their structural composition<sup>[22, 23]</sup>.

Subfamily I comprises ETR1 and ERS1. Both proteins possess a highly conserved kinase domain including the phosphate acceptor histidine and an ATP-binding motif (N-, G1- and G2-box). The N-terminal part of the receptors is composed of three transmembrane helices and is required for ethylene binding. A GAF domain of unknown function is connecting the transmembrane domain and the kinase domain. Subfamily II members ETR2, ERS2 and EIN4 contain an additional N-terminal helix, but they do not show all characteristics typical for a histidine kinase. The essential histidine residue is only present in EIN4, and ATP-binding motifs are almost completely missing. Nevertheless, the three subfamily II receptors and ERS1 have been reported to exhibit autophosphorylation on serine/threonine residues<sup>[24]</sup>.

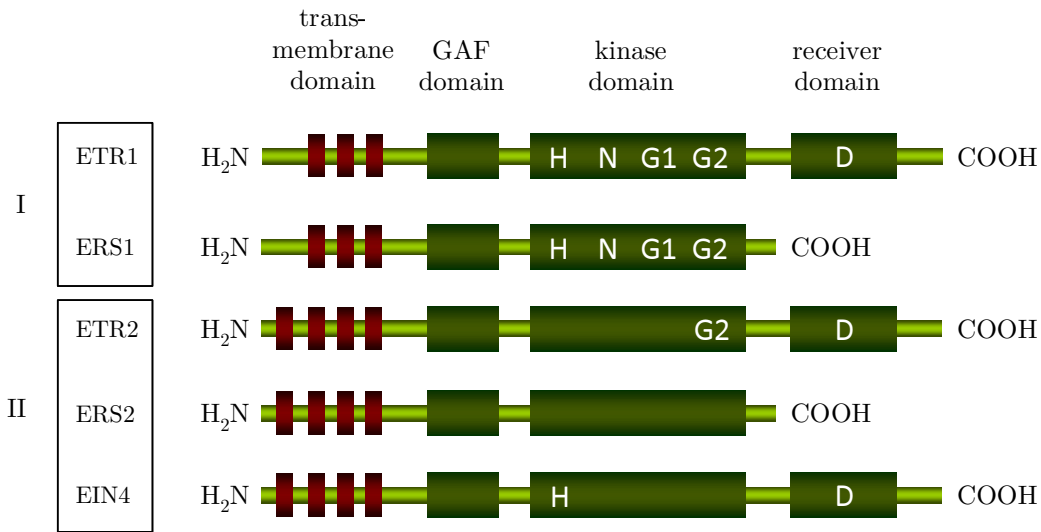


Figure 2: Modular composition of ethylene receptors from *Arabidopsis thaliana*. Members of subfamily I (ETR1 and ERS1) are characterised by three N-terminal helices and a conserved histidine kinase domain. Members of subfamily II (ETR2, ERS2 and EIN4) contain an additional transmembrane helix and have a less conserved kinase domain.

The C-terminal receiver domain, as known from bacterial two-component systems, is present only in receptors ETR1, ETR2 and EIN4.

For the five receptor proteins, a redundancy was observed regarding their functionality. A loss of one member of subfamily I can be compensated by the remaining receptors. However, when both, ETR1 and ERS1, are missing, plants will show the typical *triple response*. Deletion of all subfamily II members did not produce such phenotype indicating that ETR1 and ERS1 play a superior role in ethylene signalling in *Arabidopsis thaliana*<sup>[25]</sup>.

### 3.2.3.2 Ethylene perception by receptor protein ETR1

Ethylene receptor ETR1 from *Arabidopsis thaliana* is the best characterised component of the ethylene signalling network. The N-terminal domain of the protein comprises three helices by which the receptor can localise to the ER membrane<sup>[26]</sup>. In its functional state, the receptor forms a dimer: Cystein residues C4 and C6, that are situated outside the membrane, are involved in disulfide bonding. Both residues are necessary for dimerisation and are conserved in all five receptors<sup>[27]</sup>.

Apart from homodimers, the association of receptors from different subfamilies was observed. Extracts from *Arabidopsis thaliana* membranes contained all possible combinations of complexes of subfamily I and II members. Though, the preferential combination was made up from ETR1

and ERS1. It turned out that these complexes could be dissolved with SDS indicating that non-covalent binding might also occur among the receptors. One possible candidate for promoting the association is the GAF domain as identified by yeast two-hybrid analysis<sup>[28]</sup>.

Prior to binding of the plant hormone, the receptor dimer has to be loaded with copper(I). Complexion of the metal ion occurs also in the transmembrane domain: Residues C65 and H69 were identified to be crucial for ethylene binding. Upon dimerisation, a hydrophobic pocket is formed that stabilises the metal ion and allows for subsequent binding of the hormone<sup>[29]</sup>.

It is assumed that residues C65 and H69 are not the only residues responsible for ethylene binding. Alanine scanning mutagenesis revealed further residues in helices I and II that might play minor roles in binding of the hormone as their substitution decreased but did not abolish ethylene binding. The sequence motif for ethylene binding is not just conserved in land plants but also in green algae, fungi and cyanobacteria<sup>[30]</sup>.

The mechanism by which the signal is transferred throughout the receptor is not fully understood, but it is assumed that a conformational change is induced due to the presence of the olefin that could forward the signal<sup>[23]</sup>.

### 3.2.3.3 Signal processing within receptor protein *ETR1*

The C-terminal domain of *ETR1* holds two important elements for signalling: the kinase domain and a receiver domain. In the first domain, a conserved histidine residue (H353) is described to be autophosphorylated upon an internal trigger. The phosphoryl group is then transferred to an aspartate (D659) residue in the connecting receiver domain<sup>[31]</sup>. Autophosphorylation of all five receptor proteins was monitored *in vitro*<sup>[32, 33]</sup>, yet no information is available how exactly the signal is processed to downstream components of the signalling pathway. Though both residues are not conserved in all receptors, it was shown that they could all activate protein kinase *CTR1* suggesting that further residues including serines and threonines might be also a target for phosphorylation.

### 3.2.3.4 *MAPKK* kinase cascade

Ethylene receptor proteins *ETR1*, *ETR2*, *ERS1*, *ERS2* and *EIN4* act as negative regulators and are inactivated upon binding of the plant hormone<sup>[22]</sup>. However, for binding of the plant hormone, copper(I) is needed and is provided by the P-type ATPase copper transporter *RAN1* located at the Golgi apparatus<sup>[29, 34]</sup> (Figure 3).

Another component that has been reported to localise at the Golgi membranes as well as at the ER is the putative membrane protein RTE1<sup>[35, 36]</sup>. It is suggested that RTE1 acts on the ethylene binding domain and thereby might promote or stabilise the signalling “on” state of receptor ETR1. RTE1 could bind to an intermediate state of ETR1 in which ethylene is already bound but signalling is not yet turned off. For this change in state, most probably, a conformational

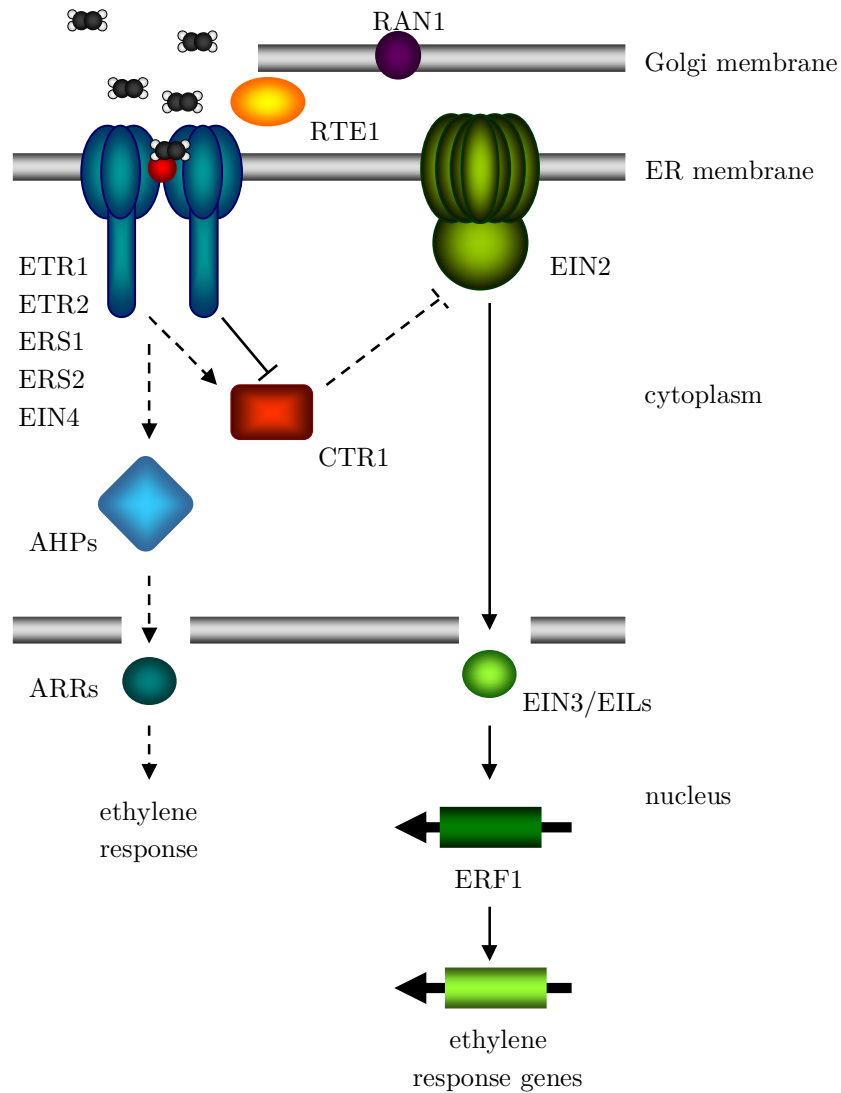


Figure 3: Schematic diagram of the ethylene signalling pathway in *Arabidopsis thaliana*. The five receptor proteins ETR1, ETR2, ERS1, ERS2 and EIN4 are located at the endoplasmic reticulum (ER). In absence of ethylene, the receptors activate CTR1 which inactivates EIN2, also located at the ER (dotted lines and arrows). For binding of ethylene, a copper ion (red dot) is necessary which is provided through RAN1, located at the Golgi membrane. Upon binding of ethylene, the receptors and CTR1 are inactivated. In consequence, EIN2 can trigger an ethylene response by activation of transcription factors EIN3/EILs which activate further components involved in transcription of ethylene response genes. Apart from regulation of CTR1, the receptor proteins can activate AHPs which regulate response regulators (ARRs). Interactions occurring upon binding of ethylene are indicated by solid arrows.

change is necessary that might be prevented by RTE1 arresting the receptor in its “on” state though ethylene is bound. However, the mechanism by which this transition is influenced still remains unclear<sup>[37]</sup>.

Downstream of ETR1 acts the negative regulator CTR1, a Raf-like serine/threonine kinase. Interaction of the N-terminus of CTR1 with receptor proteins ETR1 and ERS1 via their kinase domain was demonstrated *in vitro*, and co-localisation with ETR1 at the ER was observed by sucrose density gradient centrifugation<sup>[38, 39]</sup>. Due to the similarity of CTR1 with mitogen activated protein (MAP) kinases, it is supposed that CTR1 represents the starting point of a multi step phosphorylation dependent MAP kinase cascade<sup>[20]</sup>. In absence of ethylene, CTR1 represses further downstream components of the signalling pathway by inhibition of EIN2.

EIN2 is a positive regulator of ethylene signalling<sup>[40]</sup>. In the presence of the hormone, it activates the ethylene response through EIN3 and EIN3-like (EILs) transcription factors. These proteins accumulate in the nucleus where they can induce expression of further transcription factors such as ERF1. Finally, a transcriptional cascade is initiated that decides over the expression or repression of ethylene response genes<sup>[41]</sup>.

The initial starting point of this cascade, EIN2, has recently been demonstrated to localise at the ER membranes and physically interact with all ethylene receptor proteins<sup>[42, 43]</sup>. It was further postulated that in presence of ethylene, the non-phosphorylated receptors tightly bind to EIN2 preventing its ubiquitin targeting by proteins ETP1 and ETP2 for proteasome-dependent degradation<sup>[44]</sup>.

The N-terminus of EIN2 consists of 12 putative transmembrane helices and shows similarities to Nrap metal ion transporters<sup>[11]</sup>. Indeed, interaction with calcium was proven *in vitro*, though, its meaning remains unclear.

Signals arising from the ethylene receptor finally converge on transcription factors EIN3 and EILs<sup>[41]</sup>. It appears that almost all ethylene responses are mediated through these regulators with one exception: Inhibition of growth is divided into four phases. A first, rapid and a slowed second inhibition phase are separated by a lag phase before recovery occurs when ethylene is removed. In double mutant *ein3eil1*, the first inhibition phase was still present indicating that this response was not regulated on a transcriptional level<sup>[45, 46]</sup>.

EIN3 and EIN3-like transcription factors are under the control of two F-box proteins (EBF1 and EBF2). The latter ones belong to E3 ligases and target the transcription factors for 26S proteasome degradation in absence of the plant hormone<sup>[47, 48]</sup>.

### 3.2.3.5 Two-component signalling cascade

Two-component signalling systems are common in bacteria but are also found in fungi and plants<sup>[49, 50]</sup>. In the simplest case, the system consists of a histidine kinase composed of an input and transmitter domain and a second, individual module, the response regulator that holds a receiver and output domain (Figure 4A). Upon a specific signal, the kinase domain autophosphorylates on a conserved histidine residue, and the phosphoryl group is subsequently transferred to an aspartate residue in the receiver domain of the response regulator.

In the multi step phosphorelay, the histidine kinase is fused to an additional receiver element in which an aspartate residue is acceptor for the phosphoryl group, internally transferred from the histidine in the kinase domain (Figure 4B). The signal is further transferred by phosphorylation of an individual histidine containing transfer protein (HPt) that initiates phosphorylation of an aspartate in the response regulator. Similar to the single step system, this trigger might result in a conformational change of the second module (the output domain) and might activate or inhibit further elements of a signalling network.

While ethylene receptors ERS1 and ERS2 are similar to the histidine kinases from the single step system, ETR1, ETR2 and EIN4 show structural compositions like the hybrid kinases<sup>[51]</sup>.

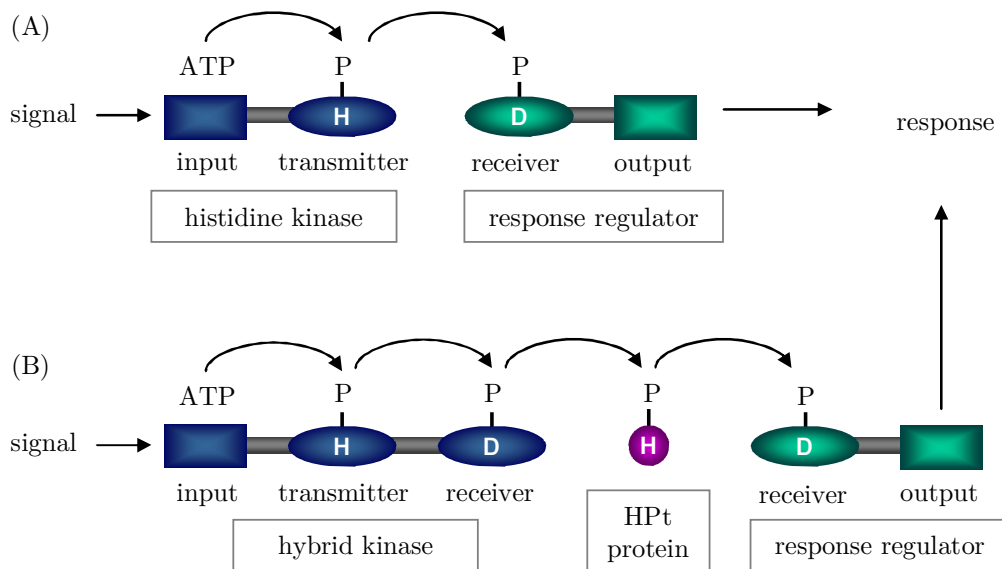


Figure 4: Schematic diagram of single (A) and multi step (B) two-component signalling systems. When a signal is perceived by the sensory input domain, the kinase autophosphorylates on a histidine in the transmitter domain. The phosphorylation is subsequently transferred to an aspartate residue in the receiver domain of the response regulator. This finally triggers the response. In multi step signalling (B), the kinase is fused to an additional receiver domain and the transfer of the phosphoryl group is mediated by a histidine containing transfer protein (HPt).



It is assumed that upon signal input—in case of ETR1 this corresponds to ethylene being absent—the kinase domain can autophosphorylate on a conserved histidine residue. The phosphoryl group might further be transferred to an aspartate residue within the receiver domain of the hybrid kinase and subsequently to an HPt protein.

In *Arabidopsis thaliana* five phosphotransfer proteins were identified (AHP1 to AHP5) that might play a role in ethylene signalling<sup>[52]</sup>. Indeed, physical interaction of ETR1 and AHP1 was confirmed *in vitro* by fluorescence spectroscopy<sup>[53]</sup>.

Apart from the AHPs, 23 response regulators (ARRs) were identified in *Arabidopsis thaliana*. These regulators can be divided into two classes: Type-B regulators act predominantly as transcription factors, type-A regulators can act in a negative feedback loop of the phosphorelay by inhibiting gene expression<sup>[54]</sup>. With the receptor proteins locating at the ER membrane and ARRs accumulating in the nucleus, AHPs might act as shuttle system between the two compartments<sup>[52]</sup>.

### 3.2.4 Cross-talk between ethylene and other plant hormones

Signalling pathways for individual plant hormones should not be considered separately. It is obvious that most physiological and developmental processes are not affected by a single hormone but require an interplay of several components to provoke a specific response. Thus, the hormones can act both in a signal amplifying manner and antagonistically<sup>[55]</sup>.

Auxin for example has been shown to increase the transcription level of ACC-synthase, thereby enhancing ethylene production. Furthermore, both hormones are responsible for the formation of the apical hook. In contrast, auxin can slow down ethylene induced senescence and ripening processes<sup>[56, 57]</sup>.

Cytokinin, another *classical* plant hormone, can also elevate ethylene biosynthesis<sup>[58]</sup>. The receptor itself shows similarities to the two-component systems and utilises AHPs as described for ethylene signalling. This indicates a direct cross-talk between the two pathways rather than effects on transcription levels of response genes for synthesis of the respective hormone<sup>[59]</sup>.

Auxin and cytokinin also act in an antagonistic mechanism to control meristemic activities<sup>[60]</sup>. Taken together these examples show the complexity of plant hormone signalling and illustrate its exciting scientific impact.

### 3.2.5 Objectives of this thesis

Molecular genetic studies identified several residues in receptor protein ETR1 from *Arabidopsis thaliana* that are important for signal perception and subsequent changes in the phosphorylation status. However, the mechanism by which the signal input is transferred by the receptor protein still remains unclear. Conformational changes due to binding of ethylene and phosphorylation events in the kinase and receiver domain are discussed but could not be proven on a molecular level.

To date, it is possible to show *in vitro* receptor activity by incorporation of  $^{32}\text{P}$  phosphate upon phosphorylation. Also effects of ethylene and of agonists and antagonists were monitored by this method. Though, the technique has a main drawback. Densitometric measurements are difficult to quantify reliably and require large amounts of protein which is always a bottleneck when working with membrane proteins.

To overcome this challenge, a highly sensitive method based on intrinsic tryptophan fluorescence should be established allowing quantitative analysis of ligand binding and phosphorylation of the receptor.

Further insights into the signal transfer mechanism might also be revealed by the three dimensional structure of the receptor protein. In a comprehensive crystallisation study, growth conditions for protein crystals suitable for X-ray diffraction analysis and subsequent structure determination should be acquired.

Apart from promoting the understanding of signal transduction in ethylene receptor ETR1, both approaches might also provide a receptor model that could be used to design and test substances with potential plant physiological effects.

## 4 Materials & Methods

### 4.1 Materials

#### 4.1.1 Equipment

Table 1: Devices and instruments (basic laboratory equipment is not listed)

<i>Instrument</i>	<i>Manufacturer</i>
<i>ÄKTAexplorer™ 100</i> chromatography system	<i>GE Healthcare Europe GmbH</i> (Munich)
<i>Avanti® J-26 XP</i> centrifuge	<i>Beckman Coulter GmbH</i> (Krefeld)
Bench-top centrifuges <i>5810R</i> and <i>5702</i>	<i>Eppendorf AG</i> (Hamburg)
<i>BioDocAnalyze®</i> gel documentation system	<i>Biometra GmbH</i> (Goettingen)
<i>Biomek® 3000</i> automation workstation	<i>Beckman Coulter GmbH</i> (Krefeld)
600 MHz <i>Bruker BioSpin</i> NMR spectrometer	<i>Bruker BioSpin GmbH</i> (Rheinstetten)
Circular dichroism spectropolarimeter <i>Jasco-715</i>	<i>Jasco GmbH</i> (Groß-Umstadt)
Crystallisation incubators	<i>Molecular Dimensions Limited</i> (Newmarket, UK)
<i>DU 800</i> UV/visible spectrophotometer	<i>Beckman Coulter GmbH</i> (Krefeld)
Electroblotting system <i>PerfectBlue</i>	<i>peqlab Biotechnologie GmbH</i> (Erlangen)
Fluorescence spectrometer <i>LS 55</i>	<i>PerkinElmer</i> (Rodgau)
Fluorescent image analyzer <i>FLA-3000</i>	<i>Fujifilm Europe GmbH</i> (Duesseldorf)
<i>French® Pressure Cell Press</i> with 40k standard cell	<i>Heinemann</i> (Schwaebisch Gmuend)
Gel systems <i>Mighty Small II</i>	<i>Hoefer Scientific Instruments</i> (San Francisco, USA)
Gel systems (large)	manufactured at University of <i>Duesseldorf</i>
Incubator shaker <i>INNOVA 44R</i>	<i>New Brunswick / Eppendorf AG</i> (Hamburg)
Luminescent image analyzer <i>LAS-1000</i>	<i>Fujifilm Europe GmbH</i> (Duesseldorf)
<i>Milli-Q® Gradient</i> water system	<i>Millipore GmbH</i> (Schwalbach)
<i>Moticam 2300</i> (digital microscope camera)	<i>Motic Deutschland GmbH</i> (Wetzlar)
<i>Optima™ L-80 XP</i> preparative ultracentrifuge	<i>Beckman Coulter GmbH</i> (Krefeld)
Rotors: <i>JA-10</i> , <i>JA-25.50</i> , <i>Type 70.1 Ti</i> , <i>SW 55 Ti</i> , <i>SW 28 Ti</i>	<i>Beckman Coulter GmbH</i> (Krefeld)
Steam steriliser <i>Varioklav S75</i>	<i>H+P Labortechnik</i> (Oberschleißheim)
Stereoscopic zoom microscope <i>SMZ-1000</i>	<i>Nikon GmbH</i> (Duesseldorf)
Thermocycler <i>TProfessional</i>	<i>Biometra GmbH</i> (Goettingen)
Ultrasonic homogeniser <i>Branson Sonifier® 250</i>	<i>Branson Ultrasonics</i> (Danbury, CT, USA)

#### 4.1.2 Chromatography supplies

Table 2: Columns, media and molecular weight markers used for affinity, ion exchange and size exclusion chromatography

<i>Chromatography supplies</i>	<i>Manufacturer</i>
<i>HiPrep 16/60 Sephacryl S-200 and S-300 HR</i> <i>PD-10 desalting columns</i> <i>HiTrap<sup>TM</sup> Q Sepharose<sup>TM</sup> XL column</i>	<i>GE Healthcare Europe GmbH (Munich)</i>
<i>Ni-NTA agarose</i> <i>HIS-Select<sup>®</sup> nickel affinity gel</i> <i>Protino<sup>®</sup> Ni-IDA resin</i>	<i>Qiagen GmbH (Hilden)</i> <i>Sigma-Aldrich Chemie GmbH (Munich)</i> <i>Macherey-Nagel GmbH &amp; Co. KG (Dueren)</i>
<i>Gel filtration molecular weight markers</i> <i>(29.000-700.000 Da)</i>	<i>Sigma-Aldrich Chemie GmbH (Munich)</i>

#### 4.1.3 Crystallographic supplies

Table 3: Crystallisation screens

<i>Screen</i>	<i>Manufacturer</i>
<i>Classics, MbClass and PEGs (Suites I and II, respectively)</i> <i>JCSG<sup>+</sup> Suite</i>	<i>Qiagen GmbH (Hilden)</i>
<i>JBScreen Membrane 1, 2 and 3</i>	<i>Jena Bioscience GmbH (Jena)</i>
<i>The Lipidic-Sponge Phase<sup>TM</sup> Screen, MemStart Screen</i>	<i>Molecular Dimensions Limited</i> <i>(Newmarket, UK)</i>

Table 4: Crystallisation plates

<i>Name</i>	<i>Manufacturer</i>
<i>72-well Terasaki plates</i> <i>96-well IMP@CT<sup>TM</sup> plates</i>	<i>Greiner Bio-One GmbH (Frickenhhausen)</i>
<i>EasyXtal 15-/24-well plates</i> <i>NeXtal Evolution <math>\mu</math>plate</i>	<i>Qiagen GmbH (Hilden)</i>

Table 5: Cryocrystallography equipment

<i>Name</i>	<i>Manufacturer</i>
<i>MicroLoops<sup>TM</sup> and MicroMeshes<sup>TM</sup></i>	<i>MiTeGen LLC (Ithaca, NY, USA)</i>
<i>Mounted CryoLoops<sup>TM</sup></i>	<i>Hampton Research Corp. (Aliso Viejo, CA, USA)</i>
<i>EMBL/ESRF sample changer kit with</i> <i>CryoCaps and CryoVials</i>	<i>Molecular Dimensions Limited (Newmarket, UK)</i>

#### 4.1.4 Kits

Table 6: For routinely performed applications like preparation of DNA or determination of protein concentration, the following kits were used according to the manufacturers' protocols.

<i>Name</i>	<i>Manufacturer</i>
<i>QIAprep Spin Miniprep Kit</i> <i>QIAquick Gel Extraction Kit</i>	<i>Qiagen GmbH (Hilden)</i>
<i>illustra GFX™ PCR DNA and Gel Band Purification Kit</i>	<i>GE Healthcare Europe GmbH (Munich)</i>
<i>Bio-Rad Protein Assay Kit</i>	<i>Bio-Rad Laboratories GmbH (Munich)</i>
<i>BCA Protein Assay Kit</i>	<i>Pierce / Thermo Fisher Scientific (Bonn)</i>

#### 4.1.5 Filters and Membranes

- *Amicon Ultra®* centrifugal filter units (*Millipore GmbH, Schwalbach*) with a molecular weight cut-off of 10 kDa, 30 kDa and 50 kDa, respectively, were used to concentrate dilute protein solutions.
- Aqueous solutions were sterile filtered through 0.2 µm cellulose acetate membranes (*Schleicher & Schuell GmbH, Dassel*).
- For western blotting two types of transfer membranes were used: *Protran BA 83* cellulose nitrate membrane, 0.2 µm (*Whatman International Ltd., Maidstone, UK*) and *Sequi-Blot* PVDF membrane, 0.2 µm (*Bio-Rad Laboratories GmbH, Munich*).

#### 4.1.6 Chemicals and Buffers

All buffers were prepared with deionised water that was sterile filtered through a 0.22 µm polyethersulfone membrane by a *Milli-Q® Gradient* water system.

If not stated otherwise, all chemicals were obtained in analytical grade from the following companies: *Anatrace Inc.* (Maumee, OH, USA); *Acros Organics* (Geel, Belgium); *AppliChem GmbH* (Darmstadt); *Becton Dickinson GmbH* (Heidelberg); *Carl Roth GmbH & Co. KG* (Karlsruhe); *Diagonal GmbH & Co KG* (Muenster); *Fisher Scientific GmbH* (Schwerte); *Fluka AG* (Buchs, Switzerland); *Glycon Biochemicals GmbH* (Luckenwalde); *Merck KGaA* (Darmstadt); *Millipore GmbH* (Schwalbach); *peqlab Biotechnologie GmbH* (Erlangen); *Riedel-de-Haën GmbH* (Seelze); *Roche GmbH* (Mannheim); *Serva Electrophoresis GmbH* (Heidelberg); *Sigma-Aldrich Chemie GmbH* (Munich); *VWR International GmbH* (Darmstadt)

#### 4.1.7 Radiochemicals

Isotopic labelled nucleotide  $\gamma$ - $^{32}\text{P}$ -ATP was purchased from *Hartmann Analytic GmbH* (*Braunschweig*) with a specific activity of 110 TBq/mmol and 3000 Ci/mmol, respectively.

#### 4.1.8 Enzymes

Restriction enzymes and polymerases for molecular biological applications as well as proteases for biochemical usage were obtained from *Finnzymes Oy* (*Espoo, FIN*), *Invitrogen GmbH* (*Darmstadt*), *New England Biolabs GmbH* (*NEB, Frankfurt/Main*), *Novagen®/Merck KGaA* (*Darmstadt*), *peqlab Biotechnologie GmbH* (*Erlangen*) and *Sigma-Aldrich Chemie GmbH* (*Munich*). All enzymes were used in their appropriate buffer as specified by the manufacturer.

Table 7: Features of enzymes used for molecular and biochemical applications. Recognition sequences of restriction enzymes and proteases are in superscript.

<i>DNA modifying enzymes</i>	<i>Application / Features</i>	<i>Manufacturer</i>
<i>peqGOLD Pwo</i> DNA polymerase	Amplification of DNA (proofreading)	<i>peqlab</i>
<i>Phusion®</i> high-fidelity DNA polymerase	Amplification of DNA (proofreading)	<i>Finnzymes</i>
<i>Taq</i> DNA polymerase	Amplification of DNA (no proofreading)	<i>NEB</i>
T4 DNA polymerase	3' → 5' exonuclease activity to create 5' overhangs for SLIC	<i>NEB</i>
T4 DNA ligase	Ligation of DNA fragments	<i>NEB</i>
BamHI <sup>G GATCC</sup>	Restriction of DNA	<i>NEB</i>
NcoI <sup>C CATGG</sup>		
NdeI <sup>CA TATG</sup>		
Antarctic phosphatase	Removal of 5' phosphates from DNA	<i>NEB</i>
<i>Protein modifying enzymes</i>	<i>Application / Features</i>	<i>Manufacturer</i>
<i>AcTEV®</i> <sup>ENLYFQ G</sup>	Removal of His <sub>10</sub> -tag present at proteins expressed in vector pTEV-16b	<i>Invitrogen</i>
Factor Xa <sup>IEGR X</sup>	Removal of His <sub>10</sub> -tag present at proteins expressed in vector pET-16b	<i>Novagen®</i>
Thrombin <sup>LVPR GS</sup>	Proteolysis of AtETR1	<i>Sigma-Aldrich</i>

#### 4.1.9 Antibodies

Table 8: Features of primary and secondary antibodies

<i>Primary Antibodies</i>	<i>Application / Features</i>	<i>Manufacturer</i>
Tetra His antibody, mouse IgG	Detection of HHHH-epitope in proteins (e.g. affinity His-tags)	<i>Qiagen GmbH (Hilden)</i>
Hexa His antibody, conjugated with horseradish peroxidase	Detection of HHHHHH-epitope in proteins (e.g. affinity His-tags)	<i>Miltenyi Biotec GmbH (Bergisch-Gladbach)</i>
Hsp70/DnaK antibody, mouse IgG	Detection of heat shock protein DnaK	<i>Calbiochem / Merck KGaA (Darmstadt)</i>
ETR1 (HRR) antibody, rabbit IgG	Identification of AtETR1 (epitope: aa 401-738)	kindly provided by <i>A.B. Bleecker</i> (Univ. of Wisconsin-Madison, USA) <sup>[27]</sup>
<i>Secondary Antibodies</i>	<i>Manufacturer</i>	
ECL mouse IgG, peroxidase-linked antibody	<i>GE Healthcare Europe GmbH (Munich)</i>	
Rabbit IgG, peroxidase-linked antibody		

#### 4.1.10 Oligonucleotides

Oligonucleotides were synthesised by *MWG-Biotech AG (Ebersberg)* or by *Sigma-Aldrich Chemie GmbH (Munich)*. The lyophilised and desalted oligonucleotides were dissolved in sterile water at a concentration of 100 µM and stored at -80 °C.

Table 9: Oligonucleotides used as primers to amplify or mutate gene sequences

<i>Name</i>	<i>Sequence (5' to 3')</i>	<i>Application</i>
<i>T7-Promotor</i>	TAATACGACTCACTATAGGG	Sequencing of T7-plasmids
<i>T7-Terminator</i>	GCTAGTTATTGCTCAGCGG	
<i>TEV16-for</i>	ATTTTGTTTAACTTTAAGAAGGAGATATAC CATGGGCCATCATCATCATCATCATCA TCATCACAGCAGCGCCATG	Replacing factor Xa site by <u>TEV site</u> in vector pET-16b
<i>TEV16-rev</i>	TTCCTTTCGGGCTTTGTTAGCAGCCGGATC CTCGAGCATATGTCCCTGAAAATACAGGTT <u>TTCATGGCCGCTGCTGTGAT</u>	
<i>AtETR1-for</i>	GTAATTCATATGGAAGTCTGCAATTG	Amplifying AtETR1
<i>AtETR1-rev</i>	TCCCGTAACTTCCTAGGCC	

<i>Name</i>	<i>Sequence (5' to 3')</i>	<i>Application</i>
<i>AtETR1-TEV16-for</i>	CATGAAAACCTGTATTTTCAGGGACATATG GAAGTCTGCAATTGTATTGA	SLIC-primer for <u>AtETR1</u> with/without membrane domain in pETEV-16b
<i>AtETR1-MD-TEV16-for</i>	CATGAAAACCTGTATTTTCAGGGACATATG ACTACACTTGTGAGCTTGG	
<i>AtETR1-TEV16-rev</i>	TTTGTTAGCAGCCGGATCCTCGAGCATATG TTACATGCCCTCGTACAGTA	
<i>AtETR1-Seq1-for</i>	TTCTTGAAAAATAAAGCT	Sequencing of AtETR1
<i>AtETR1-Seq2-for</i>	CTTTGATGGTTTTGATGCTT	
<i>AtETR1-Seq3-for</i>	CAATCTGATAAAGCCTATAG	
<i>AtETR1-Seq4-for</i>	CTTGGGATCTCAGAACGTTT	
<i>AtETR1-L55W-rev</i>	ACCAAACCTGAACCCATACAAATCTATA	<u>Amino acid substitutions</u> in transmembrane domain of tryptophan-less AtETR1 as indicated
<i>AtETR1-F58W-rev</i>	GATAAAAGCACCCCACTGAACAAGTAC	
<i>AtETR1-L64W-rev</i>	AGTTGCTCCACACCAAAACGATAAAAAGC	
<i>AtETR1-L70W-rev</i>	AAATAAGTTAATCCAATGAGTTGCTCC	
<i>AtETR1-L73W-rev</i>	AGTGAAAGTAAACCAAGTTAATAAGATG	
<i>AtETR1-F26W-rev</i>	AATCGCAATGAACCAATCGGAGATGTA	
<i>AtETR1-F27W-rev</i>	CGCAATCGCAATCCAGAAATCGGAGAT	
<i>AtETR1-F33W-rev</i>	AAGAGGAATCGACCAATACGCAATCGC	
<i>AtETR1-C65A-H69A-rev</i>	AAATAAGTTAATAAGCGCAGTTGCTCCCGC AAGAACGATAAAAAGC	
<i>AtETR1-V350W-rev</i>	TTCATGGTTCATCCACGCTAGGAAATC	<u>Amino acid substitutions</u> in kinase domain of tryptophan-less AtETR1 as indicated
<i>AtETR1-N352W-for</i>	CTAGCGGTTATGTGGCATGAAATGCGA	
<i>AtETR1-N352W-rev</i>	TCGCATTTTCATGCCACATAACCGCTAG	
<i>AtETR1-R356W-for</i>	AACCATGAAATGTGGACACCGATGCAT	
<i>AtETR1-R356W-rev</i>	ATGCATCGGTGTCCACATTTTCATGGTT	
<i>N352W-H353A-for</i>	TTCCTAGCGGTTATGTGGGCGGAAATGCG AACACCG	
<i>N352W-H353A-rev</i>	CGGTGTTTCGCATTTCCGCCCCACATAACCGC TAGGAA	
<i>N352W-H353E-for</i>	TTCCTAGCGGTTATGTGGGAAGAAATGCG AACACCG	
<i>N352W-H353E-rev</i>	CGGTGTTTCGCATTTCTTCCACATAACCGC TAGGAA	
<i>LeETR1-TEV16-for</i>	CATGAAAACCTGTATTTTCAGGGACATATG GGCAGTCTGCTGCGTATGAA	SLIC-primer for <u>LeETR1</u> with/without membrane domain in pETEV-16b
<i>LeETR1-MD-TEV16-for</i>	CATGAAAACCTGTATTTTCAGGGACATATG GATCGCCACACGATCCTGAA	
<i>LeETR1-TEV16-rev</i>	TTTGTTAGCAGCCGGATCCTCGAGCATATG TTAACTTCCAGAACCACGC	



<i>Name</i>	<i>Sequence (5' to 3')</i>	<i>Application</i>
<i>LeETR1-Seq1-for</i>	GCCGGGCGAAGTGGTTGCGG	Sequencing of LeETR1
<i>LeETR1-Seq2-for</i>	ACCGATCTGACGCCGGAACA	
<i>PpETR1-TEV16-for</i>	CATGAAAACCTGTATTTTCAGGGACATATG GATTCTTGCAATTGTGTGGA	SLIC-primer for <u>PpETR1</u> with/without membrane domain in pETEV-16b
<i>PpETR1-MD-TEV16-for</i>	CATGAAAACCTGTATTTTCAGGGACATATG GATCGTCAGACGATCCTGAA	
<i>PpETR1-TEV16-rev</i>	TTTGTTAGCAGCCGGATCCTCGAGCATATG TTAGGTTTTGCGACGGGTTT	
<i>PpETR1-Seq1-for</i>	GCACCGAACTCTCCGGTGTG	Sequencing of PpETR1
<i>PpETR1-Seq2-for</i>	GAACAGCGTAGCATGGTGGA	

#### 4.1.11 Custom gene synthesis

Gene sequences of ethylene receptor ETR1 from *Physcomitrella patens* and *Lycopersicon esculentum* were ordered codon optimised for *E. coli* from *GenScript USA Inc.* (Piscataway, NJ, USA). The sequences were supplied in vector pUC57.

#### 4.1.12 Vectors

- *pET-15b* and *pET-16b* (Novagen®/Merck KGaA, Darmstadt)

Vector pET-15b (5708 bp) carries an N-terminal hexa His-tag sequence followed by a thrombin recognition site and the MCS including sites for XhoI, BamHI and NdeI. Vector pET-16b (5711 bp) has a sequence for an N-terminal deca His-tag that can be cleaved by factor Xa. The MCS includes the same three recognition sequences as for pET-15b. Expression of genes cloned into these vectors is under the control of the T7-promoter. Additionally both vectors carry an ampicillin resistance gene (ampR) for selection.

- *pRARE* (Novagen®/Merck KGaA, Darmstadt)

The pRARE plasmid carries sequences for tRNAs that are rare in *E. coli* (proL, leuW, argW, glyT, argU and ileX). Thereby, a deficiency of these amino acids can be compensated when expressing heterologous genes. The plasmid mediates a chloramphenicol resistance.

On basis of expression vectors pET-15b and pET-16b several constructs harbouring either the complete cDNA sequences of AtETR1, PpETR1 and LeETR1 or fragments lacking the transmembrane domain as well as tryptophan-less mutants and those carrying single tryptophan

mutations were cloned during and prior to this thesis. Typically, tryptophan was substituted by leucine or phenylalanine because all three amino acids have hydrophobic side chains and are of similar size. If the primary sequence did not allow for such substitution, residues with a side chain size comparable to tryptophan were selected.

Table 10: List of expression vectors that were previously constructed by *J. Voet van Vormizeele* (University of *Duesseldorf*)<sup>[61]</sup>. Vector maps of all constructs can be found in the appendix (9.2).

<i>Vector designation</i>	<i>Protein designation</i>	<i>Mutations</i>
pET-16b::AtETR1 <sub>1-738</sub> WT	AtETR1	none
pET-15b::AtETR1 <sub>1-738</sub> W <sub>free</sub>	AtETR1[W <sub>free</sub> ]	W11L, W53F, W74F, W182L, W265L, W288L, W563L
pET-15b::AtETR1 <sub>1-738</sub> W53	AtETR1[W53]	W11L, W74F, W182L, W265L, W288L, W563L
pET-15b::AtETR1 <sub>1-738</sub> H353A	AtETR1[H353A]	as indicated
pET-15b::AtETR1 <sub>1-738</sub> D659A	AtETR1[D659A]	as indicated
pET-16b::AtETR1 <sub>165-738</sub> WT	AtETR1 <sub>165-738</sub>	none
pET-16b::AtETR1 <sub>165-738</sub> H353A	AtETR1 <sub>165-738</sub> [H353A]	as indicated

Table 11: List of expression vectors constructed in this study. Vector maps of all plasmids listed can be found in the appendix (9.2). For construction of vector pTEV-16b, please refer to section 4.3.6.

<i>Vector designation</i>	<i>Protein designation</i>	<i>Mutations</i>
pET-15b::AtETR1 <sub>1-738</sub> W <sub>free</sub> F26W	AtETR1[F26W]	W11L, W53F, W74F, W182L, W265L, W288L, W563L and as indicated
pET-15b::AtETR1 <sub>1-738</sub> W <sub>free</sub> F27W	AtETR1[F27W]	
pET-15b::AtETR1 <sub>1-738</sub> W <sub>free</sub> F33W	AtETR1[F33W]	
pET-15b::AtETR1 <sub>1-738</sub> W <sub>free</sub> L55W	AtETR1[L55W]	
pET-15b::AtETR1 <sub>1-738</sub> W <sub>free</sub> F58W	AtETR1[F58W]	
pET-15b::AtETR1 <sub>1-738</sub> W <sub>free</sub> L64W	AtETR1[L64W]	
pET-15b::AtETR1 <sub>1-738</sub> W <sub>free</sub> L70W	AtETR1[L70W]	
pTEV-16b::AtETR1 <sub>1-738</sub> W <sub>free</sub> L70W	AtETR1[L70W]-TEV*	
pET-15b::AtETR1 <sub>1-738</sub> W <sub>free</sub> L73W	AtETR1[L73W]	
pET-15b::AtETR1 <sub>1-738</sub> W <sub>free</sub> V350W	AtETR1[V350W]	
pET-15b::AtETR1 <sub>1-738</sub> W <sub>free</sub> N352W	AtETR1[N352W]	
pET-15b::AtETR1 <sub>1-738</sub> W <sub>free</sub> R356W	AtETR1[R356W]	
pTEV-16b::AtETR1 <sub>1-738</sub> W <sub>free</sub> N352W/H353A	AtETR1[N352W/H353A]	
pTEV-16b::AtETR1 <sub>1-738</sub> W <sub>free</sub> N352W/H353E	AtETR1[N352W/H353E]	

\* In AtETR1[L70W] the His-tag is linked to the receptor by a thrombin protease recognition sequence. The receptor itself holds an intrinsic thrombin site, so construct AtETR1[L70W]-TEV was cloned to replace the thrombin site by a TEV protease recognition sequence in order to remove the tag.

<i>Vector designation</i>	<i>Protein designation</i>	<i>Mutations</i>
pTEV-16b::AtETR1 <sub>1-738</sub> W53/C65A/H69A	AtETR1[W53/C65A/H69A]	W11L, W74F, W182L, W265L, W288L, W563L and as indicated
pTEV-16b::AtETR1 <sub>165-738</sub> W <sub>free</sub> V350W	AtETR1 <sub>165-738</sub> [V350W]	W182L, W265L, W288L, W563L and as indicated
pTEV-16b::AtETR1 <sub>165-738</sub> W <sub>free</sub> N352W	AtETR1 <sub>165-738</sub> [N352W]	
pTEV-16b::AtETR1 <sub>165-738</sub> W <sub>free</sub> R356W	AtETR1 <sub>165-738</sub> [R356W]	
pET-16b::AtETR1 <sub>165-738</sub> SER	AtETR1 <sub>165-738</sub> SER	18 amino acid substitutions (see 6.1.2.2 for details)
pTEV-16b::PpETR1 <sub>1-767</sub>	PpETR1 <sub>1-767</sub>	none
pTEV-16b::PpETR1 <sub>158-767</sub>	PpETR1 <sub>158-767</sub>	none
pTEV-16b::LeETR1 <sub>1-754</sub>	LeETR1 <sub>1-754</sub>	none
pTEV-16b::LeETR1 <sub>173-754</sub>	LeETR1 <sub>173-754</sub>	none

#### 4.1.13 Bacterial strains: *Escherichia coli*

##### 4.1.13.1 Host strain for cloning

- XL1-blue (*Stratagene Inc.*, La Jolla, CA, USA)  
Genotype: recA1 endA1 gyrA96 thi-1 hsdR17 supE44 relA1 lac [F' proAB lacIqZΔM15 Tn10 (Tetr)]

##### 4.1.13.2 Strains for protein expression

- BL21 (DE3) (*Stratagene Inc.*, La Jolla, CA, USA)  
Genotype: B F<sup>-</sup> dcm ompT hsdS(r<sub>B</sub><sup>-</sup> m<sub>B</sub><sup>-</sup>) gal λ(DE3)
- BL21-Gold (DE3) (*Stratagene Inc.*, La Jolla, CA, USA)  
Genotype: B F<sup>-</sup> ompT hsdS(r<sub>B</sub><sup>-</sup> m<sub>B</sub><sup>-</sup>) dcm<sup>+</sup> Tet<sup>r</sup> gal λ(DE3) endA Hte
- C41 (DE3) and C43 (DE3)  
Genotype: F<sup>-</sup> ompT gal hsdSB (r<sub>B</sub><sup>-</sup> m<sub>B</sub><sup>-</sup>) dcm lon λ(DE3) and two uncharacterised mutations<sup>[62]</sup>

Cells of all three strains can express T7-RNA polymerase upon induction with IPTG. This makes them suitable expression systems in combination with pET-vectors. While BL21 (DE3) and BL21-Gold (DE3) are mainly used for expression of soluble proteins, strains C41 (DE3) and C43 (DE3) can facilitate the expression of toxic membrane proteins. Both strains are derivatives of BL21 (DE3) that carry two uncharacterised mutations that are assumed to prevent cell death upon expression of recombinant proteins<sup>[62]</sup>.

## 4.2 Microbiological methods

### 4.2.1 Media for cultivation of *E. coli* cells

Liquid cell cultures of *E. coli* were grown in 2YT medium (0.5 % NaCl, 1 % yeast extract, 1.6 % tryptone, all w/v). Solid media were additionally supplied with 1.5 % (w/v) agar<sup>[63]</sup>.

All media were sterilised by autoclaving for 20 min at 120 °C. If necessary, appropriate antibiotics were added prior to use: For cells harbouring pET-15b and pET-16b based vectors, ampicillin was added at a concentration of 100 µg/ml. Cells containing the plasmid pRARE were selected by 34 µg/ml chloramphenicol.

### 4.2.2 Preparation and transformation of chemically competent *E. coli* cells

This protocol is a modification of *Hanahan et al.*<sup>[64, 65]</sup>:

A liquid culture of 100 ml 2YT medium was inoculated with 1 ml of an o/n culture. The cells were grown to OD<sub>600</sub> of 0.5 at 37 °C and 180 rpm and then centrifuged (2,000 x g, 4 °C, 5 min). The resulting cell pellet was resuspended in 20 ml pre-cooled TFB-1 buffer and incubated on ice for 5 min. After centrifugation (2,000 x g, 4 °C, 5 min) the pellet was resuspended in 4 ml chilled TFB-2 buffer and incubated on ice for another 30 min. Aliquots of 50 µl were transferred to sterile 1.5 ml reaction tubes, flash-frozen in liquid nitrogen and stored at -80 °C.

Chemically competent cells (50 µl) were thawed on ice, mixed with 100-300 ng DNA and incubated on ice for 10 min. The cells were heat shocked for 30 sec at 42 °C and then placed on ice for further 2 min. After addition of 400 µl 2YT medium, the cells were shaken at 37 °C for 30-60 min. The cell suspension (50-150 µl) was plated onto 2YT-agar plates supplied with appropriate antibiotics and incubated at 37 °C o/n.

**TFB-1**, pH 5.8: 30 mM potassium acetate, 10 mM CaCl<sub>2</sub>, 100 mM RbCl, 50 mM MnCl<sub>2</sub>, 15 % (w/v) glycerol

**TFB-2**, pH 6.5: 10 mM MOPS, 75 mM CaCl<sub>2</sub>, 10 mM RbCl, 15 % (w/v) glycerol

### 4.3 Molecular biological methods

#### 4.3.1 Amplification and isolation of plasmid DNA from *E. coli*

Depending on the downstream application, plasmid preparations were either performed with *Qiagen's QIAprep Spin Miniprep Kit* according to the manufacturer's manual or by precipitation with ethanol. The use of the commercial kit resulted in high purity of the samples as it was needed for sequencing whereas the preparation without kit gave higher yields of DNA with slight impurities by proteins.

To amplify plasmid DNA, XL1-blue cells were transformed with the appropriate vector (see 4.2.2) and 5 ml o/n cultures were set up with a single colony. For preparations without kit 4 ml of an o/n culture were centrifuged for 2 min at 14,000 x g, and the pellet was resuspended in 100 µl buffer DP1. Buffer DP2 was added (200 µl) and mixed by inversion. Then, 150 µl of 3 M potassium acetate buffer, pH 5.5 were added and mixed as before. The turbid solution was centrifuged for 10 min at 14,000 x g, and the supernatant was transferred to 900 µl of 100 % (v/v) ethanol. Centrifugation was repeated, and the resulting pellet was washed with 70 % (v/v) ethanol. Centrifugation was repeated once again and the pellet was dried and resuspended in 30-50 µl buffer 10 mM Tris/HCl, pH 8.5.

**DP1**, pH 8.0: 50 mM Tris/HCl, 10 mM EDTA, 100 µg/ml RNase A

**DP2**: 200 mM NaOH, 1 % (w/v) SDS

#### 4.3.2 Determination of DNA concentration

Concentration of DNA in solution was determined spectrophotometrically based on the absorbance at 260 nm. For dsDNA an OD<sub>260</sub> of 1 corresponds to a concentration of 50 µg/ml<sup>[63]</sup>.

#### 4.3.3 Polymerase chain reaction to amplify DNA

The proofreading polymerases *Pwo* from *Pyrococcus woesei* and the modified *Phusion*<sup>®</sup> were used for amplification of DNA fragments for cloning strategies because of their low error rate ( $2 \times 10^{-6}$  for *Pwo* and  $4.4 \times 10^{-7}$  for *Phusion*, respectively). For colony-PCRs, the non-proofreading *Taq* polymerase from *Thermus aquaticus* was used. Standard PCR reactions contained the components listed in Table 12. Annealing temperatures and elongation times were adjusted to primer and template composition and the size of the amplicate (Table 13).

Table 12: Composition of PCR reactions

<i>Component</i>	<i>Cloning PCR (Pwo)</i>	<i>Cloning PCR (Phusion)</i>	<i>Colony PCR (Taq)</i>
Template DNA	100-300 ng	50-100 ng	one colony
5' Primer (10 $\mu$ M)	2 $\mu$ l	2.5 $\mu$ l	1 $\mu$ l
3' Primer (10 $\mu$ M)	2 $\mu$ l	2.5 $\mu$ l	1 $\mu$ l
dNTPs (10 mM)	0.5 $\mu$ l	0.5-1 $\mu$ l	0.25 $\mu$ l
<i>Pwo</i> polymerase	0.5 U		
10x 'complete' buffer	5 $\mu$ l		
<i>Phusion</i> <sup>®</sup> polymerase		1 U	
5x <i>HF</i> buffer		10 $\mu$ l	
<i>Taq</i> polymerase			1.25 U
10x <i>ThermoPol</i> buffer			2.5 $\mu$ l
Adjust with sterile water to a final volume of:	50 $\mu$ l	50 $\mu$ l	25 $\mu$ l

Table 13: Thermal cycling profile for cloning and colony PCRs

<i>Component</i>	<i>Cloning PCR (Pwo)</i>	<i>Cloning PCR (Phusion)</i>	<i>Colony PCR (Taq)</i>
Initial denaturation	5 min / 95 °C	30 sec / 98 °C	5 min / 95 °C
Denaturation	30-60 sec / 95 °C	10 sec / 98 °C	30-60 sec / 95 °C
Annealing	30-60 sec / primer specific temperature	10-30 sec / primer specific temperature	30-60 sec / primer specific temperature
Elongation	2 min per kb / 72 °C	15-30 sec per kb / 72 °C	1 min per kb / 72 °C
Final elongation	10 min / 72 °C	10 min / 72 °C	10 min / 72 °C

#### 4.3.4 Agarose gel electrophoresis

DNA samples from PCR reactions as well as restriction assays were analysed by agarose gel electrophoresis. Agarose gels (1 %, w/v) prepared with 1x TBE buffer and 0.5  $\mu$ g/ml ethidium bromide were used to separate DNA fragments from 100 bp to 10 kb. Depending on the expected size of the fragments, two types of DNA size markers were applied: *100 bp DNA Ladder* and *1 kb DNA Ladder* (NEB GmbH, Frankfurt/Main), respectively. All samples were mixed with 10x DNA loading dye prior to loading. Electrophoresis was carried out at a constant voltage of 150 V. Afterwards DNA bands were visualised by UV transillumination at 254 nm and documented with the *BioDocAnalyze*<sup>®</sup> gel documentation system.

**10x TBE**, pH 8.2-8.4: 10.8 % (w/v) Tris/HCl, 5.5 % (w/v) boric acid, 0.93 % (w/v) EDTA

**10x DNA loading dye**: 50 % (v/v) glycerol, 0.1 % (w/v) bromophenol blue

### 4.3.5 Cloning, Mutagenesis and Sequencing

#### 4.3.5.1 Standard cloning: restriction and ligation of DNA

Vectors pET-15b and pET-16b were linearised with restriction endonucleases NdeI and BamHI and remaining 5' phosphate groups were removed by antarctic phosphatase to prevent self-ligation. The gene of interest—the insert—was amplified (see 4.3.3) using primers that introduced an N-terminal NdeI recognition site and a C-terminal BamHI site to allow directed integration into the vector of choice<sup>[63]</sup>. After agarose gel electrophoresis (see 4.3.1) the amplificate was digested with both restriction enzymes.

In a ligation reaction the vector was mixed with a five-fold molar excess of insert and incubated together with T4-DNA ligase. The reaction mix was then transformed into XL1-blue cells (see 4.2.2) and colonies were tested for successful integration of the insert by colony PCR (see 4.3.3). DNA from positive clones was amplified and isolated according to section 4.3.1 and sequenced at either *StarSEQ® GmbH (Mainz)* or *GENterprise GENOMICS GmbH (Mainz)*.

This standard cloning method was used to create single tryptophan substitution mutants of tryptophan-free AtETR1. For insertion of tryptophans in helices I and II of the receptor (F26W, F27W, F33W, L55W, F58W, L64W, L70W and L73W) 3' mutagenesis primers were applied together with 5' primer *AtETR1-for* (Table 9, page 25) to amplify small fragments of about 100-250 bp. These fragments were used as 5' primers in a second PCR together with 3' primer *AtETR1-rev* to amplify the whole gene.

For insertion of tryptophans within the kinase domain of tryptophan-free AtETR1 (V350W, N352W and R356W) overlap extension PCRs were performed<sup>[66]</sup>. Two complementary mutagenesis primers were designed per amino acid substitution, each of which was used in an independent PCR reaction together with *AtETR1-for* and *AtETR1-rev* primers, respectively. Corresponding fragments (25 ng each) were combined in a third PCR reaction as template DNA together with the primers *AtETR1-for* and *AtETR1-rev* to amplify the complete gene sequence (Figure 5). Subsequently, cloning of all mutated sequences was performed as described before.

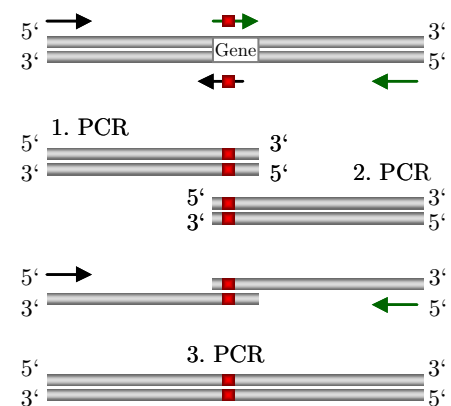


Figure 5: Schematic representation of the three steps of overlap extension PCR. The mutation site is indicated as red box, arrows represent primers.

**Restriction reaction** (30-40  $\mu$ l): Vector and insert DNA (1-6  $\mu$ g) was digested for 2-3 h at 37 °C with 40 U NdeI in NEBuffer 3 supplied with 100  $\mu$ g/ml BSA. After inactivation of NdeI by heat shock (10 min at 65 °C), 40 U BamHI were added and the mix was incubated at 37 °C for further 2-3 h. After a second heat shock, 5 U of antarctic phosphatase were added to samples containing vector DNA. Incubation continued for 1 h up to o/n at 37 °C and was terminated by a third heat shock as before.

**Ligation reaction** (10-15  $\mu$ l): Vector DNA (25-50 ng) was mixed with a five-fold molar excess of insert DNA and supplied with 400 U T4-DNA ligase in the appropriate reaction buffer. Samples were incubated at 16-20 °C for 10 min up to o/n.

#### 4.3.6 SLIC: Sequence and ligation independent cloning

In sequence and ligation independent cloning 5' ssDNA overlaps of insert and vector DNA are generated by an 3' exonuclease and are reassembled by *in vitro* homologous recombination and single-strand annealing<sup>[67]</sup>. The vector of choice is linearised by restriction enzymes, and the gene of interest is amplified by PCR using primers that create an additional 30 bp overlap corresponding to the vector sequence (Figure 6).

Both fragments are treated with T4-DNA polymerase, which has a 3'→5' exonuclease activity in absence of nucleotides. The reaction is terminated by addition of a single dNTP. Vector and insert DNA are combined in a ligation reaction lacking the enzyme ligase as it is not needed for recombination. The ligation mix is then transformed into XL1-blue cells as described in 4.2.2.

For SLIC, an expression vector was created based on *Novagen's* vector pET-16b. This vector was cleaved with restriction enzymes NcoI and BamHI to cut out the deca His-tag, the factor Xa recognition site and the multiple cloning site. In

this gap a fragment was cloned via SLIC that contained a new deca His-tag followed by a TEV recognition sequence (ENLYFQG) and sites for NdeI and XhoI. This new vector—designated pTEV-16b—was used for all further cloning. Maps of all plasmids constructed with pTEV-16b are listed in the appendix (9.2).

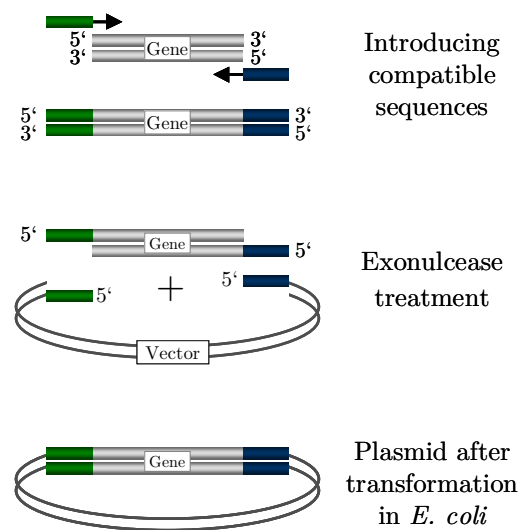


Figure 6: Preparation of insert and vector for sequence and ligation independent cloning. Primers are indicated as arrows.



**SLIC-PCR:** PCRs for preparation of gene sequences were performed as described in 4.3.3 with a split thermal cycling. The annealing temperature for the first 10 cycles considered only the sequence corresponding to the gene of interest. For the remaining 20 cycles, the complete primer sequence (including the 30 bp overhang) was taken into account.

**Exonuclease treatment** (20-40  $\mu$ l): Vector and insert DNA (400-1,000 ng) were individually mixed with 1-2 U T4-DNA polymerase in NEBuffer 2 supplied with 50  $\mu$ g/ml BSA. Samples were incubated at 22 °C for 40 min. The reaction was terminated by addition of 1 mM dCTP.

**Annealing** (10  $\mu$ l): Vector DNA (50-150 ng) was mixed with a five-fold molar excess of insert DNA in a buffer containing 50 mM Tris/HCl pH 7.5, 10 mM magnesium chloride, 1 mM ATP and 10 mM dithiothreitol. Samples were incubated at 37 °C for one hour.

## 4.4 Protein biochemical methods

### 4.4.1 Protein quantification

The concentration of a protein sample in solution was determined colorimetrically either by *Bio-Rad's Protein Assay* based on the method of *Bradford*<sup>[68]</sup> or by *Pierce's BCA Protein Assay*<sup>[69]</sup> according to the manufacturers' instruction. The choice which assay to use was depending on the composition of the sample buffer and possible interferences with the respective assay.

Proteins in buffers containing *n*-dodecyl- $\beta$ -D-maltopyranoside or *FOS-CHOLINE*<sup>®</sup> based detergents were quantified using bicinchoninic acid (BCA) whereas the *Bradford* test was applied to protein solutions with up to 8 M urea or more than 1 mM DTT.

In both cases, reference curves were setup with BSA over a range of 0-10 or 0-20 mg/ml depending on the expected protein concentration. To correct for background, the reference samples were prepared using the same buffer the protein was diluted in. By standard, protein concentrations were determined in triplicate.

The concentration of highly pure protein solutions was determined spectrophotometrically by reading absorption at 280 nm considering protein specific absorption coefficients that were calculated based on the primary sequence using *ExPASy's ProtParam*<sup>[70]</sup> software.

#### 4.4.2 SDS polyacrylamide gel electrophoresis

Purified protein samples and those from expression studies as well as potential protein crystals were analysed by discontinuous SDS-PAGE<sup>[71]</sup>. For up to 15 samples, small gels with a size of 9 x 10 x 0.1 cm were used. Large gels (32 x 20 x 0.1 cm) could separate 40-60 samples at once. Gels were composed of a 5 % (w/v) acrylamide stacking gel and a 10-15 % (w/v) acrylamide separating gel. Prior to use, all samples were supplied with 4x loading buffer. Samples from expression studies were incubated at 95 °C for 10 min to break the cells.

Depending on the downstream application, *Bio-Rad's Precision Plus Protein Standards* were used either as unstained variant when gels were silver stained or as two-coloured variant when western blotting was performed after electrophoresis. SDS-PAGE was carried out at constant current (30-50 mA) and maximum voltage (600 V) within 1-2 h for small gels and o/n for large gels, respectively.

##### Composition of SDS-PAGE gels (percentage in w/v)

**Stacking gel:** 16.7 % Rotiphorese® Gel 30, 0.2 % TEMED and 1.3 % APS in stacking gel buffer

**10% Separating gel:** 33.3 % Rotiphorese® Gel 30, 0.1 % TEMED and 0.7 % APS in separating gel buffer

**12% Separating gel:** 40 % Rotiphorese® Gel 30, 0.1 % TEMED and 0.7 % APS in separating gel buffer

**15% Separating gel:** 50 % Rotiphorese® Gel 30, 0.1 % TEMED and 0.7 % APS in separating gel buffer

##### Composition of stock solutions (percentage in w/v)

**Acrylamide stock solution:** Rotiphorese® Gel 30 (30 % acrylamide with 0.8 % bisacrylamide)

**2.5x Separating gel buffer, pH 8.9:** 1.875 M Tris/H<sub>3</sub>PO<sub>4</sub>, 0.25 % SDS

**5x Stacking gel buffer, pH 6.7:** 0.25 M Tris/H<sub>3</sub>PO<sub>4</sub>, 0.5 % SDS

**4x Loading buffer:** 30 mM Tris, 30 mM boric acid, 0.7 mM EDTA, 50 mM DTT, 6.7 % SDS, 5 mM MgCl<sub>2</sub>, 16.7 % sucrose, 0.16 % bromophenol blue

**10x Electrophoresis buffer:** 0.25 M Tris, 1.92 M glycine, 0.5 % SDS

#### 4.4.3 Silver staining of SDS-PAGE gels

With a detection limit of 50-100 pg the silver staining method is a very sensitive method to verify even slight amounts of protein in a SDS-PAGE gel<sup>[72]</sup>.

After electrophoresis, gels were incubated in fixation solution for 30-60 min followed by treatment with sensitising solution for another 30 min. The gels were washed three times with deionised water for overall 60 min. Staining solution was applied for 30-60 min, and the gels were subsequently washed with water. The staining process—the reduction of silver ions—was initiated by addition of developing solution and was terminated by 2.3 M citric acid. Incubation times apply to large gels. Times were reduced to 10 min for each step for small gels.

**Fixation solution:** 30 % ethanol, 10 % acetic acid (both technical quality, v/v)

**Sensitising solution:** 30 % ethanol (tech. quality, v/v), 0.5 % (w/v) sodium acetate, 0.2 % (w/v) sodium thiosulfate

**Staining solution:** 0.1 % (w/v) silver nitrate, 0.02 % (v/v) formaldehyde

**Developing solution:** 2.5 % (w/v) sodium carbonate, 0.02 % (v/v) formaldehyde

#### 4.4.4 Western blotting

Electrophoretically separated protein samples were transferred from acrylamide gels to either cellulose nitrate (NC) or polyvinylidene fluoride (PVDF) membranes by semi-dry western blotting<sup>[73]</sup>.

After electrophoresis gels were initially incubated with shaking in transfer buffer for about 10 min. PVDF membranes were rinsed with 100 % (v/v) ethanol prior to use. All membranes and blotting papers were briefly wetted in transfer buffer, and the blot sandwich was assembled as follows: Three sheets of paper, the transfer membrane, the gel and finally three more sheets of blotting paper were placed inside a semi-dry electroblotting system with the membrane facing the anode. Protein transfer was performed at a constant current of either 1 mA/cm<sup>2</sup> for 1.5 hours or 0.2 mA/cm<sup>2</sup> over night. After blotting, the protein transfer was confirmed by staining with *Ponceau S* solution. Before proceeding with the immunodetection of bound proteins (see 4.4.6), membranes were rinsed with deionised water to destain.

**Transfer buffer:** 25 mM Tris, 190 mM glycine in 10 % (v/v) ethanol

***Ponceau S* staining solution:** 0.5 % (w/v) *Ponceau S* in 1 % (v/v) acetic acid

#### 4.4.5 Dot blotting

*Dot blots* are a variant of western blotting (see 4.4.4) and were performed with protein samples that were not previously separated by SDS-PAGE.

A grid was drawn on dry cellulose nitrate membrane with a square size of approximately 1 x 1 cm. Protein samples were prepared with 4x loading buffer (see 4.4.2) and pipetted onto the membrane not exceeding a drop volume of 10 µl. Membranes were dried at room temperature and immunodetection was carried out as described in 4.4.6.

#### 4.4.6 Immunodetection

Transfer membranes from western and dot blotting applications (4.4.4 and 4.4.5) were further analysed by immunodetection. If not stated otherwise, all incubation steps were carried out on a laboratory shaker at room temperature. At first, membranes were placed in 1 % (w/v) casein-TBS solution to saturate free binding sites of the membrane. After 60 min of incubation, membranes were washed twice with TBT buffer and once with TBS buffer; each step lasting 10 min. Primary antibodies (Table 8, page 25) were diluted in 1 % casein-TBS solution according to the manufacturers' instructions and were applied to the membrane for 60 min at room temperature or o/n at 4 °C. Membranes were washed again three times for 10 min with TBT buffer and once more with TBS buffer. The second antibody (also diluted in 1 % casein-TBS solution) was applied for 60 min. Then, washing with TBT and TBS buffer was repeated as before. Bound secondary antibodies were detected via the linked enzyme horseradish peroxidase using *Millipore's Immobilon™ Western Chemiluminescent HRP Substrate*. Luminescent signals derived from the oxidation of luminol were detected and quantified with the luminescent image analyzer *LAS-1000* and the corresponding software *Image Gauge 3.0*.

**TBS buffer**, pH 7.5: 10 mM Tris/HCl, 150 mM NaCl

**TBT buffer**, pH 7.5: 20 mM Tris/HCl, 500 mM NaCl, 0.05 % (v/v) *Tween®* 20

#### 4.4.7 Proteolytic cleavage

##### *4.4.7.1 Removal of the deca His-tag from AtETR1 (factor Xa proteolysis)*

Purified receptor protein AtETR1 (see 4.7.1.1) was treated with factor Xa protease to cleave the N-terminal affinity tag from the fusion protein.

AtETR1 (< 1.6 mg) was diluted in a total reaction volume of maximum 5 ml. The protease-protein ratio was adjusted to 0.05 U/μg fusion protein and the sample was incubated at 4 °C on a shaker o/n. Factor Xa was removed by *Xarrest®* agarose (*Novagen®/Merck KGaA, Darmstadt*) according to the manufacturer's protocol. Cleaved His-tags and undigested tagged AtETR1 were bound to Ni-NTA pre-equilibrated twice with 1 CV buffer KA. The sample was added to the affinity agarose and placed on a shaker for 15 min at room temperature. The mixture was applied to an empty column and cleaved AtETR1 was eluted with the flow-through.

**Buffer KA**, pH 7.5: 50 mM Tris/HCl, 100 mM KCl, 0.1 % (w/v) DDM

#### 4.4.7.2 Removal of the deca His-tag from AtETR1[L70W]-TEV (*AcTEV*<sup>®</sup> proteolysis)

AtETR1[L70W]-TEV was purified as described in section 4.7.1.1 and was treated with *AcTEV*<sup>®</sup> protease to remove the N-terminal deca His-tag. Proteolytic cleavage was performed in buffer KAD at a protein concentration of 0.8 mg/ml. *AcTEV*<sup>®</sup> protease was applied in a protease/protein ratio of 0.33 U/μg fusion protein. Samples were incubated at 10°C to 20 °C o/n. Non-digested protein, cleaved affinity tags and the protease that contained a His-tag itself were removed with 4 ml Ni-NTA pre-equilibrated with 5 CV buffer KA. The affinity agarose was incubated with the protein solution for 15 min at room temperature, and then AtETR1[L70W]-TEV was collected with the flow through.

**Buffer KAD**, pH 7.5: 50 mM Tris/HCl, 100 mM KCl, 0.1 % (w/v) DDM, 1 mM DTT

#### 4.4.7.3 Proteolysis of AtETR1, AtETR1[H353A] and AtETR1[D659A] with thrombin

Wild type and mutant receptor protein was purified according to 4.7.1.1 and was treated with thrombin in a protease-protein ratio of 0.2 U/μg receptor protein. Reactions were setup at 25 °C in buffer TD in a final volume of 50-80 μl with the receptor at a concentration of 0.4 mg/ml. Samples were taken after 0 and 4 hours and cleavage with thrombin was terminated by addition of 0.02 % (w/v) PMSF in 100 % (v/v) ethanol. All samples were analysed by SDS-PAGE (4.4.2) using 4-20 % Tris/glycine gels from *biostep GmbH (Jahnsdorf)*. Western blotting was performed as described in sections 4.4.4 and 4.4.6.

**Buffer TD**, pH 7.5: 50 mM Tris/HCl, 100 mM KCl, 0.1 % (w/v) DDM, 1 mM MnCl<sub>2</sub>, 0.2 mM ATP

## 4.5 Expression of recombinant proteins in *E. coli*

### 4.5.1 Expression of full-length receptor protein AtETR1

C43 (DE3) cells were transformed with vector pET-16b::AtETR1<sub>1-738</sub>WT or a plasmid containing coding sequences for mutated AtETR1 full-length receptor proteins (Table 10 and Table 11, page 28) following the protocol described in 4.2.2. Pre-cultures were set up with a single colony in 500 ml 2YT medium supplied with 100 μg/ml ampicillin in non-baffled 1 l flasks and were incubated o/n at 30 °C with shaking at 180 rpm. Each main culture (500 ml 2YT medium, 150 μg/ml ampicillin in baffled flasks) was inoculated with 40 ml of pre-culture, and cells were

grown to an OD<sub>600</sub> of 1. Protein expression was initiated by addition of IPTG to a final concentration of 0.5 mM. About 6-8 hours after induction, cells were harvested by centrifugation (10,000 x g, 6 min, 4 °C), flash-frozen in liquid nitrogen and stored at -80 °C.

#### 4.5.2 Expression of the extramembrane domain of AtETR1

With the exception of the surface entropy reduced mutant, named AtETR1<sub>165-738</sub>SER, all AtETR1<sub>165-738</sub> constructs lacking the membrane domain were expressed in BL21 (DE3) cells harbouring the plasmid pRARE. In contrast, AtETR1<sub>165-738</sub>SER was expressed in BL21-Gold (DE3) cells co-transformed with pRARE.

Cells were transformed as described in section 4.2.2 and pre-cultures (500 ml 2YT medium supplied with 100 µg/ml ampicillin and 34 µg/ml chloramphenicol) were set up in non-baffled 1 l flasks. Cultures were inoculated with a single colony and grown o/n at 37 °C with shaking at 180 rpm. Each main culture (500 ml 2YT medium with antibiotics in final concentrations as indicated above) was supplied with 40 ml of pre-culture, and cells were grown in baffled flasks to an OD<sub>600</sub> of 0.7 (for mutant AtETR1<sub>165-738</sub>SER OD<sub>600</sub> ~ 3.0) before induction was started by addition of 0.5 mM IPTG. Protein expression continued for 4 hours (for mutant AtETR1<sub>165-738</sub>SER only 2.5 h). Then, cells were harvested by centrifugation (10,000 x g, 6 min, and 4 °C). The cell pellets were flash-frozen in liquid nitrogen and stored at -80 °C.

#### 4.5.3 Expression of PpETR1 and LeETR1

Analytical expression studies to test for optimal expression conditions were performed with bacterial strains C41 (DE3), C43 (DE3) and BL21 (DE3): Pre-cultures (5 ml 2YT medium) supplied with 100 µg/ml ampicillin were inoculated with a single colony and incubated with shaking at 180 rpm o/n at 37 °C. Pre-cultures were used to inoculate main cultures (100 ml 2YT/ampicillin medium in baffled 250 ml flasks) to an OD<sub>600</sub> of 0.05. These cultures were grown shaking at 30 °C until they reached an OD<sub>600</sub> of 0.5-0.8. Protein expression was induced by addition of 1 mM IPTG, and samples for SDS-PAGE and western blot analysis were taken 0 and 4 hours upon induction.

**Preparation of expression samples for SDS-PAGE:** An aliquot of 500 µl cell culture was centrifuged for 5 min at 14,000 rpm. The supernatant was discarded and the cell pellet was resuspended in 50 µl 4x loading buffer (see 4.4.2) and 150 µl H<sub>2</sub>O. Samples were boiled at 95 °C for 10 min. Sample volumes to apply to an SDS-PAGE gel were calculated based on the OD<sub>600</sub> of the cell culture: 15/OD<sub>600</sub> = sample volume in µl.

For preparative expression of PpETR1 and LeETR1 pre- and main cultures were scaled up to 500 ml 2YT medium (including ampicillin in a final concentration of 100 µg/ml). The IPTG concentration was reduced to 0.1 mM for the constructs lacking the membrane domain while expression duration was extended to 6 hours. Full-length PpETR1 and LeETR1 were expressed o/n at 16 °C, and for LeETR1 the IPTG concentration was also reduced to 0.1 mM.

## 4.6 Purification of recombinant proteins from *E. coli* – general methods

### 4.6.1 Cell disruption

Cells were thawed on ice and resuspended in protein specific buffer. High pressure disruption was performed with a pre-cooled *French pressure cell press* at 1,200 to 1,500 psi. By standard, the cell suspension was passed through the system twice.

#### Composition of cell disruption buffers (percentage is in w/v)

##### **AtETR1**, pH 8.0:

50 mM Tris/HCl, 200 mM NaCl, 15 % glycerol , 2 mM DTT, 0.002 % PMSF [per gram cells: 2.5 ml buffer]

##### **AtETR1<sub>165-738</sub>**, pH 6.0:

100 mM Bis-tris propane/HCl, 150 mM NaCl, 20 mM 2-mercaptoethanol, 8 M urea [per gram cells: 5-6.25 ml buffer]

##### **PpETR1<sub>158-767</sub> and LeETR1<sub>173-754</sub>**, pH 7.5:

50 mM Tris/HCl, 200 mM NaCl, 10 mM DTT, 10 % glycerol, 0.002 % PMSF [per gram cells: 5 ml buffer]

##### **PpETR1<sub>1-767</sub> and LeETR1<sub>1-754</sub>**, pH 8.0

50 mM Tris/HCl, 200 mM NaCl, 10 % glycerol, 10 mM DTT, 0.002 % PMSF [per gram cells: 2.5 ml buffer]

### 4.6.2 Isolation and solubilisation of *E. coli* membranes

*E. coli* C43 (DE3) cells were disrupted as described in 4.6.1, and membranes were separated by centrifugation at 40,000 x g and 4 °C for 30 min. Disrupted cells of strain BL21 (DE3) were centrifuged at 230,000 x g to form a solid pellet.

Depending on the downstream application, membrane proteins were either solubilised in a buffer containing 8 M urea, or a native approach referring to *Ren et al.*<sup>[74]</sup> was chosen using a set of 24 detergents (appendix 9.2.7) to test for appropriate solubilisation conditions.

Therefore, membrane pellets corresponding to 7 g of fresh cells were resuspended in 10 ml buffer S. Samples with a volume of 400 µl were set up with 1 and 2 % detergent, respectively, and incubated for 2 hours at 20 °C with slight shaking. Samples were then centrifuged at

150,000 x g and 4 °C for 30 min. The supernatant was collected, and the pellet was resuspended in 400 µl buffer S. Aliquots of each sample (10 µl) were supplied with 4x loading buffer (see 4.4.2), and dot blots with final immunodetection were performed according to 4.4.5 and 4.4.6.

**Buffer S**, pH 8.0: 50 mM Tris/HCl, 100 mM NaCl and 0.002 % (w/v) PMSF

#### 4.6.3 Isolation and purification of inclusion bodies

*E. coli* cells were disrupted as described in section 4.6.1, and the crude extract was centrifuged at 10,000 x g and 4 °C for 30 min. Pellets were resuspended in an equal volume of buffer IB-DOC, and the inclusion bodies were sonicated on ice five times for 30 sec with a 30 sec pause in between. Centrifugation was repeated as before, and the resulting inclusion body pellet was resuspended in an equal volume of buffer IB. Sonication and centrifugation were performed once again as described above. The pellet was finally resuspended in an equal volume of buffer IB, and aliquots of 10 ml were centrifuged for 15 min at 10,000 x g and 4 °C. The supernatant was discarded, and the inclusion body pellets were flash-frozen in liquid nitrogen and stored at -80 °C.

**Buffer IB-DOC**, pH 7.5: 50 mM Tris/HCl, 100 mM NaCl, 1 % (w/v) sodium deoxycholate, 0.002 % (v/v) PSMF

**Buffer IB**, pH 7.5: 50 mM Tris/HCl, 100 mM NaCl

#### 4.6.4 Solubilisation of inclusion bodies

Each aliquot of purified inclusion bodies was resuspended in 10 ml buffer IB (see 4.6.3) and sonicated on ice five times for 30 sec with a 30 sec pause in between. Small scale samples were set up to test for optimal solubilisation conditions. Aliquots of the suspension (250 µl) were transferred to 1.5 ml reaction tubes and centrifuged at 10,000 x g and 4 °C for 15 min. The supernatant was discarded, and 1 ml of solubilisation buffers SB-1 to SB-18 (modified after *Patra et al.*<sup>[75]</sup>) was added to the inclusion body pellet. The pellets were completely dissolved in the buffer by dispensing with a brush, and the suspension was incubated for 30 min at 25 °C with slight shaking. Centrifugation was repeated as before. The supernatants were collected and the pellets resuspended in buffer IBS. SDS-PAGE analysis was performed according to 4.4.2 and 4.4.3 with 10 µl of each sample supplied with 4x loading buffer.



**Buffer IBS**, pH 7.5: 50 mM Tris/HCl, 100 mM NaCl, 1 % (w/v) SDS

**SB-1**, pH 7.0: 50 mM Tris/HCl, 100 mM NaCl

**SB-2**, pH 7.0: 50 mM Tris/HCl, 100 mM NaCl, 2 M urea

**SB-3**, pH 7.0: 50 mM Tris/HCl, 100 mM NaCl, 8 M urea

**SB-4**, pH 8.0: 50 mM Tris/HCl, 100 mM NaCl

**SB-5**, pH 8.0: 50 mM Tris/HCl, 100 mM NaCl, 2 M urea

**SB-6**, pH 8.0: 50 mM Tris/HCl, 100 mM NaCl, 8 M urea

**SB-7**, pH 9.0: 50 mM Tris/HCl, 100 mM NaCl

**SB-8**, pH 9.0: 50 mM Tris/HCl, 100 mM NaCl, 2 M urea

**SB-9**, pH 9.0: 50 mM Tris/HCl, 100 mM NaCl, 8 M urea

**SB-10**, pH 10.0: 50 mM NaHCO<sub>3</sub>, 100 mM NaCl

**SB-11**, pH 10.0: 50 mM NaHCO<sub>3</sub>, 100 mM NaCl, 2 M urea

**SB-12**, pH 10.0: 50 mM NaHCO<sub>3</sub>, 100 mM NaCl, 8 M urea

**SB-13**, pH 11.0: 50 mM NaHCO<sub>3</sub>, 100 mM NaCl

**SB-14**, pH 11.0: 50 mM NaHCO<sub>3</sub>, 100 mM NaCl, 2 M urea

**SB-15**, pH 11.0: 50 mM NaHCO<sub>3</sub>, 100 mM NaCl, 8 M urea

**SB-16**, pH 12.0: 50 mM Na<sub>2</sub>HPO<sub>4</sub>, 100 mM NaCl

**SB-17**, pH 12.0: 50 mM Na<sub>2</sub>HPO<sub>4</sub>, 100 mM NaCl, 2 M urea

**SB-18**, pH 12.0: 50 mM Na<sub>2</sub>HPO<sub>4</sub>, 100 mM NaCl, 8 M urea

#### 4.6.5 Refolding of proteins solubilised from inclusion bodies

The buffers used for releasing proteins from inclusion bodies were rather harsh either because of a high pH value or the chaotropic reagent urea (see 4.6.4 for details). In consequence, a buffer exchange was performed after solubilisation to allow for proper refolding of the proteins. A set of 15 buffers was prepared according to the *QuickFold™ Protein Refolding Kit* from *Athena Environmental Sciences, Inc.* (Baltimore, MD, USA) to test for optimal refolding conditions. Composition of refolding buffers RB-1 to RB-15 can be found in appendix 9.4.

Before refolding, solubilised protein samples were diluted to a concentration of 5 mg/ml. Refolding buffers RB-1 to RB-15 (950 µl) were transferred to 1.5 ml reaction tubes, and 50 µl of the diluted protein solution were added. Samples were mixed by inversion and incubated for 30 min at 4 °C. Samples were centrifuged for 15 min at 20,000 x g and 4 °C. Then, the supernatants were collected, and the pellets were resuspended in an equal volume of buffer RF-8M. Samples from the supernatant and pellet fractions (10 µl) were supplied with 4x loading buffer and analysed by SDS-PAGE according to 4.4.2 and 4.4.3.

**Buffer RF-8M**, pH 8.0: 50 mM Tris/HCl, 100 mM NaCl, 8 M urea

#### 4.6.6 Size exclusion chromatography

Analytical size exclusion chromatography was used to determine composition and homogeneity of a protein sample. By standard, a *HiPrep 16/60 Sephacryl S-200* column from *GE Healthcare Europe GmbH* (Munich) was used. Analytical SEC was performed with a flow rate of 0.5 ml/min at room temperature with an *ÄKTAexplorer™* system. Prior to use, the column was equilibrated at a flow rate of 0.5-1 ml/min with 1.5-2 CV of the appropriate buffer. Calibration

was carried out with proteins from *Sigma-Aldrich's Gel Filtration Molecular Weight Markers Kit* ranging from 29 kDa to 700 kDa.

Choice of buffer composition and sample volume were protein specific and are listed in Table 14. Sample loops were only partially filled (max. 50 %) to ensure all protein was applied to the column\*.

Table 14: Protein specific conditions for size exclusion chromatography

<i>Protein</i>	<i>Buffer composition</i>	<i>Sample volume</i>	<i>Fraction size</i>
AtETR1 <sub>165-738</sub>	50 mM Tris/HCl pH 8.0, 150 mM	0.2-2 ml	1 ml
AtETR1 <sub>165-738</sub> SER	NaCl, 0.04 % (w/v) DDM	250-750 µl	1-2 ml
PpETR1 <sub>158-767</sub>	50 mM Tris/HCl pH 8.5, 150 mM	1 ml	1 ml
LeETR1 <sub>173-754</sub>	NaCl, 0.04 % (w/v) DDM		

#### 4.6.7 Removal of DnaK contamination

In case of DnaK contamination after IMAC purification, two approaches were tested to eliminate the impurity by the heat shock protein. In the first approach, the target protein (still bound to Ni-NTA) was incubated four times for 10 min each in buffer DR-1 on a shaker at room temperature. In between each incubation step, the suspension was applied to an empty column to remove the buffer. Afterwards, purification and elution of the target protein was proceeded according to the individual protein preparation protocols (see 4.7).

In a second approach, the elution fraction after IMAC purification was concentrated to 5 ml by ultra filtration and diluted with an equal volume of buffer DR-2. The solution was incubated on a shaker for 60 min at 4 °C and then concentrated again to a final volume of 2.5 ml by ultra filtration. Buffer exchange to buffer DR-3 was performed by *PD-10* column. The eluate was concentrated to 1 ml and centrifuged for 30 min at 14,000 x g and 4 °C.

An anion exchange chromatography was applied using a 1 ml *HiTrap<sup>TM</sup> Q Sepharose<sup>TM</sup> XL* column on *ÄKTAexplorer<sup>TM</sup>* to separate released DnaK and target protein. With a flow rate of 1 ml/min the column was equilibrated with 10 CV buffer DR-3. After sample application, a linear gradient up to 100 % was run for 10 CV with buffer DR-4 while fractions were collected with a volume of 0.5 ml. Aliquots of each fraction were analysed by SDS-PAGE (4.4.2 and 4.4.3) regarding their protein composition.

---

\* Complete filling of a sample loop will result in a loss of protein as the solution will not move even through the tubing but rather in an arrow-head like manner due to friction within the sample loop, with the effect of applying protein solution to the waste bottle instead of the column.

**Preparation of denatured *E. coli* proteins:** *E. coli* lysate from a membrane preparation of AtETR1 (see 4.6.2) was diluted into buffer DR-0 resulting in a protein concentration of 2 mg/ml. The diluted lysate was incubated for 10 min in a water bath at 65 °C. Precipitated proteins were pelleted by centrifugation at 12,000 x g for 10 min. The cleared supernatant was stored at -20 °C.

**Buffer DR-0**, pH 8.0: 50 mM Tris/HCl, 150 mM NaCl, 0.002 % (w/v) PMSF

**Buffer DR-1**, pH 8.0: 50 mM Tris/HCl, 150 mM NaCl, 0.002 % (w/v) PMSF, 0.1 mg/ml denatured *E. coli* proteins, 5 mM ATP, 5 mM MgCl<sub>2</sub>

**Buffer DR-2** pH 8.0: 20 mM Tris/HCl, 100 mM NaCl, 0.5 M arginine, 0.002 % (w/v) PMSF, 0.015 % (w/v) *FOS-CHOLINE*<sup>®</sup>-14

**Buffer DR-3** pH 6.5: 50 mM Bis-tris propane/HCl, 10 mM NaCl, 0.5 M arginine, 0.015 % (w/v) *FOS-CHOLINE*<sup>®</sup>-14

**Buffer DR-4** pH 6.5: 50 mM Bis-tris propane/HCl, 1 M NaCl, 0.5 M arginine, 0.015 % (w/v) *FOS-CHOLINE*<sup>®</sup>-14

## 4.7 Purification protocols for individual proteins

### 4.7.1 Purification of full-length receptor protein AtETR1

#### 4.7.1.1 *Purification in 8 M urea*

Membrane pellets prepared as described in section 4.6.2 were resuspended in 10 ml buffer U and incubated for 90 min at 37 °C with slight stirring. After centrifugation at 40,000 x g and 20 °C for 30 min, the supernatant was collected by a pipette, and imidazole was added to a final concentration of 20 mM.

Two plastic columns with an inner diameter of 0.75 cm were each filled with 2 ml Ni-NTA and equilibrated with 5 CV buffer U. The columns were positioned on top of each other, and the protein sample was applied to the upper column. When the sample had completely passed through, the resin was washed with 10 CV buffer U followed by 30 CV of buffer U supplied with 50 mM imidazole. For both washing steps a tubing (approx. 40-50 cm) was connected to the column outlet to accelerate flow. The target protein was eluted with 6 CV buffer U prepared with 250 mM imidazole.

The eluate was concentrated to 1 ml by ultra filtration in an *Amicon Ultra*<sup>®</sup> filter unit with a molecular weight cut-off of 50 kDa. The protein solution was diluted once with 10 ml buffer U and concentrated again to approximately 2 ml. The protein concentration was determined by the *Bradford* assay (4.4.1) and adjusted to 0.8 mg/ml with buffer U.

Aliquots of 500 µl were transferred to 15 ml reaction tubes, and 50 µl of 1 M DTT were added to each tube. After addition of 10 ml pre-cooled buffer R1 the solution was mixed by inversion and centrifuged for 30 min at 230,000 x g and 4 °C. Supernatants were pooled after centrifugation and were concentrated to 1 ml by ultra filtration at 8 °C. Samples were diluted once again with buffer R2 in a ratio of 1:10 and finally concentrated to a volume of 2.5 ml.

Buffer exchange to buffer KA was performed by a *PD-10* column. The eluate was concentrated by ultra filtration (final volume < 500 µl), and the protein sample was finally centrifuged for 30 min at 150,000 x g and 4 °C.

**Buffer U**, pH 8.0: 20 mM Tris/HCl, 100 mM NaCl, 8 M urea

**Buffer R1**, pH 8.0: 55 mM Tris/HCl, 264 mM NaCl, 11 mM KCl, 0.1 % (w/v) DDM, 10 mM DTT, 1.1 mM EDTA, 0.002 % (w/v) PMSF

**Buffer R2**, pH 8.0: 55 mM Tris/HCl, 264 mM NaCl, 11 mM KCl, 0.1 % (w/v) DDM, 2 mM DTT

**Buffer KA**, pH 7.5: 50 mM Tris/HCl, 100 mM KCl, 0.1 % (w/v) DDM

#### 4.7.1.2 Native purification of *AtETR1*

Membrane pellets prepared as described in section 4.6.2 were dissolved in 10 ml buffer SF14. Solubilisation of membrane proteins was promoted either by incubation at room temperature for 2 hours with slightly stirring or by sonication on ice for 20 min with 50 % duty cycle. The solubilise was then centrifuged for 20-30 min at 150,000-230,000 x g and 4 °C. The supernatant was collected, and sodium chloride was added to a final concentration of 2 M.

Ni-NTA (4 ml) was filled in a plastic column with an inner diameter of 1.5 cm and equilibrated with 10 CV buffer N2M. The supernatant from centrifugation was mixed with the resin in a 50 ml reaction tube and placed on a shaker for 15 min at room temperature. The suspension was filled into the column, and the resin was washed with 20 CV buffer N2M followed by 20 CV of buffer N2M supplied with imidazole in a final concentration of 50 mM. Bound target protein was eluted with 5 CV buffer NFI.

The protein solution was concentrated to a final volume of 2.5 ml by ultra filtration (MWCO 50 kDa) at 8 °C. Buffer exchange was performed by *PD-10* column into buffer NF. The eluate was concentrated again (final volume < 500 µl), and the protein solution was finally centrifuged for 30 min at 150,000 x g and 4 °C to remove aggregated proteins.

**Buffer SF14**, pH 8.0: 50 mM NaPi, 100 mM NaCl, 0.002 % (w/v) PMSF, 1 % (w/v) *FOS-CHOLINE*<sup>®</sup>-14

**Buffer N2M**, pH 8.0: 50 mM NaPi, 2 M NaCl, 0.002 % (w/v) PMSF, 0.015 % (w/v) *FOS-CHOLINE*<sup>®</sup>-14

**Buffer NFI**, pH 7.5: 50 mM NaPi, 150 mM NaCl, 0.002 % (w/v) PMSF, 0.015 % (w/v) *FOS-CHOLINE*<sup>®</sup>-14, 250 mM imidazole

**Buffer NF**, pH 8.0: 50 mM NaPi, 150 mM NaCl, 0.002 % (w/v) PMSF, 0.015 % (w/v) *FOS-CHOLINE*<sup>®</sup>-14

#### 4.7.2 Purification of the extramembrane domain of AtETR1

Receptor proteins AtETR1<sub>165-738</sub>, AtETR1<sub>165-738</sub>[H353A] and AtETR1<sub>165-738</sub>SER were expressed in inclusion bodies, so purification was performed under denaturing conditions in 8 M urea.

Cell pellets (4-5 g wet weight) were resuspended, and cells were disrupted as described in section 4.6.1. The crude extract was centrifuged at 40,000 x g and 20 °C for 20 min. The supernatant was collected by a *Pasteur* pipette, and an equal volume of buffer T9 was added.

A plastic column with an inner diameter of 1.5 cm was filled with 6.5 ml *HIS-Select*<sup>®</sup> nickel affinity gel, and the resin was equilibrated with 5 CV buffer T75. The amount of the resin was reduced to 2 ml/4-5 g wet weight cells for mutant AtETR1<sub>165-738</sub>SER, which was expressed at a lower level compared to the other truncated proteins. The protein was applied to the affinity gel and incubated on a shaker at room temperature for 20 min. The resin was then allowed to settle and 5 CV buffer T75 were applied as the first washing buffer followed by 10 CV buffer T75 supplied with 30 mM imidazole. Bound protein was eluted with 3 CV of buffer T75 with 200 mM imidazole.

The eluate was concentrated to 1 ml in an *Amicon Ultra*<sup>®</sup> filter unit (MWCO 30 kDa) and diluted to 2.25 ml with buffer T75. *N*-ethylmaleimide dissolved in dimethyl sulfoxide was added (250 µl of 100 mM NEM) and incubated for 15 min at room temperature. The buffer was exchanged to buffer T75 by a *PD-10* column to remove NEM. The eluate was submitted to centrifugation at 150,000 x g and 10 °C for 30 min.

Protein refolding was initiated by dilution with pre-cooled buffer R3 in a ratio of 1:10. The protein solution was again centrifuged for 30 min at 230,000 x g and 4 °C. The supernatant was collected and concentrated by ultra filtration to a volume of 1 ml. The remaining concentration of urea was reduced to 80 mM by diluting and concentrating the sample twice in a ratio of 1:10 with buffer R3. The protein solution was finally concentrated to 100-500 µl and centrifuged to remove aggregated proteins (150,000 x g, 4 °C and 30 min).

**Buffer T9**, pH 9.0: 50 mM Tris/HCl, 150 mM NaCl, 8 M urea

**Buffer T75**, pH 7.5: 50 mM Tris/HCl, 150 mM NaCl, 8 M urea

**Buffer R3**, pH 8.2: 50 mM Tris/HCl, 10 mM NaCl, 1 mM KCl, 10 mM DTT, 0.1 % (w/v) DDM, 0.002 % (w/v) PMSF

### 4.7.3 Purification of full-length PpETR1 and LeETR1

#### 4.7.3.1 *Native purification*

Native purification of full-length proteins PpETR1<sub>1-767</sub> and LeETR1<sub>1-754</sub> was performed as described for the receptor protein ETR1 from *Arabidopsis thaliana* (see 4.7.1.2).

#### 4.7.3.2 *Purification in 8 M urea*

Membrane pellets were prepared from 7-8 g of cells as explained previously (see 4.6.2). The crude extract was clarified by centrifugation (30 min, 230,000 x g and 4 °C), and the pellet was resuspended in 10 ml buffer PLU. The solution was stirred at 37 °C for 30 min. Then, centrifugation was repeated with the temperature increased to 20 °C. Supernatants were collected, and sodium chloride was added to a final concentration of 2 M. Ni-NTA (4 ml) was filled into a plastic column with an inner diameter of 1.5 cm and was equilibrated with 10 CV of buffer U2M. The resin was mixed with the supernatant in a 50 ml reaction tube and placed on a shaker for 15 min at room temperature. The suspension was filled back into the column and the resin was washed with 20 CV buffer U2M followed by 20 CV of buffer U2M supplied with 50 mM imidazole. The bound target protein was eluted with 5 CV buffer PLU supplied with 250 mM imidazole.

**Buffer PLU**, pH 8.0: 50 mM NaPi, 150 mM NaCl, 8 M urea

**Buffer U2M**, pH 8.0: 50 mM NaPi, 2 M NaCl, 8 M urea

### 4.7.4 Preparation of truncated PpETR1 and LeETR1 from inclusion bodies

Inclusion body pellets isolated as described in 4.6.3 were resuspended in 10 ml buffer IBU by stirring at room temperature for 30 min. Non-solubilised material was removed by 15-min centrifugation at 10,000 x g and 20 °C. The protein concentration of the supernatant was determined by the *Bradford* assay (4.4.1) and was set to 5 mg/ml with buffer IBU.

To promote refolding of the denatured proteins, 500 µl aliquots of the protein solution were diluted to 10 ml with buffer IBR and mixed by inversion. Incubation continued at 8 °C for 30 min on a shaker before aggregated protein was removed by centrifugation (30,000 x g, 4 °C, 15 min). The supernatant was concentrated to 1 ml (*Amicon Ultra*<sup>®</sup> filter unit, MWCO 30 kDa), diluted once in a ratio of 1:10 and finally constrained to 2.5 ml. Depending on the

downstream application, a buffer exchange was performed using a *PD-10* column and protein aggregates were removed by final centrifugation at 150,000 x g and 4 °C for 30 min.

**Buffer IBU**, pH 7.5: 50 mM Tris/HCl, 100 mM NaCl, 8 M urea

**Buffer IBR**, pH 8.5: 50 mM Tris/HCl, 10 mM NaCl, 1 mM DTT, 0.04 % (w/v) DDM

## 4.8 Protein characterisation

### 4.8.1 *In vitro* kinase assay

An amount of 25 µg receptor protein was purified as described before (4.7.1 to 4.7.4) and was incubated at room temperature for 10 min in 50 µl buffer KA supplied with 1 mM manganese chloride. Phosphorylation was initiated by the addition of 0.2 mM ATP mixed with radioactive labelled  $\gamma^{32}\text{P}$ -ATP to result in a specific activity of 10 µCi/25 µg protein. The assay was further incubated at room temperature for 30 min until the reaction was terminated by addition of 4x DDT<sub>free</sub> loading buffer. Samples were stored o/n at -20 °C before analysis by SDS-PAGE and western blotting was performed (4.4.2 and 4.4.4). Prior to loading, all protein samples were supplied with 60 mM DTT. After western blotting, the transfer membranes were dried, exposed to a phosphor imaging plate for 4-7 days and analysed using *Fujifilm's* image analyzer *FLA-3000* and the corresponding software *Image Gauge 3.0* for quantification of radioactive signals.

**Buffer KA**, pH 7.5: 50 mM Tris/HCl, 100 mM KCl, 0.1 % (w/v) DDM

**4x DDT<sub>free</sub> loading buffer**: 30 mM Tris, 30 mM boric acid, 0.7 mM EDTA , 6.7 % SDS, 5 mM MgCl<sub>2</sub>, 16.7 % sucrose, 0.16 % bromophenol blue (all w/v)

#### *Testing of inhibitory effects by KCN or ethephon*

Protein samples were incubated for 10 min at room temperature with 100 µM of copper(II) chloride. Then, 1 mM manganese chloride, buffer KA and KCN or ethephon were applied in a final concentration of 100 µM. The samples were incubated for further 10 min. The phosphorylation reaction was started by addition of ATP/ $\gamma^{32}\text{P}$ -ATP, and samples were treated and analysed as described before.

#### 4.8.2 Circular dichroism spectroscopy

##### 4.8.2.1 *Setup and data collection*

Far-UV CD spectra were recorded with a *Jasco-715* spectropolarimeter in quartz *SUPRASIL*<sup>®</sup> cuvettes (*Hellma GmbH & Co. KG, Muellheim*) with a path length of 1 mm and a volume of 160 µl. All measurements were performed at room temperature in buffer  $\text{KP}_i$  at a protein concentration of 0.1-0.3 mg/ml. Spectra were recorded from 260-195 nm with a step resolution of 1 nm and a bandwidth of 2 nm. The scan speed was set to 50 nm/min and by standard 10 spectra were accumulated.

**Buffer  $\text{KP}_i$** , pH 7.5: 50 mM potassium phosphate, 0.05 % (w/v) DDM

##### 4.8.2.2 *Evaluation of CD data*

All spectra were corrected for buffer absorption prior to analysis. Measured ellipticity (mdeg) was converted to mean residue weight ellipticity  $\Theta_{\text{MWR}}$  by the following equation:

$$\Theta_{\text{MWR}} = \Theta \cdot 100 \cdot \frac{MWR}{c \cdot d} \quad (\text{deg} \times \text{cm}^2 \times \text{dmol}^{-1}) \quad (\text{Eq. 1})$$

Here,  $\Theta$  is the observed ellipticity in degrees,  $MWR$  the mean residue molar weight of the protein (molecular mass in daltons/number of residues),  $c$  the protein concentration in mg/ml and  $d$  the optical path length in cm. Quantitative secondary structure estimation was carried out with the software package *CDPro* including the three programs *CONTIN*, *SELCON3* and *CDSSTR*<sup>[76]</sup>.

#### 4.8.3 Fluorescence spectroscopy

##### 4.8.3.1 *Intrinsic tryptophan fluorescence*

Protein intrinsic tryptophan fluorescence was measured with the fluorescence spectrometer *LS 55*. The excitation wavelength was set to 295 nm to selectively excite tryptophan residues. With a scan speed of 100 nm/min emission spectra were recorded within a range of 310-400 nm. By standard, five spectra were accumulated and corrected for buffer absorption. Settings of excitation and emission slits were adjusted to result in bandwidth of 4 nm and 5 nm, respectively.



#### 4.8.3.2 Monitoring phosphorylation status ETR1

Wild type and mutant full-length receptors were applied at a concentration of 2.4  $\mu\text{M}$ , truncated receptors were used at a concentration of 3.0  $\mu\text{M}$ . Samples (60  $\mu\text{l}$ ) were incubated with 1 mM manganese chloride for 10 min. If required, ATP was added at a final concentration of 200  $\mu\text{M}$  and incubation continued for further 30 min. Control samples were also set up without manganese chloride but with 0.2 mM ATP and incubated as before. Afterwards samples were measured in an ultra-micro cell (*Hellma GmbH & Co. KG, Muellheim*) with an optical path length of 3 mm and a volume of 45  $\mu\text{l}$ .

#### 4.8.3.3 Monitoring ligand binding to ETR1

Wild type and mutant full-length receptors were applied at a concentration of 2.4  $\mu\text{M}$ . Samples (60  $\mu\text{l}$ ) were incubated with 100  $\mu\text{M}$  copper(II) chloride for 10 min. If required, ethephon was added to a final concentration of 100  $\mu\text{M}$  and incubation continued for further 10 min. Control samples were set up containing ethephon but not the cofactor  $\text{Cu}^{2+}$ . Afterwards, samples were measured as described before.

For titration of ETR1 with ligands, measurements were carried out in a quartz *SUPRASIL*<sup>®</sup> macro/semi-micro cell (*PerkinElmer, Rodgau*) with an optical path length of 4 mm and a volume of 500  $\mu\text{l}$ . Mutant full-length receptors of ETR1 were applied at a concentration of 2.4  $\mu\text{M}$  and were titrated with increasing concentrations of ligands as specified in the results section. Changes in fluorescence intensity were determined by collecting emission spectra as described before.

#### 4.8.4 <sup>31</sup>P-NMR spectroscopy

NMR spectra were recorded at room temperature with a 600 MHz *Bruker BioSpin* NMR spectrometer. Deuterium oxide was supplied in concentrations of 5 to 10 % (v/v) with every sample to allow for locking. Orthophosphoric acid (85 %, v/v) was used as external standard. Data were processed and analysed with *MestReNova*<sup>®</sup> 6.2 (*Mestrelab Research*, Escondido, CA, USA).

#### 4.8.5 Protein crystallography

Structure determination by X-ray crystallography requires the production of protein monocrystals. When exposed to X-radiation, electrons from the proteins in the crystal will scatter the X-rays and produce diffraction patterns. These data are subsequently used to calculate electron density maps, from which a protein structure can be built.

Proteins can crystallise from a supersaturated solution as depicted in the phase diagram in Figure 7. When protein and precipitant reach a critical concentration, nucleation events can occur. This is usually achieved by raising the concentrations due to water evaporating from the aqueous phase.

By formation of nuclei, the actual concentration of the soluble protein in the system is slightly reduced. This results in a stop of nucleation events, and the actual crystal growth is initiated (see metastable zone in the phase diagram).

Slight changes in the ratio of protein and precipitant concentration can decide over the fate of a crystallisation drop and produce diverse liquid and solid phenomena as shown in Table 15 (page 55).

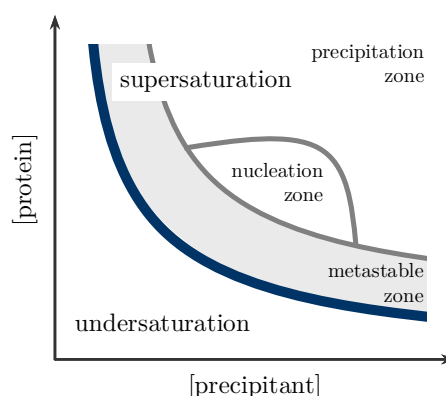


Figure 7: Simplified phase diagram for crystallisation of proteins. Crystals can only form from supersaturation, right to the solubility curve (blue line).

##### 4.8.5.1 Crystallisation techniques

###### *Microbatch under oil*<sup>[77]</sup>

Protein and precipitant solutions were combined in a small drop (1-2  $\mu$ l final volume) in either 72-well *Terasaki* plates or 96-well *IMP@CT<sup>TM</sup>* plates. The plates were covered with mineral oil to limit evaporation and stored at 4 °C, 15 °C and 20 °C, respectively. For temperature screenings using *Biometra's* thermocycler *TProfessional*, PCR plates with V-bottom were prepared with protein and precipitant, and the drops were individually covered with 30  $\mu$ l of mineral oil. Drops in standard microbatch plates were set up either manually or using the *Biomek<sup>®</sup> 3000* automation workstation.

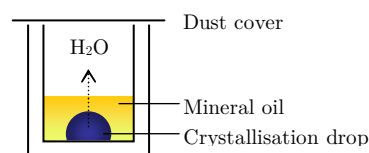


Figure 8: Microbatch setup. Evaporation of water from the crystallisation drop is limited by a thin layer of mineral oil.

### Vapour diffusion techniques: hanging and sitting drop crystallisation<sup>[78]</sup>

In the sitting drop techniques drops of protein solution and crystallisation buffer (0.75 µl each) were pipetted on small platforms within the wells of the crystallisation plates (*NeXtal Evolution µplate*). The wells also contained a separated reservoir that was filled with 70 µl of precipitant solution. Plates were sealed with *Crystal Clear Sealing Tape* from *Hampton Research Corp.* (Aliso Viejo, CA, USA) and stored at a temperature of choice.

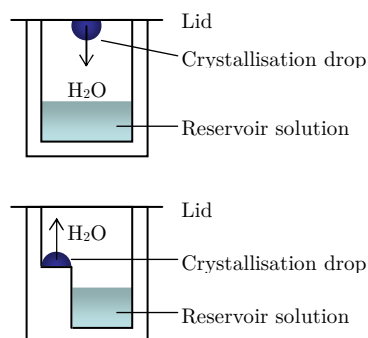


Figure 9: Setup of crystallisation chambers for hanging drop (upper figure) and sitting drop (lower figure) techniques.

For hanging drop crystallisation, *Qiagen's EasyXtal* plates were used. A drop of protein and precipitant solution was set up on the lid, and the cover was placed upside down over a reservoir filled with the appropriate crystallisation buffer (200-750 µl).

In both techniques, water will start to evaporate from the protein containing droplet as its precipitant concentration is lower than in the reservoir. The system will equilibrate creating a supersaturated condition in the drop increasing protein and precipitant concentration and the chance of crystal growth.

### Sponge Phase Crystallisation

The *Lipidic-Sponge Phase™ Screen* from *Molecular Dimensions Ltd.* (Newmarket, UK) was set up in the vapour diffusion technique. The wells of an *EasyXtal* plate were filled with 500 µl of reservoir solution (0.01 % (w/v) sodium/potassium phosphate, 0.55 M sodium acetate, 0.75 M HEPES, pH 6.3). The sponge phase (1 µl) was pipetted to the corresponding lids, and 1 µl of protein solution was added without mixing. The plates were sealed and stored at 21 °C.

#### 4.8.5.2 Microseeding

Microseeding was performed for wild type AtETR1 with *Hampton's Seed Bead™* kit. A crystal obtained from a microbatch experiment with buffer TPN was transferred to a 1.5 ml reaction tube prepared with 50 µl of AtETR1 (1 mg/ml in buffer TPN) and a PTFE bead. The crystal was sonicated twice for one minute, and another 450 µl of protein solution were added. This stock solution was diluted five times in a 1:10 ratio with buffer TPN, and new microbatch trials were set up with 2 µl drops for every dilution. Plates were incubated at 4 °C and 20 °C.

**Buffer TPN**, pH 8.5: 100 mM Tris/HCl, 11 % (w/v) PEG 1500, 0.5 % (w/v) sodium cholate

#### 4.8.5.3 Reductive methylation of proteins

Reductive methylation of lysine residues is used to alter the crystallisation properties of proteins<sup>[79, 80]</sup>. Wild type AtETR1<sub>165-738</sub> was prepared according to section 4.7.2, and the buffer was exchanged to buffer HN by a 0.5 ml *Zeba Desalt Column* from *Pierce/Thermo Fisher Scientific (Bonn)*. The protein concentration was adjusted to 1 mg/ml, and 20 µl of ABC solution as well as 400 µl of 1 M formaldehyde were added per ml protein solution and incubated at 4 °C for two hours. This step was repeated once. Finally, 100 µl ABC solution were applied per ml protein solution and incubation was continued o/n. The supernatant was collected after centrifugation at 230,000 x g and 4 °C for 30 min, and a buffer exchange was performed into buffer TN by a *PD-10* column. The eluate was concentrated to 100 µl by ultra filtration (MWCO 30 kDa) and diluted once with buffer R4 in a ratio of 1:40. The protein solution was concentrated again to a final volume of 70-80 µl and centrifuged at 18,000 x g and 4 °C for 30 min.

**Buffer HN**, pH 7.5: 50 mM HEPES/NaOH, 250 mM NaCl

**Buffer TN**, pH 7.5: 20 mM Tris/HCl, 200 mM NaCl

**ABC solution**: 1 M dimethylamine-borane complex

**Buffer R4**, pH 8.2: 50 mM Tris/HCl, 10 mM NaCl, 1 mM KCl, 0.1 % (w/v) DDM, 0.002 % (w/v) PMSF

#### 4.8.5.4 Interpretation of crystallisation results

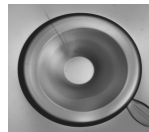

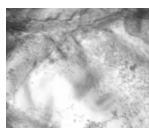
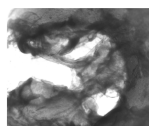
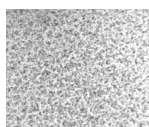

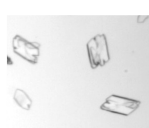
All crystallisation plates were examined using a stereomicroscope. A score was established for interpretation according to Table 15. The control intervals were chosen depending on the crystallisation method. Due to the nature of the screen, plates from sponge phase crystallisation experiments were observed on a weekly basis for the first four weeks, and then a monthly cycle was chosen. Crystallisation experiments from vapour diffusion or microbatch techniques were examined in shorter intervals of several days during the first month as equilibration in these setups occurred more quickly.


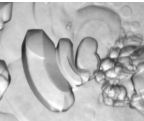
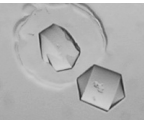
When crystals appeared, they were probed for protein or salt. The simplest yet most invasive method was to test the crystal texture with a thin needle: While salt crystals appear hard and will break with an audible cracking sound, protein crystal have a very soft texture and will not split but rather smear when probed with the needle. However, this method will definitely destroy the crystal, and it is therefore only useful when several crystals were grown at the condition tested. In a more sophisticated approach, diffraction characteristics of potential protein crystals were tested by X-ray diffraction analysis as described in 4.8.5.6.

Crystals were also analysed by SDS-PAGE. A crystal was washed three times in the same buffer that was used for crystallisation and was finally transferred to 5 µl 4x loading buffer. Extensive washing was necessary to remove any remaining protein solution from the crystal to avoid false positive results. SDS-PAGE and silver staining was carried out as described earlier (see 4.4.2 and 4.4.3).

The first two methods will only discriminate whether a crystal is protein or salt. But SDS-PAGE analysis will also give information on the protein composition. This might be of special interest when the protein to be crystallised consists of different subunits.

Table 15: Classification of crystallisation experiments.

<i>Description</i>	<i>Examples</i>
Clear drop	
Upon <u>phase separation</u> small droplets of highly concentrated protein form within the aqueous phase. This typically occurs when organic additives, such as PEG, are added to a solution containing high salt concentrations.	
<u>Skin</u> is a form of precipitate that builds a layer between crystallisation drops and oil in the microbatch technique.	
<u>Precipitate</u> can appear with a white to brownish colour. While light precipitate might redissolve and promote nucleation, dark, amorphous precipitate usually represents denatured protein.	
Non-amorphous <u>crystalline precipitate</u> can act as a precursor to crystals.	
<u>Spherulites</u> show radial pattern formation, sometimes appearing as droplets or clusters.	
<u>Plates</u> result from crystal growth in two dimensions. These rather thin crystals often occur in a stacked form.	

<i>Description</i>	<i>Examples</i>
When crystal growth is favoured in only one dimension, <u>needles</u> may form and build clusters.	
<u>Amorphous crystals</u> are three dimensional structures that show poor symmetry and contain sharp edges as well as spherical parts.	
Three dimensional <u>crystals</u> show a high degree of internal order that can be described by symmetry operations. These structures show sharp edges in all dimensions.	

#### 4.8.5.5 Freezing and storage of protein crystals

For transport and storage crystals, were harvested with nylon loops or meshes mounted to magnetic caps and flash frozen in liquid nitrogen. The caps were covered with a plastic vial to avoid uncontrolled contact with the crystal and were stored in liquid nitrogen.

If necessary, crystals were transferred to buffers with cryoprotectants prior to freezing to prevent damage arising from dehydration as well as radiation damage upon exposure to X-rays. The composition of these cryobuffers is specified in the corresponding result section.

#### 4.8.5.6 Collecting diffraction data

Screening for crystals suitable for structure solution was performed at beamlines *X11* and *X12* at the *European Molecular Biology Laboratory (EMBL)*, *Hamburg* as well as beamlines *ID 23-1*, *ID 23-2*, *ID 14-1* and *ID 14-2* at the *European Synchrotron Radiation Facility (ERSF)* in *Grenoble*, France. Crystals obtained from initial screenings were also tested with in-house *Bruker AXS* diffractometer system at a temperature of 100 K.

---

#### 4.8.6 Bioinformatics methods and software tools

- Sequence similarity searches were performed with *BLAST* algorithm<sup>[81]</sup> accessing databases *UniProtKB*<sup>[82, 83]</sup> and *NCBI's* non-redundant protein sequence database.
- For multiple alignments of protein and nucleotide sequences, *ClustalW*<sup>[84]</sup>, *ClustalW2*<sup>[85]</sup>, *MultAlin*<sup>[86]</sup> and *COBALT*<sup>[87]</sup> were used. Alignments were visualised with *Jalview 2.6*<sup>[88]</sup>.
- Translation of nucleotide sequences was done with *Translate*. For computing physico-chemical properties of a protein, the program *ProtParam* was used. Potential cleavage sites for proteases were identified with *PeptideCutter*. All three programs are part of *ExPASy's* proteomics tools<sup>[70]</sup>.
- Vector maps were created using the web server *PlasMapper Version 2.0*<sup>[89]</sup>
- Fluorescence spectra were processed and analysed with *FL WinLab*<sup>TM</sup> software from *PerkinElmer (Rodgau)*
- Molecular graphics images of protein structures deposited at the protein database *RCSB PDB* ([www.pdb.org](http://www.pdb.org)) were produced with the *UCSF Chimera* package<sup>[90]</sup>.





## 5 Part A: Functional studies on ethylene receptor ETR1 from *A. thaliana*

*In vitro* kinase activity of ETR1 from *Arabidopsis thaliana* was first demonstrated for the recombinant extramembrane domain of the receptor. In 1998, *Gamble et al.* showed incorporation of  $^{32}\text{P}$  phosphate into the soluble histidine kinase domain of ETR1<sup>[32]</sup>.

Ten years later *Groth* and *Voet van Vormizeele* extended the autoradiographic assay for the full-length receptor and demonstrated effects of ethylene, cyanide and the antagonist 1-methylcyclopropene, which are proposed to bind in the transmembrane domain of ETR1<sup>[33]</sup>.

However, the applied technique exhibits several disadvantages. The method combines multiple working steps: the initial enzyme assay, followed by SDS-PAGE analysis and western blotting. With every step, error-proneness is increased. Hence, a single step assay would be preferable. Furthermore, the method leaves radioactive waste to dispose of, a fact that should also be considered. Another major drawback is that exact densitometric analysis of an autoradiographic image is complicate due to diffuse protein bands, often characteristic for membrane proteins<sup>[91]</sup>.

Figure 10 shows the results of a phosphorylation assay performed with full-length receptor

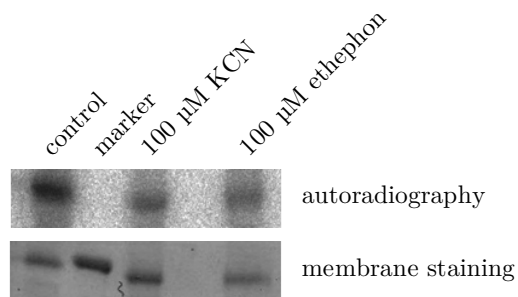


Figure 10: Phosphorylation assay with AtETR1 showing incorporation of  $^{32}\text{P}$  phosphate into the receptor protein (signals in autoradiography). The control refers to the standard assay without potassium cyanide and ethephon. Staining of the transfer membrane with *Ponceau S* (lower figure) identified equal amounts of protein in each lane and visualised a protein band (75 kDa) from the protein marker.

AtETR1. The left lane in the autoradiographic image displays a signal from  $^{32}\text{P}$  phosphate bound to the receptor protein. The middle and the right lane depict effects of cyanide and ethephon\*. Qualitatively, the signals appear weaker, but due to the shape of the spots and the background intensity, it is difficult to perform highly accurate densitometric analysis.

However, the autoradiographic assay is still applied as a more exact measuring system is not available yet. For that reason, an improved, fluorescence-based system should be developed in the first part of this thesis. In this new approach

\* Ethylene is highly volatile and was therefore replaced by potassium cyanide and ethephon in phosphorylation assays with receptor protein ETR1. Potassium cyanide has been suggested to interact with the ethylene signalling pathway as it can induce ethylene responses *in planta*<sup>[92-94]</sup>. Ethephon is a chemical compound that releases ethylene, phosphate and a chloride ion in an aqueous solution above pH 4.

ligand binding and phosphorylation events should be determined by monitoring changes in fluorescence intensity.

## 5.1 Intrinsic tryptophan fluorescence to resolve ligand binding and conformational changes in ETR1

When electrons are excited to a higher quantum state ( $S_1$  or  $S_{x>1}$ ) and subsequently relax to their ground state ( $S_0$ ), energy will be emitted in form of light or heat between the lowest vibration level of  $S_1$  and the ground state (Figure 11). In fluorescence, the relaxation process involves both, emission of heat (vibration) and light. Therefore, the wavelength of the emitted light is longer and less energetic.

The transition between individual states as well as the intensity of fluorescence can be influenced by several interactions. So-called quenching is characterised by a decrease in fluorescence intensity. In collision (dynamic) quenching, a molecule (the quencher) absorbs energy from the excited fluorophore upon contact before relaxation and emittance of light from the fluorophore can occur. Depending on size and electronic properties of quencher and fluorophore, the intensity of emitted light is either decreased or annihilated. Apart from collision quenching, static quenching can also occur. Here, the fluorophore and the quencher form a non-fluorescent complex during the ground state  $S_0$  preventing excitation of the fluorophore.

The latter effect is utilised to determine interactions between the target protein, the fluorophore, and putative ligands that might bind to the protein affecting its fluorescence properties<sup>[95]</sup>.

Another mechanism that is accompanied by a loss of fluorescence intensity is resonance energy transfer (RET). This occurs when the

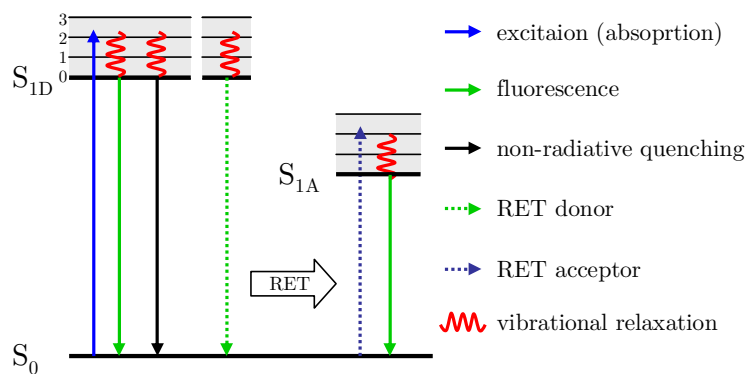


Figure 11: Jablonski diagram showing different relaxation modes after excitation. By absorption of energy a fluorophore is excited from the ground state ( $S_0$ ) to a higher vibration energy level (0 to 3 in the scheme) of state  $S_{1D}$ . Due to vibration, the fluorophore relaxes to the lowest energy level in state  $S_1$ . Starting here, further relaxation can be achieved by fluorescence or non-radiative quenching. It is also possible to transfer energy from a donor molecule to an acceptor molecule with a lower excitation state  $S_{1A}$ .

emission spectrum of one fluorophore (the donor) overlaps with the excitation wavelength for a second fluorophore (the acceptor). Energy transfer does not require the emission of actual light from the donor. A non-radiative transfer is common when both molecules are in close proximity (30 to 60 Å)<sup>[96]</sup>.

In proteins, the three aromatic amino acids tryptophan, tyrosine and phenylalanine contribute to the UV fluorescence. Their absorption maxima in water occur at 258 nm (Phe), 275 nm (Tyr) and 280 nm (Trp). Typically, a wavelength in the range of 295-300 nm is chosen to selectively excite tryptophan<sup>[97]</sup>.

Tryptophan emission is affected by the surrounding environment, especially by the polarity of the solvent. Upon hydrogen bonding to the imino group a red shift in emission spectra can be observed indicating the solvent exposure of the amino acid<sup>[98]</sup>.

This parameter is used to detect conformational changes in proteins upon folding process or binding interactions with other proteins or DNA. The method was used, for example, to show binding of calmodulin to a human neuronal receptor peptide and interactions of the *E. coli* single-stranded binding protein (SSB) with DNA<sup>[99, 100]</sup>.

#### 5.1.1 Cloning of single tryptophan substitution mutants

In the transmembrane domain of AtETR1 two residues have been identified to be involved in ethylene binding. C65 and H69 may form a hydrophobic pocket and coordinate a copper ion ( $\text{Cu}^+$ ) that is supposed to mediate binding of the gaseous molecule ethylene<sup>[29]</sup>.

To examine binding characteristics for both, the hormone and the co-factor, single tryptophan residue were cloned into helices I and II of the tryptophan-free mutant AtETR1[W<sub>free</sub>]. The first two helices were chosen because *Wang et al.* have identified several residues by alanine scanning mutagenesis that seem to play an important role in ethylene perception. Substitution of these residues almost completely abolished ethylene binding in the respective mutants<sup>[30]</sup>.

*MEMSAT3* algorithm, which uses a neuronal network for scoring amino acids typically found in helices and the adjacent cap regions, was applied for topology analysis to create a schematic model of the first two helices (Figure 12)<sup>[101-103]</sup>.

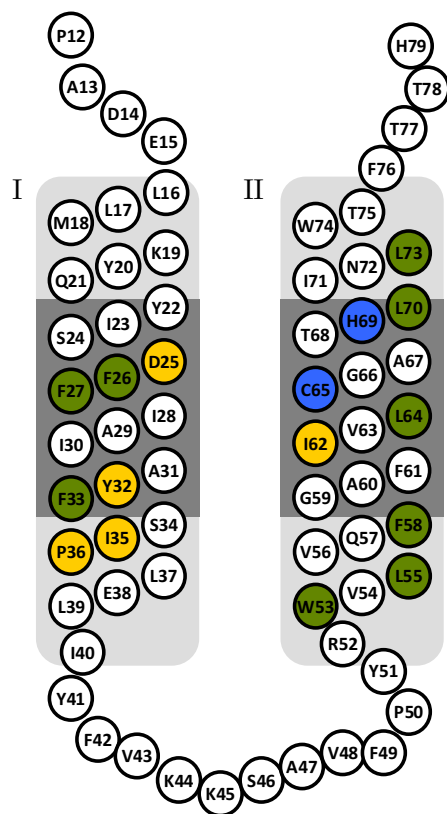


Figure 12: Topology model of transmembrane helices I and II of wild type AtETR1. Blue residues show amino acids necessary for coordination of  $\text{Cu}^+$  prior to ethylene binding. Yellow coloured amino acids were identified by alanine scanning mutagenesis to play an important role in binding of the hormone. The green residues were mutated to tryptophan, except for the naturally occurring W53. Core regions of predicted helices are in dark grey, cap regions are coloured in light grey.

Leucin and phenylalanine residues in close proximity of the identified amino acids were selected for tryptophan substitution because all three amino acids have hydrophobic side chains and are of similar size. Mutagenesis was carried out using the sequence and ligation independent cloning method as described in section 4.3.6.

In total, 9 mutants were created (F26W, F27W, F33W, L55W, F58W, L64W, L70W and L73W) including a receptor variant based on AtETR1[W53]. In this mutant both residues necessary for  $\text{Cu}^+$  coordination were replaced by alanine (C65A and H69A). Although mutants W53, L55W and F58W have no nearby residues in helix II that have been reported to be important for ethylene signalling they might be in contact with such residues from helix I (Y32, I35 and P36) if both helices are in close proximity (Figure 12).

Further mutants were created based on AtETR1[W<sub>free</sub>] to monitor the phosphorylation state of the receptor. These mutants contained single tryptophan residues in the kinase domain close to H353, which is suggested to be phosphorylated upon kinase activity<sup>[32]</sup>.

As no crystal structure is available for the soluble histidine kinase domain of AtETR1 yet, a homology

model was created to identify residues that might be suitable for mutagenesis. A *BLAST* search on structures deposit in the protein data base (PDB) with the sequence of the kinase domain of ETR1 (aa 350-585) from *A. thaliana* as query gave several hits for bacterial histidine kinase proteins<sup>[81]</sup>. The cytosolic part of a sensor histidine-kinase protein from *Thermotoga maritima* (PDB accession code: 2C2A) shares about 50 % sequence similarity over a range of 226 amino acids and was chosen for homology modelling with *Modeller/EasyModeller*<sup>[104-108]</sup>.

Figure 13 shows the calculated model for AtETR1. The putative phosphorylation site is located in the N-terminal helix. Together with the following helix, this domain might dimerise with a second monomer as it has been shown for the sensor histidine-kinase protein from *Thermotoga maritima*<sup>[109]</sup>. In consequence, *trans* phosphorylation of residue H353 might be possible upon dimerisation of AtETR1 if bound ATP and the phosphate acceptor histidine are brought in close proximity. However, a *cis* phosphorylation mechanism might also occur: There is a large loop adjacent to the two N-terminal helices that might pull these helices towards the C-terminal part upon a trigger, like binding of ATP in an induced fit mechanism. This is highly speculative and evidence for one or the other approach might be confirmed with a crystal structure of AtETR1 in different states of the phosphorylation process.

From the model, three residues were chosen for mutagenesis and were substituted by tryptophan including N352, which is next to H353, as well as V350 and R356, which are about one helix turn apart. These three mutants were also cloned as truncated receptor variants missing the transmembrane domain because heterologous expression and purification of truncated AtETR1 yielded about tenfold more protein on average (1 mg/g cells) compared to the full-length constructs (see chapter 5.1.2).

Additionally, mutants were cloned into AtETR1[N352W] with amino acid substitutions H353A and H353E. While the alanine mutant should represent a non-phosphorylatable protein, mutant H353E mimics a phosphorylated protein by providing a negative charge through its carboxyl group.

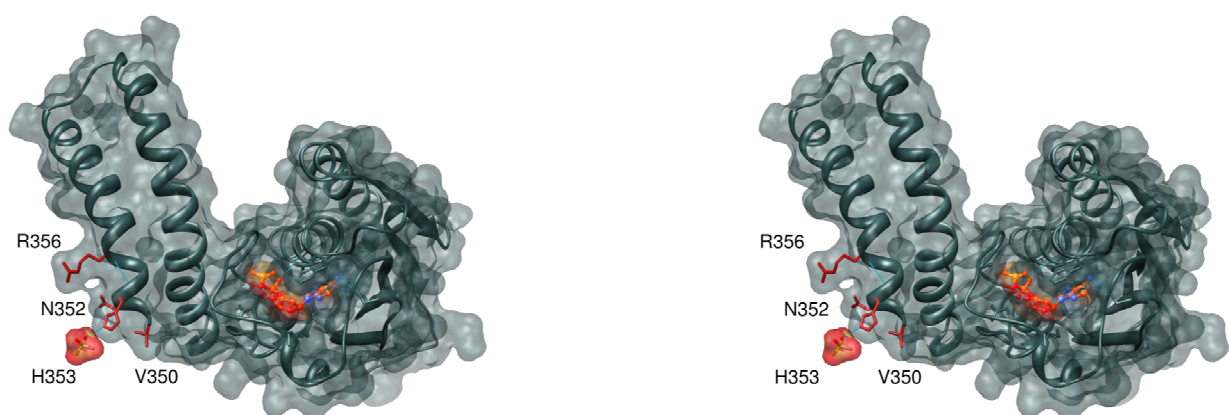


Figure 13: Cross-eye stereo image of the modelled kinase domain of AtETR1. The N-terminal part is comprised of two helices which are connected to the C-terminal part by a large loop. Bound ADP in the C-terminal part of the protein and phosphate bound to H353 were adopted from the template structure, a sensor histidine-kinase protein from *Thermotoga maritima* (PDB accession code: 2C2A) and are highlighted as ball and stick models. Residues selected for substitution mutagenesis as well as catalytic H353 are displayed in stick mode and coloured in dark red.

### 5.1.2 Expression and purification of recombinant ETR1

Wild type AtETR1 and mutant full-length receptor proteins were expressed in cells of bacterial strain C43 (DE3) as described in section 4.5.1. The proteins were purified by IMAC under denaturing conditions (8 M urea) and were subsequently refolded by dilution into an appropriate buffer (see 4.7.1.1). Individual purification steps of wild type AtETR1 are shown in Figure 14A.

Purification at denaturing conditions was necessary in order to remove contamination by the chaperon DnaK, which could not be removed from detergent solubilised AtETR1. The impact of this contamination will be discussed in detail in chapter 6.2.2.

Ethylene receptor proteins lacking the transmembrane domain—AtETR1<sub>165-738</sub> and mutant constructs—were expressed in BL21 (DE3) cells harbouring the additional plasmid pRARE, which encodes for rare *E. coli* t-RNAs (see 4.1.12). A denaturing strategy was chosen for purification (Figure 14B) as most protein was expressed in inclusion bodies<sup>[33]</sup>.

On average, about 0.1 mg purified full-length receptor protein was obtained per gram cells. Yields for the truncated constructs were about tenfold higher, an observance that is not unusual for membrane protein production. Due to highly hydrophobic membrane domains, these proteins are more difficult to handle in an aqueous environment such as the cytosol of bacterial host cells. Thereby, aggregation and degradation will occur and result in a lower overall protein yield.

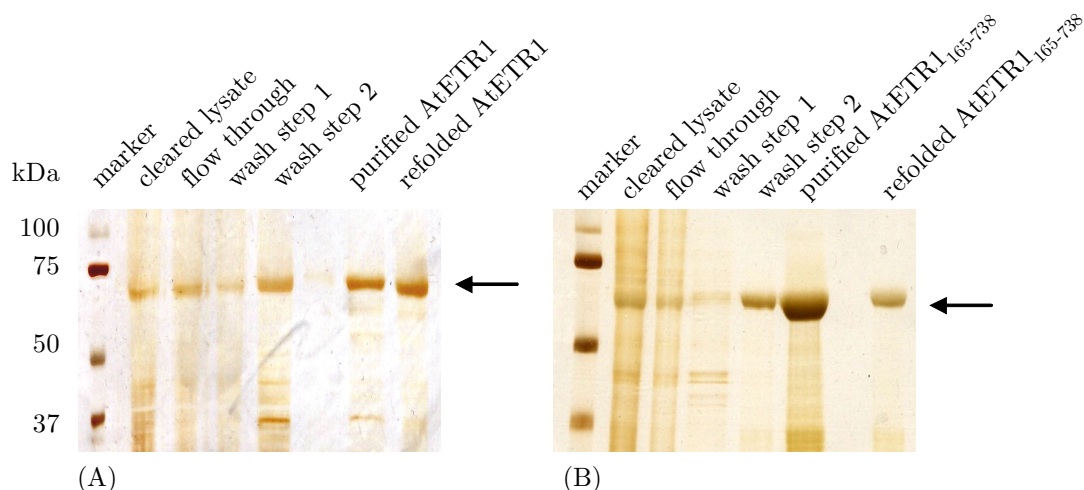


Figure 14: (A) Purification of wild type receptor protein AtETR1 (85 kDa) and (B) truncated AtETR1<sub>165-738</sub> (66 kDa). The proteins were solubilised in 8 M urea and the cleared lysates were applied to IMAC (Ni-NTA). Samples from the flow through fractions, wash steps 1 (no imidazole) and wash steps 2 (A: 50 mM imidazole, B: 30 mM imidazole) were analysed by SDS-PAGE. The right lanes in each gel show protein samples before and after refolding of the receptor constructs (indicated by arrow).

### 5.1.3 Characterisation of single tryptophan substitution mutants

Before the wild type and single tryptophan substitution mutants of AtETR1 were subjected to fluorescence studies, all proteins were tested for kinase activity to confirm that functionality was regained after refolding upon denaturing purification. Furthermore, all receptor proteins were analysed by CD spectroscopy. This characterisation should give estimation on the secondary structure composition and evaluate if amino acid substitutions caused changes or defects in the protein structure.

#### *5.1.3.1 Monitoring kinase activity by incorporation of $^{32}\text{P}$ phosphate*

Kinase activity of wild type and mutant receptor constructs was determined to check whether all proteins regained functionality after refolding. This assay was not performed with AtETR1[N352W/H353E] as this mutant could not be purified in sufficient amounts.

The kinase assay was performed according to methods section 4.8.1, and signals from  $^{32}\text{P}$  phosphate were densitometrically quantified. Figure 15 shows the effects of cyanide and ethephon on the kinase activity of each wild type and mutant receptor protein. For each protein the kinase assay was performed without the regulatory substances, and resulting activity was set to 100 % (internal reference, see black bars). For reasons of clarity, these reference activities are displayed only once for all full-length and truncated proteins.

Receptor variants comprising a transmembrane domain clearly showed a reduced activity upon treatment with cyanide (blue bars) and ethephon (green bars). Kinase activity is reduced to about 40 to 60 % in both cases. These effects were expected with exception of mutants AtETR1[W53/C65A/H69A] and AtETR1[N352W/H353A].

In the second mutant the putative phosphorylation site H353 is substituted by alanine. Thus, phosphorylation should be abolished in this mutant. However, this phenomenon has been observed before and might indicate alternative phosphorylation sites corresponding to serine, threonine or tyrosine residues<sup>[61]</sup>. In close proximity to H353 such residues can be found at position 357 (threonine) and 366/367 (serine).

In mutant AtETR1[W53/C65A/H69A] both amino acids that have been described to be essential for copper mediated ethylene binding are substituted by alanine. Hence, the observed inhibitory effects of potassium cyanide and ethylene in form of ethephon are surprising. However, copper binding might not exclusively depend on residues C65 and H69.

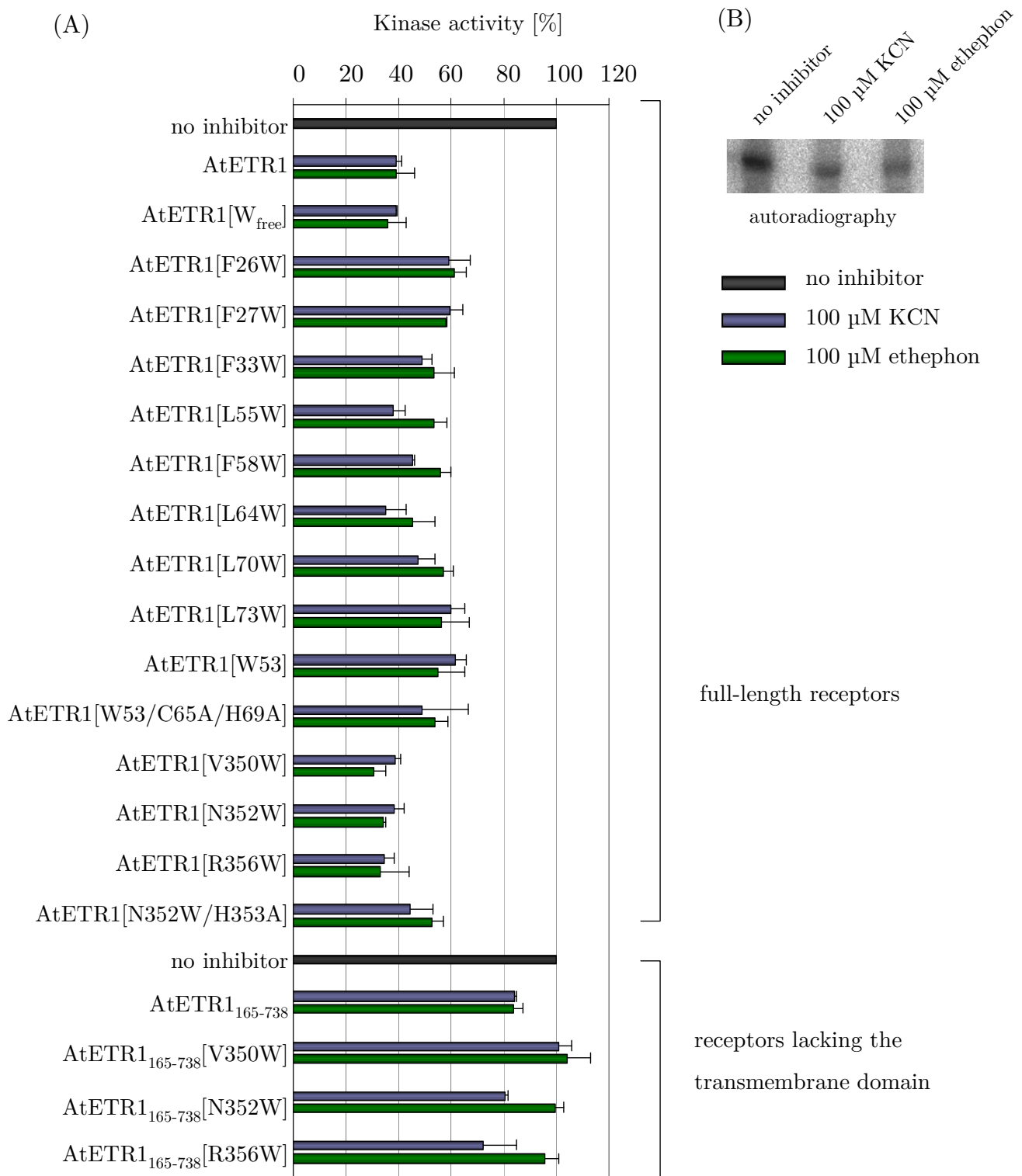


Figure 15: Monitoring kinase activity of full-length and truncated AtETR1 and mutant protein constructs by  $^{32}\text{P}$  assay. (A) shows inhibitory effects of cyanide and ethylene released from ethephon. All receptor proteins were additionally subjected to a phosphorylation assay without regulatory substances. Signals from  $^{32}\text{P}$  incorporation (B) were densitometrically quantified and results for the controls without ethephon or potassium cyanide were set to 100 % for each protein to allow for comparison of individual receptors. These references are shown once for each set of full-length and truncated receptors for reasons of clarity and thereby do not show error bars (mean error: 5 %). All measurements were performed in duplicate.



By alanine scanning, Wang *et al.*<sup>[30]</sup> have shown that further residues are conceivably involved in binding of the plant hormone including residues D25, Y32, I35, P36 and I62 (Figure 12, page 62). These amino acids are still present in mutant AtETR1[W53/C65A/H69A] and might favour binding of ethylene and agonistic cyanide.

The truncated receptor variants which are missing the ethylene binding domain showed nearly no effect upon treatment with both inhibitors as expected. Kinase activity was maintained between 80 to 100 % (Figure 15). These minor variations might be explained with the exactness of densitometric analysis as described in chapter 4.1.

In summary, all receptors showed incorporation of  $^{32}\text{P}_i$ . Full-length proteins even showed a reduced activity upon addition of ethephon and potassium cyanide indicating that refolding of the receptors was successfully.

#### 5.1.3.2 Secondary structure analysis by CD spectroscopy

CD spectra of all proteins were recorded over a range of 260-195 nm as described in section 4.8.2. Prior to measurement, proteins were diluted into 50 mM potassium phosphate buffer supplied with 0.05 % (w/v) DDM. Typically, low protein concentrations of 0.2 to 0.25 mg/ml were chosen to allow for measurements to 195 nm.

The CD spectra for full-length wild type AtETR1 and the tryptophan-less mutant AtETR1[W<sub>free</sub>] as well as for the truncated wild type AtETR1<sub>165-738</sub> are shown in Figure 16. The spectra for the both full-length constructs are almost identical and comprise the formation of secondary structure elements upon refolding. The CD spectrum of the ethylene receptor lacking the membrane domain is less distinct.

However, with the minimum at 209 nm and zero crossing between 200 and 201 nm, all spectra indicate a strong  $\alpha$ -helical content when compared to  $\alpha$ -helical reference peptides (minima at 208 and 222 nm, cross point at 202 nm)<sup>[110]</sup>. The fact that the second minimum at 222 nm is not very distinct might point to the influence of  $\beta$ -strands and random coil structures.

All spectra were processed with the software package *CDPro*<sup>[76]</sup> to give quantitative estimation on secondary structure composition of the tested receptors. *CDPro* comprises the three algorithms *CDSSTR*, *SELCON3* and *CONTIN*, which use reference sets of up to 48 proteins to estimate the secondary structure content of an unknown protein.

*PSIPRED*<sup>[110, 111]</sup> secondary structure prediction method was used to calculate theoretical values for  $\alpha$ -helices,  $\beta$ -strands and random coil structures based on the amino acid sequence of wild

type AtETR1 and AtETR1<sub>165-738</sub>. The algorithm uses neural networks to estimate secondary structure elements by analysing the output of position specific iterated *BLASTs*. In a similar strategy *BetaTPred2* was used to estimate  $\beta$ -turn elements in the protein structures<sup>[112]</sup>.

The first striking fact from the data in Table 16 is that experimental values for each set of full-length proteins and those missing the transmembrane domain are highly consistent and show a predominant  $\alpha$ -helical content. The only exception is mutant AtETR1[N352W/H353E], which should mimic a phosphorylated receptor protein.

In mutants based on the full-length receptor, the amount of  $\alpha$ -helices is

slightly increased by about 5 %. This result is in accordance to expectation as the N-terminal domain that is missing in constructs based on AtETR1<sub>165-738</sub> is comprised of three putative transmembrane helices. However, a clear disparity is apparent for the  $\alpha$ -helical content of both receptor populations obtained from experimental data and calculations with *PSIPRED*. Theoretical values are about 5 % higher for truncated receptor proteins and about 10 % for full-length constructs compared to the values calculated from experimental data.

The overall accuracy of the *PSIPRED* algorithm accounts for approximately 80 % as determined by a set of proteins with known crystal structure<sup>[110, 111]</sup>. However, accuracy varies for each secondary structure element. For example,  $\alpha$ -helices that show a strong and characteristic signal in circular dichroism can be estimated with an accuracy of more than 95 %. The CD spectrum of  $\beta$ -sheets and  $\beta$ -turns is weaker and depends on the length of respective structures. In consequence, accuracy for these elements accounts to 50 to 70 %<sup>[113, 114]</sup>.

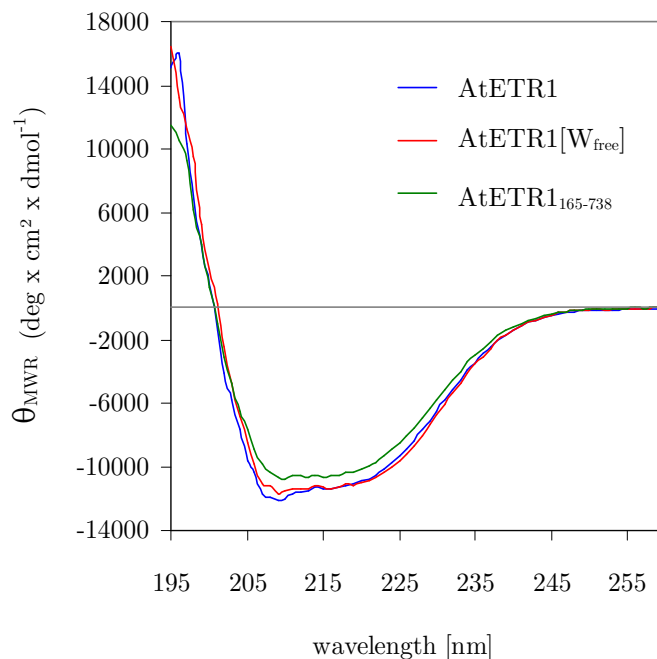


Figure 16: CD spectra obtained for the receptor proteins AtETR1, AtETR1[W<sub>free</sub>] and AtETR1<sub>165-738</sub>. Measured ellipticity (mdeg) was converted to mean residue weight ellipticity  $\Theta_{\text{MWR}}$  to allow for comparison of all spectra. For reasons of clarity, it was renounced to depict spectra of individual single tryptophan substitution mutants. However, secondary structure content of these mutants as calculated from the spectra is summarised in Table 16 (page 65).

Experimental data is subject to variation, too. Correct determination of the protein concentration is crucial for calculating  $\Theta_{\text{MWR}}$  (mean residue weight ellipticity), which is necessary for estimation of the secondary structure composition and comparison of individual CD spectra<sup>[115]</sup>. All spectra in this thesis were recorded in duplicate and were consistent ( $0.5 < \text{RMSD} < 4.2$ )\* over the range of 240 nm to 195 nm, which was used for secondary structure estimation by algorithms implemented in *CDPro*.

Table 16: Secondary structure composition of wild type and mutant AtETR1 and AtETR1<sub>165-738</sub> constructs as calculated from the amino acid sequence and from experimental data. All values are given in %.

<i>Protein</i>	<i>Data source</i>	<i><math>\alpha</math>-helices</i>	<i><math>\beta</math>-strands</i>	<i><math>\beta</math>-turn</i>	<i>Random coil</i>
AtETR1	theoretical	45 – 46	12 – 13	21 – 22	19 – 20
	experimental	34 – 36	17	19 – 21	28 – 29
AtETR1[W <sub>free</sub> ]	experimental	34 – 35	17 – 18	19 – 21	28 – 29
AtETR1[F26W]	experimental	34 – 36	17 – 18	18 – 21	28 – 29
AtETR1[F27W]	experimental	32 – 35	18 – 19	19 – 22	28 – 29
AtETR1[F33W]	experimental	33 – 36	17 – 18	19 – 21	28 – 29
AtETR1[L55W]	experimental	34 – 36	16 – 18	18 – 21	27 – 29
AtETR1[F58W]	experimental	36 – 37	15 – 18	18 – 20	27 – 28
AtETR1[L64W]	experimental	31 – 33	19 – 20	20 – 22	28 – 29
AtETR1[L70W]	experimental	31 – 34	18 – 19	20 – 22	28 – 29
AtETR1[L73W]	experimental	34 – 37	16 – 18	19 – 21	28 – 29
AtETR1[W53]	experimental	34 – 36	16 – 19	18 – 21	27 – 29
AtETR1[W53/C65A/H69A]	experimental	32 – 35	17 – 19	19 – 21	27 – 29
AtETR1[V350W]	experimental	33 – 35	16 – 19	19 – 21	27 – 29
AtETR1[N352W]	experimental	35 – 36	16 – 18	18 – 21	27 – 29
AtETR1[R356W]	experimental	35 – 37	16 – 18	18 – 21	27 – 29
AtETR1[N352W/H353A]	experimental	30 – 32	19 – 21	19 – 22	28
AtETR1[N352W/H353E]	experimental	6 – 22	18 – 41	16 – 22	27 – 33
AtETR1 <sub>165-738</sub>	theoretical	36	16	23 – 24	23 – 24
	experimental	28 – 31	21	20 – 22	29
AtETR1 <sub>165-738</sub> [V350W]	experimental	28 – 31	20 – 21	20 – 23	28 – 30
AtETR1 <sub>165-738</sub> [N352W]	experimental	29 – 32	19 – 21	19 – 22	29
AtETR1 <sub>165-738</sub> [R356W]	experimental	28 – 31	19 – 23	20 – 22	28 – 29
range	0 – 10 %	11 – 20 %	21 – 30 %	31 – 40 %	41 – 50 %

\* Equation for calculation of root mean square deviation: 
$$\text{RMSD} = \sqrt{\frac{\sum_{i=1}^n (x_{1,i} - x_{2,i})^2}{n}}$$

However, the high correlation of experimental data indicates that all receptors are folded in a similar way and allows for the assumption that they probably hold a native structure as kinase activity was observed for these proteins (see previous chapter). If misfolding occurred, it might be supposed that individual proteins exhibit individual structures, and data obtained are expected to show high variation.

There is only one mutant showing a complete different secondary structure composition: Receptor protein AtETR1[N352W/H353E] has a much reduced  $\alpha$ -helical content of only 6 to 22 % depending on the algorithm used. It was further observed that this mutant yielded hardly any protein after purification ( $< 0.05$  mg/g cells). Hence, it is reasonable to assume that aggregation of misfolded protein has occurred.

First interpretation of the AtETR1[N352W/H353E] CD data was that the introduction of a negative charge disturbs proper folding of the mutant protein. All other mutations affected large but non-charged residues (leucine, phenylalanine and tryptophan). Thus, it might be possible that this unique substitution altered the structure of the receptor remarkably. Assuming that phosphorylation is coupled to a conformational change, it might be possible that this pseudo-phosphorylated state cannot fold from scratch but requires a correctly folded un-phosphorylated protein as a starting point. It is most obvious that this information gets lost during the denaturing purification.

However, interim published data of a mutant receptor with the single H353E substitution showed no conformational difference compared to the wild type protein as determined by CD spectroscopy<sup>[116]</sup>. For that reason, it is rather likely that mutagenesis of the two adjacent amino acids caused structural defects due to steric disorder.

## 5.2 Ligand binding to ethylene receptor ETR1

### 5.2.1 Binding of copper cofactor and ethylene

Mutant receptor proteins of AtETR1 that carry single tryptophan residues in close proximity to the putative ethylene binding site (C65 and H69) were subjected to fluorescence measurements to probe for binding of the copper cofactor and the plant hormone ethylene. Measurements were performed as described in section 4.8.3.1. The receptor proteins were pre-incubated with 100  $\mu$ M copper(II) chloride for 10 min\*. In samples testing ethylene binding, the plant growth substance ethephon was added at a final concentration of 100  $\mu$ M and incubation was continued for further 10 min. With these incubation steps the setup was identical to the activity assay with  $^{32}$ P-ATP, except no nucleotide was added here. A concentration of 100  $\mu$ M ethephon was chosen because it decreased receptor activity to about 40 to 60 % as determined by the autoradiography assay (see 5.1.3.1).

All samples were measured with a fluorescence spectrometer. Tryptophan residues were selectively excited at 295 nm. Emission spectra were recorded over a range of 310-400 nm, and the emission maximum was found at 348 nm. For each receptor, control samples were set up containing only the protein. Fluorescence intensities of these references were set to 100 % for each protein, and corresponding samples containing copper(II) chloride and/or ethephon were referred to the individual basis fluorescence intensity.

Figure 17 shows effects of treatment with copper(II) and ethephon on the fluorescence intensity of the receptor proteins. Noticeably, upon incubation with the metal ion, the fluorescence intensity decreased to about 70 to 80 % in all cases (blue bars). In contrast, upon treatment with just ethephon (orange bars), fluorescence intensity was maintained at almost 100 % compared to samples that contained only the receptor protein (black bar). When ethephon was applied after treatment with copper(II), no distinct quenching effect was observed (green bars). Minor changes were detected within the error range, except for mutant AtETR1[L70W], which showed a further slight decrease of 5 % in its fluorescence intensity (blue circle in Figure 17).

---

\* Coordination of a copper ion is necessary for binding of ethylene binding in ETR1. Typically copper(I) is described in literature. However, *Kikuchi et al.* detected copper(II) in the binding domain by X-ray absorption spectroscopy and *Rodríguez et al.* successfully applied copper(II) sulfate in their *in vitro* binding studies<sup>[29, 117]</sup>. Because copper(I) chloride is hardly soluble in water, it was replaced by copper(II) chloride throughout the complete study.

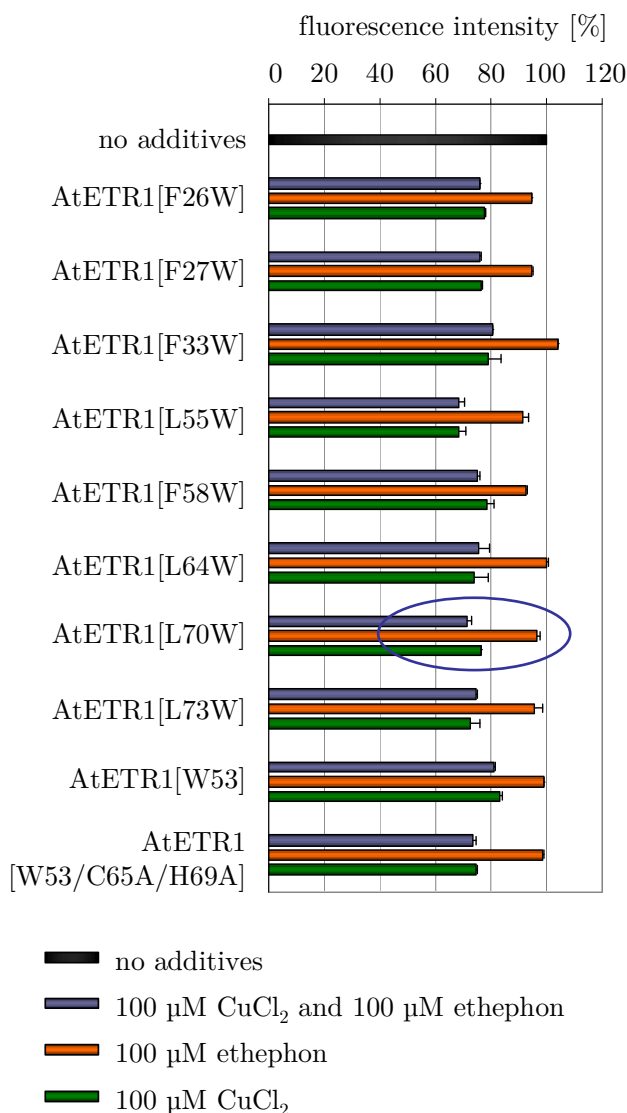


Figure 17: Fluorescence intensity measurements at 348 nm emission wavelength with mutant AtETR1 proteins. Changes in fluorescence intensity upon incubation with 100 μM copper (II) chloride (green bars) and/or ethephon (blue and orange bars) were determined and correlated to each internal reference (protein without additives and with fluorescence intensity at 348 nm set to 100 %). Note that these references are not given for each protein for reasons of clarity, but a representative bar is depicted once on top of the figure (black bar). Effects of copper(II) chloride and ethephon on mutant AtETR1[L70W] are highlighted by a blue circle.

Measurements were performed in duplicate for F26W, F27W, F33W and W53. All other mutants were measured in triplicate.

It cannot be stated which type of quenching is induced by the metal ion. Binding of copper(II) might trigger the formation of a non-fluorescent complex like in static quenching. A conformational change in the mutant receptor proteins could also be induced by binding of the metal ion and might alter the solvent exposition of the tryptophan probes. Such change in environment can either be displayed by a wavelength shift of the absorption maximum—which was not observed—or by an increase or decrease in fluorescence intensity.

The minimal change in fluorescence intensity that was observed for mutant AtETR1[L70W] might be due to a ligand induced conformational change. However, fluorescence changes in this order will not be suitable for concentration dependent measurements. Nevertheless, mutant receptor AtETR1[L70W] might be used to qualitatively test binding of potential plant growth substances in principle.

For the other mutants, no additional quenching effect was observed after treatment with ethephon and copper(II). This might indicate that the tryptophan probes were not placed correctly to monitor conformational changes. Alternatively,

the effect by copper(II) might be stronger than that for ethephon, thereby masking any further changes in fluorescence intensity. This would also explain why the effect of ethephon was only minimal for mutant AtETR1[L70W].

The observed quenching effect for mutant AtETR1[W53/C65A/H69A] is surprising but might be explained with the cofactor and the plant hormone binding to the receptor at sites other than the postulated C65-H69 site. This assumption is based on the results of *Wang et al.* who identified further residues involved ethylene binding as described in the previous chapter<sup>[30]</sup>. To further investigate the observed quenching effect, mutant AtETR1[W53/C65A/H69A] was used in titration studies with copper(II). The results will be discussed in section 5.2.2.

The copper ion could also target the His-tag, which is carried by all recombinant proteins in this study. With the N-terminal tag being a flexible structure, it could come close to helices I and II with their respective tryptophan residues and affect their fluorescence characteristics. Fluorescence measurements were repeated with tag-free mutant AtETR1[L70W]-TEV to determine the impact of the affinity tag and to rule out that the observed reduction in fluorescence intensity was due to static quenching caused by copper binding to the His-tag (see chapter 5.2.3).

In summary, the fluorescence measurements revealed interaction of copper(II) with the receptor proteins. Although it remains unclear by what quenching mechanism the observed decrease in fluorescence intensity was induced. The anticipated monitoring of ethylene binding to a mutant AtETR1 was only partially accomplished: Only one mutant, AtETR1[L70W], was identified to show a second minor change in its fluorescence intensity after treatment with ethephon. Because the effect is only minimal (5 %) quantitative binding studies will not be possible, but the mutant might be used to reflect binding of further potential regulatory substances in principle.

### 5.2.2 Characterisation of the quenching effect

As outlined in the previous chapter the mutant receptor protein AtETR1[W53/C65A/H69A] showed a quench in fluorescence intensity upon treatment with copper(II). This observance was contrary to expectation as the amino acids necessary for complexation of the metal ion were replaced in this mutant. For that reason, mutants AtETR1[W53/C65A/H69A] and AtETR1[W53] were both titrated with copper(II) chloride over a range of 0,5  $\mu\text{M}$  to 5 mM to evaluate if the monitored changes in fluorescence intensity were due to collisional or static quenching (see methods section 4.8.3.3).

The *Stern-Volmer* plot in Figure 18 shows the correlation of changes in fluorescence and the concentration of the quencher copper(II) chloride. Both, collisional and static quenching can be described by the *Stern-Volmer* equation:

$$\frac{F_0}{F} = 1 + K_{SV}[Q] \quad (\text{Eq. 2})$$

$$K_{SV} = k_q \tau_0 \quad (\text{Eq. 3})$$

Here,  $F_0$  and  $F$  are the fluorescence intensities in the absence and the presence of the quencher  $Q$ , with  $K_{SV}$  being the quenching constant ( $K_{SV}$  will be replaced by  $K_D$  for collisional/dynamic quenching and  $K_S$  for static quenching). The quenching constant is composed of  $k_q$ , the bimolecular quenching constant, and  $\tau_0$  that represents the lifetime of the fluorophore in absence of the quencher.

If only one type of quenching occurs, the *Stern-Volmer* plot will describe a linear correlation of quencher concentration and  $F_0/F$ . To distinguish between static and dynamic quenching, it is necessary to determine the lifetime of the fluorophore: The lifetime dependence on quencher concentration will be constant in static quenching as quencher and fluorophore build a non-fluorescent complex, thereby decreasing the number of excitable fluorophores. In dynamic quenching, the lifetime will be reduced due to energy transfer upon collision of quencher and fluorophore.

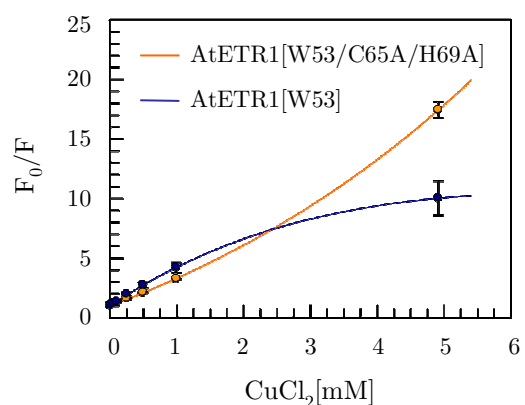


Figure 18: *Stern-Volmer* plot showing copper(II) quenching on receptors AtETR1[W53] (blue) and AtETR1[W53/C65A/H69A] (orange).



The correlation of copper(II) concentration and fluorescence intensity changes for mutant AtETR1[W53/C65A/H69A] describes a concave curve ( $\chi^2_{\text{red}} = 0.05$ ) that indicates combined dynamic and static quenching (orange curve in Figure 18)\*. Actually, no static quenching was expected for this mutant due to fact that the residues necessary for copper binding are substituted by alanine (see chapter 5.2.1). In accordance, *Stern-Volmer* constants  $K_D$  and  $K_S$  reveal predominantly dynamic quenching ( $K_D = 1.9 \pm 0.2 \text{ nM}^{-1}$ ,  $K_S = 0.13 \pm 0.03 \text{ nM}^{-1}$ ).

Complexion of copper (II) by the affinity tag might be in charge of the observed weak static quench. Furthermore, based on the topology model (Figure 12, page 62), in close proximity of residue W53 there are several residues (D25, Y32, I35, P36 and I6) that have been shown to be involved in ethylene binding, too. Those amino acids were not substituted in the mutant, so it might be possible that the metal ion was trapped in the binding site by these residues causing a static quench upon titration with copper(II) chloride.

Data for mutant AtETR1[W53] were also fitted on the assumption that the fluorophore is quenched statically and dynamically. However, the hyperbolic *Stern-Volmer* plot ( $\chi^2_{\text{red}} = 0.35$ ) as well as the negative constant  $K_S$  ( $-0.10 \pm 0.02 \text{ nM}^{-1}$ ) indicated the existence of two populations of fluorophores that are not equally exposed to the quencher (see blue curve in Figure 18). For that reason, a modified *Stern-Volmer* equation was used to estimate the amount of each fluorophore population and their respective *Stern-Volmer* constants for static and dynamic quenching.

With two populations of fluorophores ( $a$  and  $b$ ), the total fluorescence in absence ( $F_0$ ) and presence ( $F$ ) of the quencher is composed of

$$F_0 = F_{0a} + F_{0b} \quad (\text{Eq. 4})$$

$$F = F_a + F_b \quad (\text{Eq. 5})$$

The fraction  $f$  of each fluorophore population ( $f_a$  and  $f_b$ ) contributing the this initial fluorescence is given by

$$f_{a,b} = \frac{F_{0a,b}}{F_0} = \frac{F_{0a,b}}{F_{0a} + F_{0b}} \quad (\text{Eq. 6}) \quad \text{and} \quad F_{0a,b} = f_{a,b} \cdot F_0 \quad (\text{Eq. 7})$$

---

\* Data were fitted on the assumption of one fluorophore being quenched both, statically and dynamically:

$\frac{F_0}{F} = (1 + K_D[Q])(1 + K_S[Q])$  with  $F_0$  and  $F$  being the fluorescence intensities in absence and presence of the quencher  $Q$  and  $K_D$  and  $K_S$  being the quencher constants for dynamic and static quenching. The reduced chi-squared ( $\chi^2_{\text{red}}$ ) is given by  $\chi^2$  divided by the number of degrees of freedom that is defined by the number of data points minus the number of variables in the equation.

Combined dynamic and static quenching for one population is given by

$$\frac{F_0}{F} = (1 + K_D [Q])(1 + K_S [Q]) \quad (\text{Eq. 8})$$

where  $K_D$  and  $K_S$  are the quencher constants for dynamic and static quenching and  $Q$  is the quencher concentration. Rearrangement of this equation describes the initial fluorescence intensity

$$F_0 = (1 + K_D [Q])(1 + K_S [Q]) \cdot F \quad (\text{Eq. 9})$$

Combined with equation 4, the initial fluorescence intensity  $F_0$  for two populations  $a$  and  $b$  is given by

$$F_0 = (1 + K_{Da} [Q])(1 + K_{Sa} [Q]) \cdot F_a + (1 + K_{Db} [Q])(1 + K_{Sb} [Q]) \cdot F_b \quad (\text{Eq. 10})$$

In consequence of equation 5 and 9, the overall observed fluorescence  $F$ , as sum of  $F_a$  and  $F_b$  is described by

$$F = \frac{F_{0a}}{(1 + K_{Da} [Q])(1 + K_{Sa} [Q])} + \frac{F_{0b}}{(1 + K_{Db} [Q])(1 + K_{Sb} [Q])} \quad (\text{Eq. 11})$$

Subtraction of the total observed fluorescence  $F$  in presence of the quencher (equation 11) from the total initial intensity  $F_0$  (equation 4) yields  $\Delta F$ , the actual difference in fluorescence intensity

$$\Delta F = F_0 - F = \left(1 - \frac{1}{(1 + K_{Da} [Q])(1 + K_{Sa} [Q])}\right) \cdot F_{0a} + \left(1 - \frac{1}{(1 + K_{Db} [Q])(1 + K_{Sb} [Q])}\right) \cdot F_{0b} \quad (\text{Eq. 12})$$

Substituting  $F_{0a}$  and  $F_{0b}$  by equation 7 finally yields

$$\frac{\Delta F}{F_0} = \left(1 - \frac{1}{(1 + K_{Da} [Q])(1 + K_{Sa} [Q])}\right) \cdot f_a + \left(1 - \frac{1}{(1 + K_{Db} [Q])(1 + K_{Sb} [Q])}\right) \cdot f_b \quad (\text{Eq. 13})$$

With  $f_b = 1 - f_a$  equation 14 is given

$$\frac{\Delta F}{F_0} = \left(1 - \frac{1}{(1 + K_{Da} [Q])(1 + K_{Sa} [Q])}\right) \cdot f_a + \left(1 - \frac{1}{(1 + K_{Db} [Q])(1 + K_{Sb} [Q])}\right) \cdot (1 - f_a) \quad (\text{Eq. 14})$$

Data for mutant receptor protein AtETR1[W53] were fitted according to equation 14 and are shown in Figure 19. The curve-fitting on the assumption of two populations of fluorophores being quenched statically and dynamically yielded a slightly improved  $\chi^2_{\text{red}}$  of 0.0007 compared to the fit considering only one fluorophore population\* ( $\chi^2_{\text{red}} = 0.004$ ). The difference between the goodness of both fits is not distinct enough to confirm one or two fluorophore populations.

However, although AtETR1[W53] holds only one tryptophan residue, it is possible that two

populations of fluorophores are present. These fluorophores could be minor contamination or degradation products not detectable by SDS-PAGE analysis. The two populations could also represent different conformations of AtETR1[W53] as a result from copper(II) binding: One fraction might correspond to protein that is loaded with the metal ion while the other fraction is not. Upon binding of copper(II) a conformational change might alter the solvent exposition of residue W53 that could be reflected in a change of its fluorescence intensity.

Furthermore, it is possible that upon excitation at 295 nm deprotonated tyrosines (tyrosinates) are excited in addition to the single tryptophan. Those residues show excitation and emission characteristic such as tryptophans (absorption maximum at 295 nm, emission maximum at 345 nm) and might thereby contribute to the observed fluorescence<sup>[118, 119]</sup>. Side chains like aspartate and glutamate residues can act as proton acceptors at neutral pH and favour the formation of tyrosinates<sup>[120]</sup>. Also the alkaline pH of 8.0 of the medium might have promoted deprotonation of tyrosine residues. Although the quantum yield of tyrosinates is about tenfold lower than that of tryptophans ( $\Phi_{\text{F(Tyr)}} = 0.015$  compared to  $\Phi_{\text{F(Trp)}} = 0.14$ , at neutral pH), tyrosinate fluorescence has been reported for tryptophan-free proteins<sup>[96, 121-123]</sup>. In mutant AtETR1[W53] the copper ion is supposed to be complexed by C65 and H69. Assuming that helices I and II are in close proximity of each other, residues Y20, Y22 and Y32 (see Figure 12, page 62) are possible candidates to form tyrosinates. Their fluorescence might be affected upon binding of copper(II) to C65 and H69 resulting in a static quench of the fluorescence.

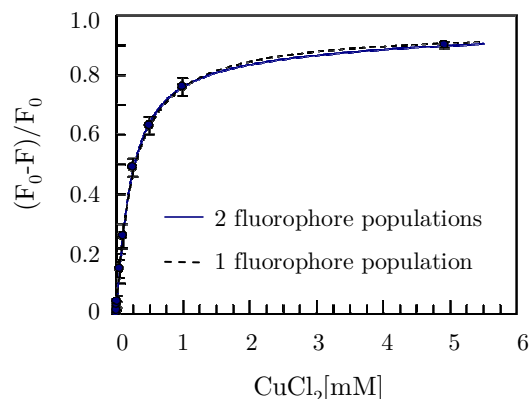


Figure 19: Modified *Stern-Volmer* plot showing copper(II) quenching for AtETR1[W53]. Data were fitted on the assumption of one ( $\chi^2_{\text{red}}=0.004$ ) or two ( $\chi^2_{\text{red}}=0.0007$ ) populations of fluorophores being quenched statically and dynamically (equation 14).

\* Data were fitted with equation 14 considering only one population of fluorophores ( $f_a=0$ ).

The collisional quench that was observed for both mutants is probably owed to the localisation of residue W53 in the cap region of helix II where it is probably exposed to the solvent and soluble quenchers.

### 5.2.3 Effect of His-tag on copper binding

In order to remove the N-terminal His-tag after purification of AtETR1[L70W] a new construct containing a TEV cleavage site was cloned into vector pTEV-16b. This new construct, AtETR1[L70W]-TEV, was subjected to analytical TEV cleavage experiments to determine a condition most efficient for removal of the affinity tag (see 4.4.7.2).

Figure 20 shows SDS-PAGE analysis of protein samples taken upon setup of the cleavage reaction as well as 4 hours later and over night. Though the reaction was performed at up to 20 °C, complete removal of the affinity tag was not obtained. Even after incubation over night, a minor fraction of AtETR1[L70W]-TEV still contained the affinity tag as shown by immunodetection. Such reduced cleavage efficiency is not uncommon for detergent solubilised membrane proteins. It has been reported that either the detergent itself might inhibit the protease or the detergent-protein complex could prevent proper cleavage due to steric occlusion<sup>[124, 125]</sup>.

However, for preparative cleavage, AtETR1[L70W]-TEV was treated with *AcTEV*<sup>®</sup> over night at 20 °C as this condition yielded mostly tag-free receptor protein. Non-cleaved protein as well as removed tag peptides and the His-tagged protease itself were removed by IMAC. The mutant receptor was subsequently applied to fluorescence measurements as described for the tagged AtETR1[L70W] mutant before. Samples were set up with 100 µM copper(II) chloride and/or 100 µM ethephon. Also a control sample was prepared that contained only the protein. Fluorescence intensities of all samples were

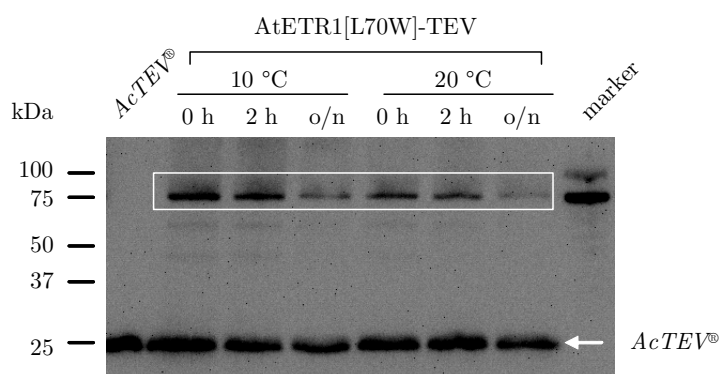


Figure 20: Removal of deca His-tag from AtETR1[L70W]-TEV. The receptor (24 µg) was incubated with *AcTEV*<sup>®</sup> protease at a ratio of 0.33 U/µg target protein at 10 °C and 20 °C. Samples taken upon setup as well as after 2 hours and over night (o/n) were analysed by western blotting and immunodetection (His-antibody). The white box indicates signals from the receptor protein, the white arrow points to those from His-tag labelled *AcTEV*<sup>®</sup> protease.

determined and related to the sample without additives (set to 100 %). Figure 21 shows data obtained with the tagged receptor AtETR1[L70W] and the tag-free mutant AtETR1[L70W]-TEV. Results for the cleaved protein are almost identical to those of the unmodified receptor. Again, a decrease in fluorescence intensity to about 70 % is observed after treatment with copper(II) chloride (green bars). However, this quench was neither enhanced nor reduced upon further incubation with the plant growth regulator ethephon (blue bars). This indicates that the affinity tag is not responsible for the monitored decrease in fluorescence intensity.

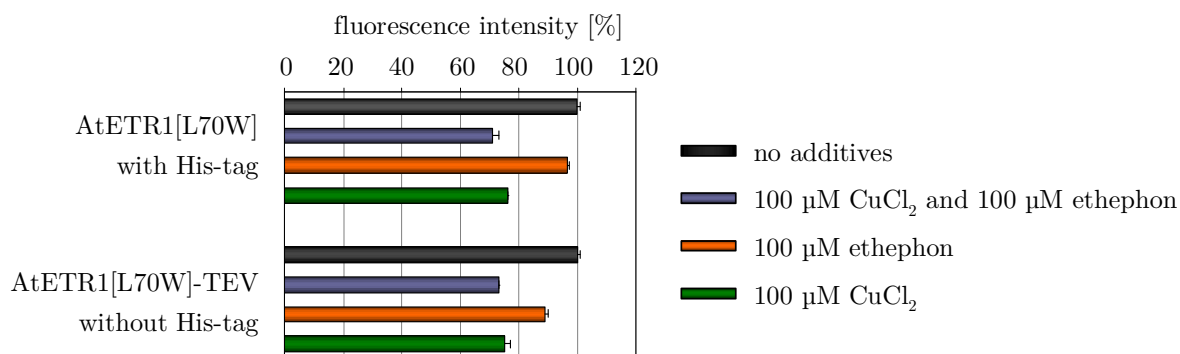


Figure 21: Fluorescence intensity measurements at 348 nm emission wavelength with mutant AtETR1[L70W] (containing the His-tag) and tag-free AtETR1[L70W]-TEV. Changes in fluorescence intensity upon incubation with 100 μM copper(II) chloride (green bars) and/or ethephon (blue and orange bars) were determined and correlated to each internal reference (protein without additives and with fluorescence intensity at 348 nm set to 100 %; see black bars in upper figure). All measurements were performed in duplicate.

Although distinct effects of ethephon—in terms of activity regulation—were demonstrated by autoradiography, it remains unclear why binding of the plant growth regulator could not be proven to the same extent in the fluorescence assay. As already stated, it might be assumed that the quenching effect of copper is masking any effects of further applied substances. Hence, measurements were also performed with AtETR1[L70W], which was incubated with 100 μM copper(II) chloride, but prior to monitoring fluorescence intensity, the excess metal ion was removed by size exclusion chromatography. The protein solution was then treated with ethephon as before. Analysis of the fluorescence data revealed no changes in intensity upon application of the plant growth substance (data not shown). This means that either the cofactor was removed from the receptor protein during buffer exchange or that binding occurred, but if it was accompanied by a conformational change, it was not detectable by the incorporated tryptophan probes.

In summary, the previous experiments revealed that the affinity tag was not responsible for the observed quench. Mutant AtETR1[L70W] showed the same fluorescence intensity changes upon treatment with copper(II) independent of the presence of its affinity tag.

When the protein was pre-incubated with copper(II) and measurements were performed in copper-free buffer, no quench was detected at all. To determine whether loading of the receptor protein with the metal ion was actually successful, alternative detection methods, for example, EPR spectroscopy have to be used.

Apparently, without any structural information on the transmembrane domain, allowing a correct placement of an intrinsic reporter, the fluorescent approach will not be suitable to replace the autoradiography assay in terms of quantitative ligand binding analysis. As already outlined in the previous chapter, mutant AtETR1[L70W] showed a minimal decrease in its fluorescence intensity after treatment with ethephon and might be used to reflect fundamental binding of potential regulatory substances. However, this mutant is not suitable for determination of concentration dependent parameters. In measurements with AtETR1[L70W], a concentration of 100  $\mu$ M ethephon resulted in a reduction of only 5 % in its fluorescence intensity. This implies that the resolution in the fluorescence measurements is not high enough to allow for quantitative binding analysis of potential plant growth regulators.

### 5.3 Characterisation of the ETR1 phosphorylation state

Reversible phosphorylation of a protein kinase is mostly coupled to a conformational change. Due to its charge, the phosphoryl group can alter the properties of amino acids and introduce hydrophilic moieties that can induce a structural change in the protein. This effect has been observed for various proteins and was monitored by changes in fluorescence properties. In similar approaches, the activation of p47<sup>phox</sup>, a subunit of NADPH oxidase, was studied<sup>[126]</sup>. Similarly, the activation mechanism of the chloride channel CTRF (cystic fibrosis transmembrane conductance regulator) was addressed by fluorescence quenching studies<sup>[127]</sup>.

In order to probe conformational changes in ETR1 that might occur upon phosphorylation, single tryptophan mutants were created carrying tryptophan residues in close proximity to the putative phosphate acceptor H353. These mutants would be suitable to evaluate new ethylene agonists and antagonists by fluorescence spectroscopy in a quick and sensitive assay.

### 5.3.1 Conformational changes upon phosphorylation of ETR1 probed by engineered Trp reporter groups

Phosphorylation experiments were performed as endpoint measurements according to section 4.8.3.2. Wild type and mutant receptor proteins of AtETR1 and AtETR1<sub>165-738</sub> with single tryptophan substitutions close to residue H353 were incubated with 1 mM manganese(II) chloride and 0.2 mM ATP to initiate autophosphorylation as observed by autoradiography (see 5.1.3.1). Samples were set up in triplicate and incubated at room temperature for 30 min before fluorescence intensity was measured. Tryptophan residues were selectively excited at 295 nm. Emission spectra were recorded over a range of 310 to 400 nm.

Analysis of the spectra revealed an emission maximum at 348 nm. Control samples were set up for each receptor containing only the protein. Fluorescence intensities of these samples were set to 100 % for each protein and corresponding samples containing manganese(II) chloride and/or ATP were compared to the internal reference of each protein variant.

As shown in Figure 22 fluorescence intensity was maintained at almost 100 % in all samples. Minimal changes were within the standard deviation. Neither incubation with manganese(II) chloride (green bars) nor with ATP (orange bars) or a combination of both (blue bars) corresponding to the setup in the radioactive kinase assay had any effect on the fluorescence intensity.

The fact that no fluorescence quench was detectable upon incubation of the receptor mutant with ATP and the manganese cofactor might be explained by the fact that phosphorylation did not occur. However, this is quite unlikely as all proteins were treated as in the radioactive phosphorylation assay where clear incorporation of  $^{32}\text{P}_i$  in the receptor protein was detectable reflecting the autokinase activity of ETR1<sup>[32, 33]</sup>.

Alternatively, phosphorylation occurred but was not accompanied by a conformational change. Then again, the conformational change was too small to be monitored by the fluorescence probe. However, it is also possible that the selected tryptophan probes were not placed in a proper location of the receptor to sense structural changes. If phosphorylation did not occur at residue H353 as postulated but at positions 357 (threonine) or 366/367 (serine) as described earlier (see 5.1.3.1), the tryptophan residues might be too far apart to detect any conformational changes.

ETR1 is a multi domain receptor protein (Figure 23). With its N-terminal part—including the kinase domain—and the C-terminal receiver domain, it shows similarity to bacterial two-component signal transduction systems that signal by histidine to aspartate phosphotransfer<sup>[32, 128, 129]</sup>. Each of the two structural domains of ETR1 contains a putative

phosphorylation site: residue H353 in the sensory kinase domain and residue D659 in the receiver domain<sup>[31, 129]</sup>. Individual phosphorylation at both sites was shown *in vitro*, but the intramolecular phosphoryl transfer between both domains was not demonstrated yet<sup>[32]</sup>.

The absence of any detectable quench in the ethylene receptor protein upon addition of ATP (Figure 22) might be also explained by the fact that the phosphoryl group does not remain at

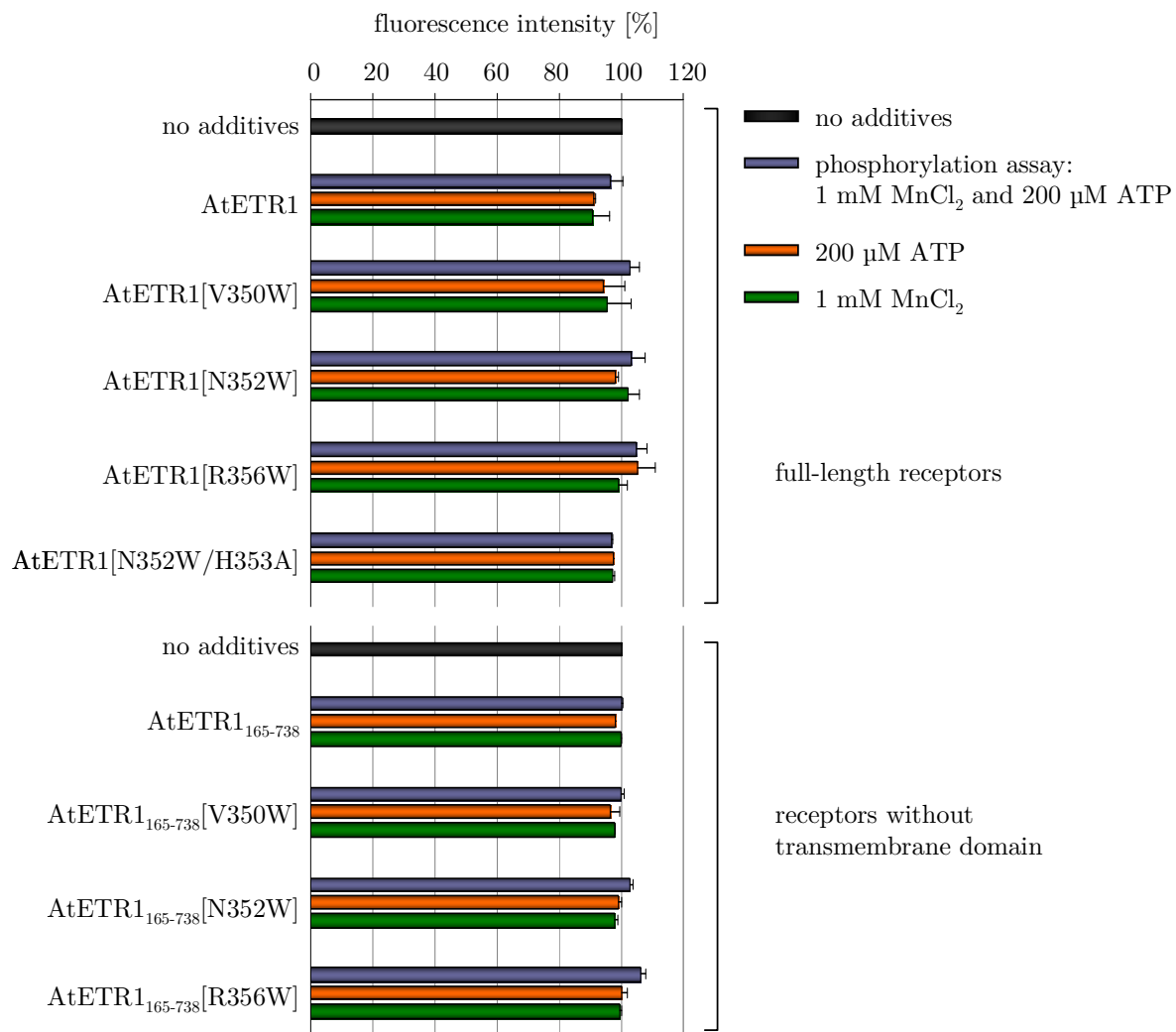


Figure 22: Fluorescence intensity measurements at 348 nm emission wavelength with mutant AtETR1 and AtETR1<sub>165-738</sub> receptors carrying single tryptophan residues in close proximity to the putative phosphorylation site His353. Changes in fluorescence intensity upon incubation with 1 mM manganese(II) chloride (green bars) and/or 200 μM ATP (blue and orange bars) were determined and related to an internal reference (protein without additives, fluorescence intensity at 348 nm set to 100 %, see black bars). All measurements were performed in triplicate. For reasons of clarity, references (black bars) are depicted only once for each set of full-length and truncated constructs.



residue H353 but is directly transferred to the aspartate in the receiver domain. In consequence, the residues selected for substitution to tryptophan are too distant to reveal conformational changes in the other domain. In this context, time-resolved fluorescence spectroscopy might grasp phosphorylation events at residue H353 before the phosphoryl group is intramolecularly transferred to residue D659.

#### 5.3.1.1 Phosphoryl transfer in ETR1: a hypothesis based on proteolysis of radiolabelled receptors

In an attempt to identify the phosphorylation site in ETR1, kinase activity assays with radiolabelled  $^{32}\text{P}$ -ATP were performed with wild type AtETR1 and mutant proteins where phosphoryl group acceptors H353 and D659 were substituted by alanine. Because these protein variants would give information only which residue is phosphorylated but would not show the

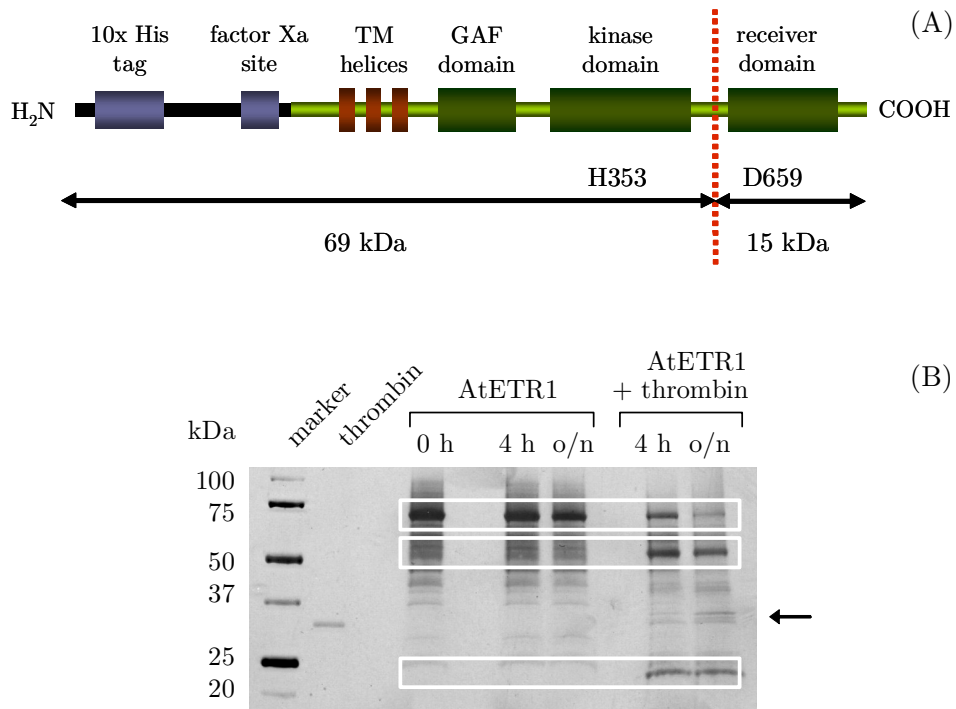


Figure 23: (A) Schematic domain structure of AtETR1. The N-terminal 10x His-tag is linked to the target protein by a factor Xa recognition sequence (blue). The three predicted N-terminal helices (red) are followed by a GAF domain (green). Due to a thrombin recognition sequence (red dotted line), the protein can be cleaved into a 69 kDa fragment (including residue H353) and a second fragment with the size of 15 kDa (including phosphoryl group acceptor D659). Efficiency of proteolysis of AtETR1 with thrombin was analysed by SDS-PAGE (B). Samples were taken upon setup and after 4 h as well as over night (o/n). From top to bottom, white boxes label protein bands of the full-length protein, the 69 kDa fragment and the 15 kDa product. The black arrow points to protein bands attributed to thrombin (29 kDa).

transfer of the phosphoryl group from the kinase to the receiver domain, it was necessary to analyse both parts of the protein individually.

Due to a thrombin protease cleavage site present in all three receptor forms, it was possible to split the protein into a 69 kDa sized N-terminal part carrying H353 in the kinase domain and a smaller fragment of 15 kDa that comprises the receiver domain including residue D659 (see Figure 23A). The receptor proteins were treated with thrombin as described in section 4.4.7.3. The cleavage reaction was carried out at room temperature as the kinase assay was performed at the same temperature. Complete cleavage of the receptor proteins could not be achieved, but incubation for 4 h yielded distinct fractions of both fragments as shown for the wild type receptor (Figure 23B).

Phosphorylation studies according to the protocol described in 4.8.1 were carried out before and after treatment with the protease. In the latter case, thrombin was inhibited by 1 mM PMSF prior to the radioactive assay. Individual phosphorylation events in the full-length proteins and the fragments comprising the kinase or the receiver domain are summarised in Table 17.

The radioactive assay showed that all full-length receptor proteins are able to incorporate radiolabelled  $^{32}\text{P}$ . For wild type AtETR1 and the mutant AtETR1[D659A] this result was expected as both proteins hold the putative H353 phosphorylation site. In case of the mutant H353A phosphorylation might be explained by threonine or serine residues in close proximity to the substituted histidine 353 as outlined in chapter 5.1.3.1.

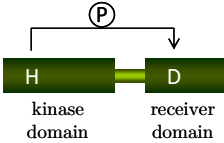
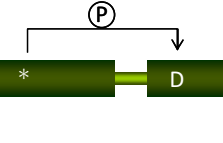
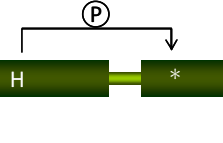
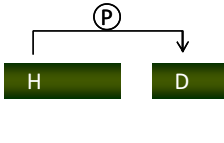
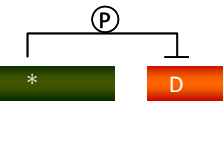
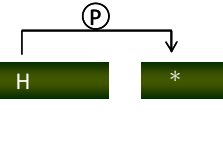
Cleavage with thrombin after phosphorylation further revealed incorporation of  $^{32}\text{P}$  phosphate into each fragment (see schematic models in Table 17). For mutant AtETR1[D659A] incorporation of the label in both domains indicated that there have to be residues in addition to D659 that can act as an acceptor for the phosphoryl group. According to the crystal structure of the receiver domain, the active site is comprised by residues D616, E617 and D659 and both aspartates are in close proximity (Figure 25, page 91)<sup>[130]</sup>. In consequence, phosphorylation of amino acid D616 instead of D659 might occur in the D659A mutant. To verify this hypothesis, additional mutants have to be tested in further phosphorylation studies.

As the phosphorylation reaction was not inhibited by cyanide prior to thrombin cleavage, the isolated kinase domain seems to be still able to autophosphorylate explaining the incorporation of the radiolabel in the kinase domain fragments of all receptors.

Another remarkable result of the autokinase assay was that a transfer of phosphoryl groups from the split kinase domain to the receiver domain was observed for wild type AtETR1 and mutant AtETR1[D659A]. This observation corresponds to phosphotransfer in typical two-

component systems known from prokaryotes: An ATP-binding kinase domain, which is typically located to a plasma membrane, serves as the first component whereas the second element that is usually found in the cytoplasm is a regulatory receiver domain<sup>[131]</sup>. Obviously, the information to operate individually is still implemented in the combined module found in the plant hybrid histidine kinases. Signalling might be processed faster in the combined hybrid system as recruitment of individual components is not necessary.

Table 17: Putative phosphoryl transfer in wild type AtETR1 and mutants AtETR1[H353A] and AtETR1[D659A] before and after treatment with thrombin. Domains coloured in green indicate phosphorylation. The orange coloured domain did not contain <sup>32</sup>P phosphate. Phosphorylatable residues in each domain other than H353 (kinase domain) and D659 (receiver domain) are marked by asterisks.

<i>Experimental setup</i>	<i>AtETR1</i>	<i>AtETR1[H353A]</i>	<i>AtETR1[D659A]</i>
1. phosphorylation  2. proteolysis			
1. proteolysis  2. phosphorylation			

The question that still remains is why a phosphoryl group transfer was not detected between the cleaved domains in the AtETR1[H353A] mutant. Bacterial two-component systems show an exclusive phosphoryl group transfer from histidine to aspartate. Hence, phosphotransfer between the individual elements in the split plant system might not be feasible from a serine or threonine to the aspartate in the receiver component. This hypothesis might be explained by a unique conformation of the kinase domain caused by phosphorylation of H353 that might be a crucial prerequisite for binding of the cleaved receiver domain. Such a crucial induced conformational change was found for the two component system CheA/CheY involved in the bacterial chemotaxis signalling pathway<sup>[131]</sup>. Upon phosphorylation of other residues in the kinase domain of AtETR1, a slightly different conformation might be adopted which in consequence prevents binding of the receiver domain and transfer of the phosphoryl group to D659.

In summary, experiments presented in this section revealed a phosphotransfer between the putative phosphorylation sites H353 in the kinase domain and the receiver domain (D659) of AtETR1. In addition, phosphorylation of other residues seems to occur when the primary phosphorylation targets H353 and D659 are substituted by alanine.

In the context of the fluorescence quenching studies, these results indicate that the tryptophan probes placed in close proximity of H353 were not capable to monitor the phosphorylation state as they were not located at the final phosphorylation site in the receiver domain. All fluorescence measurements were carried out 30 min after incubation with ATP, so most of the protein was probably already phosphorylated at residue D659. A modified approach using time-resolved fluorescence spectroscopy to monitor fluorescent changes immediately after application of ATP might elude this issue and reveal structural changes due to phosphorylation at residue H353. If conformational changes are still not detectable, further mutants should be created with tryptophan probes placed close to the active site of the receiver domain. A crystal structure of this component is already available facilitating steric reasonable substitution of residues by tryptophan<sup>[130]</sup>.

### 5.3.2 <sup>31</sup>P-NMR spectroscopy to assign the phosphorylation sites in ETR1

In the previous chapter, individual phosphorylation of the kinase and receiver domain was observed by a radioactive kinase assay. Experiments with mutants AtETR1[H353A] and AtETR1[D659A] indicated that residues other than H353 and D659 are potential targets for phosphorylation. In order to assign these residues <sup>31</sup>P-NMR was applied<sup>[132]</sup>.

Nuclear magnetic resonance (NMR) arises when certain nuclei are placed in a magnetic field and are excited with an electromagnetic pulse. This phenomenon is not elicited by all atomic nuclei but those with a so-called *spin* resulting from individual spins of protons and neutrons in the nucleus. This spin induces a magnetic moment that is responsible for interferences with an external magnetic field. When such a field is applied to nuclei with an overall spin of  $\frac{1}{2}$  (<sup>1</sup>H, <sup>13</sup>C, <sup>15</sup>N and <sup>31</sup>P), the nuclei can either align parallel or anti-parallel to the external field. Transition between these two orientations is induced by electromagnetic radiation. Upon subsequent relaxation, energy is emitted at a specific resonance frequency. Obtained data are processed by *Fourier* transformation to give typical NMR spectra as shown in Figure 24.

These spectra contain several information: The *chemical shift* ( $\delta$ , expressed in ppm) is characteristic for functional groups in a specific environment. Integration of the peak area gives

information on the amount of the respective chemical group and *spin-spin coupling* (recognisable by splitting of peaks into multiplets) will provide information on the chemical environment as individual nuclei can interact with each other<sup>[133]</sup>.

While this information is usually used to assess the structure of chemical compounds, peptides and small proteins (< 30 kDa), it was used here to identify and assign phosphorylated amino acids. The major advantage of  $^{31}\text{P}$  for NMR analysis is its natural abundance of 100 % that obviates expensive or inconvenient labelling of proteins. This procedure is necessary for isotopes  $^{13}\text{C}$  or  $^{15}\text{N}$ , which both occur at lower natural rates of only 1.1 and 0.4 %. Compared to  $^1\text{H}$ -,  $^{13}\text{C}$ - or  $^{15}\text{N}$ -NMR,  $^{31}\text{P}$  spectra show less signals facilitating their interpretation. Obtained signals are only caused by externally applied  $^{31}\text{P}$  as proteinogenic amino acids do not contain phosphor.

However,  $^{31}\text{P}$ -NMR experiments require several milligrams of highly concentrated protein. This might not be a drawback for soluble proteins but membrane proteins that usually express at a low level and are prone to aggregation at high concentrations<sup>[134]</sup>.

$^{31}\text{P}$ -NMR measurements were performed with the truncated wild type receptor AtETR1<sub>165-738</sub> in a phosphorylation assay. In addition, individual reference spectra were recorded with 100 mM AMP, ADP and ATP supplied with 10 % (v/v) deuterium oxide (see section 4.8.4).

Figure 24 shows individual spectra for nucleotides and for the kinase assay. AMP (blue spectrum) gave one distinct signal at 3.5 ppm corresponding to the  $^{\alpha}\text{P}$  atom. ADP (green spectrum) showed two signals, one for  $^{\alpha}\text{P}$  and the other one for  $^{\beta}\text{P}$  (-10.7 and -6.6 ppm at pH 7.5). Both signals were in accordance to published data (-11.0 and -5.6 to -6.2 ppm at pH 8.0)<sup>[135]</sup>. Furthermore, two small peaks appeared at 3.4 ppm and 1.9 ppm. The first signal was in accordance to AMP and the second one was assigned to orthophosphate (reference data: 2.3 to 3.0 ppm) indicating ADP hydrolysis. The red spectrum shows three signals for  $^{\alpha}\text{P}$  (-11.0 ppm),  $^{\beta}\text{P}$  (-21.5 ppm) and  $^{\gamma}\text{P}$  (-6.0 ppm), which correspond all to published data for ATP (-11, -21.0 to -23.0 and -5.6 to -6.2 ppm). The nucleotide reference spectra were collected to obtain chemical shifts for each phosphate species in the kinase assay buffer.

Subsequently, the phosphorylation assay was set up with the receptor protein (75  $\mu\text{M}$ ), 1 mM manganese(II) chloride, 43 mM ATP and 5 % (v/v) deuterium oxide. The ATP concentration was increased by the factor of 215 compared to the  $^{32}\text{P}$  assay to give distinct signals in the NMR spectrum. The sample was measured after 10 minutes incubation at room temperature. Although the  $^{32}\text{P}$  assay is usually incubated for 30 minutes, it was tested if a signal was already detectable at that point. Strikingly, the sample showed only noise (see black spectrum in Figure 24). Even the ATP typical signals were no longer detectable.

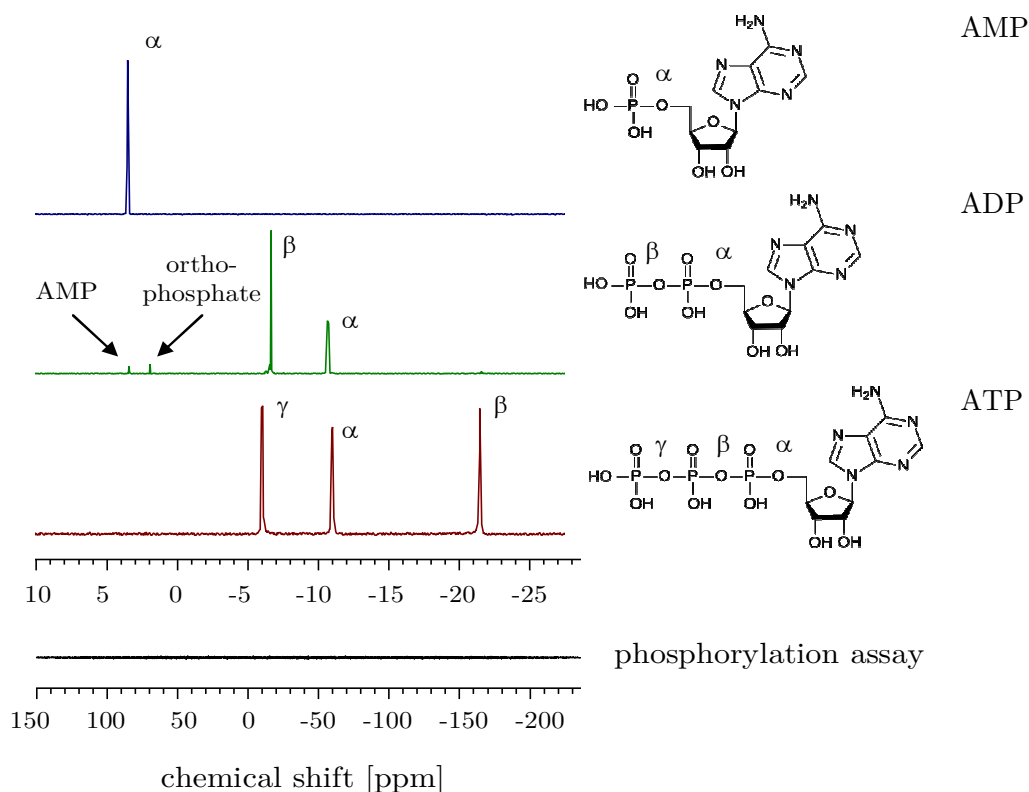


Figure 24:  $^{31}\text{P}$ -NMR spectra of AMP (blue), ADP (green) and ATP (red), 100  $\mu\text{M}$  each nucleotide supplied with 10 %  $\text{D}_2\text{O}$ . Structural formulas are given for each nucleotide and individual peaks are assigned to  $^{\alpha}\text{P}$ ,  $^{\beta}\text{P}$  and  $^{\gamma}\text{P}$  in the respective spectrum. The black spectrum at the bottom was recorded for AtETR1<sub>165-738</sub> supplied with 1 mM manganese(II) chloride, 43 mM ATP and 5 % deuterium oxide 10 minutes after setup of the phosphorylation assay. The chemical shift is given in ppm.

Analysis of all buffer components revealed that the observed noise signal and the elimination of the three ATP signals was caused by manganese(II). In fact, manganese(II) is used as a *shift reagent*\* in  $^{31}\text{P}$ -NMR to probe the lamellarity of phospholipid vesicles. With its paramagnetic nature the metal ion affects the phosphate groups in the lipids of the external layer of vesicles causing peak broadening. In multilamellar vesicles the effect is neglectable, in unilamellar vesicles the  $^{31}\text{P}$  signal will be significantly reduced<sup>[137]</sup>.

Nevertheless, it is not principally impossible to carry out  $^{31}\text{P}$ -NMR measurements in the presence of manganese(II). However, it is necessary to adjust the ratio of the NMR active species, the substrate ATP and the *shift reagent*. With the appropriate adjustments,  $^{31}\text{P}$ -NMR might turn out as a valuable tool to identify phosphorylation sites in ethylene receptor ETR1.

\* Shift reagents are paramagnetic ions that affect nuclei in NMR spectroscopy by inducing an internal, local magnetic field. This effect is utilised to separate peak signals<sup>[136]</sup>.

## 5.4 Synopsis

Functional studies on ethylene receptor ETR1 from *A. thaliana* were performed to elucidate two main aspects of ethylene signalling: perception of the gaseous hormone in the sensor domain and the related phosphorylation in the kinase and receiver domain of the receptor.

In order to address signal perception, mutant receptor proteins were generated carrying single tryptophan residues in close proximity of the putative ethylene binding site located at C65 and H69. Binding of the plant hormone is described to occur via a copper ion. Hence, the receptors were pre-incubated with this cofactor and subsequently supplied with the growth regulator ethephon. It turned out that the initial fluorescence signal from the protein was substantially decreased by copper. Further distinct quenching effects of the plant hormone were not detectable. Only mutant AtETR1[L70W] showed minimal decrease in its fluorescence intensity upon treatment with ethephon. However, the observed effect is too small to enable ligand binding studies considering quantitative analysis. Though, the mutant might be used to reflect binding of potential plant growth substances in principle.

Mutant AtETR1[W53/C65A/H69A], which was assumed not to bind the metal ion because residues C65 and H69 were substituted by alanine, showed a distinct reduction in fluorescence intensity. Titration studies with copper(II) on this mutant and AtETR1[W53] revealed static and dynamic quenching effects for both mutants. This indicates that both receptors could bind the metal ion. Binding of copper to the histidine affinity tag was disproven in controls with receptor proteins lacking the tag. However, there are further residues in the transmembrane helices I and II (D25, Y32, I35, P36 and I62) that have been reported to play a role in binding of ethylene and presumably also in copper binding<sup>[30]</sup>.

Based on the data obtained in the fluorescence quenching studies, the strategy of applying internal reporters such as tryptophan residues to monitor binding of ethylene agonists and antagonists seems not suitable. It is obvious that copper is interfering with the measurement, thereby preventing the significant detection of possible effects due to further substances.

An alternative to the tryptophan fluorescence spectroscopy seems to be electron paramagnetic resonance (EPR) spectroscopy. This method reveals information on type, structure and local environment of paramagnetic species which are characterised by unpaired electrons as in copper(II). The principle of EPR spectroscopy is similar to NMR, however, the spin of *electrons* is observed and transition between individual states is induced by micro waves instead of radio waves. The electrons are influenced by the local environment, so the presence or absence of further ions or ligands will be reflected in individual EPR spectra.

EPR spectroscopy has been applied successfully to show copper mediated binding of inhibitors to laccase from *Rhus vernicifera* as well as binding of cyanide and azide to the copper site of a dopamine  $\beta$ -monooxygenase<sup>[138, 139]</sup>. Receptor protein AtETR1 might be applied in similar measurements to prove binding of the copper ion and to analyse binding of ethylene agonists or antagonists. Binding of these substances will most probably be reflected in the EPR spectra.

However, copper (II) EPR spectroscopy requires protein concentration of at least 100 to 250  $\mu\text{M}$ <sup>[139, 140]</sup>. For AtETR1 this corresponds to about 9 to 20 mg/ml. With the established expression and purification protocols for AtETR1 (yielding 0.1 mg receptor protein per gram cells), preliminary EPR studies might be performed, but comprehensive measurements will require a modification of the preparation method to obtain more protein.

Similar to the fluorescence quenching studies applied for probing ligand binding, experiments were carried out to monitor the phosphorylation state of the receptor by quenching of tryptophan residues that have been placed close to the putative phosphorylation site H353 in the kinase domain of the ethylene receptor. Although fluorescence studies with these mutants were performed according to the radioactive assay, no changes in fluorescence intensity were detected.

The conclusion drawn from these experiments is that intermolecular phosphoryl group transfer from H353 to D659 had occurred in the *in vitro* experiment. To evaluate this hypothesis, the  $^{32}\text{P}$  assay was carried out with wild type AtETR1, which had been proteolytically cleaved between the kinase and the receiver domain. By this approach, phosphorylation of the two individual domains was demonstrated reflecting a typical split two-component signal transduction system as found in bacteria.

Phosphorylation of mutant receptors AtETR1[H353A] and AtETR1[D659A] suggests that the kinase domain as well as the receiver domain contain additional residues in close proximity of the already described residues H353 and D659 that can be phosphorylated, too (see 5.3.1.1).

$^{31}\text{P}$ -NMR was applied to identify these residues. Preliminary measurements revealed that the original setup of the  $^{32}\text{P}$  assay cannot be used as the manganese(II) cofactor serves as a paramagnetic metal ion disturbing the magnetic field and repressing any  $^{31}\text{P}$  characteristic signals. Although the NMR spectroscopic studies could not successfully be completed yet, the method has high potential to identify the phosphorylation sites in ETR1 by replacing manganese(II) with the non-paramagnetic magnesium or by reducing the concentration of manganese(II) to prevent quenching of the NMR signal. A modification of expression and purification protocols might be necessary, too, in order to increase the yield of recombinant receptor protein required for NMR measurements.



## 6 Part B: Crystallisation of ETR1 from *A. thaliana*

*Mueller-Dieckmann et al.* have crystallised the cytosolic C-terminal receiver domain (amino acids 604-738) of the ethylene receptor ETR1 from *Arabidopsis thaliana* in 1999<sup>[130]</sup>. The structure was solved at a resolution of 2.5 Å and revealed first insights into a eukaryotic receiver domain. The core is build from five stranded  $\beta$ -sheets that are clasped on two sides by two and three  $\alpha$ -helices (Figure 25).

In the crystal structure the receiver domain is dimerised. The dimerisation interface partially comprises the C-terminal part of the molecule. Three residues form an additional  $\beta$ -strand that can slot between two other  $\beta$ -strands from the core of the second monomer. The active site is comprised of residues Asp14, Glu15 and Asp57, which provide an acidic pocket and together with Lys112 contribute to a hydrogen-bonding network where Asp57 (Asp659 in full-length ETR1) can be phosphorylated.

The receiver domain of ETR1 is lacking an output domain as found in many bacterial response regulators where dimerisation typically regulates their activity. For that reason it has been suggested that phosphorylation dependent dimerisation of the receiver domain affects interaction of the receptor with downstream components of the ethylene signalling cascade<sup>[130]</sup>.

To further understand this mechanisms as well as the perception of the gaseous signal molecule and the phosphoryl transfer within the receptor protein (His353 to Asp659), it is necessary to obtain a structure for full-length ETR1. In this thesis both, the complete receptor and a truncated variant lacking the transmembrane sensor domain (aa 165-738) were subjected to crystallisation studies.

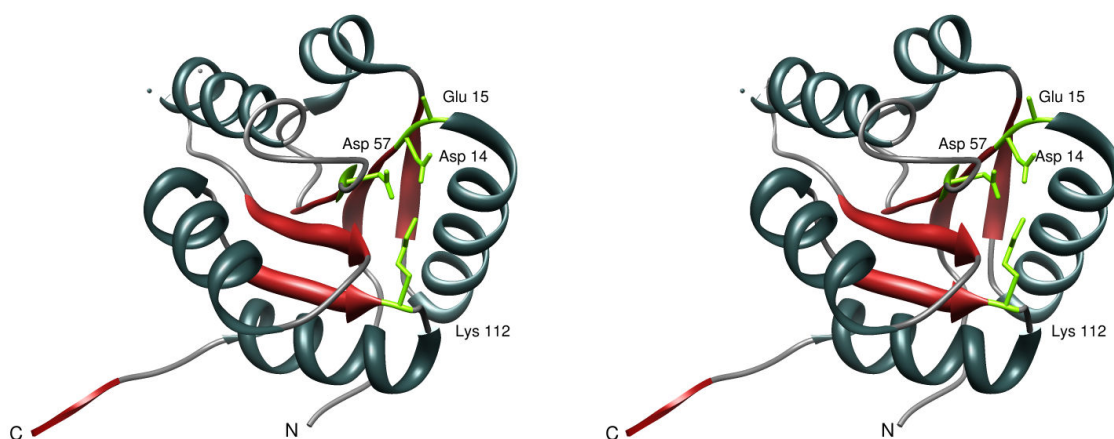


Figure 25: Cross-eye stereo image of the receiver domain of AtETR1 (pdb code: 1DCF).  $\beta$ -sheet structures are coloured red;  $\alpha$ -helices are in dark cyan. Noticeably, the C-terminus sticks out of the core structure of the receptor allowing for dimerisation. Residues forming the active site (top view) are displayed in stick mode and coloured in green.

## 6.1 Crystallisation of the extra membrane domain of ETR1

Successful identification of appropriate crystallisation conditions for AtETR1<sub>165-738</sub> lacking the transmembrane domain was obtained by Thomas Classen in his bachelor thesis<sup>[141]</sup>. This initial study screened about 800 crystallisation buffers by microbatch under oil technique using *Qiagen's Classics* and *PEGs Suites I and II*, the *JCSG<sup>+</sup> Suite*, the *PACT Suite* and the *AmSO<sub>4</sub> Suite*.

A buffer composed of 11 % (w/v) PEG 1500 and 100 mM Tris/HCl, pH 8.5 mixed with an equal volume of the purified receptor gave hexagonal crystal plates (about 15 x 60 µm). However, the plates formed stacks and were unsuitable for

diffraction analysis. Nevertheless, SDS-PAGE demonstrated that the crystals contain AtETR1<sub>165-738</sub>. Based on this initial hit, the crystallisation project was continued in the present thesis.

First setups were performed identical to the initial parameters including protein preparation (IMAC under denaturing conditions, see 4.7.2), crystallisation technique (microbatch under oil), incubation temperature (20 °C), equipment (*IMP@CT<sup>TM</sup>* and *Terasaki* crystallisation plates) as well as the protein-precipitant drop size (2 µl final volume).

However, crystals grown from the initial buffer showed a different morphology than those observed in the first trials (Figure 27A). The crystals (1 to 5 per well in 5 % of all wells) were rather large with an edge length of about 200 to 500 µm and appeared usually within 1 to 5 days after crystallisation setup. Viewed laterally the crystals mimicked a hexagonal shape, but viewed from the top they showed an almost circular form.

The crystals were harvested, washed twice in buffer to remove any residual protein solution and were subsequently analysed by SDS-PAGE. In silver stained polyacrylamide gels the crystals showed distinct proteins bands corresponding to the molecular weight of the purified ethylene receptor (Figure 27B).

Despite their morphology the crystals were tested for their diffraction quality and typically revealed patterns as shown in Figure 27C with a maximum resolution of 11 to 12 Å. Even at that low resolution secondary structure elements like  $\alpha$ -helices might be allocated in an electron



Figure 26: Schematic model of truncated ethylene receptor AtETR1 (amino acids 165-738). The N-terminal 10x His-tag is linked to the protein by a factor Xa protease recognition sequence. Both parts are coloured blue. The receptor (green) has an N-terminal GAF domain followed by a kinase domain and the C-terminal receiver domain.

density map. However, indexing of all collected diffraction patterns with *iMosflm/Mosflm*<sup>[142]</sup> failed preventing processing of collected data. This is probably due to the high mosaicity of the crystals that is reflected in the smeared form of individual spots on the diffraction image: The more centred the spots are located, the more streaked they appear. This phenomenon is based on irregular crystal packing causing a shift in the crystal lattice. This effect can be observed in the diffraction pattern. Spots are not focussed to circular points but rather appear in an oval shape. This makes it difficult for analysing software to find the centre of each spot—a prerequisite to index a set of images<sup>[143]</sup>.

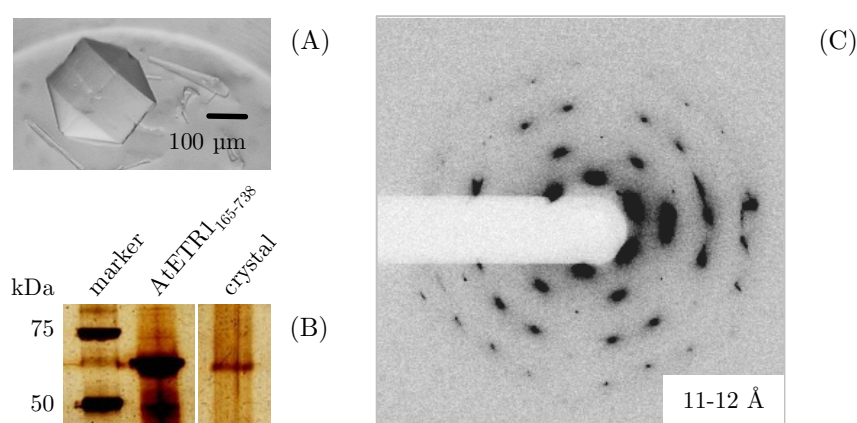


Figure 27: Crystal (A) obtained in 11 % (w/v) PEG 1500 and 100 mM Tris/HCl, pH 8.5. The image was taken 7 weeks after setup. (B) Analysis of crystal content by SDS-PAGE. AtETR1<sub>165-738</sub> was identified by comparison of a harvested crystal to a reference sample of purified receptor protein (lane AtETR1<sub>165-738</sub>). Figure (C) shows a typical diffraction image collected at beamline *ID 23-2* at *ESRF*, Grenoble. Outer spots appear at about 11-12 Å resolution.

Mosaicity is often enhanced during flash freezing of protein crystals, which are crossed by solvent containing channels. Crystalline ice may form inside upon freezing increasing disorder in crystal packing. To overcome this problem, the solvent in the crystal is replaced by a cryoprotectant that allows for vitrification<sup>[144]</sup>. These agents usually comprise glycerol and small to large molecular weight PEGs. Oils such as *Paratone-N* (*Hampton Research*) are also used to coat the crystals minimising dehydration during crystal handling.

No visible ice was detected on AtETR1<sub>165-738</sub> crystals upon freezing, most probably because the crystals were grown under oil. Further cryoprotectants were tested for their effect on mosaicity and diffraction: Glycerol was applied in concentrations above 50 % (w/v), otherwise crystals immediately dissolved. Higher molecular weight PEG 4000 was also tested and the crystals were stable for freezing up to concentrations of 25 % (w/v). The crystals were dragged through *Paratone-N* in order to coat them with an additional outer layer.

However, all attempts did not improve diffraction quality. Mosaicity—judged by eye, as it was still not possible to index the images—was not reduced and the resolution was still in the range of 11–12 Å.

Temperature annealing is another chance to reduce mosaicity<sup>[145]</sup>. Here, the cryo stream in which crystals are placed during X-ray measurement to prevent radiation damage is blocked briefly. The crystal can thaw and refreeze, eventually improving overall diffraction quality by realigning the protein molecules within the lattice. Again, this method did not work for AtETR1<sub>165-738</sub> crystals.

Another major problem occurring with crystal growth and probably also a reason for the low scattering quality observed for AtETR1<sub>165-738</sub> is related to the fact that almost all crystals stuck firmly to the crystallisation plates. Only minor defects caused by touching them with a nylon loop during harvesting could easily damage the internal order which would explain the observed diffraction results. Treatment of the plates with *n*-decane prior to crystallisation setup did not prevent the attachment of the crystals to the plastic surface.

#### 6.1.1 Optimising crystallisation conditions

Although crystals were grown for truncated ethylene receptor protein AtETR1<sub>165-738</sub>, these crystals were unsuitable for data collection and structure determination. Furthermore, about 75 % of all wells contained amorphous, spherulitic structures rather than crystals (Figure 28). In order to improve crystal quality, a comprehensive optimisation study was performed. First, modifications of the crystallisation conditions were tested including buffer composition and crystallisation setup. Later, these studies were accompanied by chemical and genetic modification of the receptor protein.

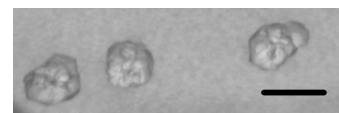


Figure 28: Globular structures grown in 11 % (w/v) PEG 1500 and 100 mM Tris/HCl, pH 8.5. Scale bar corresponds to 100 µm

##### 6.1.1.1 *Crystallisation buffer composition*

The protein concentration was maintained between 5 to 10 mg/ml depending on protein yield after IMAC purification (see 4.7.2). The protein concentration had only a minor effect on crystallisation. Basically, the more protein present in a setup the more crystals or spherulites appeared.

Several components of the crystallisation buffer were varied during optimisation:

- Starting with 100 mM Tris/HCl buffer at pH 8.5 supplied with 11 % (w/v) PEG 1500, a factorial screen was set up covering buffer strength in a range of 25 to 175 mM and PEG concentration from 3 to 19 % in increments of 25 mM and 2-3 %, respectively.
- Tris buffer was substituted by Tricine and Bicine in a range of 10 to 500 mM while the pH was maintained at 8.5 using hydrochloric acid for adjustment. The PEG 1500 concentration was not changed in this approach.

Additives were added to the initial buffer composition for different reasons:

- Nickel sulfate was applied in concentrations from 1  $\mu$ M to 5 mM to complex the N-terminal His-tag of the receptor to give this flexible domain a more rigid structure which otherwise might prevent ordered crystal packing.
- 2-mercaptoethanol (1 to 100 mM) was added to create a reducing environment and inhibit formation of unspecific disulfide bonds. Although the transmembrane domain which is postulated to be responsible for dimerisation via amino acids Cys4 and Cys6 is missing, further cysteines in the protein might bind and cause a heterogeneous protein composition<sup>[27]</sup>.
- Up to 10 % ethanol (v/v) was applied to lower the dielectric constant of water, thereby reducing protein solubility. This may result in crystal growth as solid states of macromolecules are favoured. In contrast, aggregation is also possible<sup>[146]</sup>.
- AMP-PNP (adenosin-5'-( $\beta,\gamma$ -imido)triphosphate) is a non-hydrolysable ATP analogue. The molecule can bind to the ATP-binding domain in the histidine kinase domain of ETR1 and thereby arrest the enzyme in a rigid state more suitable for crystallisation. The ATP analogue was applied in a concentration of 0.5 mM.

Optimisation attempts were carried out with wild type AtETR1<sub>165-738</sub> and the mutant AtETR1<sub>165-738</sub>[H353A]. The mutant protein might show better homogeneity as the wild type can occur in phosphorylated and non-phosphorylated states that will probably adopt different conformations.

Individual results for every optimisation step are listed in Table 18. All variations of the crystallisation buffer did not affect the morphology of the crystals. If crystals appeared, they were shaped like a short sharpened pencil. While the buffering substance had no influence on crystallisation, the PEG concentration could decide the fate of each crystallisation setup. The drops remained clear at concentrations less than 11 % (w/v). When increased up to 13 %, precipitate occurred, and at concentration between 13 and 19 % spherulites and few crystals

were formed. The results from the optimisation study are in clear contrast to the first crystallisation experiments where crystals were obtained at a PEG 1500 concentration of 11 %. This discrepancy illustrates the low reproducibility of the crystallisation trials. The reason might rather be the protein than the crystallisation buffer: Even when the buffer composition was kept constant, different crystallisation results for AtETR1<sub>165-738</sub> were obtained in setups with protein from different preparations. This indicates that the protein quality varied between individual preparations. In order to favour protein homogeneity, several additives that could interfere with the receptor were tested regarding their influence on crystal formation.

AMP-PNP, 2-mercaptoethanol and nickel sulfate did not improve crystallisation but had a rather negative effect as the formation of precipitate was observed in various setups. Ni<sup>2+</sup> might have introduced a conformational change in the protein due to disruption of salt bridges or formation of coordinate-covalent bonds. The reductant 2-mercaptoethanol might prevent the formation of unspecific disulfide bonds but might also inhibit those necessary for proper tertiary structure. Only the addition of ethanol had a positive effect on the crystallisation. The crystal shape did not change, but the overall number of crystals and spherulites almost doubled when ethanol was applied in a concentration of 10 % (v/v). Ethanol will reduce solubility and enhance electrostatic interactions between protein molecules, thereby favouring crystal growth<sup>[147]</sup>. However, as diffraction of crystals grown at this condition showed no improvement, this approach was not further continued.

Table 18: Effects of buffer components on crystallisation of wild type AtETR1<sub>165-738</sub> (WT) and the mutant AtETR1<sub>165-738</sub>[H353A] (HA). The only component showing a positive effect is highlighted in blue. Percentages are given in (w/v).

<i>Parameter</i>	<i>Effect</i>	<i>Crystallisation Result</i>	<i>Protein</i>
Ion strength of Tris/HCl buffer	none	Spherulites and crystals	WT HA
PEG 1500 concentration	concentration dependent	< 11 % clear 11 % - 13 % precipitate > 13 % spherulites, few crystals	WT HA
Substitution of Tris by Bicine/Tricine	none	Spherulites and crystals	WT
Nickel sulfate	negative	Spherulites and precipitate	WT HA
2-mercaptoethanol	none / negative	Spherulites and precipitate, few crystals	WT HA
Ethanol	positive	Increased number of crystals, less spherulites and precipitate	WT
AMP-PNP	none	Spherulites and few crystals	HA

Even though the results from the buffer optimisation study indicated that the reason for the low quality of obtained crystals was rather due to the protein itself than external factors, several approaches were made considering crystallisation setup and storage. For all experiments the initial buffer composed of 100 mM Tris/HCl, pH 8.5 and 11 % (w/v) PEG 1500 was used.

#### *6.1.1.2 Variation of incubation temperature*

A temperature gradient from 5 to 35 °C in increments of 2.5 °C was applied to the crystallisation trials. Crystals grown at 20 °C usually appeared 24 h after setup and grew to large sizes (up to several hundred µm) within a few days. On one hand, a decrease in temperature should slow down this process to favour an ordered crystal packing. On the other hand, an increase in temperature might influence crystallisation by affecting solubility and supersaturation of the sample and the precipitants. *Christopher et al.* showed temperature dependence on crystal growth for 30 proteins proving that only minor changes in temperature can have a huge effect on the outcome of a crystallisation experiment.  $\alpha$ -Amylase, for example, will produce crystals from 4 to 17 °C. However, when increasing the temperature to 18 °C, only precipitate will be formed<sup>[148]</sup>.

In the case of the truncated wild type ethylene receptor, the gradient was set in a PCR thermal cycler. For that reason crystallisation plates had to be substituted by PCR plates with V-shaped bottom. Each well was filled with 2 µl of protein-precipitant solution and was individually covered with 30 µl mineral oil.

Within the first 5 days, precipitate formed in all setups no matter which temperature was applied. Even at 20 °C neither spherulites nor crystals were grown. This supports the conclusion that the PCR plate itself caused the precipitation. It is possible that surface interactions between protein, precipitant and the material of the plate caused the precipitation of all protein. Indeed, when incubated in a *Terasaki* or *IMP@CT<sup>TM</sup>* plate at constant 4 °C, crystals appeared though slightly smaller but with the same shape as before. In summary, no crystal improvement was obtained by varying the incubation temperature.

#### *6.1.1.3 Heterogeneous nucleating agents*

As already described, harvesting of crystals was rather difficult as they stuck to the surface of the crystallisation plates. Touching with a nylon loop damaged crystals in most cases. To overcome this problem, the application of a heterogeneous nucleating agent was tried. Small

polystyrene particles from a grounded *Terasaki* plate were added to the crystallisation buffer in a ratio of 0.5 µg/µl prior to crystallisation setup. These small particles were supposed to initiate nucleation as it was observed that crystals preferentially grew on impurities within a crystallisation drop<sup>[149]</sup>. If the particles were small enough, a crystal attached to it might have been harvested with the synthetic grain.

Nevertheless, this approach ultimately failed. On one hand, crystals with known shape still adhered to the wall of the wells, but no crystals were detected attached to the particles. On the other hand, grains from the *Terasaki* plate were rather large (several hundred µm) although they were prepared in a mortar filled with liquid nitrogen. It is possible that during this process the surface of the plastics was altered disavouring crystal growth. However, even if crystals had been grown there, it is questionable if harvesting them together with the particles was possible at all.

#### 6.1.1.4 Crystallisation in agarose gels

Though offering quite remarkable properties, the use of agarose gels in protein crystallography is rather seldom reported in literature<sup>[150, 151]</sup>.

Agarose matrices create an environment that avoids sedimentation of crystals or precursors as these are trapped inside the pores of the gel. They can further promote nucleation, favour a high internal order and can generate crystals with low mosaicity. The main reason for this is a reduced convection inside the gelatinous matrix that allows for controlled crystal growth in three dimensions. It has also been observed that agarose gels could eliminate twinning of ADH crystals and prevent the incorporation of impurities<sup>[152]</sup>. With all these characteristics, agarose gels seemed to be most suitable for crystallisation of ETR1.

Agarose solutions (*Roti<sup>®</sup>garose MEEO*, *Carl Roth GmbH*) were prepared with demineralised water in concentrations of 0.6 to 3.0 % (w/v) in increments of 0.6 %. These solutions were briefly boiled to solve the agarose and then cooled down to 40 °C. Crystallisation buffer (100 mM Tris/HCl, pH 8.5 and 11 % (w/v) PEG 1500) was also pre-warmed to 40 °C and mixed with the agarose solution in equal amounts. 2 µl of the gel solutions were mixed in a microbatch plate with 1 µl of protein solution (5 mg/ml). Plates were covered with mineral oil and stored at 21 °C. To evaluate if the temperature of the pre-warmed agarose-precipitant mix had an influence on crystal growth, controls were set up with protein solution without agarose that was briefly incubated at 40 °C.



The results of this screen are shown in Figure 29. Crystals with known amorphous shape were obtained only in agarose-free crystallisation drops. Also heavy precipitate was found here, most probably due to denatured protein upon incubation at 40 °C. All other drops remained clear in terms of crystalline structures. However, the gelatinous texture of the agarose is visible.

Though no improvement was made for crystals of truncated AtETR1, it might be considered to expand this study. It is obvious that concentrations above 0.4 % (w/v) agarose lead to rough structured matrices, probably unsuitable for crystallisation.

In setups with less than 0.4 % (w/v) agarose the gel looks uniform and although no crystals were obtained, precipitate was not formed either. The fact that formation of disordered structures such as denatured protein is inhibited is a good indicator that the agarose gel serves its purpose.

Evidently, the composition of the initial crystallisation buffer was altered by the water in which the agarose was solved probably preventing potential crystal growth. Though setting up the agarose screen with water was according to published protocols<sup>[150, 152]</sup>, it might be worth testing if crystal growth can be achieved for lower concentrations of agarose solved in crystallisation buffer.

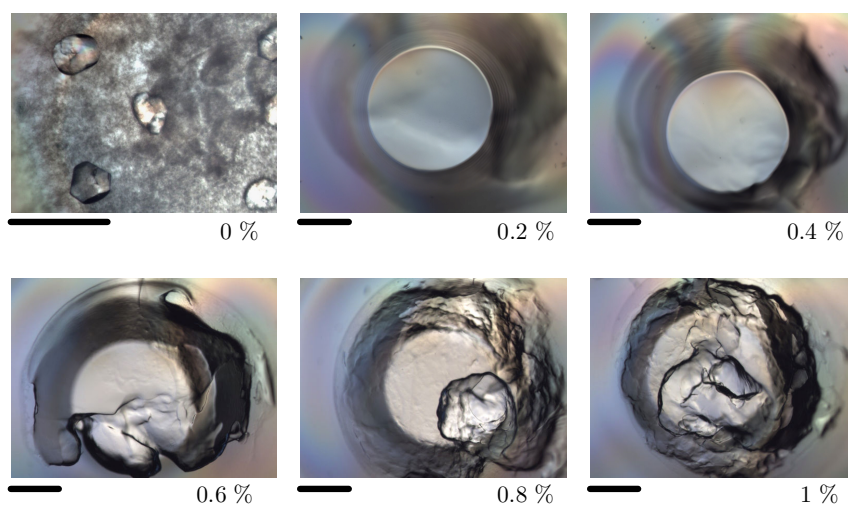


Figure 29: Crystallisation of wild type AtETR1<sub>165-738</sub> in 0.2 to 1 % (w/v) agarose gels. Images were taken 30 days after setup. The scale bar corresponds to 400  $\mu\text{m}$ . The condition without agarose (0 %) yielded crystals with known shape.

Among the optimisation trials presented in the previous sections, changes in crystallisation setup including different crystallisation methods (micro batch, hanging and sitting drop vapour diffusion) and use of a pipetting robot were compared. Unfortunately, none of these strategies did improve crystal growth and diffraction quality, respectively.

### 6.1.2 Protein modification

Variation of several external factors did not improve crystal growth. Thus, two approaches were taken to modify the receptor protein to improve crystallisation. It is obvious that flexible parts of a protein will obstruct formation of highly ordered crystals. These flexible structures might either be protein internal domains that can perform conformational changes, for example, upon phosphorylation or low structured loops and surface exposed flexible side chains. To eliminate such flexibility in AtETR1<sub>165-738</sub>, the purified receptor protein was either genetically or chemically modified.

#### 6.1.2.1 Reductive methylation

A very common approach to chemically alter a protein surface is reductive methylation of primary amines in lysines and the N-terminus<sup>[79, 80]</sup>. This method has been proven to initiate crystal growth for various proteins that did not crystallise in the first place including virulence factors of *Yersinia pestis* and the head portion of myosin (subfragment-1) from chicken<sup>[153, 154]</sup>.

The target protein is treated with formaldehyde, which forms a *Schiff* base with the  $\epsilon$ -amino group of a lysine residue (Figure 30A). Under reducing conditions, this intermediate reacts to a secondary amine. The reaction is repeated, and a second methyl group is added.

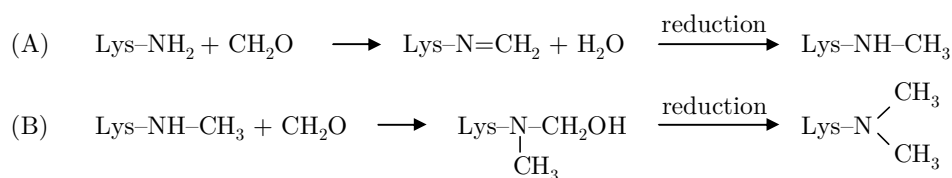


Figure 30: Reaction scheme of reductive methylation of lysine residues. During the first reaction (A) the amino group of a lysine residue is reduced to a secondary amine. The reaction is repeated to result in di-methylated lysine (B).

AtETR1<sub>165-738</sub> was subjected to reductive methylation as described in section 4.8.5.3. Protein modification was accompanied by a significant loss of protein (over 75 %) due to precipitation. This effect is rather common when methylation is performed at protein concentrations > 1 mg/ml but not with the low protein concentration used with AtETR1<sub>165-738</sub>. Nevertheless, the modification of a protein surface alters its pI and thereby its solubility which might explain the observed aggregation<sup>[79]</sup>.

Remaining protein was used in *Qiagen's Classics Suite I*. Additional setups were prepared in microbatch with the known buffer (100 mM Tris/HCl, pH 8.5 and 11 % (w/v) PEG 1500). It

turned out that neither crystals nor spherulites were grown in the Tris-PEG buffer. All drops remained clear over a period of several weeks until they finally dried up. This result indicates that methylation had a huge impact on crystallisation properties of the truncated receptor protein. Obviously, the modifications did alter its structure strongly, so a comprehensive buffer screening would have to be applied to find a new suitable crystallisation condition. However, due to the low yield of methylated protein only the *Classics I* screen was applied, which showed heavy precipitate but no crystalline structures.

#### 6.1.2.2 Surface entropy reduction

To overcome disordered crystal packing, the truncated ETR1 receptor was genetically modified aiming to reduce the surface entropy of the protein. This effect is usually achieved by substituting clusters of two or three residues with large, flexible and solvent exposed side chains by amino acids with lower conformational variability. Typically, lysine, glutamic acid and glutamine residues are replaced by alanine<sup>[155]</sup>. This modification can ultimately initiate crystallisation by providing homogenous protein surfaces that can form intermolecular contacts and pack tightly to a crystal lattice as shown in Figure 31.

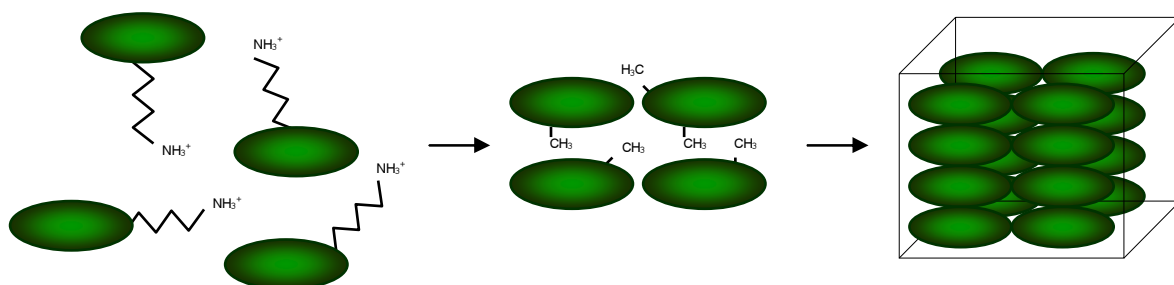


Figure 31: Effect of surface entropy reduction on crystal packing. Lysine side chains on protein surfaces (green spheres) are mutated to alanine residues favouring packing of the molecules into a tight crystal cluster (right).

Identification of highly entropic side chains in a target sequence is done by web-based *SERp* server<sup>[156]</sup>. Submitted sequences (amino acid or DNA) are analysed from three aspects. These include secondary structure prediction by *PSIPRED*<sup>[111, 110]</sup>, a *PSI-BLAST* search to identify conserved residues that may be of involved in functional sites and a side chain conformational entropy profile. The latter one produces an entropy score for each amino acid considering allowed conformations of residues and their solvent exposure frequency as determined from

known structures. The *PSIPRED* algorithm uses neural networks to estimate secondary structure elements by analysing the output of position specific iterated *BLAST* searches. In this approach, not structured elements like  $\alpha$ -helices and  $\beta$ -sheets are of interest but flexible loops with potential solvent exposed amino acids.

Taken together, these three processes can identify residues suitable for mutation studies. Typically, these residues are non-conserved and clustered in protein regions that are predicted to be highly entropic, such as surface exposed amino acids. Refinement of the obtained results includes a meta search on the PDB database to identify solvent exposed residues in proteins of known structure.

Using the surface entropy reduction method, several structures of proteins were solved that did not produce crystals in the wild type form including human choline acetyltransferase and Hsp33 from *B. subtilis*<sup>[157, 158]</sup>.

```

MKTTLVELGRTLALEECALWMPTRTGLELQ
LSYTLRHQHPVEYTVPIQLPVINQVFGTSRAV
KISPNSPVARLRPVSGKYMLGEVVAVRVPLH
LSNFQINDWPELSTKRYALMVLMLPSDSARQW
HVHELELVEVVADQVAVALSHAAILEESMRAR
DLLMEQNALDLARREAETAIRARNDFLAVMN
HEMRTPMHAIIALSSLLQETELTPEQRLM
VETILKSSNLLATLMNDVLDLSRLEDGSLQLE
LGTFLNLHTLFREVLNLKPIAVVKKLPITL
NLAPDLPEFVVGDKRLMQIILNIVGNAV
FSKQGSISVTALVTKSDTRAADFFVPTGS
HFYLRVKVKDSGAGINPDIPKIFTKFAQTQS
LATRSSGGSGGLAISKRFVNLMEGNIWIESD
GLGKGCTAIFDVKLGISERSNESKQSGIPK
VPAIPRHSNFTGLKVLVMDENGVSVMVTKGLL
VHLGCEVTTVSSNEECLRVVSHEHKVVFMDVC
MPGVENYQIALRIHEKFTKQRHQRPLLVAL
SGNTDKSTKEKCMSFGLDGVLKPVSLDN
IRDVLSDLLEPRVLYEGM

```

Figure 32: Amino acid sequence of receptor protein AtETR1<sub>165-738</sub>. Residues identified by the *SERp* web server are highlighted bold red.

In case of AtETR1<sub>165-738</sub> 18 residues in eight clusters were recognised to potentially interfere with crystallisation and ordered crystal packing (Figure 32).

In consequence, all amino acids were mutated to alanine by sequence and ligation independent cloning (see methods section 4.3.6), and the construct was designated AtETR1<sub>165-738</sub>SER.

The standard expression protocol for wild type AtETR1<sub>165-738</sub> was employed, but analysis of the expression samples by SDS-PAGE and western blotting revealed that no protein of the mutant was produced at this condition (data not shown).

Successful production of the SER mutant was obtained by replacing the expression strain BL21 (DE3) to BL21-Gold (DE3) and a rather late induction of

protein production at OD<sub>600</sub> ~ 3.0. Cells continued to grow for about 2-3 hours at these conditions, and target protein was faintly visible in silver stained acrylamide gels (Figure 33A). There is no rationale why the derivate strain BL21-Gold (DE3) yielded protein but BL21 (DE3) did not. The improved variant is just lacking endonuclease I which makes this strain suitable for cloning but should have no influence on protein expression.

Isolation of the mutant receptor was carried out using denaturing IMAC purification as described for the wild type receptor (see 4.7.2). Purification steps of the wild type protein and samples of both proteins after refolding are shown in Figure 33B. On average, preparation yielded about 3 mg highly pure wild type AtETR1<sub>165-738</sub> per litre cell culture. Yields for the mutant protein were noticeably lower and amounted to less than 1 mg/l.

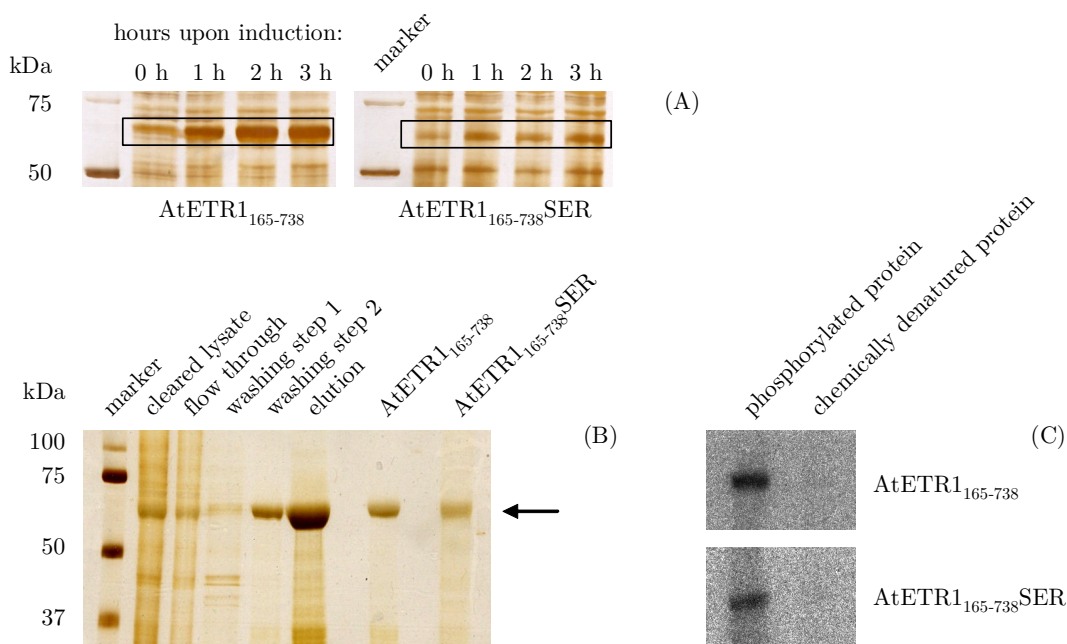


Figure 33: (A) SDS-PAGE analysis of samples from expression of wild type and mutant AtETR1<sub>165-738</sub>. Boxes indicate the protein bands corresponding to receptor protein in silver stained acrylamide gels. In the lower figure (B) purification of wild type receptor protein is shown. Cleared lysate after centrifugation was applied to Ni-NTA matrix and samples from the flow through fraction, two wash steps and the elution fraction were analysed by SDS-PAGE. Buffer for washing step 1 did not contain imidazole. Buffer for washing step 2 was supplied with 30 mM imidazole. Elution of bound target protein was achieved by 200 mM imidazole. Both proteins were refolded by dilution and samples are shown in the two right lanes of figure (B) indicated by arrow. Figure (C) displays an autoradiography showing incorporation of <sup>32</sup>P phosphate into receptor protein AtETR1<sub>165-738</sub> and the SER mutant. Chemical denaturation of both proteins prior to phosphorylation was achieved by incubation with SDS. These proteins showed no incorporation of radiolabelled <sup>32</sup>P.

Both proteins regained functionality after refolding as proven by incorporation of <sup>32</sup>P phosphate upon autokinase activity (Figure 33C). To determine possible structural changes caused by the genetic modification, CD spectra were recorded over a range of 260-195 nm as described in section 4.8.2. Proteins were diluted to 0.25 mg/ml into 50 mM potassium phosphate buffer supplied with 0.05 % (w/v) DDM. Recorded spectra were processed with the software package *CDPro* as described earlier to give estimation on secondary structure

composition. Data were compared to those calculated by *PSIPRED*<sup>[110]</sup> and *BetaTPred2*<sup>[112]</sup> and are summarised in Table 19.

Table 19: Secondary structure composition of wild type AtETR1<sub>165-738</sub> and the surface entropy reduced mutant AtETR1<sub>165-738</sub>SER as calculated from the amino acid sequence and from experimental data. All values are given in %.

<i>Protein</i>	<i>Data source</i>	$\alpha$ -helices	$\beta$ -strands	$\beta$ -turn	<i>Random coil</i>
AtETR1 <sub>165-738</sub>	experimental	28 – 31	21	20 – 22	29
	theoretical	36	16	23 – 24	23 – 24
AtETR1 <sub>165-738</sub> SER	experimental	34 – 36	16 – 17	19 – 21	28 – 29
	theoretical	37	15 – 16	21 – 23	24 – 25
range		0 – 10 %	11 – 20 %	21 – 30 %	31 – 40 %

Even though the three putative transmembrane helices are missing, AtETR1<sub>165-738</sub> and the mutant protein still show a strong  $\alpha$ -helical content of over 30 %. Experimental values for the wild type receptor show about 5-8 % less  $\alpha$ -helices as predicted by *PSIPRED* algorithm. In contrast, the amount of  $\beta$ -sheets is increased by that figure. These minor changes might be due to the accuracy of data processing as outlined in chapter 5.1.3.1. Predicted and experimental data for the surface entropy reduced mutant AtETR1<sub>165-738</sub>SER show better agreement.

In summary, the CD measurements indicate that substitution of the 18 residues that are supposed to favour surface entropy and amount to 3 % of the receptor's total amino acids did not significantly alter the structure of the receptor protein.

Prior to use in crystallisation setups, the mutant AtETR1<sub>165-738</sub>SER protein was further characterised by size exclusion chromatography (see 4.6.6). Approximately 2 mg of wild type protein and about 0.4 mg of the mutant receptor, both diluted in the same volumes, were applied to a *HiPrep 16/60 Sephacryl S-200* column (effective molecular weight range: 5 – 250 kDa).

Figure 34A illustrates that the wild type protein eluted almost completely in the void volume of the column indicating severe aggregation of the receptor. A second minor protein peak at about 60 kDa can be assigned to monomeric AtETR1<sub>165-738</sub>, which has a calculated molecular weight of 66.3 kDa (including the affinity tag). Figure 34B shows the results for the SER mutant (65.3 kDa). Here, three peaks are detectable in the chromatogram that can be assigned

molecular weights of 260, 131 and 59 kDa. Apart from protein eluting in the void volume—as for the wild type receptor—the two other peaks could account for receptor monomers and dimers, respectively. The fact that the second and the third peak gave hardly any signal in SDS-PAGE analysis might be due to the overall low amount of protein that was applied to size exclusion chromatography.

Though looking promising, it turned out that aggregation of the SER mutant receptor was concentration dependent and increased dramatically with higher protein concentrations. In preparative approaches, the protein concentration was set to 8 mg/ml to allow for application of a small sample volume to avoid dilution and peak broadening upon chromatography. Furthermore, this concentration was chosen to be used in later crystallisation studies. When performing SEC under this condition, almost all protein eluted in the void volume producing a chromatogram like AtETR1<sub>165-738</sub> in Figure 34A.

Aggregation of the SER mutant was quite unexpected as wild type AtETR1<sub>165-738</sub> formed precipitate already during concentration, but no aggregation was observed for the mutant receptor at this point. Hence, it was expected that the mutant receptor was less prone to aggregation.

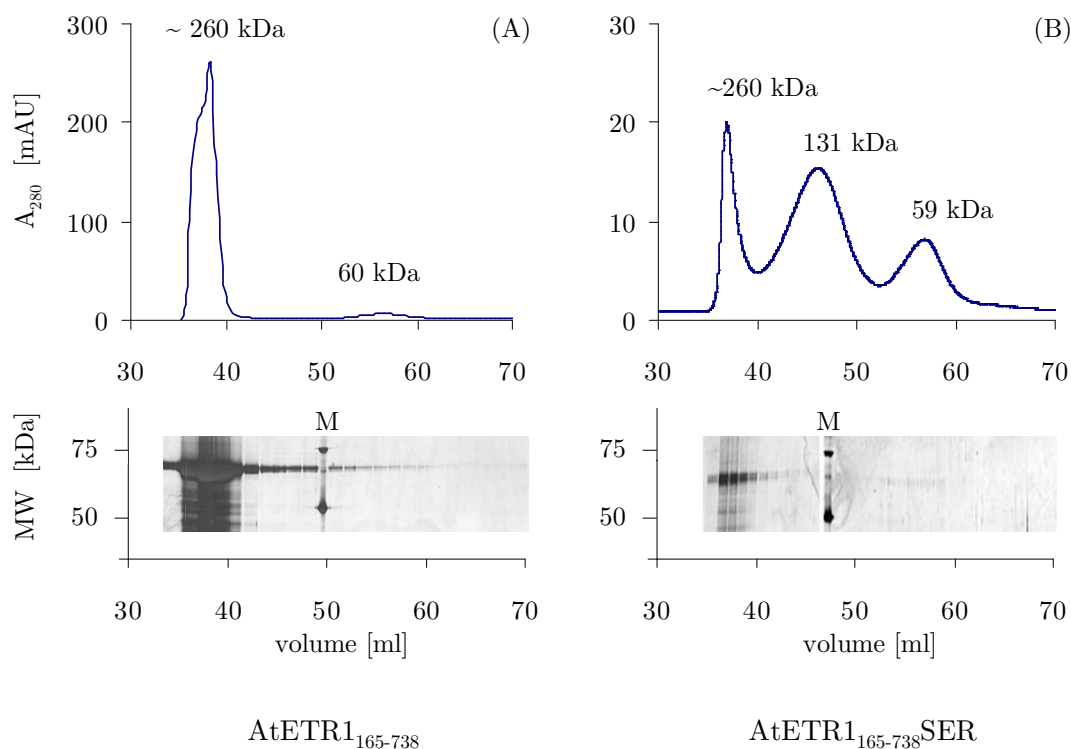


Figure 34: Size exclusion chromatograms of receptor proteins AtETR1<sub>165-738</sub> (A) and AtETR1<sub>165-738</sub>SER (B). Samples from elution fractions were analysed by SDS-PAGE. The gels are aligned with the chromatograms to show protein composition of each peak. Note that magnitude of ordinates differs by a factor of 10. M = protein marker



The results from size exclusion chromatography and CD spectroscopy support two conclusions. First, the severe aggregation of wild type AtETR1<sub>165-738</sub> is probably in charge for the observed amorphous crystal growth. If the crystal is mainly build from precipitated protein, an ordered lattice cannot form even if partially monomeric protein is present.

Second, it is highly probably that reduction in surface entropy altered the proteins secondary and eventually tertiary structure. However, it did not prevent precipitation at high concentrations. Membrane proteins often contain hydrophobic patches on their surface. If these regions are brought together in spatial proximity, aggregation could still occur. The fact that this event did not occur in solution, at least not visibly, might indicate that a trigger is needed to initiate precipitation like *surface-induced* aggregation caused by the column matrix<sup>[159]</sup>.

In spite of the problems with the SER mutant at high concentrations, the receptor protein was applied to microbatch crystallisation at a concentration of 5 mg/ml (see 4.8.5.1). *Qiagen's Classics Suites I and II*, the *JCSG<sup>+</sup>* screen and the standard Tris-PEG buffer, which had already produced crystals for the wild type were used. Crystallisation drops were set up in *IMP@CT<sup>TM</sup>* plates by mixing equal shares of protein and precipitant solution to a final volume of 1.5 µl. Plates were layered with mineral oil and stored at 21 °C. Over a period of 1 to 3 months, the drops were examined for potential crystal growth until they finally dried up.

Inspection of the crystallisation trials revealed amorphous shaped structures in several conditions including the Tris-PEG buffer (Figure 35). These structures formed within the first week after setup. Other conditions containing PEGs almost exclusively formed a skin, a phenomenon often observed in membrane protein crystallography where polyethylene glycols together with detergent and denatured protein can create a layer covering the drop and preventing further equilibration<sup>[160]</sup>.

Taken together, the SER approach did not improve crystallisation of the receptor but had a rather counter-productive effect. While the wild type protein crystals showed minor symmetry at least, the bulky structures obtained with the SER mutant missed edges and visible order and were not suitable for diffraction analysis.

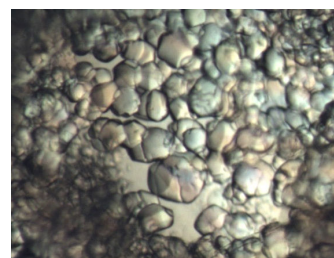


Figure 35: Amorphous crystals of receptor AtETR1<sub>165-738</sub>SER grown in 100 mM sodium phosphate citrate pH 4.2, 40 % (v/v) ethanol and 5 % (w/v) PEG 1000. The image was taken 14 days after setup. The scale bar corresponds to 100 µm.



## 6.2 Crystallisation of full-length ETR1

In spite of many efforts on optimising crystallisation conditions for the soluble kinase and receiver domain of the ETR1, the receptor protein did not produce crystals suitable for diffraction studies.

Parallel to crystallisation experiments with truncated AtETR1<sub>165-738</sub>, the full-length receptor was subjected to crystallisation trials with the standard Tris-PEG buffer (100 mM Tris/HCl pH 8.5, 11 % (w/v) PEG 1500) supplied with 1-2 % (w/v) sodium cholate, *n*-octyl- $\beta$ -D-glucopyranoside and *n*-dodecyl- $\beta$ -D-maltopyranoside. It turned out that a buffer containing sodium cholate induced crystal growth of full-length receptor. The crystals obtained showed a morphology similar to that of the truncated receptor fragment and are characterised as barrel-like structure with edges at top and bottom (Figure 36A). The crystals gave distinct protein bands in SDS-PAGE analysis corresponding to the molecular weight of the purified full-length receptor AtETR1 (Figure 36B). Albeit this familiar forms, further structures grew showing a more angular shape. As with the crystals of the kinase and receiver domain, the crystals were very fragile and stuck firmly to the crystallisation plates. Diffraction measurements revealed a low resolution of about 12 Å, anisotropic scattering and high mosaicity preventing indexing and processing of the data obtained (Figure 36C). Anisotropic diffraction is often observed for membrane proteins and is caused by inherent flexibility of the proteins and disordered detergent molecules that interfere with crystal packing<sup>[161]</sup>.

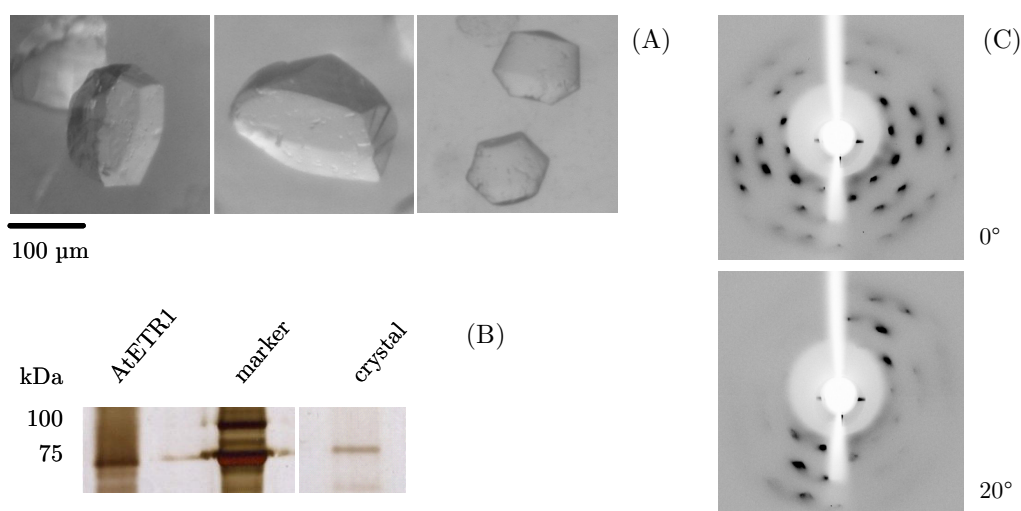


Figure 36: Crystals (A) obtained in 100 mM Tris/HCl pH 8.5, 11 % (w/v) PEG 1500 and 1 % (w/v) sodium cholate. Images were taken 7 days after setup. (B) Analysis of crystal content by SDS-PAGE. Receptor AtETR1 was identified by comparison to a reference sample of purified full-length receptor (lane AtETR1). Figure (C) shows diffraction images collected at an interval of 20°. Outer spots appear at about 12 Å resolution.

Comprehensive optimising efforts like with the truncated receptor AtETR1<sub>165-738</sub> were applied to improve diffraction. However, all approaches to improve crystal quality failed.

In addition, microseeding was tested as another variation of the external parameter. Formation of a protein crystal is a two step process: First, nucleation occurs followed by crystal growth. However, both events will require different solution conditions. In order to obtain large, well-ordered crystals, it might be necessary to separate both events<sup>[162]</sup>. In microseeding, a previously grown crystal is pulverised, and a dilution series is set up in mother liquor with the crystalline particles. These seeds are then introduced to new crystallisation setups with a reduced protein or precipitant concentration to allow crystal growth but no nucleation.

According to methods section 4.8.5.2 an AtETR1 crystal was grounded, and the resulting particles were introduced to new crystallisation drops. Plates were incubated at 4 °C and 20 °C but did not produce any solid structures. Over a period of 3 months the drops stayed clear until they finally dried up. It can only be assumed that the mother liquor was too dilute in terms of protein concentration. So, supersaturation necessary for crystal growth was not achieved.

In consequence, further efforts focussed on modifications of the receptor protein starting with the removal of the affinity tag.

### 6.2.1 Effect of histidine affinity tag

Conformational variability in a protein is mainly caused by flexible, low structured regions like loops. Affinity tags such as the deca His-tag in case of AtETR1 can also contribute to the overall entropy as they do not exhibit an ordered secondary structure.

Full-length receptor protein prepared under denaturing condition (see 4.7.1.1) was subjected to cleavage with factor Xa\*. Analytical studies identified a protease-protein ratio of 0.05 U/μg protein and incubation at 4 °C over night as optimum cleavage condition (Figure 37). Undigested protein as well as

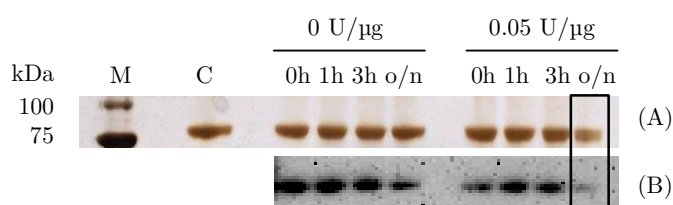


Figure 37: SDS-PAGE analysis (A) and western blot (B) of samples from analytical digest of full-length AtETR1 with protease factor Xa. The condition chosen for preparative cleavage is framed. C = control sample (AtETR1 without protease), M = marker, o/n = over night.

\* Wild type AtETR1 was cloned into vector pET-16b. There, the N-terminal deca His-tag is linked to the target protein by a factor Xa protease recognition sequence.

the peptide tags were removed by Ni-NTA chromatography. This subsequent purification by IMAC resulted in a major loss of protein (approximately 50 to 75 %) yielding less than 0.05 mg tag-free ETR1 per gram cells.

The tag-free receptor protein was concentrated to 5-8 mg/ml and applied in microbatch crystallisation setups (2 µl final drop size) with Tris-PEG buffer supplied with 1 % (w/v) sodium cholate. The plates were stored at 21 °C as before, and crystals with the known barrel-like structure were obtained. Of course, removal of the tag might change the crystallisation characteristics of a protein in principle. Hence, further crystallisation conditions were screened applying crystallisation kits *JBScreen Membrane 1* and *2* and *MemStart* from *Molecular Dimensions*. However, none of the other conditions resulted in crystals during the next three months. In summary, these experiments indicate that the affinity tag is not in charge for the amorphous shape of the crystals.

### 6.2.2 Influence of the purification method on crystallisation of ETR1

A native purification protocol was established for AtETR1 to allow for non-destructive solubilisation of the receptor protein from its bacterial host membranes. The aim of this approach was to avoid complete lipid depletion of the receptor protein.

In their native environment, lipids can play a structural role on integral membrane proteins. For the light harvesting complex of photosystem II (LHC-II) from pea chloroplasts, delipidation of LHC-II completely abolished crystal growth<sup>[163]</sup>. A similar effect was observed for the cytochrome  $b_6f$  complex from the cyanobacterium *Mastigocladus laminosus*. When structural important lipids were absent, the complex would only crystallise in a proteolysed form<sup>[164]</sup>.

To identify a surface-active agent most suitable for solubilisation, a set of 23 detergents covering non-ionic and zwitter-ionic substances was incubated with bacterial membranes containing receptor AtETR1 (see 4.6.2). Depending on their chemical properties, detergents were applied in concentrations of 1 to 2 % (w/v) according to appendix 9.3.

As shown in Figure 38A two detergents, *FOS-CHOLINE*<sup>®</sup>-13 and -14, effectively released the receptor from its bacterial host membranes. Eventually, *FOS-CHOLINE*<sup>®</sup>-14 was chosen because of its lower CMC (0.0046 %, compared to 0.027 %).

Solubilised proteins were applied to Ni-NTA for subsequent purification according to section 4.7.1.2. Binding to the affinity matrix was only possible when ion strength of the buffer was increased to 2 M NaCl, thereby promoting hydrophobic interactions<sup>[165]</sup>.

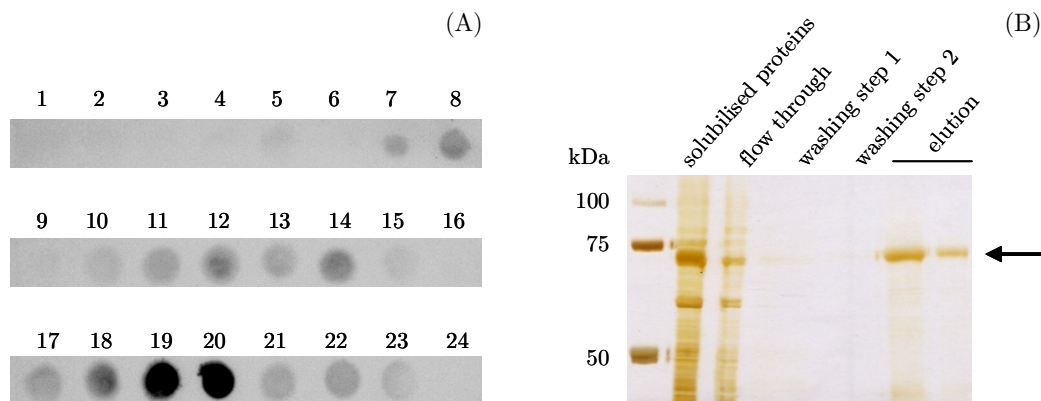


Figure 38: (A) Dot blot for detection of AtETR1 solubilised from *E. coli* membranes. Supernatant fractions after centrifugation were applied, and solubilised protein was identified by a His antibody. The following detergents were used in concentrations of 1 or 2 % (w/v):

- 1) ANAPOE<sup>®</sup>-20, 2) ANAPOE<sup>®</sup>-35, 3) ANAPOE<sup>®</sup>-58, 4) ANAPOE<sup>®</sup>-C10E6, 5) ANAPOE<sup>®</sup>-X-114,
- 6) ANAPOE<sup>®</sup>-X-405, 7) ANZERGENT<sup>®</sup>-3-10, 8) ANZERGENT<sup>®</sup> 3-12, 9) ANZERGENT<sup>®</sup> 3-14,
- 10) C-DODECAFOS<sup>TM</sup>, 11) CYCLOFOS<sup>TM</sup>-4, 12) CYCLOFOS<sup>TM</sup>-5, 13) CYCLOFOS<sup>TM</sup>-6,
- 14) CYCLOFOS<sup>TM</sup>-7, 15) FOS-CHOLINE<sup>®</sup>-9, 16) FOS-CHOLINE<sup>®</sup>-10, 17) FOS-CHOLINE<sup>®</sup>-11,
- 18) FOS-CHOLINE<sup>®</sup>-12, 19) FOS-CHOLINE<sup>®</sup>-13, 20) FOS-CHOLINE<sup>®</sup>-14, 21) *n*-octyl- $\beta$ -D-glucopyranoside,
- 22) *n*-dodecyl- $\beta$ -D-maltopyranoside, 23) *n*-octyl- $\beta$ -D-thiomaltopyranoside, 24) no detergent

(B) Purification of solubilised full-length AtETR1 by IMAC. Washing buffer 1 did not contain imidazole. Buffer 2 was supplied with 50 mM imidazole. Release of bound target protein was achieved by iterative elution with 250 mM imidazole.

The purified protein was tested for autokinase activity, and CD spectroscopy demonstrated a secondary structure composition highly similar to AtETR1 purified under denaturing condition (data not shown).

The native purification protocol was used to isolate ETR1 orthologs from *Physcomitrella patens* and *Lycopodium obscurum*, too (see section 7.2.2.1). In those preparations a contamination with heat shock protein Hsp70 (DnaK) was observed. Analysis of proteins samples from purified AtETR1 revealed the same contamination (Figure 39). In conventional SDS-PAGE the chaperon was not detected as AtETR1 and DnaK run at the same apparent molecular weight although they differ about 15 kDa in their calculated size (DnaK: 70 kDa, AtETR1: 85 kDa). This *gel shifting* is a phenomenon often observed for membrane proteins where helical structures may be embedded in SDS micelles rather than being unfolded. In consequence, these more compact structures facilitate faster migration in acrylamide gels<sup>[166]</sup>.

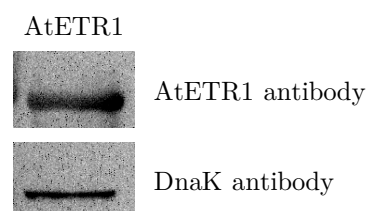


Figure 39: Western blot analysis of samples from native purification of full-length AtETR1.

The cross contamination of the natively purified ETR1 receptors by DnaK might result from the specific affinity of the chaperone to the connector peptide region of pET-vectors<sup>[167]</sup>. The binding motif for DnaK consists of a core formed by 4-5 hydrophobic residues (preferably a random combination of Leu, Ile, Val, Phe and Tyr). Two adjacent regions of four residues with basic amino acids favour the binding of the chaperone. This motif is rather common and occurs on average every 36 residues in a protein sequence<sup>[168]</sup>. In folded proteins, these motifs are usually not exposed. Hence, DnaK binding is commonly considered at non-structured regions such as the affinity tag including the linker region.

Expression vector pET-16b::AtETR1<sub>1-738</sub>WT does not hold such a motif in its starting sequence (MGHHHHHHHHHHSSGHIEGRH...). There is only one hydrophobic amino acid present (Ile) that probably cannot affect DnaK binding on its own.

In contrast, in cloning vector pTEV-16b, which was used for expression of PpETR1 and LeETR1, this sequence is composed of MGHHHHHHHHHHSSGHENLYFQGH... which is fused N-terminally to the target protein and thereby provides a putative hydrophobic core region (underlined sequence). The basic His residues present in the left and right region might promote the observed DnaK binding (see section 7.2.2.1).

As the contamination with the chaperon was equally present in preparations of AtETR1, LeETR1 and PpETR1, there have to be further reasons for the presence of DnaK. A straight forward is that the chaperone assists in protein folding as AtETR1 and its orthologs might contain unfolded or misfolded regions<sup>[169]</sup>. This possibility cannot be ruled out because aggregation due to exposure of hydrophobic regions is a phenomenon common in heterologous expression. When synthesis occurs faster than folding, non-folded protein will accumulate in the host cell and is targeted by DnaK.

To overcome the contamination with DnaK, two non-invasive approaches were tested for receptor protein AtETR1. According to *Rial et Ceccarelli*<sup>[170]</sup> release of DnaK can be promoted by incubation of the target protein with  $Mg^{2+}$ •ATP because substrate binding and release of DnaK is coupled to its ATPase activity. By binding of ATP, a conformational state with low substrate affinity is induced while this effect is reversed when ADP is bound<sup>[171]</sup>. To enhance release of DnaK from a target protein, denatured proteins can be provided as a kind *bait* for DnaK.

In a second approach referring to *Pastorino et al.*<sup>[169]</sup>, incubation of the target protein with 0.5 M arginine might remove DnaK contaminations, too. Arginine has previously been described as useful additive for refolding and stabilising of recombinant proteins, thereby reducing

aggregation. *Ishibashi et al.*<sup>[172]</sup> showed that arginine could prevent aggregation but did not induce protein denaturation at concentrations up to 2 M. The mechanism of this effect is not understood yet. It is proposed that arginine may interact with  $\pi$ -electrons of aromatic side chains through its guanidinium group, thereby suppressing interaction with amino acid residues of DnaK<sup>[173]</sup>. It is also possible that due to the chaotropic effect of arginine, hydrogen bonds that are responsible for binding of the chaperon to the protein are broken.

Both methods were performed according to section 4.6.7. The advantage of the first method is that it can be performed while the target protein is still bound to a Ni-NTA column. This does not work for the second method as protein binding to the affinity matrix is prevented by arginine. For the second approach anion exchange chromatography was used to trap released DnaK (pI 4.8) whereas AtETR1 (pI 7.7) should elute with the flow trough. However, both methods did not remove the heat shock protein. Obviously, affinity of DnaK for the receptor protein was stronger than for the denatured *E. coli* proteins. Probably, these *bait* proteins were aggregated in solution leaving no contact area for the chaperon which in consequence bound to AtETR1 again. Furthermore, it is possible that aromatic side chains were covered with detergent, thereby preventing possibly interactions of arginine with side chains of DnaK participating in binding.

With no option to remove the contaminating chaperon, it was considered to subject AtETR1 to crystallisation studies on a trial basis and accept the contamination in a kind of co-crystallisation approach. This is certainly a very hypothetical assumption, but the addition of soluble proteins in crystallisation setups had previously been successful in favouring crystal growth and improving diffracting qualities<sup>[174]</sup>. However, in those cases, proteins were intentionally brought together rather than accepting a contamination that might not be eliminated. On one hand, antibody fragments are often applied to enlarge hydrophilic parts of membrane proteins to promote intermolecular forces between individual protein molecules<sup>[175]</sup>. On the other hand, a second protein which has been identified as putative interaction partner can bind to the target protein and lock it in a defined structure, thereby enhancing ordered crystal packing<sup>[176]</sup>.

Crystallisation studies with natively purified AtETR1 were done with two different detergents: the zwitter-ionic *FOS-CHOLINE*<sup>®</sup>-14 used for solubilisation of the receptor and the non-ionic detergent *n*-dodecyl- $\beta$ -D-maltopyranoside (DDM), which is often successfully applied in membrane protein crystallography<sup>[177]</sup>. Detergent exchange from *FOS-CHOLINE*<sup>®</sup>-14 to DDM was performed during IMAC purification while the receptor was still bound to the affinity

matrix. Subsequent concentration of eluted protein showed that the sugar-based detergent promoted precipitation of AtETR1. Typically, about 0.5 mg purified receptor were obtained per gram cells when solubilised in *FOS-CHOLINE*<sup>®</sup>-14. Application of DDM reduced the yield by approximately 75 %.

Protein loss is probably related to an excess in detergent. Due to its size (~ 75 kDa) empty micelles of DDM are concentrated together with receptor containing micelles in ultra filtration units with a molecular weight cut-off of 50 kDa. Increasing detergent will remove structurally important lipids that stick to the target protein at a moderate concentration resulting in destabilisation and aggregation of the proteins<sup>[178]</sup>. *FOS-CHOLINE*<sup>®</sup>-14 micelles are distinct smaller (~ 40 kDa). So, they can pass through the filtration unit and will not induce delipidation.

Receptor AtETR1 in *FOS-CHOLINE*<sup>®</sup>-14 or DDM containing buffer was applied in microbatch crystallisation trials using *Qiagen's MbClass* and *PEGs Suites I* and *II* as well as *JBScreen Membrane 1*, *2* and *3* kits from *Jena Bioscience*. Crystallisation drops were set up in *IMP@CT*<sup>TM</sup> plates by mixing equal amounts of protein and precipitant solution to a final drop volume of 1-2 µl. Plates were layered with mineral oil and incubated at 21 °C. AtETR1 in *FOS-CHOLINE*<sup>®</sup>-14 was also tried to crystallise with the *Lipidic-Sponge Phase*<sup>TM</sup> *Screen* from *Molecular Dimension* (see section 4.8.5.1). In protein crystallography, *sponge phases* are composed of lipids, usually monoolein, that form flexible liquid bilayers in solution that mimic a native membrane environment and are therefore used to promote crystallisation of integral membrane proteins<sup>[179, 180]</sup>.

Within one day salt crystals appeared in various microbatch conditions containing either magnesium or calcium chloride. These crystals were most probably phosphate crystals as the protein solution contained sodium phosphate. Further growth of sharp-edged crystals was not observed over a period of 80 days. However, spherulites as shown in Figure 40 were obtained in several conditions. Their formation did not depend on the detergent applied in the screen.



Figure 40: Pictures (A) to (C) were taken 24 hours after crystallisation setup and show spherulites grown in (A) 50 mM MES pH 6.5, 100 mM zinc acetate, 1 M ammonium sulfate; (B) 100 mM HEPES pH 7.5 and 1.5 M lithium sulfate; (C) 100 Tris pH 8.5 and 1.5 M lithium sulfate. Black scale bars correspond to 100 µm.

Spherulitic growth is by far not the favoured trend in protein crystallisation because spherulites show only minor order in crystal packing and are thereby unsuitable for X-ray diffraction analysis. Nevertheless, crystallisation conditions that lead to these structures might guide to the right condition for getting crystals with a distinct higher order.

Spherulites usually grow from a core of either heterogeneous impurities or microscopic droplets formed as the result of phase separation<sup>[181]</sup>. Alternatively, the spherulite cores might be of crystalline precipitate. Thus, an option is to spin down the crystallisation sample after setup to remove initial aggregates. In further crystallisation trials, it might also be advisable to develop a factorial screen based on the conditions given in Figure 40. Often only slight changes in pH or precipitant concentration can have a huge impact on crystallisation and might favour optimisation of crystal growth<sup>[182, 183]</sup>.

Sharp edged crystals with a size of about 100  $\mu\text{m}$  edge length (Figure 41, A-C) were obtained with two *Lipidic-Sponge Phase*<sup>TM</sup> conditions. The crystals appeared two months after setup, but when exposed to X-rays they revealed diffraction corresponding to salt (Figure 41D).

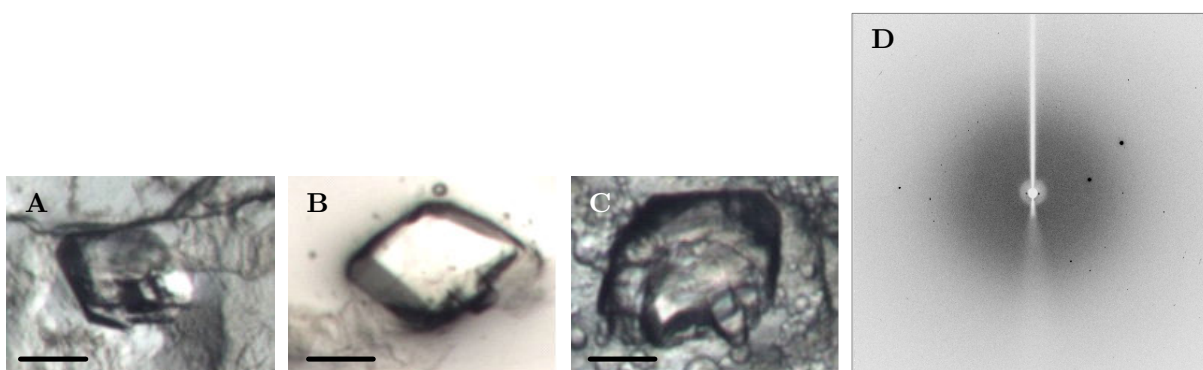


Figure 41: (A) and (B) show images of crystals grown in monoolein, Tris pH 9.0, sodium chloride, magnesium chloride and PEG 400 (concentrations are not given by the manufacturer). In condition (C) PEG 400 was substituted by PEG 1500. Black scale bars correspond to 100  $\mu\text{m}$ . Images were taken 8 weeks after setup. Image (D) shows few intense spots, typical for salt crystals (B). Outer spots appear at a resolution of 1.9  $\text{\AA}$ .



### 6.3 Synopsis

Two ETR1 constructs from *Arabidopsis thaliana* were expressed, purified and subjected to crystallisation studies. The shorter variant is lacking the transmembrane sensor domain whereas the other variant is the full-length protein.

Purification of the truncated variant AtETR1<sub>165-738</sub>, which was expressed in inclusion bodies was performed by denaturing IMAC with subsequent refolding by dilution<sup>[33]</sup>. On average, 1 mg protein was obtained from 1 g of cells.

With a buffer composed of 100 mM Tris/HCl pH 8.5 and 11 % (w/v) PEG 1500 crystals were grown with a barrel-like structure and a lateral hexagonal shape. Crystals with this morphology showed anisotropic diffraction to a maximum resolution of about 11 Å and were not suitable for structure solution because processing of collected data was not possible. Various efforts were taken to optimise these crystals including changes of external parameters, like buffer composition or experimental setup as well as modification of the protein itself (reductive methylation and surface entropy reduction by amino acid substitution).

A change of these parameters did not improve crystal shape and diffraction. Thus, focus was put on the full-length receptor protein AtETR1. When purified under denaturing conditions according to *Voet van Vormizeele* and *Groth*<sup>[33]</sup> typical protein yields of 0.1 mg/g cells were obtained.

Purified full-length AtETR1 crystallised under similar conditions as the truncated receptor variant (100 mM Tris/HCl pH 8.5 and 11 % (w/v) PEG 1500 and 1-2 % (w/v) sodium cholate). The crystals showed the known barrel-like morphology and did not allow collection of diffraction data suitable for structure analysis. The low quality of crystals obtained might be related to packing defects caused by partially disordered protein rather than flexible domains. These protein defects might be explained with complete delipidation of the receptor protein upon denaturing purification resulting in removal of structural important lipids<sup>[178]</sup>.

For that reason a native purification protocol was established by solubilising the receptor in *FOS-CHOLINE*<sup>®</sup>-14 micelles followed by subsequent metal affinity chromatography. However, the heat shock protein DnaK was co-purified and could not be removed. Accepting the chaperon as co-crystallisation reagent, natively prepared ETR1 was subjected to further crystallisation trials. Several conditions produced spherulitic crystals that are not suitable for diffraction analysis but might indicate a starting point for further screening.



## 7 Part C: Crystallisation of ETR1 orthologs from *P. patens* and *L. esculentum*

An alternative approach to solve the structure of a particular protein that resists crystallisation or shows only poor diffraction is to screen for orthologs of this protein from different organisms. This approach was taken for the tRNA-modifying enzyme QueA (S-adenosyl-methionine:tRNA ribosyl transferase/isomerase). From 12 orthologs of different eubacteria only the protein from *Bacillus subtilis* yielded crystals that diffracted to 3.2 Å resolution allowing for structure determination of QueA<sup>[184]</sup>.

In this thesis, crystals were obtained for ETR 1 from *Arabidopsis thaliana*. However, these crystals diffracted only to about 11 Å resolution and their diffraction could not be improved by numerous variations of extrinsic and intrinsic parameters.

For that reason ETR1 orthologs from two other organisms, the moss *Physcomitrella patens* (*subsp. patens*) and the tomato *Lycopersicon esculentum*, both plants being subject to current research<sup>[185, 186]</sup>, were selected for heterologous expression in *E. coli* and crystallisation studies.

ETR1s from *A. thaliana* and *L. esculentum* show a sequence identity of 80 % and a similarity of 90 %. For the moss *P. patens* these values are slightly lower. PpETR1 has a sequence identity of 63 % compared to the other species, the sequence similarity amounts to 77 % compared to *L. esculentum* and 78 % in comparison to ETR1 from *A. thaliana*.

Ethylene receptor proteins from other organisms show higher identity to AtETR1. ETR1 from the wild cabbage (*Brassica oleracea*), for example, has a sequence identity of about 95 % as identified by *BLAST* search<sup>[81]</sup>.

The observed variation in sequence identity is not surprising considering taxonomic distances of the different organisms. While *A. thaliana* and *B. oleracea* share the same family (*Brassicaceae*), the moss *P. patens* is more distantly related to the other organisms. The evolutionary separation occurred between phylum and class with the *Brassicaceae* and



Figure 42: Images of (A) inflorescence of *Arabidopsis thaliana* (cc, A. Salguero), (B) fruits of *Lycopersicon esculentum* (cc, L. Chiesa) and the moss *Physcomitrella patens* (C).

*L. esculentum* as a representative of the *Solanaceae* belonging to the *Tracheophyta* (vascular plants) whereas *P. patens* is associated to the *Bryophyta* (mosses).

However, ethylene receptors from *P. patens* and *L. esculentum* were chosen precisely because of their lower conservation to AtETR1. This fact might be reflected in the three dimensional structure which might lead to better crystallisation of these receptors compared to orthologs with higher identity.



Figure 43: *ClustalW2* alignment of ETR1 from *A. thaliana*, *L. esculentum* and *P. patens*. The *Zappo* colour scheme was set to colour amino acid residues according to their physicochemical properties. A conservation index of 50 % was chosen to show conservation by modifying the colour intensity at each amino acid position. The most conserved regions appear in a darker colour than those regions with low conservation. In addition, conservation is also indicated by vertical bars. The height of the bar corresponds to the degree of conservation. Putative catalytic residues at positions 369 (H/Y) and 703 (D) are encircled. The predicted transmembrane helices from AtETR1 and the beginning of the GAF domain are indicated by coloured boxes.

An alignment of ETR1 sequences from the three organisms is shown in Figure 43. Remarkably, the sequence similarity varies between different regions of the proteins. The transmembrane part with its three predicted helices as well as the sequence up to the GAF domain shows the highest conservation, despite the fact that LeETR1 has an extended N-terminus of 14 residues. In particular helix 2, which harbours the putative ethylene binding site (C65 and H69 in AtETR1), is completely identical in all three sequences emphasising the importance of this region<sup>[29]</sup>.

Interestingly, not both putative phosphorylation sites of AtETR1 (H353 and D659) are conserved in all three sequences. H353 (position 369 in alignment, encircled) is substituted by tyrosine in PpETR1. In contrast, D659 (position 703 in alignment, encircled) is found in all sequences. Substitution of histidine by tyrosine in the putative kinase domain is not unusual as tyrosine is the third most common amino acid that gets phosphorylated apart from serine and threonine<sup>[187]</sup>.

## 7.1 Cloning and expression of receptor constructs

The main bottleneck in crystallisation of membrane proteins is the production of protein amounts sufficient for initial crystallisation trials<sup>[134]</sup>. Especially if no automated systems are available allowing setups in the nanoliter range, several milligrams of the target protein are required for first screenings.

However, when protein production is carried out in a heterologous expression system, the codon bias of host and target organism is crucial for an effective expression. The relative usage of codons is organism specific and can severely vary among different species. For *Physcomitrella patens* and *Lycopersicon esculentum* the mean difference in codon bias compared to *Escherichia coli* is approximately 26 %.

To overcome the problem of a limited expression level in *E. coli* caused by a foreign codon bias, it is possible to provide the bacterial host with an additional expression plasmid encoding for rare tRNAs to compensate the host's deficiency in these amino acids (see description of plasmid pRARE in section 4.1.12). In a more sophisticated approach the complete DNA sequence of a gene is modified by silent mutations to adopt the codon usage of the host organism. In case of PpETR1 and LeETR1 the second approach was chosen, and both sequences were artificially synthesised with an optimised codon usage for *E. coli*.

### 7.1.1 Cloning of receptor constructs

Following the approach for crystallisation of AtETR1 different constructs of both receptor proteins were designed. Initially, a modified expression vector, designated pTEV-16b, was created to express fusion proteins with an N-terminal deca His-tag that is linked to the target protein by a TEV protease recognition site (ENLYFQ|G) for cleavage of the affinity tag (see section 4.3.6).

For the moss as well as for the tomato, full-length constructs and truncated versions lacking the membrane domain of the receptor proteins were cloned into vector pTEV-16b by the SLIC method (see 4.3.6). Even though removing the membrane associated part of a protein will not guarantee formation of a soluble variant, it might help to reduce hydrophobic parts that could initiate aggregation of expressed protein within the host cell<sup>[188]</sup>.

Four expression vectors were constructed for PpETR1 and LeETR1 according to Table 11 (page 28). Figure 44 illustrates the schematic structure of the full-length constructs and the truncated variants.

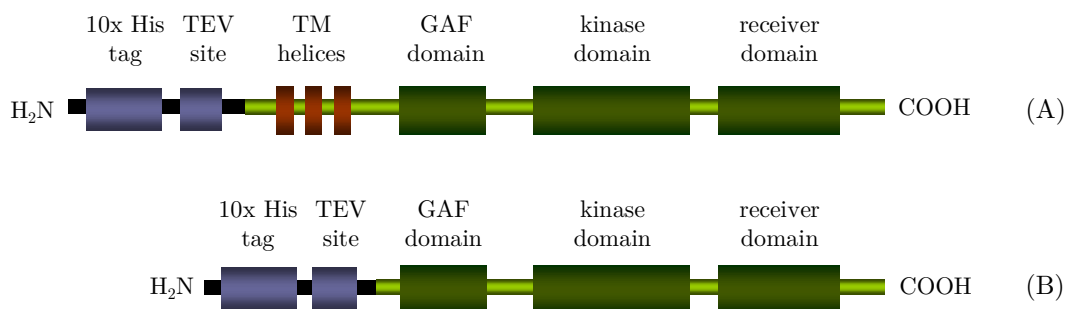


Figure 44: Schematic representation of truncated and full-length receptor proteins of PpETR1 and LeETR1. The upper figure (A) shows the different domains of the full-length receptors PpETR1<sub>1-767</sub> and LeETR1<sub>1-754</sub>. The N-terminal 10x His-tag is linked to the target protein by a TEV protease recognition sequence, both parts are coloured blue. The receptor protein (green) has an N-terminal transmembrane (TM) domain consisting of three putative helices (red). Next to this transmembrane domain is a GAF domain followed by a kinase domain and the C-terminal receiver domain. At the bottom (B) a schematic picture of the receptor proteins lacking the membrane domain is given. This model refers to PpETR1<sub>158-767</sub> and LeETR1<sub>173-754</sub>.

### 7.1.2 Expression studies

Analytical expression studies were performed with bacterial strains C41 (DE3), C43 (DE3) and BL21 (DE3) according to protocol 4.5.3. Liquid cultures of 2YT medium with a volume of 100 ml were set up at 30 °C. Protein expression was induced by the addition of IPTG to a final

concentration of 1 mM. The objective of these expression studies was to test whether the proteins can be expressed in *E. coli*: Membrane proteins are often toxic to their host cells. In consequence, the protein yield might be very low due to cell death, or the proteins might form aggregates within the cells in form of inclusion bodies<sup>[134, 189]</sup>. For receptor constructs giving positive results in this initial expression screening, conditions should be further optimised to allow maximum production of the functional protein.

In the analytical expression studies, both constructs lacking the three putative membrane helices were overexpressed in all host cells tested. However, the expression level was highest in BL21 (DE3) as shown in Figure 45B.

The protein gels show clear expression bands at a molecular weight range of 60 to 70 kDa corresponding to the calculated molecular sizes of PpETR1<sub>158-767</sub> (71.2 kDa, including the affinity tag) and LeETR1<sub>173-754</sub> (67.4 kDa, also with deca His-tag). This result was confirmed by detection of the 10x His-tag in western blot analysis (Figure 46).

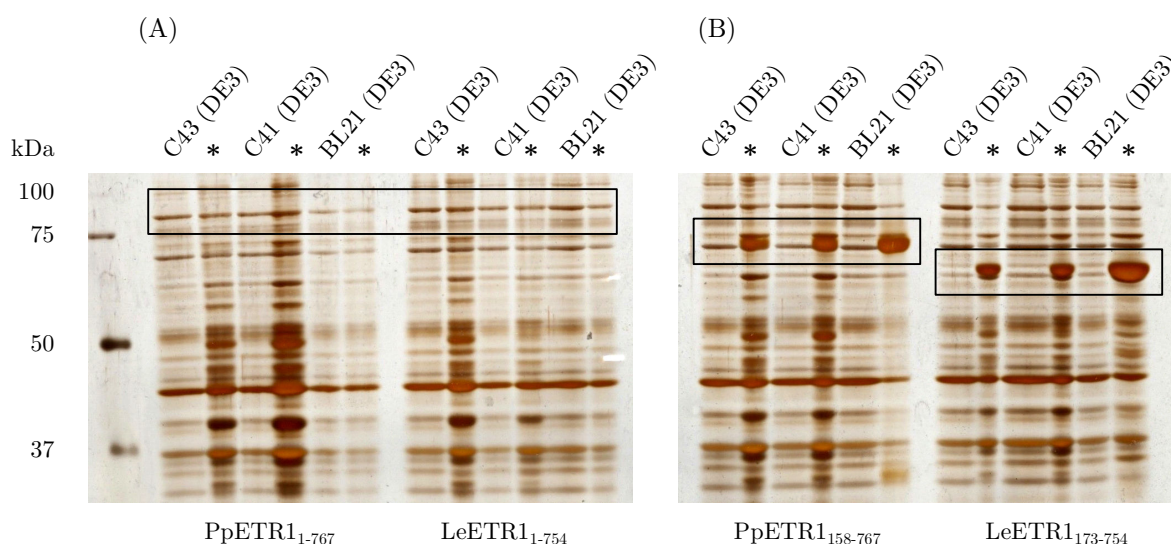


Figure 45: Separation of cell culture samples from analytical expression studies with full-length and truncated PpETR1 and LeETR1; SDS-PAGE analysis with a 12 % silver stained gel. Expression samples were taken upon induction and four hours (\*) later. Boxes indicate the molecular weight range in which protein bands from expressed receptor proteins were expected.

Western blot analysis revealed that further proteins in the range of 40 to 50 kDa were detected in cells of BL21 (DE3) upon IPTG induction. These proteins might correspond to degradation products as the N-terminus was detected by the affinity tag. Alternatively, the target proteins were not fully translated.

Protein bands for the full-length constructs were expected at 89.1 kDa (PpETR1<sub>1-767</sub>) and 87.1 kDa (LeETR1<sub>1-754</sub>). No protein expression was detectable for both receptors in the silver stained SDS-PAGE gel (Figure 45A), but analysis of expression samples by western blotting revealed that full-length protein was expressed in BL21 (DE3) (Figure 46).

This result is surprising as BL21 (DE3) is usually used for expression of soluble proteins. In contrast, *E. coli* strains C43 (DE3) and C41 (DE3) are derivatives selected precisely for expression of toxic membrane proteins<sup>[62]</sup>.

The expression level for full-length constructs was very low compared to the truncated receptor proteins (equal amounts of cell culture samples were tested by western blot analysis, Figure 46). While samples of PpETR1<sub>158-767</sub> and LeETR1<sub>173-754</sub> showed clear signals after 30 seconds exposure time, membranes with samples of the full-length receptors had to be exposed for 10 min to show faint luminescent signals.

Based on these first results, expression conditions were optimised independently for both types of constructs as described in the following sections.

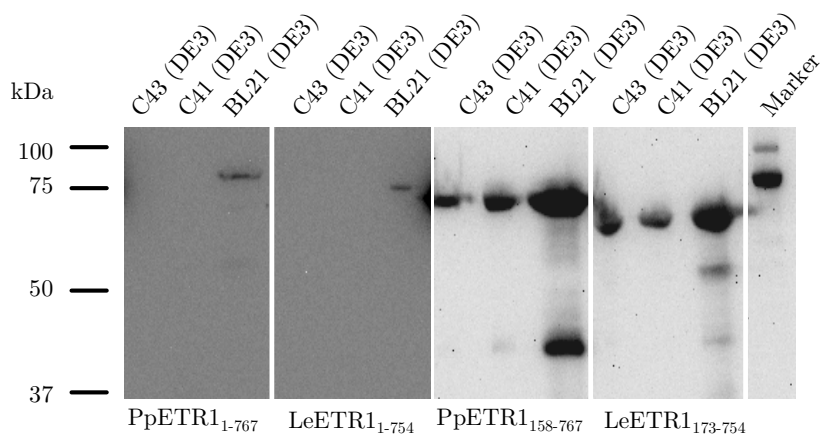


Figure 46: Western blot analysis of liquid culture samples from analytical expression of full-length and truncated ethylene receptor ETR1 from *P. patens* and *L. esculentum*. Heterologously expressed proteins were detected with HRP-labelled antibodies directed against the deca His-tag. All samples were taken 4 hours after induction with 1 mM IPTG.



### 7.1.2.1 Optimisation of expression of constructs lacking the transmembrane sensor domain

Analytical expression studies have shown the highest expression level in *E. coli* strain BL21 (DE3). However, a minor part of the protein was degraded as determined by western blot analysis. In order to obtain high expression with reduced degradation, the cell culture volume was scaled up to 500 ml 2YT medium, but the inducer concentration was reduced to 0.1 and 0.5 mM. Controls were induced with 1 mM IPTG (see section 4.5.3).

Cell pellets were analysed for inclusion body formation—a common phenomenon when expressing membrane proteins<sup>[190]</sup>—that was observed at expression of AtETR1<sub>165-738</sub>. The bacterial cells were disrupted (see 4.6.1), and the crude extract was subjected to differential centrifugation. During a 15 minute spin at 2,000 x g, non-disrupted cells and cell debris were removed. The next step, 30 min at 10,000 x g, was used to separate inclusion bodies while large membrane systems typically found with C43 (DE3) and C41 (DE3) were pelleted at 30,000 x g (30 min). A final centrifugation step was performed at 150,000 x g for 60 min to collect small membrane fragments and associated proteins. Equal volumes of pellet and supernatant samples were analysed by SDS-PAGE and western blotting (see protocols 4.4.2 - 4.4.6).

As shown in Figure 47 most of the protein accumulated as inclusion bodies or was removed with the cell debris fraction. This result indicates that cell disruption was incomplete, and non-

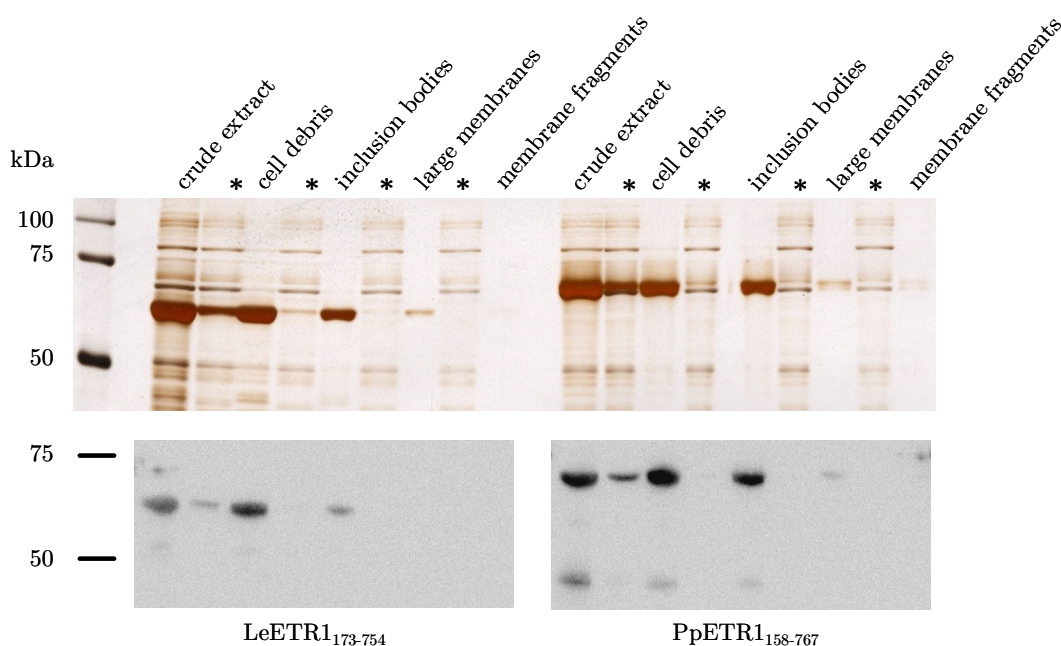


Figure 47: Cellular localisation of LeETR1<sub>173-754</sub> and PpETR1<sub>158-767</sub> in BL21 (DE3) host cells induced with 0.1 mM IPTG. Separation of pellet and supernatant (\*) fractions was performed by SDS-PAGE on 12 % acrylamide gels and western blot analysis with an antibody directed against the fused affinity His-tag.

disrupted cells with inclusion bodies were detected in this step or that these fractions already contained isolated protein aggregates. Because the efficiency of the differential centrifugation depends on the size of the inclusion bodies, an overlap with the cell debris fraction might have occurred<sup>[191]</sup>. Western blot analysis showed a faint signal for PpETR1<sub>158-767</sub> in the membrane fraction indicating that a small amount of the receptor was located to the cytoplasmic membrane, probably due to hydrophobic domains in the receptor that associate with the membrane.

The formation of inclusion bodies was detected in all induced BL21 (DE3) cells whether or not protein expression was initiated by high (1 mM) or low (0.1 mM) inducer concentrations.

The accumulation of protein aggregates can be reduced by a decrease in temperature. Cell cultures were grown at 16 °C to slow down the cellular protein production machinery<sup>[192, 193]</sup>. In addition, 2 % (v/v) ethanol was added to the culture as exposure to organic solvents will upregulate synthesis of up to 30 heat shock proteins in *E. coli* to prevent cellular damage. Though the function of many heat shock proteins is still unknown, several have been characterised as chaperones and chaperonins involved in protein folding and prevention of protein aggregation<sup>[194]</sup>.

However, neither the reduced incubation temperature nor the addition of ethanol decreased or prevented accumulation of inclusion bodies for PpETR1<sub>158-767</sub> or LeETR1<sub>173-754</sub>. Therefore, preparative expression of both receptor fragments was obtained in liquid cell cultures of 500 ml 2YT medium at the initial

30 °C. The inducer IPTG was used at a reduced concentration of 0.1 mM (see 4.5.3 for details). Figure 48 shows the expression level for both proteins at different times after induction. Expression of LeETR1<sub>173-754</sub> was usually slightly lower than for PpETR1<sub>158-767</sub>, but both constructs showed an equal increase in protein expression after induction. For the receptor construct of *P. patens* a

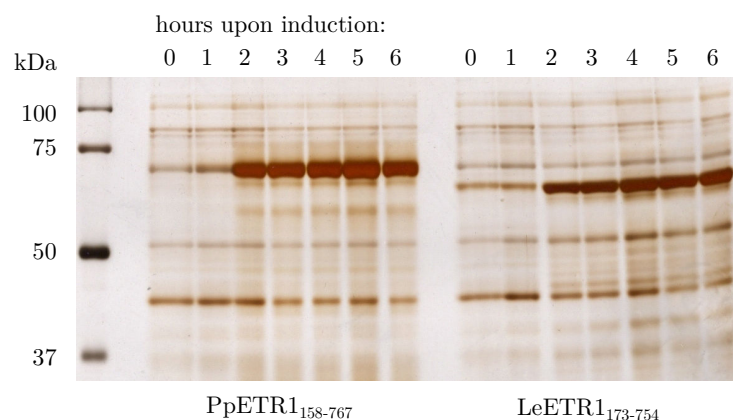


Figure 48: Analysis of cell culture samples from preparative expression of PpETR1<sub>158-767</sub> and LeETR1<sub>173-754</sub> by SDS-PAGE (12 % silver stained gel). Samples were taken every hour upon induction with IPTG for six hours in total. Sample volumes to apply were calculated based on the optical density of the culture to allow comparison of expression levels dependent on expression duration.

decreased expression level was observed six hours after induction. Thus, the cell cultures were terminated at that point and typically yielded 3.5 to 4.0 g cells per litre medium.

#### 7.1.2.2 Optimisation of the expression of full-length receptors

Initial studies have shown that full-length ETR1 from *P. patens* and *L. esculentum* was expressed to minor amounts in BL21 (DE3). Further analytical expression studies were performed with the bacterial strains BL21 (DE3), C41 (DE3) and C43 (DE3) in order to test whether synthesis of the full-length receptors can be triggered by variation of external parameters.

Cell cultures were grown at a reduced temperature (16 °C) and IPTG concentration (0.1 mM). It turned out that the decrease of the incubation temperature had a major impact on protein expression. As shown in Figure 49 expression of both receptor proteins was found in BL21 (DE3) as demonstrated by silver stained SDS-PAGE gel and confirmed by western blot analysis. Cell growth was severely slowed down at 16 °C. Hence, expression was extended to 24 hours to increase cell masses to a maximum of 3 g per litre medium for LeETR1<sub>1-754</sub> and up to 6 g per litre for full-length ETR1 from the moss *P. patens*. Even at these optimised conditions no expression was detected in cells of C43 (DE3) and C41 (DE3).

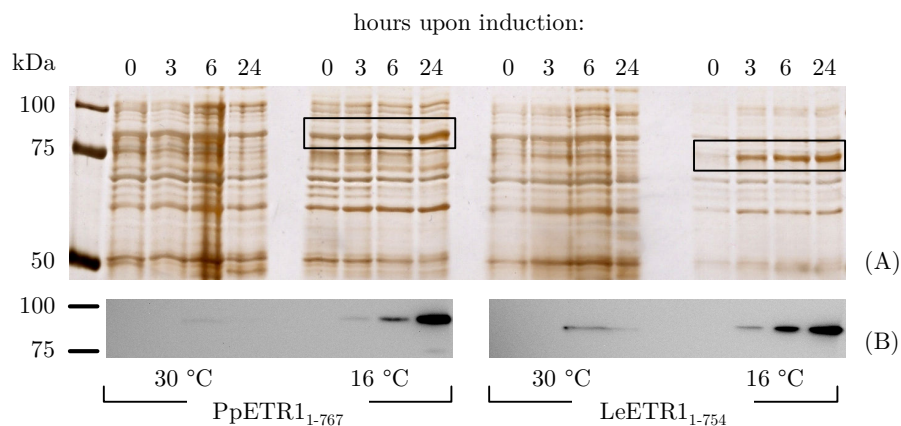


Figure 49: Expression of full-length ethylene receptor ETR1 from *P. patens* and *L. esculentum* in BL21 (DE3) at 30 °C and 16 °C. IPTG concentration was maintained at 1 mM. Samples from liquid cell cultures were examined on a 12 % silver-stained SDS-PAGE gel (A) and protein bands corresponding to recombinant receptor proteins were identified by western blot analysis (B) using an antibody directed against the deca His affinity tag. Sample volumes applied were calculated based on the optical density of the cell culture to allow comparison of expression levels.

To enhance growth of cells harbouring plasmid pTEV-16b::LeETR1<sub>1-754</sub>, the inducer concentration was reduced to 0.1 mM as afore-mentioned. The main problem with the lactose analogue IPTG—apart from its high costs—is its influence on the growth rate of *E. coli*. It can cause a stress response by acting as a competitive inhibitor of  $\beta$ -galactosidase disturbing glucose/lactose metabolisms in *E. coli*<sup>[195]</sup>.

For LeETR1<sub>1-754</sub> cell yields were only minor affected by IPTG, and the cell mass per litre culture volume was only increased to a maximum of 4 g/l by reduction of the inhibitor (starting condition: 3 g/l). The effect of a tenfold lower inducer concentration was also tested for PpETR1<sub>1-767</sub>. However, no protein expression was found at these concentrations.

Summarised, both full-length receptor proteins were heterologously expressed in *E. coli* strain BL21 (DE3). Expression conditions had to be modified compared to analytical studies. The incubation temperature was reduced to 16 °C, and expression was extended to 24 hours after induction with IPTG. As expected the expression level was low compared to the truncated receptor variants (Figure 48). On one hand, this might be related to the fact that the full-length proteins are larger (approximately by 20 kDa) requiring more cellular resources for synthesis. On the other hand, there are distinct hydrophobic domains in the full-length receptors that have to be integrated into *E. coli* membranes to avoid aggregation in the host cell.

## 7.2 Purification and characterisation of PpETR1 and LeETR1

### 7.2.1 Receptor constructs lacking the membrane domain

#### 7.2.1.1 *Purification from inclusion bodies*

The truncated receptor variants were expressed in *E. coli* BL21 (DE3) as described in section 4.5.3. Localisation studies have shown that both receptor fragments were expressed as protein aggregates in the cytoplasm (Figure 47, page 123). This effect is often observed when overexpressing heterologous proteins in prokaryotic hosts. Incomplete or incorrect folding during protein synthesis can result in aggregation and accumulation of the recombinant protein<sup>[196, 197]</sup>. In the past, these encapsulations have been considered as dead-end of protein synthesis. Now it is known that these cellular entrapments often contain partially correctly folded proteins with distinct secondary structures<sup>[198]</sup>. There are several methods to release functional active protein from these inclusion bodies. *In vivo* approaches use chloramphenicol to arrest protein synthesis and allow refolding of the target protein by components of the bacterial protein folding

machinery within the cell<sup>[199]</sup>. Also the application of organic solvents (such as ethanol, tested in this study) might upregulate chaperone activity and could therefore prevent or reverse aggregation of recombinant proteins<sup>[194]</sup>.

In this study an *in vitro* approach was chosen to isolate and refold the C-terminal fragments of the ethylene receptors. Although aggregation of protein is not intended, inclusion bodies bring along two major advantages: First, they usually consist of highly pure recombinant protein and second, they can easily be isolated by centrifugation due to their size<sup>[200]</sup>.

BL21 (DE3) cells containing PpETR1<sub>158-767</sub> and LeETR1<sub>173-754</sub> were disrupted (see 4.6.1) and the crude extract was treated as described in section 4.6.3. To remove contaminating *E. coli* proteins associated by hydrophobic interactions, the inclusion bodies were washed twice in a buffer containing 1 % (w/v) sodium deoxycholate<sup>[201]</sup>.

Figure 50 shows the different purification steps resulting in highly pure recombinant receptor protein. Residual detergent was removed by a final wash step with 50 mM Tris/HCl buffer, pH 7.5 supplied with 100 mM sodium chloride.

Subsequently, solubilisation of the receptors from the inclusion bodies was tested. As these aggregations often contain partially correctly folded protein, buffers containing 8 M urea as well as lower concentrations of the chaotropic agent were applied at different pH. According to *Patra et al.* who applied this method for preparation of recombinant human growth hormone (r-hGH), buffers within a range of pH 7 to pH 12 were chosen<sup>[197]</sup>. These buffers were prepared with urea in final concentrations of 2 M and 8 M.

Aliquots of isolated inclusion bodies containing PpETR1<sub>158-767</sub> and LeETR1<sub>173-754</sub> were resuspended in each buffer, and after centrifugation at 10,000 x g samples from supernatant and pellet fractions were analysed by SDS-PAGE 4.6.4. Figure 51 demonstrates that both receptor

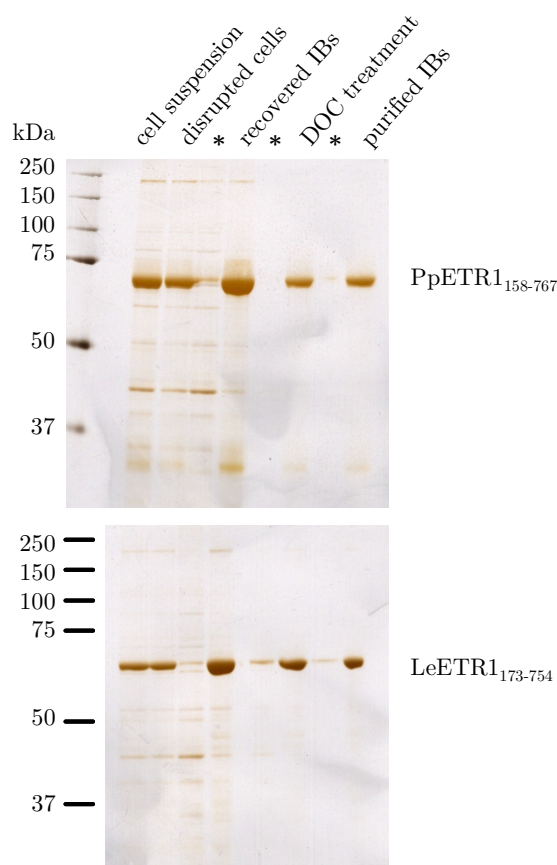


Figure 50: Isolation and purification of inclusion bodies (IBs) containing receptors PpETR1<sub>158-767</sub> and LeETR1<sub>173-754</sub>. Supernatants after centrifugation are indicated by asterisk. DOC: deoxycholate

proteins were solubilised from inclusion bodies by 8 M urea. Changing the pH of the buffer had no obvious effect on solubilisation.

Changes in pH affect the stability of a protein by changing the charge distribution in the molecule which can promote unfolding<sup>[202]</sup>. In the above mentioned example of r-hGH, an alkaline pH had been proven to be most effective for releasing the growth hormone from the aggregation state<sup>[197]</sup>.

By solubilising PpETR1<sub>158-767</sub> in 50 mM Tris/HCl, pH 8.0 supplied with 100 mM sodium chloride and 8 M urea, on average,  $48 \pm 4$  mg protein per gram cells were obtained. For the receptor variant from tomato, values were slightly lower and amounted to  $29 \pm 4$  mg per gram cells.

Based on the solubilisation screen, a refolding protocol was established to retrieve soluble and preferably functional receptor proteins. Several aspects in refolding of proteins have to be considered. Identification of the appropriate buffer is basically a *trial and error process*, but other external factors determine whether refolding is successful<sup>[203]</sup>.

One crucial aspect is protein concentration. *Lilie et Rudolph* suggested 10-50 µg/ml as the concentration limit for effective refolding in terms of maximum yield of active protein<sup>[204]</sup>. On one hand, these very low concentrations will require large volumes of refolding buffer and further dilute the protein requiring time consuming ultra filtration for concentration before crystallisation trials. On the other hand, refolding of higher concentrated protein solutions might cause new protein aggregates as refolded and partially unfolded protein can precipitate again due to their exposed hydrophobic regions.

If the target protein contains disulfide bonds, the addition of low molecular weight thiols such as DTT or 2-mercaptoethanol or the oxido shuffling system GSH/GSSG may improve protein folding<sup>[205]</sup>. Several other additives have shown stabilising effects on refolded protein. Up to

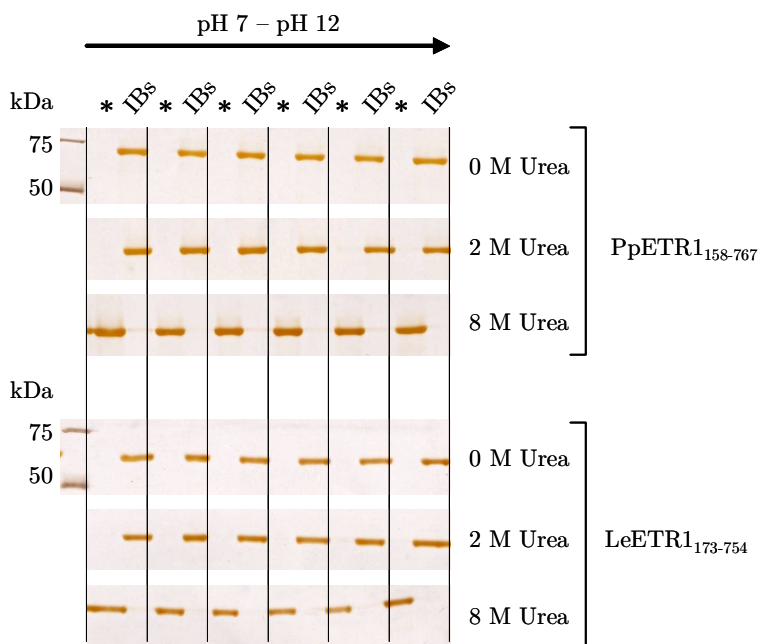


Figure 51: Solubilisation of PpETR1<sub>158-767</sub> and LeETR1<sub>173-754</sub> from inclusion bodies (IBs). Supernatants after centrifugation that might contain solubilised receptor proteins are indicated by asterisk. Each column represents a change in pH by one unit.

0.5 M of arginine or guanidine hydrochloride can be used to promote proper refolding. Also ionic, non-ionic and zwitter-ionic detergents and mixtures composed of phospholipids and detergents can enhance correct protein folding by providing polar and non-polar moieties in mixed micelles<sup>[206]</sup>.

The most common methods used in protein refolding are dilution, dialysis and buffer exchange by gel filtration chromatography. In analytical studies to test for optimal buffer conditions protein refolding was tested in a total volume of 1 ml by diluting solubilised inclusion bodies into refolding buffers at a ratio of 1:20.

A set of 15 buffers was applied, prepared according to Table 22 in appendix 9.4. Refolding studies were performed as described in section 4.6.5 at 5 mg/ml taking into account potential loss of protein due to the high protein concentration applied. Refolding efficiency was confirmed by analysing supernatant and pellet fractions of each sample by SDS-PAGE. While soluble and thus potentially correctly folded PpETR1<sub>158-767</sub> and LeETR1<sub>173-754</sub> were found in the supernatant after centrifugation, re-aggregated protein precipitated and formed a pellet. From 15 buffers tested, six yielded soluble protein for both receptors (No. 3, 6, 10, 11, 13 and 15). The buffer with the most basic composition (No. 11) was chosen for further preparative studies.

Buffer 11 is composed of 50 mM Tris/HCl, pH 8.5, 9.6 mM sodium chloride, 0.4 mM potassium chloride, 1 mM EDTA, 0.5 % (w/v) *Triton*<sup>®</sup> X-100 and 1 mM DTT. In the preparative studies potassium chloride was omitted and sodium chloride was adjusted to a concentration of 10 mM. Also EDTA was excluded to provide the opportunity to refold Ni-NTA immobilised receptor proteins. Refolding on a Ni-NTA column reduces the volume of the refolding buffer and the refolded target proteins are eluted in a few millilitres. However, this method failed for PpETR1<sub>158-767</sub> and LeETR1<sub>173-754</sub> as proteins in their unfolded state did not bind strongly to the affinity matrix. A protein loss of more than 90 % was observed even though the affinity His-tags of both proteins should be accessible for binding to Ni-NTA in their unfolded state. Nevertheless, most of the protein eluted with the flow-through fraction even before the refolding buffer was applied. In consequence, further refolding was performed by the dilution technique. Two iterative dilution steps were carried out as described in section 4.7.4 to reduce buffer volumes and to decrease the final urea concentration to 40 mM.

Finally, the detergent *Triton*<sup>®</sup> X-100 was substituted by 0.04 % (w/v) DDM. *n*-dodecyl- $\beta$ -D-maltopyranoside in the refolding buffer was chosen as DDM was successfully applied in refolding of the receptor ortholog AtETR1. Furthermore, DDM was included in the kinase activity assay buffer as well as in the buffer used for measurements of CD spectra. Moreover, as both proteins were intended for crystallisation experiments, *Triton*<sup>®</sup> X-100 had to be substituted.



*Triton*<sup>®</sup> X-100 forms micelles of approximately 107 kDa that are expected to interfere with the crystallisation process by preventing contacts between individual receptor molecules<sup>[207, 208]</sup>. In contrast, DDM micelles are on average about 30 % smaller which might enhance the chance of successful crystallisation<sup>[209]</sup>. Another problem with *Triton*<sup>®</sup> X-100 arises from its chemical heterogeneity: *Triton*<sup>®</sup> X-100 contains 9-10 ethylene oxide units per molecule which makes the detergent unsuitable for protein crystallisation as it disturbs uniform crystal packing required for high resolution structures.

Preparative refolding of PpETR1<sub>158-767</sub> and LeETR1<sub>173-754</sub> was performed in a volume of 10 ml per batch according to protocol 4.7.4. Samples were taken before and after dilution and centrifugation and were analysed by SDS-PAGE. Figure 52 illustrates that the efficiency of the refolding process differed between both receptor proteins. While receptor PpETR1<sub>158-767</sub> gave almost exclusively soluble protein, LeETR1<sub>173-754</sub> showed precipitation of most protein in the pellet. This result was in contrast to the initial analytical studies but can be explained with a higher centrifugal force and a reduced urea concentration (40 mM compared to 0.4 M) used in the preparative approach. Samples were finally centrifuged at 150,000 x g (in contrast to 20,000 x g in analytical studies) to remove any protein aggregates.

Overall, preparative refolding of the receptor proteins into 50 mM Tris/HCl buffer, pH 8.5 supplied with 1 mM DTT, 10 mM sodium chloride and 0.04 % (w/v) DDM yielded on average

$7.2 \pm 1.8$  mg soluble protein per gram bacterial cells for receptor construct PpETR1<sub>158-767</sub> and  $2 \pm 0.3$  mg for LeETR1<sub>173-754</sub>.

Compared to the numbers obtained for solubilised inclusion bodies there was a severe loss of protein (85 % for *P. patens* and 97 % for *L. esculentum*). Obviously, the high protein concentration employed at refolding (5 mg/ml) was in charge for the observed precipitation. Nevertheless, above-stated protein yields were still sufficient for further functional and structural studies.

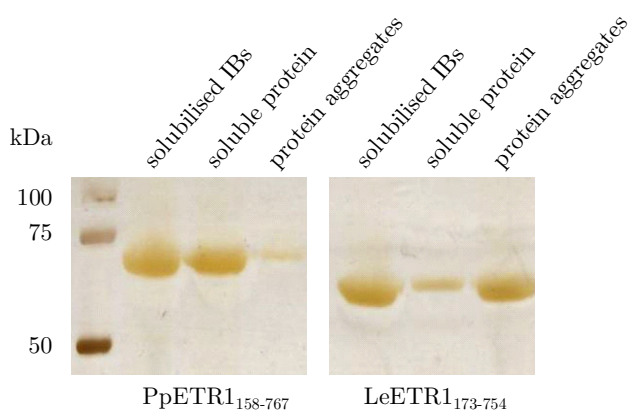


Figure 52: Refolding of truncated ethylene receptors PpETR1<sub>158-767</sub> and LeETR1<sub>173-754</sub>. Supernatant fractions with soluble protein and pellet fractions with protein aggregates were compared to solubilised inclusion bodies (IBs) by SDS-PAGE.



### 7.2.1.2 Characterisation of the truncated receptors

Both receptor proteins have been successfully refolded in terms of protein solubility. But did the proteins retain their native three dimensional structure during the *in vitro* folding process? For ETR1 successful refolding can be checked by testing functionality of the receptor in the autokinase assay<sup>[32]</sup>. Furthermore, CD spectroscopy can be used to analyse the secondary structure content of the refolded proteins. Both methods were applied for the refolded ETR1 constructs from *P. patens* and *L. esculentum* and will be discussed in this section.

PpETR1<sub>158-767</sub> and LeETR1<sub>173-754</sub> were prepared from purified inclusion bodies as described in section 4.7.4, and phosphorylation of both receptors was tested according to 4.8.1.

Proteins denatured by SDS prior to application of <sup>32</sup>P-ATP served as negative control in the phosphorylation assay. No regulatory effects of ethylene or cyanide could be evaluated because both receptors are missing the sensory transmembrane domain.

Figure 53 illustrates that both receptor fragments phosphorylated upon treatment with radiolabelled ATP (left lanes). In contrast, protein denatured by SDS prior to the activity assay did not show incorporation of <sup>32</sup>P phosphate (right lanes). These results support the assumption that refolding of both receptor proteins was successful and yielded active and functional protein.

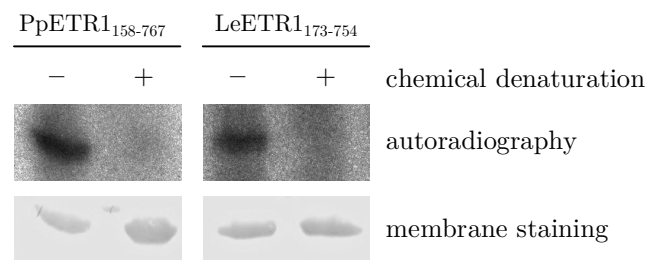


Figure 53: Autoradiography showing incorporation of <sup>32</sup>P phosphate into receptor proteins PpETR1<sub>158-767</sub> and LeETR1<sub>173-754</sub>. Chemical denaturation of both proteins prior to the phosphorylation assay was achieved by incubation with SDS. Staining of the transfer membrane with *Ponceau S* identified equal amounts of protein in each lane.

Furthermore, PpETR1<sub>158-767</sub> and LeETR1<sub>173-754</sub> were analysed by CD spectroscopy to resolve the secondary structure composition of the refolded receptors. CD spectra of both proteins were recorded over a range of 260-195 nm as described in section 4.8.2. Proteins were diluted into 50 mM potassium phosphate buffer supplied with 0.05 % (w/v) DDM. Typically, protein concentrations of 0.1 to 0.3 mg/ml were chosen to allow for measurements to 195 nm.

The recorded spectra were processed with the software package *CDPro* as described earlier for calculation of the secondary structure content of both receptors (see 5.1.3).

The *PSIPRED* secondary structure prediction method was used to calculate theoretical values for  $\alpha$ -helices,  $\beta$ -strands and random coil structures based on the amino acid sequence of each receptor protein. As this algorithm does not cover estimation of  $\beta$ -turn elements in protein structures, these were calculated by

*BetaTPred2*<sup>[112]</sup>.

CD data for both proteins are shown in Figure 54. The spectra are almost identical and indicate formation of secondary structure elements upon refolding. With a minimum at 209 nm and zero crossing between 200 and 201 nm, both spectra suggest a strong  $\alpha$ -helical conformation of the refolded receptors<sup>[110]</sup>. The fact that the second minimum at 222 nm is not that distinct reflects the influence of  $\beta$ -strands and random coil structures. CD data were processed with *CDPro* to estimate the content of each structural element ( $\alpha$ -helices,  $\beta$ -strands and

random coil), and results were compared to theoretical values obtained from the amino acid sequence by *PSIPRED* and *BetaTPred2*. CD analysis in Table 20 further confirms proper refolding of both receptor proteins. Theoretical and experimental values obtained for  $\alpha$ -helices and  $\beta$ -strands fit well. With an estimated overall  $\alpha$ -helical content of about 34 to 37 % data agree with the assumption that PpETR1<sub>158-767</sub> and LeETR1<sub>173-754</sub> are predominantly  $\alpha$ -helical proteins as already indicated by the shape of the spectra in Figure 54. Calculated amounts for  $\beta$ -turn and random coil structures differ slightly when compared to theoretical data. This slight discrepancy might be due to the fact that  $\beta$ -turns are rather small motifs consisting of four amino acids giving false positives when predicting secondary structure elements. Together with

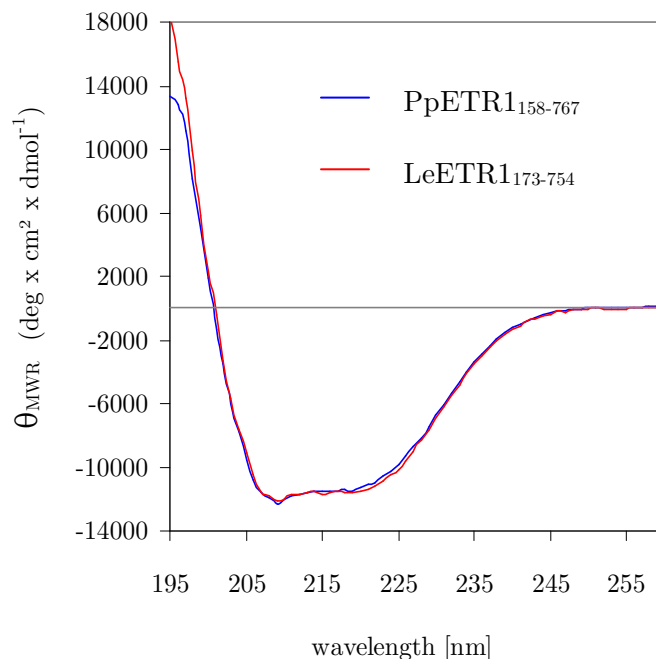


Figure 54: CD spectra obtained for receptor proteins PpETR1<sub>158-767</sub> and LeETR1<sub>173-754</sub>. Measured ellipticity (mdeg) was converted to mean residue weight ellipticity  $\Theta_{\text{MWR}}$  to allow for comparison of both spectra.

the results from the autokinase activity assay, CD experiments indicate successful refolding of both truncated receptors upon denaturing purification.

Table 20: Secondary structure composition of PpETR1<sub>158-767</sub> and LeETR1<sub>173-754</sub> as calculated from the amino acid sequence and from experimental data. All values are given in %.

<i>Protein</i>	<i>Data source</i>	<i><math>\alpha</math>-helices</i>	<i><math>\beta</math>-strands</i>	<i><math>\beta</math>-turn</i>	<i>Random coil</i>
PpETR1 <sub>158-767</sub>	experimental	34 – 37	17	19 – 21	28 – 30
	theoretical	37	15 – 17	28 – 30	19
LeETR1 <sub>173-754</sub>	experimental	35 – 37	16 – 17	18 – 20	28 – 29
	theoretical	36	16 – 17	23 – 24	24
range		0 – 10 %	11 – 20 %	21 – 30 %	31 – 40 %

Based on the results obtained with the receptor ortholog AtETR1<sub>165-738</sub>, these facts on their own, however, might not necessarily imply that the proteins will crystallise. The surface entropy reduced mutant AtETR1<sub>165-738</sub>SER was functional and showed regular secondary structure elements, too (see 6.1.2.2). However, size exclusion chromatography identified that most of the protein formed aggregates which most likely have prevented uniform crystal growth. To rule out that aggregates form with PpETR1<sub>158-767</sub> and LeETR1<sub>173-754</sub>, too, both proteins were analysed by size exclusion chromatography.

Samples of 1 ml of the refolded receptor proteins PpETR1<sub>158-767</sub> and LeETR1<sub>173-754</sub> at a concentration of 1 mg/ml were applied to a *HiPrep 16/60 Sephacryl S-200* column for size exclusion chromatography. Experiments were performed at room temperature (see methods section 4.6.6). Elution fractions of 1 ml were collected and analysed by SDS-PAGE. The retention volume was determined for every peak maximum and corresponding molecular weights were estimated based on previous calibration of the column with a set of five reference proteins ranging from 43 kDa (ovalbumin) to 200 kDa ( $\beta$ -amylase).

Both chromatograms in Figure 55 show a main peak containing most of the receptor proteins as proven by SDS-PAGE. With an estimated molecular weight of about 340 kDa, the proteins eluted in the void volume probably corresponding to higher molecular weight aggregates of the receptors. The SDS-PAGE gels also indicate the formation of aggregates as there is protein detected at the top of the gels that did not enter the separating gel. Furthermore, proteins were detected in these fractions with molecular weights of up to 50 kDa which might represent degradation products of the receptors. In this context, it can be assumed that aggregation

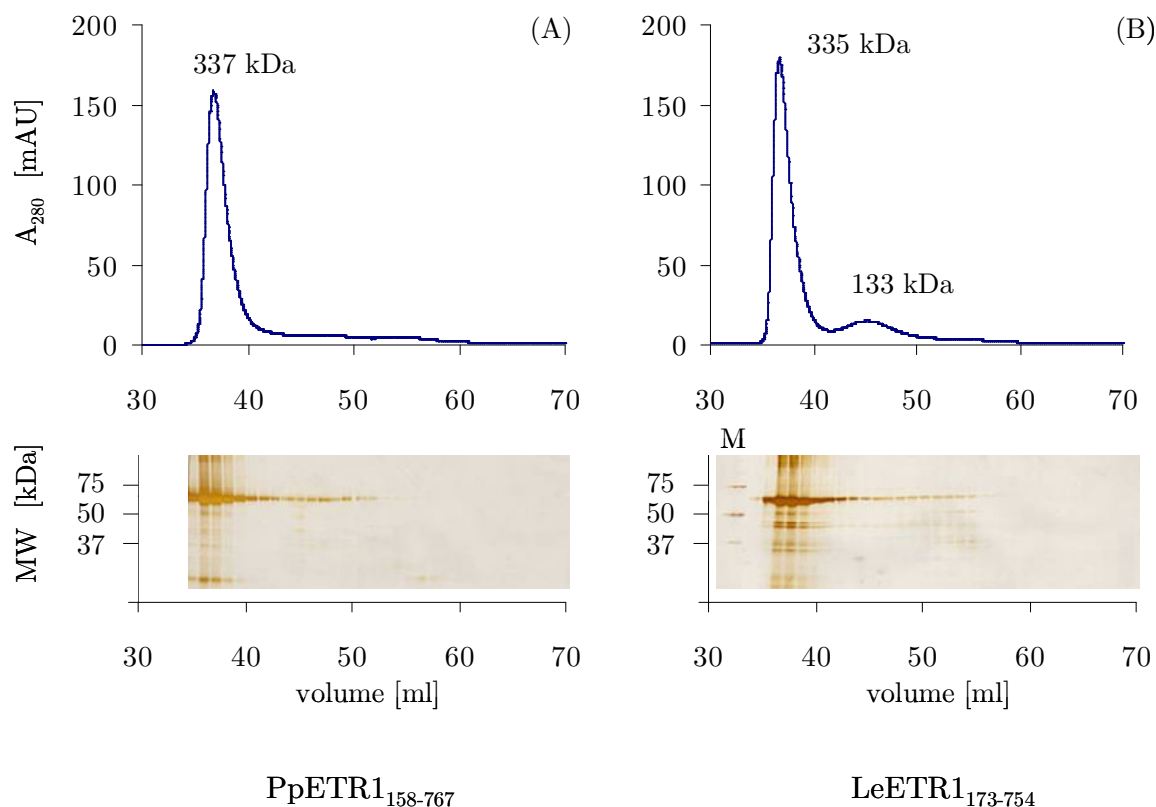


Figure 55: Chromatograms of size exclusion chromatography applied to receptor proteins PpETR1<sub>158-767</sub> (A) and LeETR1<sub>173-754</sub> (B). UV absorption was recorded at 280 nm and is displayed in mAU. Samples from elution fractions were analysed by SDS-PAGE. The protein gels are aligned with the chromatograms to show the protein composition of each peak.

already took place during refolding rather than size exclusion chromatography and the fragmented proteins might have served as aggregation cores.

A second peak in chromatogram (B) was assigned to LeETR1<sub>173-754</sub> and indicates that the sample also contained a minor fraction of non-aggregated protein. The deviation of the apparent molecular weight (133 kDa) from the calculated number for receptor monomers (67.4 kDa) might be explained with dimerisation of the receptors through their kinase domain like it has been shown for a sensor histidine-kinase protein from *Thermotoga maritima*<sup>[109]</sup>. Dimerisation might also occur via the receiver domain as described for ETR1 from *A. thaliana*<sup>[130]</sup>.

In contrast, it is possible that detergent molecules partially cover the proteins and contribute to their overall size. Hydrophobic parts of the proteins can be in charge for the detergent coating causing the observed increase in the apparent molecular weight.

The peak size of precipitated and non-precipitated protein suggests that almost all protein has aggregated. On the background of the low protein yield obtained from refolding, the total protein available is not sufficient for crystallisation studies.

In order to improve yield, solubility of both truncated proteins might be enhanced by an extensive buffer screening. Increased solubility might be obtained by retesting refolding buffers containing arginine to reduce precipitation<sup>[172]</sup>. In this context, it might also be worth to set up systematic pH screening. Though pH of the applied solutions was more than one unit off the pI of both proteins (buffer Tris/HCl pH 8.0 compared to pI 6.6 for PpETR1<sub>158-767</sub> and pI 6.8 for LeETR1<sub>173-754</sub>) a change to a more acidic pH might affect or prevent aggregation. The effect of each buffer can be checked by size exclusion chromatography.

Alternatively, crystallisation trials could focus on the full-length proteins. Contemporaneous to the work on ethylene receptors ETR1 from *P. patens* and *L. esculentum*, it was shown that the membrane protein ETR1 from *A. thaliana* was easily solubilised into *FOS-CHOLINE*<sup>®</sup>-14 micelles (see chapter 6.2.2). This approach seemed more promising than an extensive screening of new refolding conditions for the truncated receptors. Thus, the preparation protocol for AtETR1 was applied to PpETR1<sub>1-767</sub> and LeETR1<sub>1-754</sub>, too.

## 7.2.2 Full-length receptor constructs

### 7.2.2.1 *Native purification*

BL21 (DE3) cells overexpressing PpETR1<sub>1-767</sub> or LeETR1<sub>1-754</sub> were disrupted by *French Press*, and membranes containing the receptor proteins were harvested by centrifugation at 230,000 x g and 4 °C for 30 min. The membrane pellet was solubilised in a buffer containing 1 % (w/v) *FOS-CHOLINE*<sup>®</sup>-14, and non-solubilised material was removed by centrifugation as described before. The supernatant was applied to immobilised metal affinity chromatography according to protocol 4.7.3, and samples of every washing and elution step were analysed by SDS-PAGE.

Figure 56 shows protein samples from the native purification strategy that were separated and visualised on a silver stained acrylamide gel. With two washing steps at 0 and 50 mM imidazole, highly pure protein was obtained for both ETR1 receptors. Distinct proteins bands were detected between 50 kDa and 100 kDa corresponding to receptors PpETR1<sub>1-767</sub> (89.1 kDa) and LeETR1<sub>1-754</sub> (87.1 kDa). Only in elution fractions of PpETR1<sub>1-767</sub> a very faint additional band at about 75 kDa is visible (see arrow in Figure 56).

Though rather minor, this contamination was alarming: In a previous thesis a member of the heat shock protein family Hsp70 (namely DnaK, molecular weight 70 kDa) was co-purified along with the receptor AtETR1 in native purification<sup>[61]</sup>. In order to exclude contamination by Hsp70, proteins samples from both elution fractions were analysed by western blotting using a DnaK specific antibody as well as an antibody directed against AtETR1, kindly provided by *A. B. Bleecker* (University of Wisconsin-Madison, USA)<sup>[27]</sup>. Although designed for ETR1 from *Arabidopsis thaliana*, the antibody can also be used for the orthologous proteins from *P. patens* and *L. esculentum* because of the high conservation of the three receptors.

Figure 57 shows that all samples contain the receptors PpETR1<sub>1-767</sub> and LeETR1<sub>1-754</sub>, respectively. But DnaK was detected in all samples, too. The fact that signals of the receptor orthologs are in general much weaker than those for DnaK is owed to the reduced specificity of the AtETR1 antibody against ETR1 from other species.

As described in section 6.2.2 contamination with DnaK was also observed in native purification of AtETR1, which

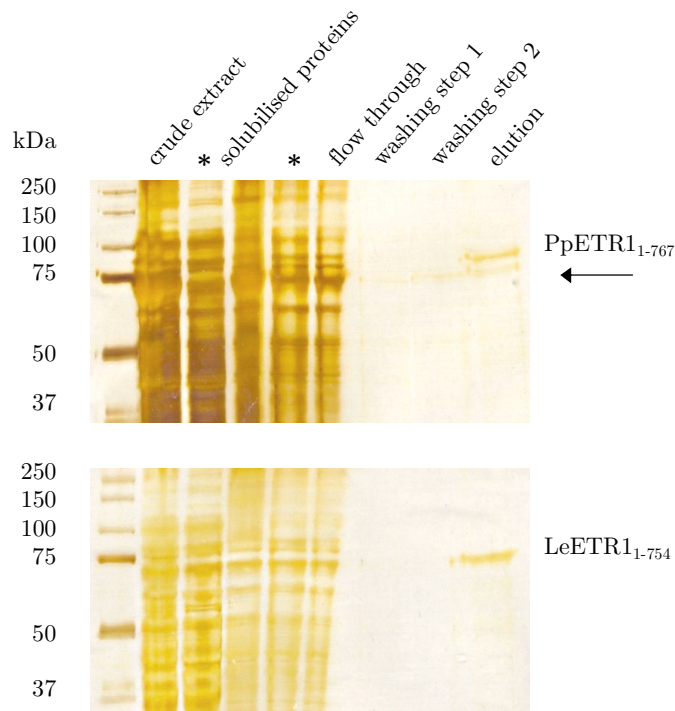


Figure 56: Native purification of PpETR1<sub>1-767</sub> and LeETR1<sub>1-754</sub> by IMAC. Samples from purification were analysed by SDS-PAGE and gels were silver stained. Supernatants after centrifugation are indicated by asterisk. The black arrow points to a contamination in the elution fraction of PpETR1<sub>1-767</sub>. Imidazole was omitted from buffers for washing step 1 and was applied at a concentration of 50 mM in buffers for washing step 2. Elution of bound target proteins was achieved by a buffer with 250 mM imidazole.

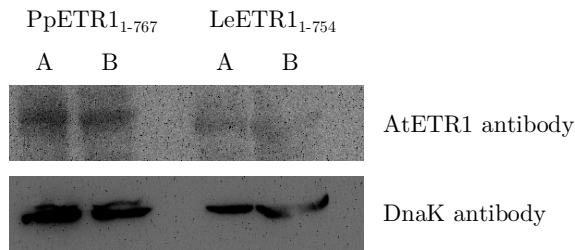


Figure 57: Western blot analysis of samples (elution fractions) from native purification of PpETR1<sub>1-767</sub> and LeETR1<sub>1-754</sub>. (A) and (B) refer to samples from two independent purifications.

was solubilised with *FOS-CHOLINE*<sup>®</sup>-14. There, several approaches have been tested to remove the chaperone including incubation with ATP and arginine<sup>[169, 172]</sup>. Unfortunately, none of these methods promoted the release of DnaK from AtETR1. Thus, denaturing purification of PpETR1<sub>1-767</sub> and LeETR1<sub>1-754</sub> was tested as an alternative approach to provide sufficient and highly pure material for crystallisation trials.

#### 7.2.2.2 Protein purification under denaturing conditions

Membrane pellets containing PpETR1<sub>1-767</sub> and LeETR1<sub>1-754</sub> were prepared from BL21 (DE3) cells as described in methods section 4.6.2. The pellets were dissolved in buffer supplied with 8 M urea to solubilise and unfold membranes and proteins. According to protocol 4.7.3.2, the crude extracts were clarified by centrifugation at 230,000 x g, and the supernatants were applied to Ni-NTA resin. Samples were taken for every washing and elution step to check for protein purity and purification efficiency. All samples were analysed by SDS-PAGE. Elution fractions were also tested by western blot to analyse whether chaperone DnaK had been successfully removed by treatment with 8 M urea.

Western blot analysis revealed that the DnaK contamination was clearly eliminated from both protein samples (Figure 58, A.2 and B.2). However, the silver stained SDS-PAGE gels showed only a weak protein band for receptor LeETR1<sub>1-754</sub> (B.1), and hardly any protein was detected for PpETR1<sub>1-767</sub> (A.1).

In spite of the successful removal of the contaminating chaperon, the denaturing purification approach was not applicable for crystallisation trials because of the of the

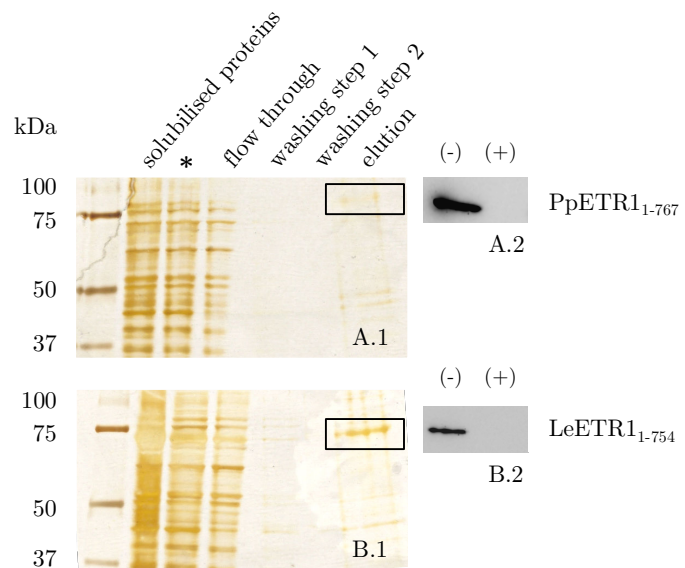


Figure 58: Purification of PpETR1<sub>1-767</sub> and LeETR1<sub>1-754</sub> by IMAC under denaturing conditions (8 M urea). A.1 and B.1: Silver stained SDS-PAGE gels documenting different steps of purification. A.2 and B.2: Immunodetection of DnaK in samples containing receptor proteins prepared under native (-) and denaturing (+) conditions. Supernatants after centrifugation are indicated by asterisk. Buffers for washing steps 1 and 2 contained 0 and 50 mM imidazole. Elution of bound target protein was achieved with 250 mM imidazole in elution buffer.

very low protein yield ( $<0.01$  mg/g cells for PpETR1<sub>1-767</sub> and  $<0.1$  mg/g cells for LeETR1<sub>1-754</sub>). Thus, as with AtETR1, crystallisation studies of PpETR1 and LeETR1 were set up with the natively prepared full-length receptors albeit the contamination with DnaK. Assuming that the chaperone is bound to the connector peptide region of the receptor, co-crystallisation of both receptors with DnaK was intended.

### 7.2.2.3 Characterisation of natively prepared protein

Before crystallisation trials were set up with PpETR1<sub>1-767</sub> and LeETR1<sub>1-754</sub>, both proteins were subjected to a phosphorylation assay to test for functionality (see 4.8.1). Figure 59 illustrates that both receptors showed incorporation of  $^{32}\text{P}$  phosphate upon treatment with radiolabelled  $\gamma\text{-}^{32}\text{P}\text{-ATP}$  (see lane “no additives”). Protein that was denatured by SDS before applying it to the autokinase assay did not show a signal in the autoradiography. An effect of potassium cyanide and ethephon was only demonstrated for receptor PpETR1<sub>1-767</sub> where less radiolabelled  $^{32}\text{P}_i$  was

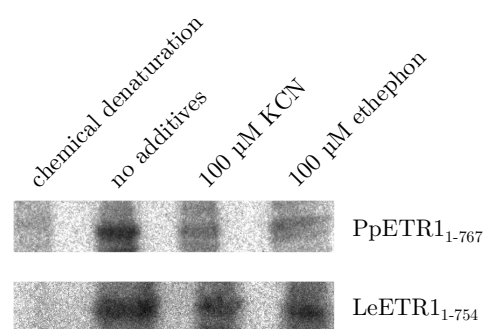


Figure 59: Autoradiography showing incorporation of  $^{32}\text{P}$  phosphate into receptor proteins PpETR1<sub>1-767</sub> and LeETR1<sub>1-754</sub>.

Denaturation prior to the phosphorylation assay was achieved by incubation with SDS.

incorporated in the purified receptor than in the control without additives. In contrast, no effects were observed for full-length ETR1 from *L. esculentum*. This result can be explained by the DnaK contamination. The chaperone can also autophosphorylate *in vitro* and might contribute to the overall signal in the LeETR1<sub>1-754</sub> assay<sup>[210, 211]</sup>. DnaK appears at the same molecular weight level on a SDS-PAGE gel as full-length LeETR1 (Figure 56). In contrast, PpETR1<sub>1-767</sub> is detected in acrylamide gels at a molecular weight level slightly above DnaK. Hence, phosphorylated DnaK and PpETR1<sub>1-767</sub> are clearly separated in the autoradiography and DnaK will not interfere with the signal from PpETR1<sub>1-767</sub> as shown here.

Summarised, the native purification method yielded active and functional ETR1 receptor protein for *P. patens*. Whether purification of the ethylene receptor from *L. esculentum* was also successful, cannot be determined exactly as the contribution of DnaK to the radioactive signal cannot be separated from the potential signal originating from the receptor. Due to the DnaK contamination CD measurements were not applicable for both receptor proteins. Like all



spectroscopic methods, circular dichroism is an extreme sensitive technique, so it was estimated that results for LeETR1<sub>1-754</sub> and PpETR1<sub>1-767</sub> would be falsified by the presence of DnaK.

Taken together, native purification of ethylene receptor protein ETR1 from *P. patens* yielded up to 0.25 mg protein per gram cells whereas only 0.1 mg/g cells were obtained for the full-length protein from *L. esculentum*. However, these numbers have to be taken with some caution due to the contamination by DnaK.

## 7.3 Crystallisation studies

### 7.3.1 Full-length ethylene receptor ETR1 from *L. esculentum*

Ethylene receptor LeETR1<sub>1-754</sub> was natively purified by IMAC according to protocol 4.7.3.1. The protein concentration was set to 10 mg/ml and the receptor protein was applied in microbatch crystallisation trials using *Qiagen's MbClass* and *PEGs Suites I and II*, the *JCSG<sup>+</sup> Screen* and *JBScreen Membrane 1, 2 and 3* kits from *Jena Bioscience*. Crystallisation setups were also prepared with the *Lipidic-Sponge Phase<sup>TM</sup> Screen* according to the manufacturer's instruction (see section 4.8.5.1). All plates were stored at 21 °C.

The plates were examined for potential crystal growth over a period of 50 days. Already after 24 hours sharp-edged crystals appeared in various microbatch conditions, most of which included magnesium or calcium chloride. When probed with a needle, all crystals were identified as salt crystals that probably had formed from phosphate buffer and the divalent cations.

Further crystal growth was not observed in any microbatch condition. However, solid structures with partial short-range order as in spherulites were detected in few conditions (see Figure 60, A-C). These structures have already been discussed for AtETR1 in section 6.2.2. As outlined there, conditions that favour spherulitic growth should be further screened because only minor changes in buffer composition might produce ordered, well-diffracting crystals.

Angular shaped structures with a size of about 50 µm edge length were detected in a *Lipidic-Sponge Phase<sup>TM</sup>* condition 5 months after setup (Figure 60D). When the crystallisation well was opened to analyse these structures, they immediately dissolved.

This indicates that the crystal-like objects are artefacts from the lipid containing crystallisation buffer. It has been reported for lipidic mesophases that voids, droplets or the lipid itself can produce shapes similar to crystals<sup>[212]</sup>.

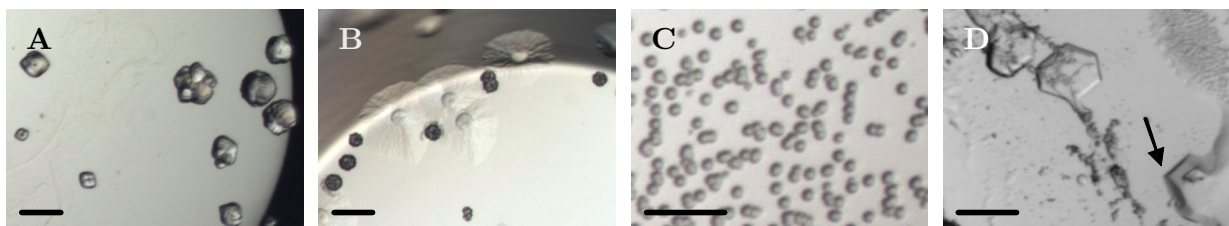


Figure 60: Pictures (A) to (C) were taken 5 days after crystallisation setup and show spherulites grown in (A) 0.2 M zinc acetate, 0.1 M sodium cacodylate, pH 6.5 and 10 % (v/v) isopropanol; (B) 1 M ammonium sulfate, 50 mM MES sodium salt, pH 6.5 and 100 mM zinc acetate; (C) 0.6 M magnesium sulfate, 100 mM HEPES, pH 7.5 and 4 % (w/v) PEG 400. Figure (D) shows angular structures in a buffer composed of monoolein, PEG 400 and HEPES, pH 7.5 (individual concentrations are not given by the manufacturer). The arrow points to a sharp-edged structure protruding from the lipid phase. Picture (D) was taken 5 months after setting up the crystallisation experiment. Black scale bars correspond to 50  $\mu\text{m}$ .

### 7.3.2 Full-length ethylene receptor ETR1 from *P. patens*

Ethylene receptor PpETR1<sub>1-754</sub> was prepared like LeETR1 (see 4.7.3.1). As already stated, the protein yield for PpETR1<sub>1-754</sub> was on average about 2.5 fold lower compared to full-length ETR1 from *L. esculentum*. A modified sitting drop method was applied by using the protein at a reduced concentration of only 2 mg/ml to allow for a first screening of at least 400 crystallisation conditions: Precipitant solutions were diluted 1:5 with sterile filtered water prior to use and crystallisation drops were set up in *NeXtal Evolution*  $\mu$ plates by mixing protein and precipitant solutions in equal amounts to a final volume of 1.5  $\mu\text{l}$ . The reservoirs of the plates were filled with 70  $\mu\text{l}$  of undiluted crystallisation buffer, and the plates were stored at 21  $^{\circ}\text{C}$ .

In classical vapour diffusion a high concentrated protein solution is diluted equally with a precipitant containing buffer—as result both solutions are only half concentrated after mixing. With the reservoir filled with precipitant solution at its original concentration, water will start to evaporate from the protein-precipitant drop until equilibrium is reached. When using protein solved in pure water without any additional substances, the drop will shrink to almost half of its starting volume, and the protein will reach the original concentration again. This approach works quite nice for proteins with starting concentration of about 5-10 mg/ml. However, if the protein is highly diluted, the concentration might still be too low to initiate nucleation even after equilibrium. The protein-precipitant drop would have to be concentrated even further to allow for crystal growth under these conditions. This is achieved by diluting the crystallisation buffer by a factor of five to ten. Thus, the drops can equilibrate to a few hundred nanoliters which was actually the original purpose of this method. Setups are often prepared with drop

volumes in the nanoliter scale to minimise the amount of protein required in crystallisation studies. As these experiments cannot be set up by hand, the diluting method might be applied when no pipetting robot is available<sup>[213]</sup>.

For an initial screening with receptor protein PpETR1<sub>1-767</sub>, *Qiagen's MbClass* and *PEGs Suites I* and *II* were used. Again, in several conditions containing Ca<sup>2+</sup>, plate and needle shaped salt crystals appeared. These salt crystals resulted probably from the phosphate buffer and the calcium ions<sup>[214]</sup> and have been observed for receptor ortholog LeETR1<sub>1-754</sub>, too.

In various conditions also spherulitic structures were found again (Figure 61). These conditions might be used as starting point for further crystallisation studies as described for receptor AtETR1. Apart from establishing factorial screens by variation of pH, salt or precipitant concentrations, the spherulites could be used in seeding experiments. It might also be tested if a reduction of the incubation temperature has a positive effect on crystal growth. The fact that rather large spherulites with a size of up to 100 µm appeared after only 5 days might indicate that the chosen temperature was too high preventing homogenous crystal packing.

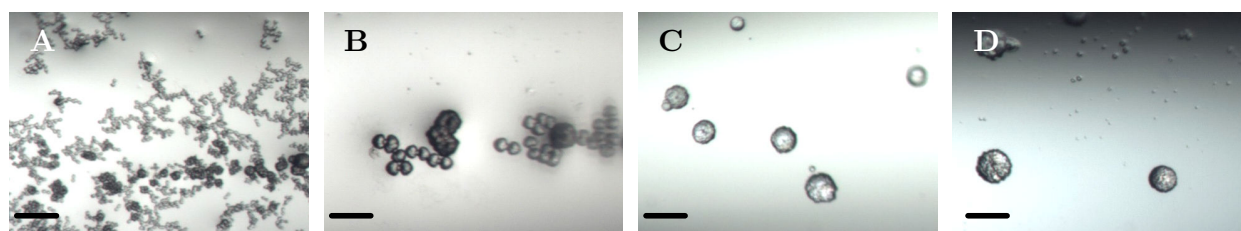


Figure 61: Pictures were taken 5 days after crystallisation setup and show spherulites grown in (A) 0.1 M Tris, pH 8.5 and 1.5 M lithium sulfate; (B) 100 mM HEPES sodium salt, pH 7.5 and 1.5 M lithium sulfate; (C) and (D) 0.2 M zinc acetate, 100 mM imidazole, pH 6.5 and 10 % (w/v) PEG 8000. Scale bars correspond to 100 µm.

## 7.4 Synopsis

Codon optimised synthetic DNA of ethylene receptor ETR1 from *Physcomitrella patens* and *Lycopersicon esculentum* coding for full-length and truncated versions lacking the transmembrane domain was cloned into bacterial expression vectors. Heterologous expression was obtained for both variants in *E. coli* strain BL21 (DE3). Expression levels and cell yields differed substantially. In general, significantly higher amounts of recombinant protein were produced for the truncated receptor proteins. In spite of higher yields in cell mass, cells harbouring full-length constructs expressed the proteins only at a low level. On average,

expression yielded about 4 g cell/l for the receptor constructs lacking the membrane domain and up to 6 g/l for cell cultures expressing the full-length proteins.

For purification of the receptors, two different strategies were applied. PpETR1<sub>158-767</sub> and LeETR1<sub>173-754</sub>, which were expressed as inclusion bodies were resolved in 8 M urea. Refolding of the receptors was performed by dilution. About 2-7 mg purified and functional protein was obtained per gram cells. However, size exclusion chromatography revealed that most of the protein forms aggregates that are not suitable for crystallisation.

Hence, full-length receptors of PpETR1 and LeETR1 were purified by IMAC after solubilisation of the receptors into *FOS-CHOLINE*<sup>®</sup> 14 micelles. Unfortunately, the isolated protein contained a contamination by the heat shock protein DnaK, which could not be separated from the receptors. Thus, functional studies demonstrating autokinase activity of ETR1 have to be considered carefully as DnaK also shows phosphorylation *in vitro*<sup>[210, 211]</sup>.

Nevertheless, purified PpETR1<sub>1-767</sub> and LeETR1<sub>1-754</sub> were used in first crystallisation studies that yielded spherulitic crystals for both receptor proteins. Though not applicable for diffraction analysis, these results outline a starting point for further crystallisation trials.

#### 7.4.1 Perspective on further crystallisation studies

A critical issue for crystallisation trials of ETR1 from *P. patens* and *L. esculentum* is the cross-contamination by DnaK when receptors are obtained by the native purification protocol. The chaperon might act as a flexible part of a putative receptor-chaperon complex and might disturb an ordered crystal packing. Therefore, an attempt should be made to remove DnaK. Washing with ATP and arginine should be tried even though these methods did not work with AtETR1 (see section 6.2.2).

Another possibility to prevent co-purification could be usage of a DnaK deficient *E. coli* strain for expression<sup>[215]</sup>. Also a change of the expression system from prokaryote to eukaryote might improve expression. Though no localisation studies have been performed for PpETR1 and LeETR1, it might be assumed that both receptors localise to the ER as described for AtETR1<sup>[26]</sup>. Since this cellular structure is not found in *E. coli* as well as posttranslational modification processes and advanced protein folding pathways, it might be reasonable to change to an eukaryotic expression system for the production of the receptor proteins<sup>[216]</sup>. Thereby, not just the expression level but also proper folding and prevention of inclusion body formation might be favoured.

#### 7.4.2 Taxonomic distribution of ethylene receptors in kingdom *Viridiplantae*

To further pursue the crystallisation project, it might be necessary to expand the study to a broader range of species containing ETR1 orthologs or ETR1-like proteins. As no molecular structure has been obtained for AtETR1, PpETR1 or LeETR1 so far, a structure from a related protein could provide the basis for homology modelling of ethylene receptor proteins.

To identify potential ethylene receptor proteins in species of *Viridiplantae*, a *BLAST*<sup>[81]</sup> search (*blastp* algorithm) with AtETR1 as query sequence was used. With a maximum of 1000 target sequences, 94 organisms were identified and from each the sequence with the highest score according to *BLOSUM62* was chosen for multiple alignment with *COBALT*<sup>[87]</sup>. Results are displayed in a phylogenetic tree (Figure 62) considering neighbour joining and a maximum sequence difference of 0.85<sup>[217]</sup>.

The majority of proteins similar to AtETR1 was found in the clade of *eudicots* comprising two representatives namely *Arabidopsis thaliana* and *Lycopersicon esculentum*, both of which were already tested for crystallisation in this thesis.

With *Oryza sativa* and *Zea mays*, the second largest clade, the *monocots*, contains two model organisms that are subject to intensive current research<sup>[218, 219]</sup>. Monocots produce less amounts of ethylene and are less sensitive to the plant hormone when applied exogenously<sup>[220]</sup>. It is interesting to reveal whether this fact is affected by structural differences of the receptor proteins. Therefore, it is most reasonable to expand the study to ethylene receptors from monocotyle plants.

*Physcomitrella patens* and its subspecies are the only representatives of the clade *moss* that have been annotated so far in terms of ethylene perceiving proteins. The same applies to the clade *club-mosses* covered by *Selaginella moellendorffii*.

Proteins similar to AtETR1 are also found in the taxa *algae* including the genera *Chlamydomonas*, *Volvox*, *Micromonas* and *Ostreococcus*. However, respective organisms were excluded from the phylogenetic tree as they showed sequence differences  $> 0.85$ .

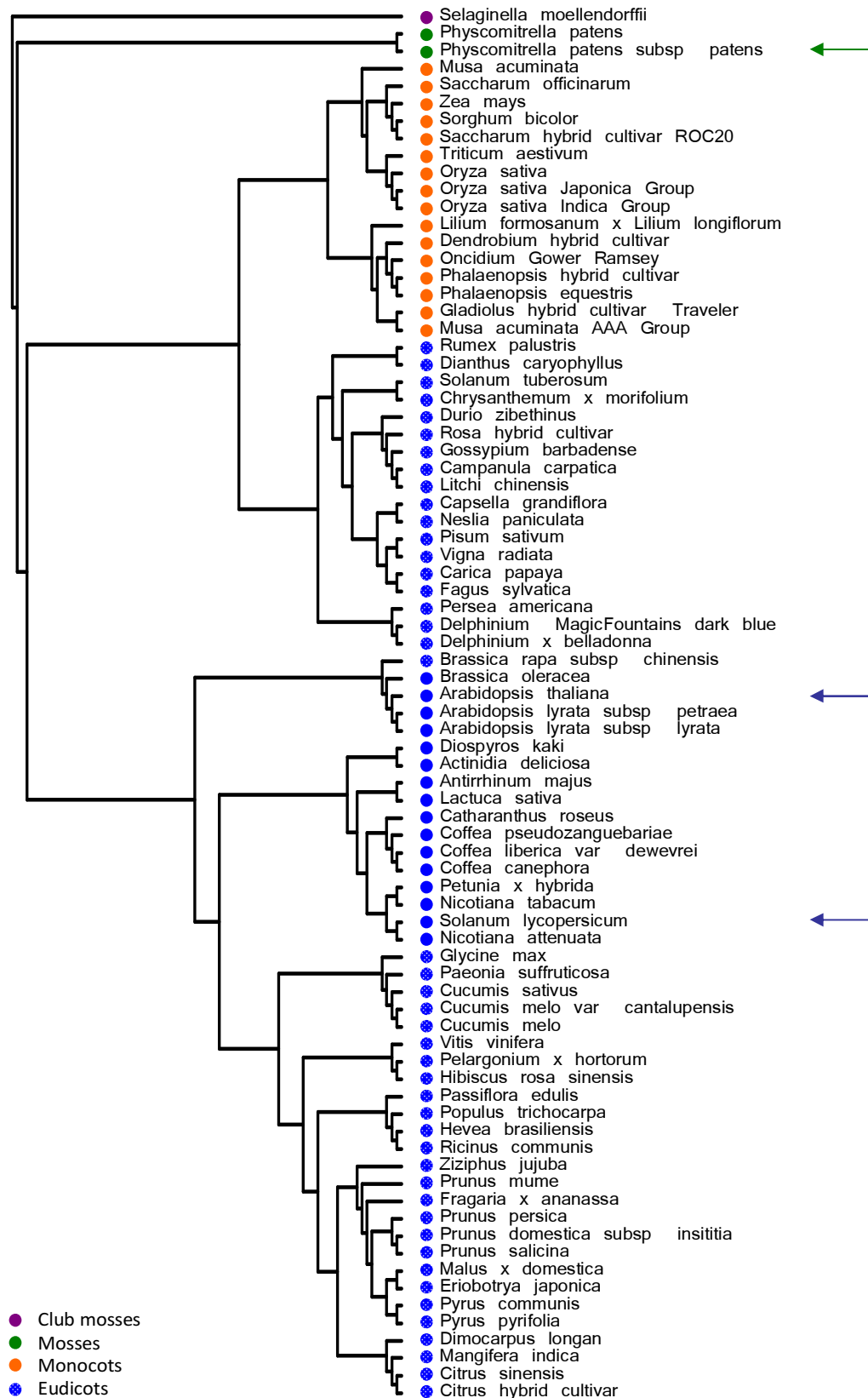


Figure 62: Taxonomic distribution of ethylene receptor proteins in green plants (*Viridiplantae*) including green algae and land plants. Species are clustered according to similarity of the respective proteins. Organisms that were chosen for this thesis are indicated by green and blue arrows. *Solanum lycopersicum* is a synonym for *Lycopersicon esculentum*. Affiliation of individual species to the taxa *club-mosses*, *mosses*, *monocots* and *eudicots* (*dicots*) are indicated by coloured dots according to the colour scheme as displayed on the bottom left.

### 7.4.3 Secondary structure analysis of orthologs AtETR1, PpETR1 and LeETR1

To date, only the cytosolic receiver domain of AtETR1 has been crystallised giving structural information for amino acids 605 to 736<sup>[130]</sup>. During this thesis, crystallisation experiments with full-length ethylene receptor AtETR1 as well as with the orthologous proteins PpETR1 and LeETR1 were performed but did not produce crystals suitable for structure determination.

However, to obtain a better understanding of the build-up and putative structural elements in the ethylene receptor proteins, primary sequences of all three ETR1 receptor were analysed regarding their secondary structure composition. Results were assigned to an alignment of the respective sequences to show conservation of these elements (Figure 63). All three ethylene

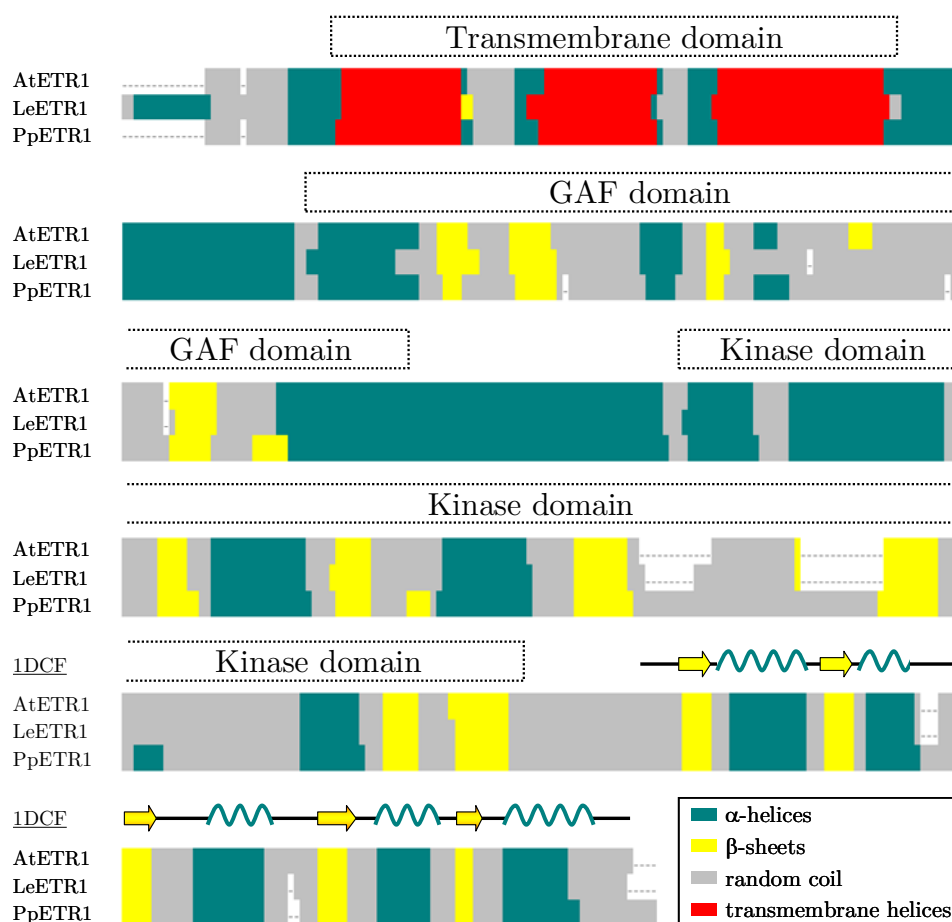


Figure 63: Secondary structure alignment for receptor proteins AtETR1, LeETR1 and PpETR1. The *PSIPRED* secondary structure prediction method was used to estimate the secondary structure composition for each receptor protein. Regions coloured in dark cyan correspond to  $\alpha$ -helices, yellow parts represent  $\beta$ -sheets and random coils structures are displayed in grey. The red coloured regions reflect putative transmembrane helices as calculated by *MEMSAT-SVM* algorithm. Structural elements derived from the crystal structure of the receiver domain of AtETR1 (PDB accession code: 1DCF) are depicted using the same colour scheme.

receptor proteins share a high degree of structural conservation although sequence identity was calculated to be only 63 % for PpETR1 relating to the other two receptors (see section 1). Notably, these differences occur mainly in low complexity regions, like in random coil structures (grey coloured sections in Figure 63). So, the tertiary structure is most likely not influenced.

The N-terminal part of the proteins comprises three transmembrane helices as predicted by *MEMSAT-SVM* algorithm using a neural network for identification and orientation of each transmembrane segment<sup>[101-103]</sup>. This method also identified an additional helix prior to the transmembrane domain of LeETR1 that might function as a possible signal peptide: As the receptor protein of tomato has been evidenced on transcript level, it might be suggested that this sequence still contains a targeting information that might have been cleaved on other receptor proteins that were detected on protein level including subfamily I from *A. thaliana* (ETR1 and ERS1). However, *BLAST* search on translated genome gave only one further hit for the peptide sequence namely in ETR1-3 of *Petunia x hybrida*.

Members of *Arabidopsis* subfamily II (ETR2, ERS2 and EIN4) all contain a fourth N-terminal helix, though it remains unclear whether it constitutes a targeting signal peptide or a transmembrane segment<sup>[221, 222]</sup>. These facts give rise to the assumption that ethylene receptor ETR1 from *L. esculentum* might take an exceptional position among the receptor proteins. With its conserved kinase domain containing all essential residues of a typical histidine kinase, it belongs to subfamily I. However, due to the fourth N-terminal helix, it could also be classified as a member of subfamily II even though these receptors show Ser/Thr kinase activity<sup>[30]</sup>.

The transmembrane domain is C-terminally flanked by a putative GAF domain. Based on a structure from *S. cerevisiae* (PDB accession code: 1F5M), this ubiquitous domain motif consists of a central part build of six anti-parallel  $\beta$ -sheets that are enclosed by four  $\alpha$ -helices<sup>[223]</sup>. While all helices can be found in the ETR1 secondary structure model in Figure 63, the number of  $\beta$ -sheets varies from 4 to 5. Most probably, very short  $\beta$ -strands (three amino acids) were not acquired by *PSIPRED*. GAF domains are usually involved in binding of cyclic GMP, but their function in ethylene receptors is still unknown<sup>[26]</sup>.

The kinase domain forms the largest segment of the receptor proteins. Several structures have been solved for bacterial kinases, for example, CheA and ThkA from *Thermotoga maritima* and DesK from *Bacillus subtilis*<sup>[224-226]</sup>.



---

The cytosolic part of a sensor histidine-kinase protein from *Thermotoga maritima* (HK853) shares about 50 % sequence similarity over a range of 226 amino acids. It is composed of two N-terminal  $\alpha$ -helices that show a hairpin structure and allow for dimerisation. The catalytic core is build of five  $\beta$ -sheets and three  $\alpha$ -helices that form a cavity for ATP-binding. At the C-terminus, the kinase contains an additional pair of short  $\beta$ -strands with unknown function<sup>[109]</sup>. Although the overall number of  $\beta$ -sheets is slightly higher than depicted in Figure 63, the secondary structure model shows a distinct consensus with the structural elements of the bacterial kinase.

The quality of the secondary structure model is reflected by a comparison of calculated and empirically determined structural information for the receiver domain of AtETR1. Structural elements derived from the crystal structure as depicted by arrows ( $\beta$ -sheets) and waves ( $\alpha$ -helices) in Figure 63 show the high accuracy of the predicted secondary structure model. Only minor shifts of about one or two amino acids were detected.

A secondary structure alignment as shown for ETR1 from *A. thaliana*, *P. patens* and *L. esculentum* provides structural information beneficial for designing biochemical experiments as well as crystallisation studies. Although individual proteins might not show a high conservation in their amino acid sequence, they can adopt similar structures. This is due to the fact that structural elements of proteins are more conserved than the corresponding primary sequences<sup>[227]</sup>. In consequence, an alignment of such features displays the structural similarity of even distantly related proteins and emphasises their homology.

Referring to the crystallisation studies with receptor ETR1, the information from a secondary structure alignment can also be used to identify ethylene receptor proteins that show a *different* secondary structure composition. These proteins will probably show crystallisation characteristics other than those observed for the three ETR1 proteins applied in this thesis, which are all structurally highly conserved, and might lead to successful crystallisation and structure solution. The alignment can also be used to identify low structured regions like loops. Deletion of such flexible structures might also favour crystallization.

The model also allows narrowing down individual domains of the proteins more precisely than in secondary structure analysis of single sequences. This information is important if domains are going to be analysed individually like in yeast two-hybrid screenings or crosslinking approaches.



## 8 Concluding remarks

The scientific understanding of phytohormones and their impact on plant growth and physiological development has been progressive in the last years. For the majority of the plant hormones, receptor proteins were identified and signalling networks were proposed considering cross-talk between individual pathways.

In the view of agricultural importance of the signalling substances, it is necessary to further unravel the signalling mechanisms on a molecular level to grasp signal perception and transduction concepts. In this context, structural models of the hormone receptors will help to disclose the individual modes of action and to develop new regulatory substances.

Due to their size, most receptor proteins including ETR1 have to be applied to X-ray crystallography for structure solution at an atomic level. The work in the present thesis showed that this approach is a sophisticated endeavour. Although various improvements have been made in membrane protein crystallography including development of specific techniques like crystallisation in lipid phases, these methods do not apply to all membrane proteins.

In addition to structural characterisation of the receptor proteins, functional studies will provide information on the signalling mechanisms. Activation and regulation of the kinase domain of ETR1 might be deciphered by spectroscopic methods like NMR or EPR. Both techniques could show influences of putative regulatory substances and identify further residues involved in the signal transduction, thereby contributing to a general understanding of hormone signalling in plants.



## 9 Appendix

### 9.1 Abbreviations

Amino acids are abbreviated in three- and one-letter code according to *IUPAC-IUB Commission on Biochemical Nomenclature*<sup>[228]</sup>. SI units are not listed.

<b>A</b>		<b>E</b>	
Å	Angstrom	<i>E. coli</i>	<i>Escherichia coli</i>
aa	amino acids	ECL	enhanced chemiluminescence
ACC	1-aminocyclopropane-1-carboxylic acid	EDTA	ethylenediaminetetraacetic acid
ADP	adenosine-5'-diphosphate	EIL	ethylene insensitive3 like
AHP	<i>Arabidopsis</i> histidine-containing phosphotransfer protein	EIN	ethylene insensitive
AMP	adenosine-5'-monophosphate	EMBL	European Molecular Biology Laboratory
AMP-PNP	adenosin-5'-( $\beta,\gamma$ -imido)triphosphate	EPR	electron paramagnetic resonance
APS	ammonium persulfate	Eq.	equation
ARR	<i>Arabidopsis</i> response regulator	ER	endoplasmic reticulum
At/ <i>A. thaliana</i>	<i>Arabidopsis thaliana</i>	ERF	Ethylene responsive factor
ATP	adenosine-5'-triphosphate	ERS	ethylene response sensor
AU	arbitrary unit	ESRF	European Synchrotron Radiation Facility
<b>B</b>		ETP	EIN2 targeting protein
BCA	bicinchoninic acid	ETR	ethylene response/resistant
Bicine	<i>N,N</i> -Bis(2-hydroxyethyl)glycine	<b>F</b>	
Bis-tris propane	1,3-bis(tris(hydroxymethyl)-methylamino)propane	FRET	<i>Foerster</i> resonance energy transfer
BLAST	Basic Local Alignment Search Tool	<b>G</b>	
bp	base pair(s)	GMP	guanosine-5'-monophosphate
BSA	bovine serum albumin	GSH	glutathione
<b>C</b>		GSSG	glutathione disulfide
c	complementary	<b>H</b>	
cc	creative commons	h	hour
CD	circular dichroism	HEPES	4-(2-hydroxyethyl)-1-piperazineethanesulfonic acid
Ci	Curie (decays per second)	hGH	human growth hormone
CMC	critical micelle concentration	HPt	histidine-containing phosphotransfer protein
CTR	constitutive triple response	HRP	horseradish peroxidase
CV	column volume	Hsp	heat shock protein
<b>D</b>		<b>I</b>	
Da	Dalton	IB	inclusion body
DDM	<i>n</i> -dodecyl- $\beta$ -D-maltopyranoside	IgG	immunoglobulin G
deg	degree	IMAC	immobilised metal affinity chromatography
DNA	deoxyribonucleic acid	IPTG	isopropyl- $\beta$ -D-1-thiogalactopyranoside
dNTP	deoxyribonucleotide		
DOC	deoxycholate		
ds	double stranded		
DTT	dithiothreitol		

**K**

kb kilo base(s)

**L**Le/*L. esculentum* *Lycopersicon esculentum***M**

MAPKK mitogen activated protein kinase  
kinase  
MCS multiple cloning site  
MES 2-(*N*-morpholino)ethanesulfonic acid  
min minute  
MTA methylthioadenosine  
MW molecular weight  
MWCO molecular weight cut-off  
MWR mean residue weight ellipticity

**N**

NADPH nicotinamide adenine dinucleotide  
phosphate  
NC cellulose nitrate  
NEM *N*-ethylmaleimide  
NMR nuclear magnetic resonance  
NTA nitrilotriacetic acid

**O**

o/n over night  
OD optical density

**P**

PAGE polyacrylamide gel electrophoresis  
PCR polymerase chain reaction  
PDB Protein Data Bank  
PEG polyethylene glycol  
 $\Phi_F$  quantum yield  
Pi inorganic phosphate  
pI isoelectric point  
PMSF phenylmethylsulfonyl fluoride  
Pp/*P. patens* *Physcomitrella patens* (subsp.  
*patens*)  
ppm parts per million  
psi pound per square inch  
PTFE polytetrafluoroethylene  
PVDF polyvinylidene fluoride  
*Pwo* *Pyrococcus woesei*

**R**

r recombinant  
RAN responsive to antagonist  
x g relative centrifugal force  
*RCSB* Research Collaboratory for  
Structural Bioinformatics  
RET resonance energy transfer  
RMSD root mean square deviation  
rpm revolutions per minute  
RTE reversion to ethylene sensitivity

**S**

SAM *S*-adenosyl methionine  
SDS sodium dodecyl sulfate  
SEC size exclusion chromatography  
SER surface entropy reduction  
SI *The International System of Units*  
SLIC sequence and ligation independent  
cloning  
 $S_n$  electronic state  
ss single stranded

**T**

*Taq* *Thermus aquaticus*  
TEMED *N,N,N',N'*-tetramethyl-  
ethane-1,2-diamine  
TEV tobacco etch virus  
TM transmembrane  
Tricine *N*-  
(Tri(hydroxymethyl)methyl)glycine  
Tris Tris(hydroxymethyl)aminomethane  
tRNA transfer ribonucleic acid

**U**

U unit  
UV ultraviolet

**V**

v/v volume per volume

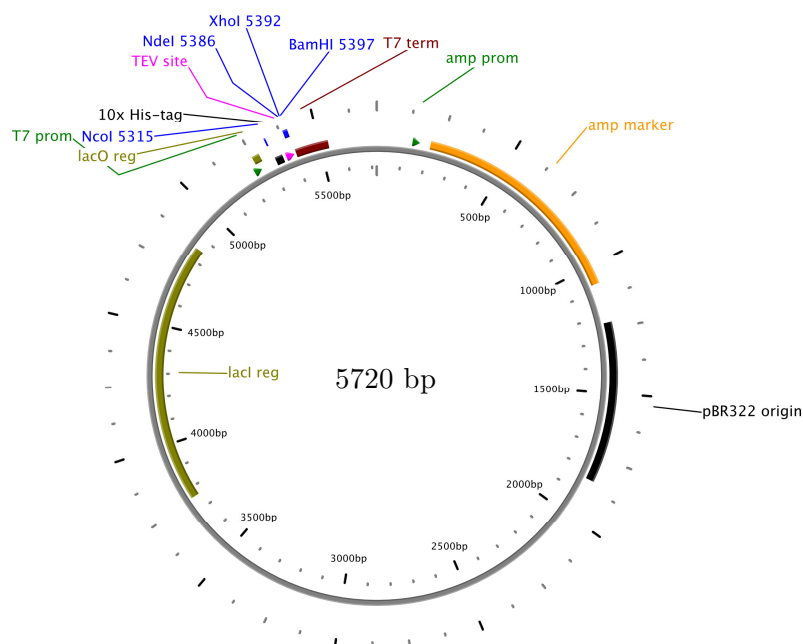
**W**

w/v weight per volume  
WT wild type

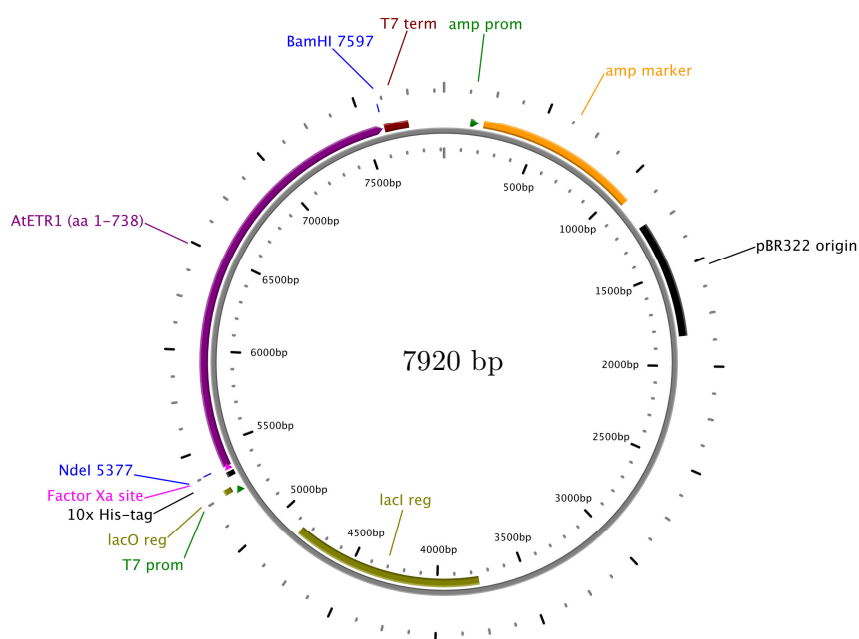
## 9.2 Maps of expression vectors

Abbreviations used in all vector maps: *prom* (transcription promoter), *term* (transcription terminator), *amp* (ampicillin), *reg* (regulator)

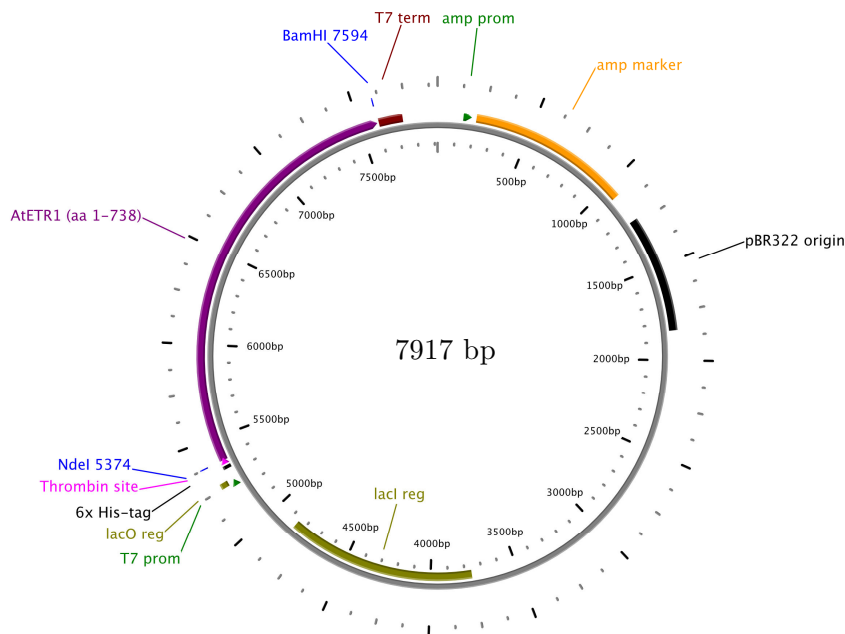
### 9.2.1 Vector pTEV-16b



### 9.2.2 Vector pET-16b::AtETR1<sub>1-738</sub>WT



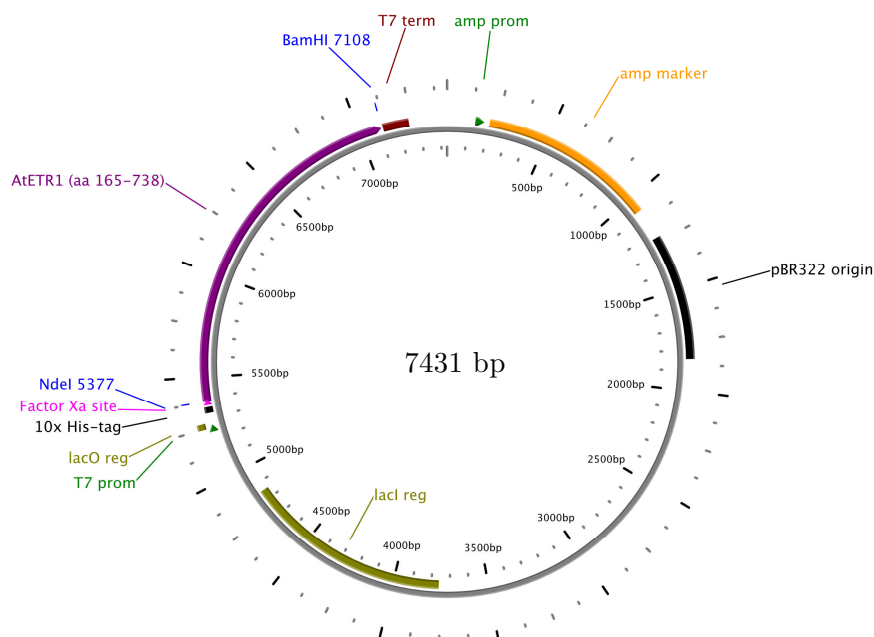
### 9.2.3 Vectors based on pET-15b::AtETR1<sub>1-738</sub>



The following vectors are based on pET-15b::AtETR1<sub>1-738</sub>:

pET-15b::AtETR1<sub>1-738</sub>W<sub>free</sub>  
 pET-15b::AtETR1<sub>1-738</sub>W53  
 pET-15b::AtETR1<sub>1-738</sub>H353A  
 pET-15b::AtETR1<sub>1-738</sub>D659A  
 pET-15b::AtETR1<sub>1-738</sub>W<sub>free</sub>F26W  
 pET-15b::AtETR1<sub>1-738</sub>W<sub>free</sub>F27W  
 pET-15b::AtETR1<sub>1-738</sub>W<sub>free</sub>F33W  
 pET-15b::AtETR1<sub>1-738</sub>W<sub>free</sub>L55W  
 pET-15b::AtETR1<sub>1-738</sub>W<sub>free</sub>F58W  
 pET-15b::AtETR1<sub>1-738</sub>W<sub>free</sub>L64W  
 pET-15b::AtETR1<sub>1-738</sub>W<sub>free</sub>L70W  
 pET-15b::AtETR1<sub>1-738</sub>W<sub>free</sub>L73W  
 pET-15b::AtETR1<sub>1-738</sub>W<sub>free</sub>V350W  
 pET-15b::AtETR1<sub>1-738</sub>W<sub>free</sub>N352W  
 pET-15b::AtETR1<sub>1-738</sub>W<sub>free</sub>R356W

### 9.2.4 Vectors based on pET-16b::AtETR1<sub>165-738</sub>

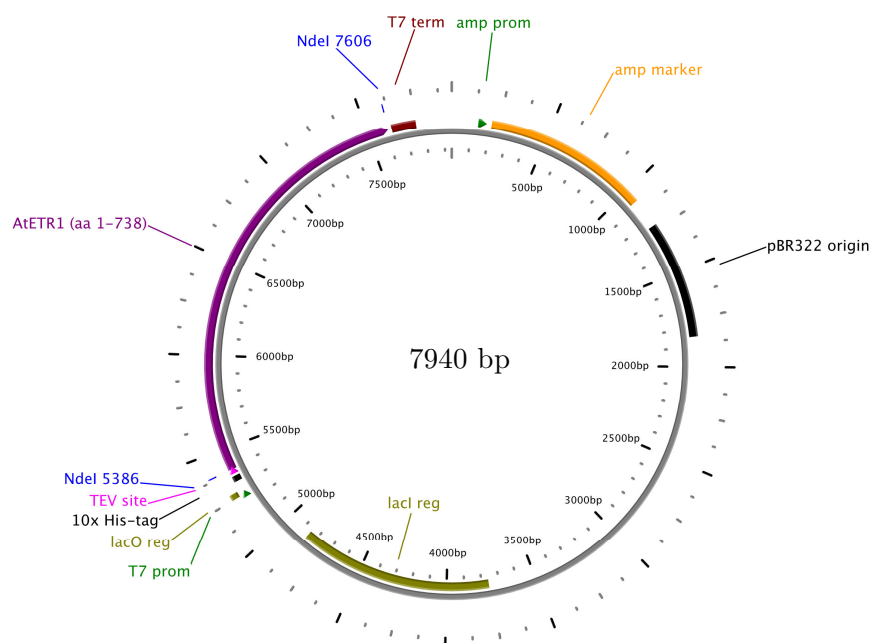


The following vectors are based on pET-16b::AtETR1<sub>165-738</sub>:

pET-16b::AtETR1<sub>165-738</sub>WT  
 pET-16b::AtETR1<sub>165-738</sub>H353A  
 pET-16b::AtETR1<sub>165-738</sub>SER



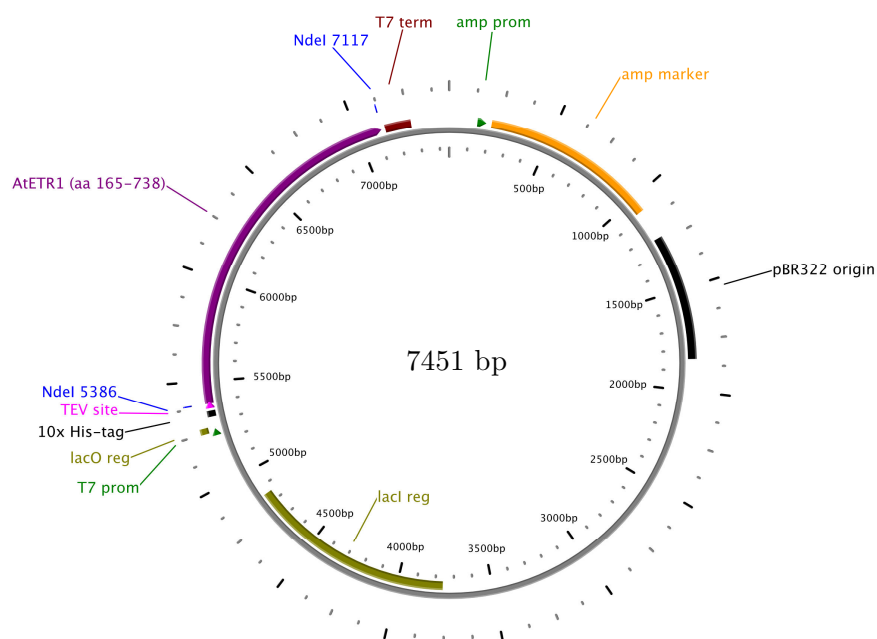
### 9.2.5 Vectors based on pTEV-16b::AtETR1<sub>1-738</sub>



The following vectors are based on pTEV-16b::AtETR1<sub>1-738</sub>:

pTEV-16b::AtETR1<sub>1-738</sub>W<sub>free</sub>L70W  
 pTEV-16b::AtETR1<sub>1-738</sub>W<sub>free</sub>N352W/H353A  
 pTEV-16b::AtETR1<sub>1-738</sub>W<sub>free</sub>N352W/H353E  
 pTEV-16b::AtETR1<sub>1-738</sub>W<sub>free</sub>53/C65A/H69A

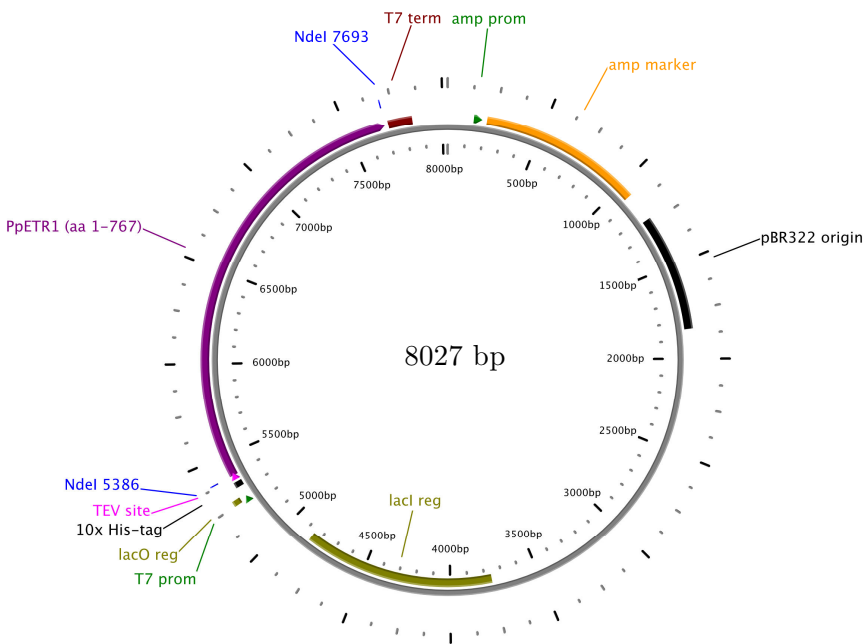
### 9.2.6 Vectors based on pTEV-16b::AtETR1<sub>165-738</sub>



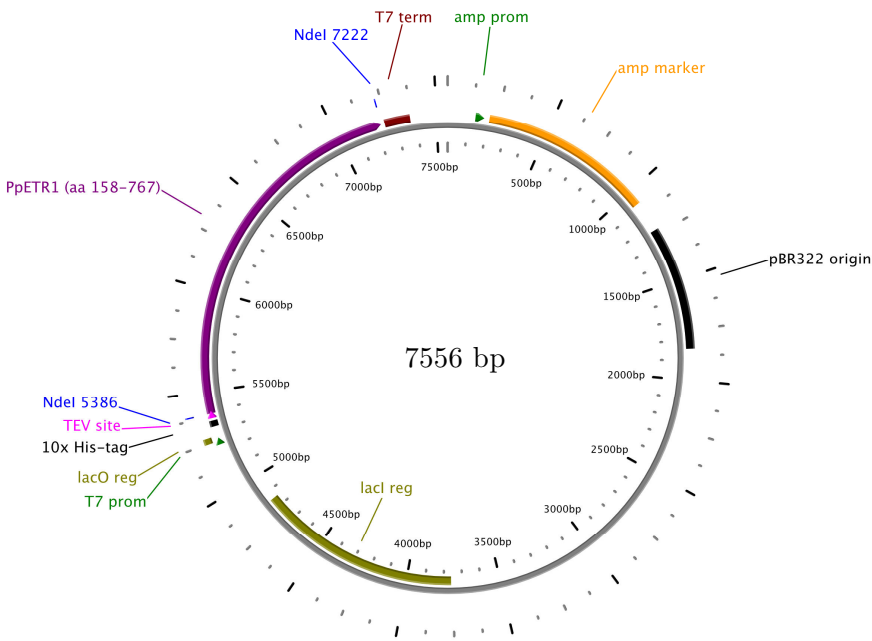
The following vectors are based on pTEV-16b::AtETR1<sub>165-738</sub>:

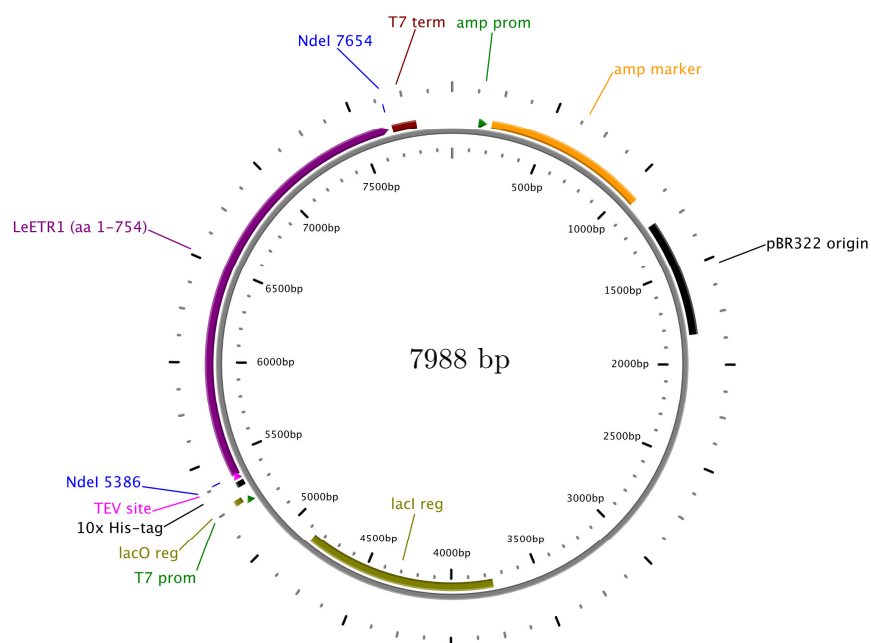
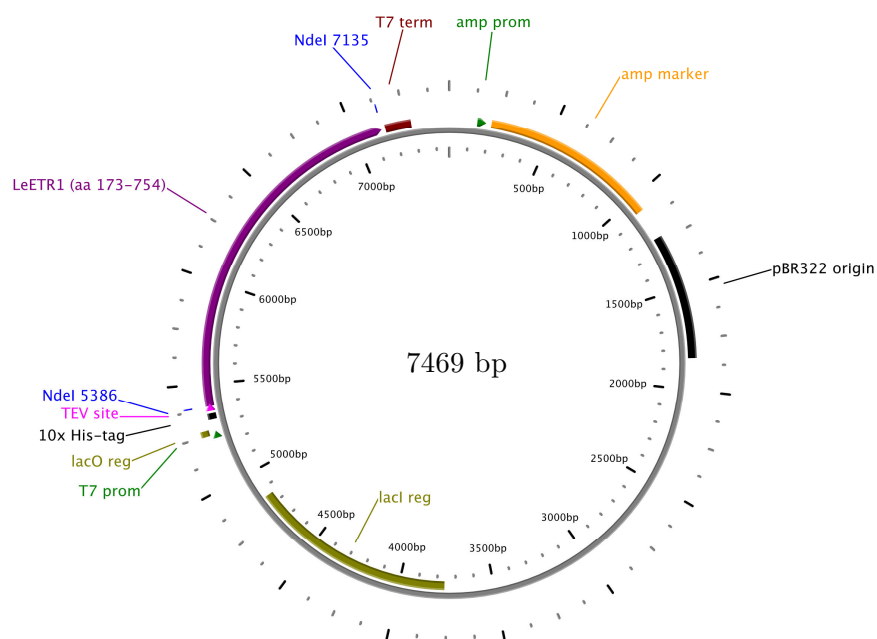
pTEV-16b::AtETR1<sub>165-738</sub>W<sub>free</sub>V350W  
 pTEV-16b::AtETR1<sub>165-738</sub>W<sub>free</sub>N352W  
 pTEV-16b::AtETR1<sub>165-738</sub>W<sub>free</sub>R356W

9.2.7 Vector pTEV-16b::PpETR1<sub>1-767</sub>



9.2.8 Vector pTEV-16b::PpETR1<sub>158-767</sub>



9.2.9 Vector pTEV-16b::LeETR1<sub>1-754</sub>9.2.10 Vector pTEV-16b::LeETR1<sub>173-754</sub>

### 9.3 List of detergents used in this thesis

Table 21: Properties of detergents as specified by the manufacturer (*Anatrace Inc.*, Maumee, OH, USA). The different types of detergents are abbreviated by N for *non-ionic* and Z for *zwitter-ionic* detergents. Percentages are given in (w/v).

<i>Detergent</i>	<i>Type</i>	<i>MW</i> (g/mol)	<i>CMC mM (%)</i>	<i>Aggregation</i> <i>number</i> (if available)	<i>Concentration</i> <i>used for solu-</i> <i>bilisation (%)</i>
ANAOE <sup>®</sup> -20	N	1228	0.059 (0.0072 %)		1
ANAOE <sup>®</sup> -35	N	1198	0.091 (0.0010 %)	40	1
ANAOE <sup>®</sup> -58	N	1122	0.004 (0.00045 %)		1
ANAOE <sup>®</sup> -C10E6	N	423	0.9 (0.0250 %)	40	1
ANAOE <sup>®</sup> -X-114	N	536	0.2 (0.011 %)		1
ANAOE <sup>®</sup> -X-405	N	1967	0.81 (0.16 %)		1
ANZERGENT <sup>®</sup> 3-10	Z	307.6	39 (1.2 %)	41	2
ANZERGENT <sup>®</sup> 3-12	Z	335.5	2.8 (0.094 %)	55-87	1
ANZERGENT <sup>®</sup> 3-14	Z	363.6	0.2 (0.007 %)	83-130	1
C-DODECAFOS <sup>TM</sup>	Z	349.17	22 (0.77 %)		2
CYCLOFOS <sup>TM</sup> -4	Z	320.92	14 (0.45 %)		2
CYCLOFOS <sup>TM</sup> -5	Z	334.95	4.5 (0.15 %)		1
CYCLOFOS <sup>TM</sup> -6	Z	349.17	2.68 (0.094 %)		1-2
CYCLOFOS <sup>TM</sup> -7	N	363.3	0.62 (0.022 %)		1-2
FOS-CHOLINE <sup>®</sup> -9	Z	309.4	39.5 (1.2 %)		2
FOS-CHOLINE <sup>®</sup> -10	Z	323.4	11 (0.35 %)		2
FOS-CHOLINE <sup>®</sup> -11	Z	337.4	1.85 (0.062 %)		1
FOS-CHOLINE <sup>®</sup> -12	Z	351.5	1.5 (0.047 %)	50-60	1
FOS-CHOLINE <sup>®</sup> -13	Z	365.5	0.75 (0.027 %)		1
FOS-CHOLINE <sup>®</sup> -14	Z	379.5	0.12 (0.0046 %)	108	1
FOS-CHOLINE <sup>®</sup> -16	Z	407.5	0.013 (0.00053 %)		1-2
<i>n</i> -octyl- $\beta$ -D-glucopyranoside	N	292.4	18 (0.53 %)	78	2
<i>n</i> -dodecyl- $\beta$ -D-maltopyranoside	N	510.6	0.17 (0.0087 %)	78-149	1
<i>n</i> -octyl- $\beta$ -D-thiomaltopyranoside	N	470.6	8.5 (0.40 %)		2

## 9.4 Refolding buffers

Table 22: Composition of refolding buffers from the *QuickFold™ Protein Refolding Kit* as specified by the manufacturer (*Athena Environmental Sciences, Inc.*, Baltimore, MD, USA).

<i>Buffer</i>	<i>Contents</i>
RB-1	50 mM MES/HCl pH 6.0, 9.6 mM NaCl, 0.4 mM KCl, 2 mM MgCl <sub>2</sub> , 2 mM CaCl <sub>2</sub> , 0.75 M guanidine HCl, 0.5 % (w/v) <i>Triton</i> <sup>®</sup> X-100, 1 mM DTT
RB-2	50 mM MES/HCl pH 6.0, 9.6 mM NaCl, 0.4 mM KCl, 2 mM MgCl <sub>2</sub> , 2 mM CaCl <sub>2</sub> , 0.5 M arginine, 0.05 % (w/v) polyethylene glycol 3,550, 1 mM GSH, 0.1 mM GSSH
RB-3	50 mM MES/HCl pH 6.0, 9.6 mM NaCl, 0.4 mM KCl, 1 mM EDTA, 0.4 M sucrose, 0.75 M guanidine HCl, 0.5 % (w/v) <i>Triton</i> <sup>®</sup> X-100, 0.05 % (w/v) polyethylene glycol 3,550, 1 mM DTT
RB-4	50 mM MES/HCl pH 6.0, 240 mM NaCl, 10 mM KCl, 2 mM MgCl <sub>2</sub> , 2 mM CaCl <sub>2</sub> , 0.5 M arginine, 0.5 % (w/v) <i>Triton</i> <sup>®</sup> X-100, 1 mM GSH, 0.1 mM GSSH
RB-5	50 mM MES/HCl pH 6.0, 240 mM NaCl, 10 mM KCl, 1 mM EDTA, 0.4 M sucrose, 0.75 M guanidine HCl, 1 mM DTT
RB-6	50 mM MES/HCl pH 6.0, 240 mM NaCl, 10 mM KCl, 1 mM EDTA, 0.5 M arginine, 0.4 M sucrose, 0.5 % (w/v) <i>Triton</i> <sup>®</sup> X-100, 0.05 % (w/v) polyethylene glycol 3,550, 1 mM GSH, 0.1 mM GSSH
RB-7	50 mM MES/HCl pH 6.0, 240 mM NaCl, 10 mM KCl, 2 mM MgCl <sub>2</sub> , 2 mM CaCl <sub>2</sub> , 0.75 M guanidine HCl, 0.05 % (w/v) polyethylene glycol 3,550, 1 mM DTT
RB-8	50 mM Tris/HCl pH 8.5, 9.6 mM NaCl, 0.4 mM KCl, 2 mM MgCl <sub>2</sub> , 2 mM CaCl <sub>2</sub> , 0.4 M sucrose, 0.5 % (w/v) <i>Triton</i> <sup>®</sup> X-100, 0.05 % (w/v) polyethylene glycol 3,550, 1 mM GSH, 0.1 mM GSSH
RB-9	50 mM Tris/HCl pH 8.5, 9.6 mM NaCl, 0.4 mM KCl, 1 mM EDTA, 0.5 M arginine, 0.75 M guanidine HCl, 0.05 % (w/v) polyethylene glycol 3,550, 1 mM DTT
RB-10	50 mM Tris/HCl pH 8.5, 9.6 mM NaCl, 0.4 mM KCl, 2 mM MgCl <sub>2</sub> , 2 mM CaCl <sub>2</sub> , 0.5 M arginine, 0.4 M sucrose, 0.75 M guanidine HCl, 1 mM GSH, 0.1 mM GSSH
RB-11	50 mM Tris/HCl pH 8.5, 9.6 mM NaCl, 0.4 mM KCl, 1 mM EDTA, 0.5 % (w/v) <i>Triton</i> <sup>®</sup> X-100, 1 mM DTT
RB-12	50 mM Tris/HCl pH 8.5, 240 mM NaCl, 10 mM KCl, 1 mM EDTA, 0.05 % (w/v) polyethylene glycol 3,550, 1 mM GSH, 0.1 mM GSSH
RB-13	50 mM Tris/HCl pH 8.5, 240 mM NaCl, 10 mM KCl, 1 mM EDTA, 0.5 M arginine, 0.75 M guanidine HCl, 0.5 % (w/v) <i>Triton</i> <sup>®</sup> X-100, 1 mM DTT
RB-14	50 mM Tris/HCl pH 8.5, 240 mM NaCl, 10 mM KCl, 2 mM MgCl <sub>2</sub> , 2 mM CaCl <sub>2</sub> , 0.5 M arginine, 0.4 M sucrose, 0.75 M guanidine HCl, 0.5 % (w/v) <i>Triton</i> <sup>®</sup> X-100, 0.05 % (w/v) polyethylene glycol 3,550, 1 mM GSH, 0.1 mM GSSH
RB-15	50 mM Tris/HCl pH 8.5, 240 mM NaCl, 10 mM KCl, 2 mM MgCl <sub>2</sub> , 2 mM CaCl <sub>2</sub> , 0.4 M sucrose, 1 mM DTT



## 10 References

1. Kende H, Zeevaart J (1997) The five "classical" plant hormones. *Plant Cell* 9:1197-1210.
2. Jun JH, Fiume E, Fletcher JC (2007) The CLE family of plant polypeptide signaling molecules. *Cell Mol Life Sci.* 65:743-755.
3. Bishopp A, Mähönen AP, Helariutta Y (2006) Signs of change: hormone receptors that regulate plant development. *Development* 133:1857-1869.
4. Lund ST, Stall RE, Klee HJ (1998) Ethylene regulates the susceptible response to pathogen infection in tomato. *Plant Cell* 10:371-382.
5. Gazzarrini S, McCourt P (2003) Cross-talk in plant hormone signalling: what Arabidopsis mutants are telling us. *Ann Bot.* 91:605-612.
6. Abeles FB, Morgan PW, Saltveit Jr ME (1992) *Ethylene in Plant Biology, Second Edition* (Academic Press).
7. Bleeker AB, Kende H (2000) Ethylene: a gaseous signal molecule in plants. *Annu Rev Cell Dev Biol.* 16:1-18.
8. Gonzalez-Carranza ZH, Whitelaw CA, Swarup R, Roberts JA (2002) Temporal and spatial expression of a polygalacturonase during leaf and flower abscission in oilseed rape and Arabidopsis. *Plant Physiol.* 128:534-543.
9. Sagee O, Goren R, Riov J (1980) Abscission of citrus leaf explants: interrelationships of abscisic acid, ethylene and hydrolytic enzymes. *Plant Physiol.* 66:750-753.
10. Riov J (1974) A polygalacturonase from citrus leaf explants: role in abscission. *Plant Physiol.* 53:312-316.
11. Chen Y, Etheridge N, Schaller GE (2005) Ethylene signal transduction. *Ann Bot.* 95:901 -915.
12. Tanimoto M, Roberts K, Dolan L (1995) Ethylene is a positive regulator of root hair development in Arabidopsis thaliana. *Plant J.* 8:943-948.
13. Lorbiecke, Sauter (1999) Adventitious root growth and cell-cycle induction in deepwater rice. *Plant Physiol.* 119:21-30.
14. Johnson PR, Ecker JR (1998) The ethylene gas signal transduction pathway: a molecular perspective. *Annu Rev Genet.* 32:227-254.
15. O'Donnell PJ et al. (2003) Multiple hormones act sequentially to mediate a susceptible tomato pathogen defense response. *Plant Physiol.* 133:1181-1189.
16. Penninckx IAMA, Thomma BPHJ, Buchala A, Metraux J, Broekaert WF (1998) Concomitant activation of jasmonate and ethylene response pathways is required for induction of a plant defensin gene in Arabidopsis. *Plant Cell* 10:2103-2114.
17. Yang SF, Hoffman NE (1984) Ethylene biosynthesis and its regulation in higher plants. *Annu Rev Plant Physiol.* 35:155-189.
18. Guzmán P, Ecker JR (1990) Exploiting the triple response of Arabidopsis to identify ethylene-related mutants. *Plant Cell* 2:513-523.
19. Guo H, Ecker JR (2004) The ethylene signaling pathway: new insights. *Curr Opin Plant Biol.* 7:40-49.
20. Etheridge N, Chen Y, Schaller GE (2005) Dissecting the ethylene pathway of Arabidopsis. *Brief Funct Genomic Proteomic.* 3:372-381.
21. Grefen C, Harter K (2004) Plant two-component systems: principles, functions, complexity and cross talk. *Planta* 219:733-742.
22. Hua J, Meyerowitz EM (1998) Ethylene responses are negatively regulated by a receptor gene family in Arabidopsis thaliana. *Cell* 94:261-271.

23. Bleeker AB, Esch JJ, Hall AE, Rodríguez FI, Binder BM (1998) The ethylene-receptor family from Arabidopsis: structure and function. *Philos Trans R Soc Lond B Biol Sci.* 353:1405-1412.
24. Moussatche P, Klee HJ (2004) Autophosphorylation activity of the Arabidopsis ethylene receptor multigene family. *J Biol Chem.* 279:48734 -48741.
25. Qu X, Hall BP, Gao Z, Schaller GE (2007) A strong constitutive ethylene-response phenotype conferred on Arabidopsis plants containing null mutations in the ethylene receptors ETR1 and ERS1. *BMC Plant Biol.* 7:3.
26. Chen Y, Randlett MD, Findell JL, Schaller GE (2002) Localization of the ethylene receptor ETR1 to the endoplasmic reticulum of Arabidopsis. *J Biol Chem.* 277:19861 -19866.
27. Schaller GE, Ladd AN, Lanahan MB, Spanbauer JM, Bleeker AB (1995) The ethylene response mediator ETR1 from Arabidopsis forms a disulfide-linked dimer. *J Biol Chem.* 270:12526 -12530.
28. Gao Z et al. (2008) Heteromeric interactions among ethylene receptors mediate signaling in Arabidopsis. *J Biol Chem.* 283:23801-23810.
29. Rodríguez FI et al. (1999) A copper cofactor for the ethylene receptor ETR1 from Arabidopsis. *Science* 283:996-998.
30. Wang W et al. (2006) Identification of important regions for ethylene binding and signaling in the transmembrane domain of the ETR1 ethylene receptor of Arabidopsis. *Plant Cell* 18:3429-3442.
31. Cho Y, Yoo S (2007) ETHYLENE RESPONSE 1 histidine kinase activity of Arabidopsis promotes plant growth. *Plant Physiol.* 143:612-616.
32. Gamble RL, Coonfield ML, Schaller GE (1998) Histidine kinase activity of the ETR1 ethylene receptor from Arabidopsis. *Proc Natl Acad Sci. USA* 95:7825-7829.
33. Voet-van-Vormizeele J, Groth G (2008) Ethylene controls autophosphorylation of the histidine kinase domain in ethylene receptor ETR1. *Mol Plant* 1:380-387.
34. Hirayama T et al. (1999) RESPONSIVE-TO-ANTAGONIST1, a Menkes/Wilson disease-related copper transporter, is required for ethylene signaling in Arabidopsis. *Cell* 97:383-393.
35. Zhou X, Liu Q, Xie F, Wen C (2007) RTE1 Is a Golgi-associated and ETR1-dependent negative regulator of ethylene responses. *Plant Physiol.* 145:75-86.
36. Resnick JS, Wen C, Shockey JA, Chang C (2006) REVERSION-TO-ETHYLENE SENSITIVITY1, a conserved gene that regulates ethylene receptor function in Arabidopsis. *Proc Natl Acad Sci. USA* 103:7917-7922.
37. Resnick JS, Rivarola M, Chang C (2008) Involvement of RTE1 in conformational changes promoting ETR1 ethylene receptor signaling in Arabidopsis. *Plant J.* 56:423-431.
38. Clark KL, Larsen PB, Wang X, Chang C (1998) Association of the Arabidopsis CTR1 Raf-like kinase with the ETR1 and ERS ethylene receptors. *Proc Natl Acad Sci. USA* 95:5401-5406.
39. Gao Z et al. (2003) Localization of the Raf-like kinase CTR1 to the endoplasmic reticulum of Arabidopsis through participation in ethylene receptor signaling complexes. *J Biol Chem.* 278:34725-34732.
40. Alonso JM, Hirayama T, Roman G, Nourizadeh S, Ecker JR (1999) EIN2, a bifunctional transducer of ethylene and stress responses in Arabidopsis. *Science* 284:2148-2152.
41. Solano R, Stepanova A, Chao Q, Ecker JR (1998) Nuclear events in ethylene signaling: a transcriptional cascade mediated by ETHYLENE-INSENSITIVE3 and ETHYLENE-RESPONSE-FACTOR1. *Genes Dev.* 12:3703-3714.
42. Bisson MMA, Groth G (2010) New insight in ethylene signaling: autokinase activity of ETR1 modulates the interaction of receptors and EIN2. *Mol Plant* 3:882-889.
43. Bisson M, Bleckmann A, Allekotte S, Groth G (2009) EIN2, the central regulator of ethylene signalling, is localized at the ER membrane where it interacts with the ethylene receptor ETR1. *Biochem J.* 424:1-6.



44. Qiao H, Chang KN, Yazaki J, Ecker JR (2009) Interplay between ethylene, ETP1/ETP2 F-box proteins, and degradation of EIN2 triggers ethylene responses in Arabidopsis. *Genes Dev.* 23:512-521.
45. Alonso JM et al. (2003) Five components of the ethylene-response pathway identified in a screen for weak ethylene-insensitive mutants in Arabidopsis. *Proc Natl Acad Sci. USA* 100:2992-2997.
46. Binder BM, Mortimore LA, Stepanova AN, Ecker JR, Bleecker AB (2004) Short-term growth responses to ethylene in Arabidopsis seedlings are EIN3/EIL1 independent. *Plant Physiol.* 136:2921-2927.
47. An F et al. (2010) Ethylene-induced stabilization of ETHYLENE INSENSITIVE3 and EIN3-LIKE1 is mediated by proteasomal degradation of EIN3 binding F-Box 1 and 2 that requires EIN2 in Arabidopsis. *Plant Cell* 22:2384-2401.
48. Gagne JM et al. (2004) Arabidopsis EIN3-binding F-box 1 and 2 form ubiquitin-protein ligases that repress ethylene action and promote growth by directing EIN3 degradation. *Proc Natl Acad Sci. USA* 101:6803-6808.
49. Stock AM, Robinson VL, Goudreau PN (2000) Two-component signal transduction. *Annu Rev Biochem.* 69:183-215.
50. Koretke KK, Lupas AN, Warren PV, Rosenberg M, Brown JR (2000) Evolution of two-component signal transduction. *Mol Biol Evol.* 17:1956 -1970.
51. Hwang I, Chen H, Sheen J (2002) Two-component signal transduction pathways in Arabidopsis. *Plant Physiol.* 129:500-515.
52. Lohrmann J, Harter K (2002) Plant two-component signaling systems and the role of response regulators. *Plant Physiol.* 128:363-369.
53. Scharein B, Voet-van-Vormizeele J, Harter K, Groth G (2008) Ethylene signaling: identification of a putative ETR1-AHP1 phosphorelay complex by fluorescence spectroscopy. *Anal Biochem.* 377:72-76.
54. Mizuno T (2005) Two-component phosphorelay signal transduction systems in plants: from hormone responses to circadian rhythms. *Biosci Biotechnol Biochem.* 69:2263-2276.
55. Wang KLC, Li H, Ecker JR (2002) Ethylene biosynthesis and signaling networks. *Plant Cell* 14 Suppl:S131-151.
56. Grierson D, Kear R, Thompson J, Garcia-Mora R (1982) Stimulation of in vitro RNA synthesis by pre-treating plants with auxins is due to auxin-induced ethylene production. *Zeitschrift für Pflanzenphysiologie* 107:419-429.
57. Raz V, Ecker JR (1999) Regulation of differential growth in the apical hook of Arabidopsis. *Development* 126:3661-3668.
58. Woeste KE, Ye C, Kieber JJ (1999) Two Arabidopsis mutants that overproduce ethylene are affected in the posttranscriptional regulation of 1-aminocyclopropane-1-carboxylic acid synthase. *Plant Physiol.* 119:521-530.
59. Hutchison CE et al. (2006) The Arabidopsis histidine phosphotransfer proteins are redundant positive regulators of cytokinin signaling. *Plant Cell* 18:3073-3087.
60. Moubayidin L, Di Mambro R, Sabatini S (2009) Cytokinin-auxin crosstalk. *Trends Plant Sci.* 14:557-562.
61. Voet van Vormizeele JH (2006) Funktionelle und molekulare Charakterisierung des Ethylenrezeptorproteins ETR1 aus *A. thaliana*, Dissertation, Heinrich-Heine-Universität Düsseldorf.
62. Miroux B, Walker JE (1996) Over-production of proteins in *Escherichia coli*: mutant hosts that allow synthesis of some membrane proteins and globular proteins at high levels. *J Mol Biol.* 260:289-298.
63. Sambrook J, Russell DW (2006) *The condensed protocols from Molecular cloning : a laboratory manual* (CSHL Press).

64. Hanahan D (1983) Studies on transformation of *Escherichia coli* with plasmids. *J Mol Biol.* 166:557-580.
65. Hanahan D, Jessee J, Bloom FR (1991) Plasmid transformation of *Escherichia coli* and other bacteria. *Meth Enzymol.* 204:63-113.
66. Ho SN, Hunt HD, Horton RM, Pullen JK, Pease LR (1989) Site-directed mutagenesis by overlap extension using the polymerase chain reaction. *Gene* 77:51-59.
67. Li MZ, Elledge SJ (2007) Harnessing homologous recombination in vitro to generate recombinant DNA via SLIC. *Nat Meth.* 4:251-256.
68. Bradford MM (1976) A rapid and sensitive method for the quantitation of microgram quantities of protein utilizing the principle of protein-dye binding. *Anal Biochem.* 72:248-254.
69. Smith PK et al. (1985) Measurement of protein using bicinchoninic acid. *Anal Biochem.* 150:76-85.
70. Walker JM ed. (2005) *The Proteomics Protocols Handbook* (Humana Press)
71. Laemmli UK (1970) Cleavage of structural proteins during the assembly of the head of bacteriophage T4. *Nature* 227:680-685.
72. Heukeshoven J, Dernick R (1988) Improved silver staining procedure for fast staining in PhastSystem Development Unit. I. Staining of sodium dodecyl sulfate gels. *Electrophoresis* 9:28-32.
73. Towbin H, Staehelin T, Gordon J (1979) Electrophoretic transfer of proteins from polyacrylamide gels to nitrocellulose sheets: procedure and some applications. *Proc Natl Acad Sci. USA* 76:4350 - 4354.
74. Ren H et al. (2009) High-level production, solubilization and purification of synthetic human GPCR chemokine receptors CCR5, CCR3, CXCR4 and CX3CR1. *PLoS ONE* 4(2): e4509
75. Patra AK et al. (2000) Optimization of inclusion body solubilization and renaturation of recombinant human growth hormone from *Escherichia coli*. *Protein Expr Purif.* 18:182-192.
76. Sreerama N, Woody RW (2000) Estimation of protein secondary structure from circular dichroism spectra: comparison of CONTIN, SELCON, and CDSSTR methods with an expanded reference set. *Anal Biochem.* 287:252-260.
77. Chayen NE, Shaw Stewart PD, Blow DM (1992) Microbatch crystallization under oil -- a new technique allowing many small-volume crystallization trials. *J Cryst Growth* 122:176-180.
78. Drenth J (1999) *Principles of protein x-ray crystallography* (Springer).
79. Walter TS et al. (2006) Lysine methylation as a routine rescue strategy for protein crystallization. *Structure* 14:1617-1622.
80. Shaw N, Cheng, C, Liu ZJ (2007) Procedure for reductive methylation of protein to improve crystallizability. *Nat Protoc.* DOI:10.1038/nprot.2007.287
81. Altschul SF et al. (1997) Gapped BLAST and PSI-BLAST: a new generation of protein database search programs. *Nucleic Acids Res.* 25:3389-3402.
82. The UniProt Consortium (2009) The Universal Protein Resource (UniProt) in 2010. *Nucleic Acids Res.* 38:D142-D148.
83. Jain E et al. (2009) Infrastructure for the life sciences: design and implementation of the UniProt website. *BMC Bioinformatics* 10:136.
84. Thompson JD, Higgins DG, Gibson TJ (1994) CLUSTAL W: improving the sensitivity of progressive multiple sequence alignment through sequence weighting, position-specific gap penalties and weight matrix choice. *Nucleic Acids Res.* 22:4673-4680.
85. Larkin M et al. (2007) Clustal W and Clustal X version 2.0. *Bioinformatics* 23:2947 -2948.
86. Corpet F (1988) Multiple sequence alignment with hierarchical clustering. *Nucleic Acids Res.* 16:10881-10890.
87. Papadopoulos JS, Agarwala R (2007) COBALT: constraint-based alignment tool for multiple protein sequences. *Bioinformatics* 23:1073-1079.

- 
88. Waterhouse AM, Procter JB, Martin DMA, Clamp M, Barton GJ (2009) Jalview Version 2--a multiple sequence alignment editor and analysis workbench. *Bioinformatics* 25:1189-1191.
  89. Dong X, Stothard P, Forsythe IJ, Wishart DS (2004) PlasMapper: a web server for drawing and auto-annotating plasmid maps. *Nucleic Acids Res.* 32:W660-664.
  90. Pettersen EF et al. (2004) UCSF Chimera-a visualization system for exploratory research and analysis. *J Comput Chem.* 25:1605-1612.
  91. Hartinger J, Stenius K, Högemann D, Jahn R (1996) 16-BAC/SDS-PAGE: a two-dimensional gel electrophoresis system suitable for the separation of integral membrane proteins. *Anal Biochem.* 240:126-133.
  92. Sislert EC, Shang FY (1984) Anti-ethylene effects of cis-2-butene and cyclic olefins. *Phytochemistry* 23:2765-2768.
  93. Oracz K, El-Maarouf-Bouteau H, Bogatek R, Corbineau F, Bailly C (2008) Release of sunflower seed dormancy by cyanide: cross-talk with ethylene signalling pathway. *J Exp Bot.* 59:2241-2251.
  94. Solomos T, Laties GG (1974) Similarities between the actions of ethylene and cyanide in initiating the climacteric and ripening of avocados. *Plant Physiol.* 54:506-511.
  95. Cho Y, Batt CA, Sawyer L (1994) Probing the retinol-binding site of bovine beta-lactoglobulin. *J Biol Chem.* 269:11102-11107.
  96. Lakowicz JR (2006) *Principles of Fluorescence Spectroscopy* (Springer).
  97. Jiskoot W, Crommelin DJA (2005) *Methods for structural analysis of protein pharmaceuticals* (Springer).
  98. Vivian JT, Callis PR (2001) Mechanisms of tryptophan fluorescence shifts in proteins. *Biophys J* 80:2093-2109.
  99. Akyol Z et al. (2004) Apo-calmodulin binds with its C-terminal domain to the N-methyl-D-aspartate receptor NR1 C0 region. *J Biol Chem.* 279:2166-2175.
  100. Kozlov AG, Lohman TM (2002) Stopped-flow studies of the kinetics of single-stranded DNA binding and wrapping around the Escherichia coli SSB tetramer. *Biochemistry* 41:6032-6044.
  101. Nugent T, Jones D (2009) Transmembrane protein topology prediction using support vector machines. *BMC Bioinformatics* 10:159.
  102. Jones DT (2007) Improving the accuracy of transmembrane protein topology prediction using evolutionary information. *Bioinformatics* 23:538 -544.
  103. Jones DT, Taylor WR, Thornton JM (1994) A model recognition approach to the prediction of all-helical membrane protein structure and topology. *Biochemistry* 33:3038-3049.
  104. Eswar N et al. (2007) Comparative protein structure modeling using MODELLER. *Curr Protoc Protein Sci.* Chapter 2:Unit 2.9.
  105. Martí-Renom MA et al. (2000) Comparative protein structure modeling of genes and genomes. *Annu Rev Biophys Biomol Struct.* 29:291-325.
  106. Sali A, Blundell TL (1993) Comparative protein modelling by satisfaction of spatial restraints. *J Mol Biol.* 234:779-815.
  107. Fiser A, Do RK, Sali A (2000) Modeling of loops in protein structures. *Protein Sci.* 9:1753-1773.
  108. Kuntal B, Aparoy P, Reddanna P (2010) EasyModeller: a graphical interface to MODELLER. *BMC Research Notes* 3:226.
  109. Marina A, Waldburger CD, Hendrickson WA (2005) Structure of the entire cytoplasmic portion of a sensor histidine-kinase protein. *EMBO J.* 24:4247-4259.
  110. Jones DT (1999) Protein secondary structure prediction based on position-specific scoring matrices. *J Mol Biol.* 292:195-202.
  111. Bryson K et al. (2005) Protein structure prediction servers at University College London. *Nucleic Acids Res.* 33:W36-38.

112. Kaur H, Raghava GPS (2003) Prediction of beta-turns in proteins from multiple alignment using neural network. *Protein Sci.* 12:627-634.
113. Creighton TE (1997) *Protein structure: a practical approach* (Oxford University Press).
114. Manavalan P, Johnson WC (1987) Variable selection method improves the prediction of protein secondary structure from circular dichroism spectra. *Anal Biochem.* 167:76-85.
115. Hennessey JP, Johnson WC (1982) Experimental errors and their effect on analyzing circular dichroism spectra of proteins. *Anal Biochem.* 125:177-188.
116. Bisson MMA, Groth G (2010) New insight in ethylene signaling: autokinase activity of ETR1 modulates the interaction of receptors and EIN2. *Mol Plant* 3:882-889.
117. Kikuchi A, Adachi S, Nakamura H, Shiro Y (2001) Structural characterization of ethylene binding site in ethylene sensor protein ETR1 by XAFS. *KEK Prog Rep.* 256.
118. Donovan JW (1973) in *Part D: Enzyme Structure* (Academic Press).
119. Cornog Jr. J, Adams W (1963) The fluorescence of tyrosine in alkaline solution. *Biochim Biophys Acta* 66:356-365.
120. Willis KJ, Szabo AG (1991) Fluorescence decay kinetics of tyrosinate and tyrosine hydrogen-bonded complexes. *J Phys Chem.* 95:1585-1589.
121. Groen B et al. (1996) Spectroscopic characterization of recombinant follicle stimulating hormone. *Spectrochim Acta Part A: Mol Biomol Spectrosc.* 52:1331-1346.
122. Pundak S, Roche RS (1984) Tyrosine and tyrosinate fluorescence of bovine testes calmodulin: calcium and pH dependence. *Biochemistry* 23:1549-1555.
123. Szabo AG, Lynn K, Krajcarski D, Rayner DM (1979) Tyrosine fluorescence at 345 nm in proteins lacking tryptophan. *J Luminesc.* 18-19:582-586.
124. Lundbäck A, van den Berg S, Hebert H, Berglund H, Eshaghi S (2008) Exploring the activity of tobacco etch virus protease in detergent solutions. *Anal Biochem.* 382:69-71.
125. Mohanty AK, Simmons CR, Wiener MC (2003) Inhibition of tobacco etch virus protease activity by detergents. *Protein Expr Purif.* 27:109-114.
126. Swain SD, Helgersen SL, Davis AR, Nelson LK, Quinn MT (1997) Analysis of activation-induced conformational changes in p47 phox using tryptophan fluorescence spectroscopy. *J Biol Chem.* 272:29502 -29510.
127. Grimard V et al. (2004) Phosphorylation-induced conformational changes of cystic fibrosis transmembrane conductance regulator monitored by attenuated total reflection-Fourier transform IR spectroscopy and fluorescence spectroscopy. *J Biol Chem.* 279:5528 -5536.
128. Chang C, Kwok SF, Bleecker AB, Meyerowitz EM (1993) Arabidopsis ethylene-response gene ETR1: similarity of product to two-component regulators. *Science* 262:539-544.
129. Chang C, Meyerowitz EM (1995) The ethylene hormone response in Arabidopsis: a eukaryotic two-component signaling system. *Proc Natl Acad Sci. USA* 92:4129-4133.
130. Müller-Dieckmann H, Grantz AA, Kim S (1999) The structure of the signal receiver domain of the Arabidopsis thaliana ethylene receptor ETR1. *Structure* 7:1547-1556.
131. Stewart RC, Jahreis K, Parkinson JS (2000) Rapid phosphotransfer to CheY from a CheA protein lacking the CheY-binding domain. *Biochemistry* 39:13157-13165.
132. James TL (1985) Phosphorus-31 NMR as a probe for phosphoproteins. *CRC Crit Rev Biochem.* 18:1-30.
133. Lottspeich F, Engels JW, Simeon A (2006) *Bioanalytik* (Spektrum Akademischer Verlag).
134. Schertler GF (1992) Overproduction of membrane proteins. *Curr Opin Struct Biol.* 2:534-544.
135. Matheis G, Whitaker JR (1984) <sup>31</sup>P NMR chemical shifts of phosphate covalently bound to proteins. *Int J Biochem.* 16:867-73.
136. Sanders JKM, Williams DH (1972) Shift reagents in NMR spectroscopy. *Nature* 240:385-390.

137. Fröhlich M, Brecht V, Peschka-Süss R (2001) Parameters influencing the determination of liposome lamellarity by  $^{31}\text{P}$ -NMR. *Chem Phys Lipids* 109:103-112.
138. Peyratout CS, Severns JC, Holm SR, McMillin DR (1994) EPR studies of ligand binding to the type 2/type 3 cluster in tree laccase. *Arch Biochem Biophys*. 314:405-411.
139. Blackburn NJ, Collison D, Sutton J, Mabbs FE (1984) Kinetic and e.p.r. studies of cyanide and azide binding to the copper sites of dopamine (3,4-dihydroxyphenethylamine) beta-mono-oxygenase. *Biochem J*. 220:447-454.
140. Aronoff-Spencer E et al. (2000) Identification of the  $\text{Cu}^{2+}$  binding sites in the N-terminal domain of the prion protein by EPR and CD spectroscopy. *Biochemistry* 39:13760-13771.
141. Classen T (2007) Reinigung und Kristallisation der Extramembran-Domäne des Ethylenrezeptors ETR1, Bachelorarbeit, Heinrich-Heine-Universität Düsseldorf.
142. Leslie A (1992) Recent changes to the MOSFLM package for processing film and image plate data. *Joint CCP4 + ESF-EAMCB Newsletter on Protein Crystallography*, No. 26.
143. Rhodes G (2006) *Crystallography made crystal clear: a guide for users of macromolecular models* (Academic Press).
144. Garman EF, Owen RL (2006) Cryocooling and radiation damage in macromolecular crystallography. *Acta Crystallogr D Biol Crystallogr*. 62:32-47.
145. Harp JM, Timm DE, Bunick GJ (1998) Macromolecular crystal annealing: overcoming increased mosaicity associated with cryocrystallography. *Acta Crystallogr D Biol Crystallogr*. 54:622-628.
146. McPherson A (2004) Introduction to protein crystallization. *Methods* 34:254-265.
147. Myerson AS (2002) *Handbook of industrial crystallization* (Butterworth-Heinemann).
148. Christopher GK, Phipps AG, Gray RJ (1998) Temperature-dependent solubility of selected proteins. *J Cryst Growth* 191:820-826.
149. Thakur AS et al. (2007) Improved success of sparse matrix protein crystallization screening with heterogeneous nucleating agents. *PLoS ONE* 2(10):e1091.
150. Biertümpfel C, Basquin J, Suck D, Sauter C (2002) Crystallization of biological macromolecules using agarose gel. *Acta Crystallogr D Biol Crystallogr*. 58:1657-1659.
151. Tanabe K et al. (2009) Promotion of crystal nucleation of protein by semi-solid agarose Gel. *Appl Phys Express*. 2:125501.
152. Sica F et al. (1994) Elimination of twinning in crystals of *Sulfolobus solfataricus* alcohol dehydrogenase holo-enzyme by growth in agarose gels. *Acta Crystallogr D Biol Crystallogr*. 50:508-511.
153. Schubot FD, Waugh DS (2004) A pivotal role for reductive methylation in the de novo crystallization of a ternary complex composed of *Yersinia pestis* virulence factors YopN, SycN and YscB. *Acta Crystallogr D Biol Crystallogr*. 60:1981-1986.
154. Rayment I et al. (1993) Three-dimensional structure of myosin subfragment-1: a molecular motor. *Science* 261:50-58.
155. Derewenda ZS (2004) Rational protein crystallization by mutational surface engineering. *Structure* 12:529-535.
156. Goldschmidt L, Cooper DR, Derewenda ZS, Eisenberg D (2007) Toward rational protein crystallization: A Web server for the design of crystallizable protein variants. *Protein Sci*. 16:1569-1576.
157. Kim A, Dobransky T, Rylett RJ, Shilton BH (2005) Surface-entropy reduction used in the crystallization of human choline acetyltransferase. *Acta Crystallogr D Biol Crystallogr*. 61:1306-1310.
158. Janda I et al. (2004) The crystal structure of the reduced,  $\text{Zn}^{2+}$ -bound form of the B. subtilis Hsp33 chaperone and its implications for the activation mechanism. *Structure* 12:1901-1907.
159. Philo JS (2009) Mechanisms of protein aggregation. *Curr Pharm Biotechnol*. 10:348-351.
160. DeLucas LJ, Delucas L (2009) *Membrane protein crystallization* (Academic Press).
161. Rasmussen SGF et al. (2007) Crystal structure of the human [bgr]2 adrenergic G-protein-coupled receptor. *Nature* 450:383-387.

162. Bergfors T (2003) Seeds to crystals. *J Struct Biol.* 142:66-76.
163. Nußberger S, Dörr K, Wang DN, Kühlbrandt W (1993) Lipid-protein interactions in crystals of plant light-harvesting complex. *J Mol Biol.* 234:347-356.
164. Zhang H, Kurisu G, Smith JL, Cramer WA (2003) A defined protein-detergent-lipid complex for crystallization of integral membrane proteins: the cytochrome b6f complex of oxygenic photosynthesis. *Proc Natl Acad Sci. USA* 100:5160 -5163.
165. Li Y, Agrawal A, Sakon J, Beitle RR (2001) Characterization of metal affinity of green fluorescent protein and its purification through salt promoted, immobilized metal affinity chromatography. *J Chromatogr. A* 909:183-190.
166. Rath A, Glibowicka M, Nadeau VG, Chen G, Deber CM (2009) Detergent binding explains anomalous SDS-PAGE migration of membrane proteins. *Proc Natl Acad Sci. USA* 106:1760-1765.
167. Rial DV, Ceccarelli EA (2002) Removal of DnaK contamination during fusion protein purifications. *Protein Expr Purif.* 25:503-507.
168. Rudiger S, Germeroth L, Schneider-Mergener J, Bukau B (1997) Substrate specificity of the DnaK chaperone determined by screening cellulose-bound peptide libraries. *EMBO J.* 16:1501-1507.
169. Pastorino B et al. (2008) Improvement of the purification of Saint Louis encephalitis virus NS2B-NS3 recombinant protease expressed in *Escherichia coli*. *J Chromatogr. B* 868:58-63.
170. Rial DV, Ceccarelli EA (2002) Removal of DnaK contamination during fusion protein purifications. *Protein Expr Purif.* 25:503-507.
171. Bukau B, Horwich AL (1998) The Hsp70 and Hsp60 chaperone machines. *Cell* 92:351-366.
172. Ishibashi M et al. (2005) Is arginine a protein-denaturant? *Protein Expr Purif.* 42:1-6.
173. Tsumoto K et al. (2004) Role of arginine in protein refolding, solubilization, and purification. *Biotechnol Prog.* 20:1301-1308.
174. Sundara Baalaji N, Acharya KR, Singh TP, Krishnaswamy S (2005) High-resolution diffraction from crystals of a membrane-protein complex: bacterial outer membrane protein OmpC complexed with the antibacterial eukaryotic protein lactoferrin. *Acta Crystallogr Sect F Struct Biol Cryst Commun.* 61:773-775.
175. Röthlisberger D, Pos KM, Plückthun A (2004) An antibody library for stabilizing and crystallizing membrane proteins - selecting binders to the citrate carrier CitS. *FEBS Lett.* 564:340-348.
176. Warke A, Momany C (2007) Addressing the protein crystallization bottleneck by cocrystallization. *Cryst Growth Des.* 7:2219-2225.
177. Newstead S, Ferrandon S, Iwata S (2008) Rationalizing  $\alpha$ -helical membrane protein crystallization. *Protein Sci.* 17:466-472.
178. Privé GG (2007) Detergents for the stabilization and crystallization of membrane proteins. *Methods* 41:388-397.
179. Wadsten P et al. (2006) Lipidic sponge phase crystallization of membrane proteins. *J Mol Biol.* 364:44-53.
180. Wöhri AB et al. (2008) A lipidic-sponge phase screen for membrane protein crystallization. *Structure* 16:1003-1009.
181. Chow PS, Liu XY, Zhang J, Tan RBH (2002) Spherulitic growth kinetics of protein crystals. *Appl Phys Lett.* 81(11):1975-1977
182. Rupp B, Wang J (2004) Predictive models for protein crystallization. *Methods* 34:390-407.
183. Bergfors TM (2009) *Protein Crystallization* (Internat'l University Line).
184. Grimm C, Klebe G, Ficner R, Reuter K (2000) Screening orthologs as an important variable in crystallization: preliminary X-ray diffraction studies of the tRNA-modifying enzyme S-adenosyl-methionine:tRNA ribosyl transferase/isomerase. *Acta Crystallogr D Biol Crystallogr.* 56:484-488.
185. Cove DJ et al. (2009) The moss *Physcomitrella patens*: a novel model system for plant development and genomic studies. *Cold Spring Harb Protoc.* 2009:pdb.emo115.

186. de Jong M, Mariani C, Vriezen WH (2009) The role of auxin and gibberellin in tomato fruit set. *J Exp Bot.* 60:1523 -1532.
187. Hanks S, Quinn A, Hunter T (1988) The protein kinase family: conserved features and deduced phylogeny of the catalytic domains. *Science* 241:42-52.
188. Shaw AZ, Miroux B (2003) A general approach for heterologous membrane protein expression in *Escherichia coli*: the uncoupling protein, UCP1, as an example. *Methods Mol Biol.* 228:23-35.
189. Grisshammer R, Tate CG (1995) Overexpression of integral membrane proteins for structural studies. *Q Rev Biophys.* 28:315-422.
190. Mukhopadhyay A (1997) Inclusion bodies and purification of proteins in biologically active forms. *Adv Biochem Eng Biotechnol.* 56:61-109.
191. Batas B, Schiraldi C, Chaudhuri JB (1999) Inclusion body purification and protein refolding using microfiltration and size exclusion chromatography. *J Biotechnol.* 68:149-158.
192. Schein CH (1989) Production of soluble recombinant proteins in bacteria. *Nat Biotech.* 7:1141-1149.
193. Sørensen HP, Mortensen KK (2005) Soluble expression of recombinant proteins in the cytoplasm of *Escherichia coli*. *Microb Cell Fact.* 4:1.
194. Thomas JG, Baneyx F (1997) Divergent effects of chaperone overexpression and ethanol supplementation on inclusion body formation in recombinant *Escherichia coli*. *Protein Expr Purif.* 11:289-296.
195. Kosinski M, Rinas U, Bailey J (1992) Isopropyl- $\beta$ -D-thiogalactopyranoside influences the metabolism of *Escherichia coli*. *Appl Microbiol Biotechnol.* 36(6):782-784.
196. Ventura S, Villaverde A (2006) Protein quality in bacterial inclusion bodies. *Trends Biotechnol.* 24:179-185.
197. Patra AK et al. (2000) Optimization of inclusion body solubilization and renaturation of recombinant human growth hormone from *Escherichia coli*. *Protein Expr Purif.* 18:182-192.
198. Oberg K, Chrnyk BA, Wetzel R, Fink AL (1994) Native-like secondary structure in Interleukin-1 beta inclusion bodies by attenuated total reflectance FTIR. *Biochemistry* 33:2628-2634.
199. Carrió MM, Villaverde A (2001) Protein aggregation as bacterial inclusion bodies is reversible. *FEBS Lett.* 489:29-33.
200. Lilie H, Schwarz E, Rudolph R (1998) Advances in refolding of proteins produced in *E. coli*. *Curr Opin Biotechnol.* 9:497-501.
201. Raina K, Panda AK, Ali MM, Talwar GP (2004) Purification, refolding, and characterization of recombinant LHRH-T multimer. *Protein Expr Purif.* 37:8-17.
202. Nall BT, Osterhout JJ, Ramdas L (1988) pH Dependence of folding of iso-2-cytochrome c. *Biochemistry* 27:7310-7314.
203. Tsumoto K, Ejima D, Kumagai I, Arakawa T (2003) Practical considerations in refolding proteins from inclusion bodies. *Protein Expr Purif.* 28:1-8.
204. Rudolph R, Lilie H (1996) In vitro folding of inclusion body proteins. *FASEB J.* 10:49-56.
205. Clark EDB (1998) Refolding of recombinant proteins. *Curr Opin Biotechnol* 9:157-163.
206. Zardeneta G, Horowitz PM (1994) Protein refolding at high concentrations using detergent /phospholipid mixtures. *Anal Biochem.* 218:392-398.
207. le Maire M, Champeil P, Møller JV (2000) Interaction of membrane proteins and lipids with solubilizing detergents. *Biochim Biophys Acta Biomembr.* 1508:86-111.
208. Eiselé J et al. (1991) Membrane protein crystallization: observations and use of short chain phospholipids as amphiphiles. *J Cryst Growth* 110:96-102.
209. Strop P, Brunger AT (2005) Refractive index-based determination of detergent concentration and its application to the study of membrane proteins. *Protein Sci.* 14:2207-2211.
210. McCarty JS, Walker GC (1991) DnaK as a thermometer: threonine-199 is site of autophosphorylation and is critical for ATPase activity. *Proc Natl Acad Sci. USA* 88:9513-9517.

- 211. Dalie BL, Skaleris DA, Köhle K, Weissbach H, Brot N (1990) Interaction of DnaK with ATP: binding, hydrolysis and  $\text{Ca}^{2+}$ -stimulated autophosphorylation. *Biochem Biophys Res Commun* 166:1284-1292.
- 212. Caffrey M, Cherezov V (2009) Crystallizing membrane proteins using lipidic mesophases. *Nat Protoc.* 4:706-731.
- 213. Dunlop KV, Hazes B (2003) When less is more: a more efficient vapour-diffusion protocol. *Acta Crystallogr D Biol Crystallogr.* 59:1797-1800.
- 214. Walker JM, Doublé S eds. (2007) *Macromolecular Crystallography Protocols* (Humana Press).
- 215. Ratelade J et al. (2009) Production of recombinant proteins in the lon-deficient BL21(DE3) strain of Escherichia coli in the absence of the DnaK chaperone. *Appl Environ Microbiol.* 75:3803-3807.
- 216. Verma R, Boleti E, George AJT (1998) Antibody engineering: comparison of bacterial, yeast, insect and mammalian expression systems. *J Immunol Methods* 216:165-181.
- 217. Saitou N, Nei M (1987) The neighbor-joining method: a new method for reconstructing phylogenetic trees. *Mol Biol Evol.* 4:406-425.
- 218. Izawa T, Shimamoto K (1996) Becoming a model plant: the importance of rice to plant science. *Trends Plant Sci.* 1:95-99.
- 219. Strable J, Scanlon MJ (2009) Maize (Zea mays): A model organism for basic and applied research in plant biology. *Cold Spring Harb Protoc.* 2009:pdb.emo132.
- 220. Maria IA, Hitoshi S, Satoshi Y, Atsushi H (2002) Differences in the rates of ethylene production and growth between the calluses derived from rice (Oryza sativa L.) and soybean (Glycine max (L.) Merr.). *Plant Prod Sci.* 5:11-16.
- 221. Xie F, Liu Q, Wen C (2006) Receptor signal output mediated by the ETR1 N-terminus is primarily subfamily I receptor dependent. *Plant Physiol.* 142:492-508.
- 222. Zhong S, Lin Z, Grierson D (2008) Tomato ethylene receptor-CTR interactions: visualization of NEVER-RIPE interactions with multiple CTRs at the endoplasmic reticulum. *J Exp Bot.* 59:965-972.
- 223. Ho YJ, Burden LM, Hurley JH (2000) Structure of the GAF domain, a ubiquitous signaling motif and a new class of cyclic GMP receptor. *EMBO J.* 19:5288-5299.
- 224. Bilwes AM, Alex LA, Crane BR, Simon MI (1999) Structure of CheA, a signal-transducing histidine kinase. *Cell* 96:131-141.
- 225. Yamada S et al. (2009) Structure of PAS-linked histidine kinase and the response regulator complex. *Structure* 17:1333-1344.
- 226. Albanesi D et al. (2009) Structural plasticity and catalysis regulation of a thermosensor histidine kinase. *Proc Natl Acad Sci. USA* 106:16185-16190.
- 227. Vesterstrøm J, Taylor WR (2011) Flexible secondary structure based protein structure comparison applied to the detection of circular permutation. *J Comput Biol.* 13:43-63.
- 228. IUPAC-IUB Commission on Biochemical Nomenclature (1968) A one-letter notation for amino acid sequences. Tentative rules. *Eur J Biochem.* 5:151-153.



## 11 Acknowledgements

A special thank goes to my supervisor Prof. Dr. Georg Groth for his continuous support and guidance throughout the last years. He gave me scope for development and his enthusiasm and encouragement were always inspiring.

I would like to thank Prof. Dr. Dieter Willbold for accepting to be co-referee and the opportunity to use the CD spectrometer at the Institute of Physical Biology.

Thanks also go to Prof. Dr. Jörg Pietruszka, Institute for Bioorganic Chemistry, for providing access to a NMR spectrometer – and to Rainer Goldbaum for technical support with the equipment.

Warm thanks go to my present and former colleagues at the Institute for Biochemical Plant Physiology. I am not even going to try to list all of you here, so as not to miss anyone, but special thanks have to go to Benny, Judith, Meli, Silke and Jan for many inspirational moments and discussions. And last but not least, thanks to Nicole who assisted in cloning and – as well as Patricia – provided me with fresh bacterial cells every now and then. Thanks to both of you.

Very special thanks go to my family for sharing all ups and downs that go along with research. For Tom, who did not just struggle through endless pages of manuscript but who always believed in me and gave me advice and encouragement. Thank you so much for your support – especially during the last stage of this project.

Cheers!



## 12 Erklärung

Die hier vorgelegte Dissertation habe ich eigenständig und ohne unerlaubte Hilfe angefertigt. Die Dissertation wurde in der vorgelegten – oder in ähnlicher Form – noch bei keiner anderen Institution eingereicht. Ich habe bisher keinen erfolglosen Promotionsversuch unternommen.

Düsseldorf, \_\_\_\_\_

Elisa Buchen

